LIGHT & ENGINEERING

LIGHT & ENGINEERING
(Svetotekhnika)

СВЕТО ТЕХНИКА

Moscow, 2016

Light & Engineering" is an international scientific Journal subscribed to by readers in many different countries. It is the Englishedition of the journal "Svetotekhnika" the oldest scientific publication in Russia, established in 1932.

Establishing the englishedition "Light and Engineering" in 1993 allowed Russian illumination science to be presented the colleagues abroad. It attracted the attention of experts and a new generation of scientists from different countries to Russian domestic achievements in light and engineering science. It also introduced the results of international research and their industrial application on the Russian lighting market.

The scope of our publication is to present the most current results of fundamental research in the field of illumination science. This includes theoretical bases of light source development, physiological optics, lighting technology, photometry, colorimetry, radiometry and metrology, visual perception, health and hazard, energy efficiency, semiconductor sources of light and many others related directions.The journal also aims to cover the application illumination science in technology of light sources, lighting devices, lighting installations, control systems, standards, lighting art and design, and so on.

"Light & Engineering" is well known by its brand and design in the field of light and illumination. Each annual volume has four issues, with about 80–140 pages per issue. Each paper is reviewed by recognisedworld experts.

To promote the work of the Journal, the editorial staff is in active communication with Thomson Scientific (Citation index) and other international publishing houses and agencies, such as Elsevier and EBSCO Publishing.

CONTENTS

VOLUME 24 **NUMBER 2** **2016**

LIGHT & ENGINEERING
(SVETOTEKHNIKA)

3

SOLATUBE® TECHNOLOGY: PROSPECTIVE APPLICATIONS IN ARCHITECTURE AND BUILDING IN RUSSIA

Alexander T. Ovcharov[1] and Jury N. Selyanin[2]

[1]Light systems Open Company, Tomsk; [2]Solar Open Company, Krasnodar
E-mail: oat_08@mail.ru

ABSTRACT

Solatube® Daylighting Systems intended for natural illumination are considered in the context of energy efficiency in illumination and the formation of a high quality light medium. A new model is described with multiple consumer parameters presented as a prospective technological solution for effective natural illumination of large rooms with high ceilings, (6–30) m.

Keywords: hollow tubular light guides, natural illumination, energy saving

Effective use of natural light in buildings is considered to be a powerful method for saving energy and resources. Worldwide trends in illumination tend towards a comfortable light medium and growing energy production and consumption. There is an obvious solution to the apparent conflict of interest between light comfort and the energy crisis: transitioning to energy saving technologies and renewable energy sources [1, 2]. Therefore, facilities and technologies applying natural light become important. Typical models representative of this technology are illumination systems (IS) with hollow tubular light guides (HTLG).

The introduction of ISs with HTLGs is gradually growing in Russia due to their properties as effective energy saving light devices of high quality. On the Russian market natural illumination is represented by several foreign companies: American (USA) *Solatube International Inc.* (*Solatube®* IS *Daylighting Systems*) [3], Italian *Solarspot International S.r.l.* (*Solarspot®* IS) [4–6] and Czech *Lightway* (*ALLUX* IS) [7].

Solatube International Inc. products occupy up to 80% of the world market of ISs with HTLGs. An effective stimulus for development of *Solatube® Daylighting Systems* ISs is the US state program supporting the use of alternative energy sources. In Russia, there are a number of government efforts, including Law № 261-ФЗ adopted in 2009 "On energy saving and increase of power efficiency ...", as well as very conscientious efforts made by progressive professionals on the building market.
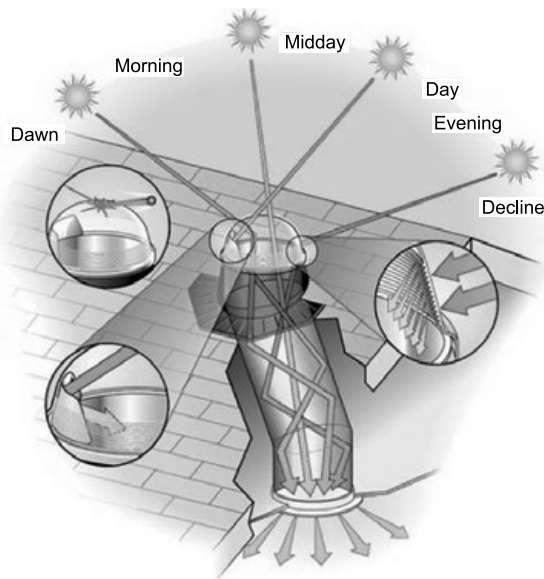
Fig. 1. Operating principle of the *Solatube®* Daylighting Systems Record optical characteristics of HTLGs keep the main advantages of sunlight: a continuous spectrum, the daily rhythm of natural light corresponding to the human "biological clock" and dynamics, which indicate weather conditions in real time

Modern ISs with HTLGs intended for natural illumination, produced by leading global companies, are made to a high standard and equipped with various means of creating a comfortable light medium in rooms. It should be noted that their structures are similar and their levels of technological perfection are approximately identical. The leadership of such ISs on the market is determined by their technological, operational and price benefits. Certain features of design draw special attention to the *Solatube® Daylighting Systems (Solatube®)* system. It contains the following main structural elements (Fig. 1):

• **Light-collecting dome (a light-receiving device)** of shock-resistant acryl located on a roof or on a building wall. The dome has notches on its inner surface, which give it properties of a Fresnel lens directing diffused light along the light guide axis, reducing the number of reflections and raising the efficiency of light transmission;

• **Flashing,** a seamless metal adapter for different roof types with a protective cover, which provides the interface between the HTLG structure and the roof, as well as its reliable hydro- and thermo-insulation;

• **Light guide (HTLG),** a set of joinable aluminium tubes, rectilinear or bent in configuration, covered from the interior with a multi-layered polymeric film with a reflection factor of 99.7% in the visible wavelength range. Light from the light-receiving device, passing through the light guide's hollow interior after multiple reflections, arrives into the illuminated room through a light diffuser. The configuration and structure of the tubes makes it easy to integrate into the architecture of different types of building;

• **Light diffuser** with a wide light distribution installed in the room's ceiling and providing a uniform diffusion of natural light in the room.

HTLGs provide rooms with natural light, providing the necessary daylight factor level and a more uniform distribution of illuminance over the entire area of a room than by means of traditional vertical light openings (lateral windows) (Fig. 2). A high reflection factor (light transmission) of an HTLG allows transporting light over a distance of more than 20 m and illuminating the rooms inaccessible to traditional technologies (cellars, central rooms of wide buildings located on ground floors, etc.).
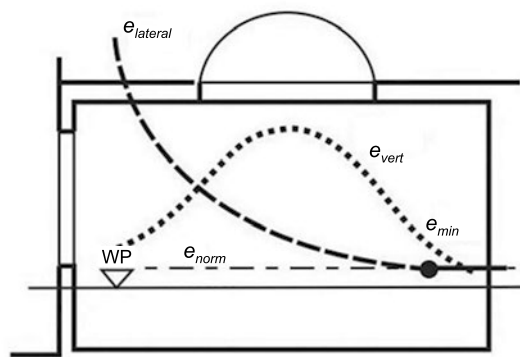
Fig. 2. Relative distributions of natural illuminance in rooms with lateral (window) and top (*Solatube®*) light opening location: E_{min} – minimum value of normalised illuminance; WP -working plane; e_{norm} – normalised daylight factor; $e_{lateral}$ – lateral daylight factor; e_{vert} – top daylight factor

Collector of a sunlight, *SkyVaut*

Internal protective dome

Bordyurny fleshing (the element of interface to a roof, is established on a border)

The light guide extender with a mirror covering of *Spectralight® Infinity*

Amplifier of a luminous flux

External dome

Element for protection against penetration

Ring for fixing of a pipe

Ring for fixing of the amplifier

Prismatic diffuser

Fig. 3. Structure of the *Solatube®* M74 model of Skycalotte series

Fig. 4. *Solatube*® M74 collector of SkyVault series (740 mm) on a roof of a building. A combination of the collector and Fresnel lenses on the dome (Raybender® technology) provides constancy of luminous flux within all light day, including morning and evening periods due to catching light rays at low angles of the sun above the horizon
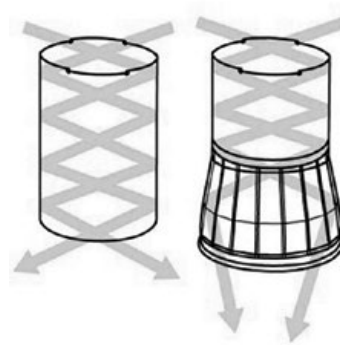
Fig. 5. Operation principle of the amplifier
The amplifier focuses luminous flux on the diffuser plane, reduces reflection and scattering losses, increases luminous flux arriving to a room and allows forming light distribution effective for illumination of rooms with high ceilings

Fig. 6. *Solatube*® M74 model illuminating rooms with high ceilings

Due to a high quality of materials and units, modern HTLGs have efficiency up to 99%, with a general efficiency of ISs with HTLGs reaching 83%.

An essential benefit of *Solatube*® in comparison with traditional light openings is the considerably reduced heat loss during cold seasons and less heat input in summer time. This provides additional energy savings for heating, ventilation and cooling of the rooms. The main economic advantage of the *Solatube*® is the reduction in costs for artificial illumination. Use of natural light as an alternative to artificial light in the day-time, depending on the resource of solar energy in a particular region allows decreasing expenses for illumination by 50–75%. Some evaluations show that: 1) transmitting sunlight to the internal space of a room is 50 times more economic than artificial illumination; 2) extending the use of natural light by one hour a day in industrial buildings achieves saving of about three million kW·h a year all over Russia.

Modern effective ISs with HTLGs change traditional ideas about the arrangement of a room's natural illumination and due to their unique pro-

Fig. 7. *Solatube®* system illuminating a kindergarten (Krasnodar)

perties start to influence modern architecture and construction. In the context of optimising power consumption and of increasing uniformity of the light medium of a room, the use of HTLGs as a main or an additional source of natural light appears to be most effective [8]. Luminous efficacy of HTLGs in comparison with traditional light structures (zenith lanterns, vertical windows) is 2−3 times higher.

The creation and development history, as well as the operating principles and concepts of architecture using ISs with HTLGs, are fully described in [9]. In this article, information on *Solatube®* ISs with HTLGs intended for designers and potential customers is given, and prospective application of these OSs in Russia are considered. The *Solatube®* model range reflects development stages of their structure and production. It is presented by *Solatube® Daylighting Systems* models of *Brighten Up®* series with HTLGs of different diameters: *160 DS* (250 mm), *290 DS* (350 mm) and of *SolaMaster®* series (530 mm), as well as by *Solatube® M74* model of *SkyVault* series (740 mm).

The first three models with a traditional structure were the basis upon which the fourth model was created, the *M74* (with record parameters) opening new opportunities for development of the natural illumination technology and expanding the scope of ISs with HTLG application.

A distinctive feature of *Solatube®* compared to similar products from other manufacturers, is the unsurpassed reflective ability of the tube coating. The *Spectralight® Infinity* coating has an integral reflection factor up to 99.7% in the visible radiation interval.

An important structural difference of the *Solatube®* from ISs with HTLGs of other manufac-

turers is the application of a Fresnel lens in the light-collecting dome (*Raybender® 3000*), which provides a steady standardised light characteristic of the system at a level utterly achievable for modern materials.

The *M74* of the *SkyVault* series model can be easily referred to zenith lanterns of a new generation. It contains several progressive solutions, some of which can be considered as revolutionary (Fig. 3). One of them is the use of a light-collecting accumulator (Fig. 3 and 4) considerably expanding the capture area and increasing light collection efficiency threefold[1].

Another progressive solution is the light amplifier (collimator) (Fig. 3 and 5). This is a cone-shaped element at the end of the light guide, which focuses luminous flux on the diffuser plane increasing the portion of light transmitted through it by approximately 15−16%.

Modular structure of the *Solatube® M74* model opens wide application opportunities of such ISs with HTLGs for providing effective natural illumination to large rooms with high (6 − 30) m ceilings (Fig. 6). A complete set of ISs with HTLGs of the

---

[1] In the collector, the *LightTracker*™ (*LITD®*) reflecting plate with *Spectralight® Infinity* reflecting coating and "cold light guide" technology are applied, due to which the IR component of sunlight is cut off. Protection of the room against IR radiation continues along the entire light transportation tube of the light guide, because of the cold tube technology. The *Spectralight® Infinity* coating works as an optical filter providing an effective transportation of visible radiation along the light guide. The coating is transparent for IR radiation, which after penetrating through the coating to the tube metal, is absorbed by the metal and dissipated into the surrounding space, outside of the illuminated room.

Fig. 8. *Solatube®* 290DS model illuminating underground
rooms of the Legal Academy (Nizhny Novgorod)

Fig. 9. *Solatube®* 330DS model illuminating underground
car service centre of the KIA car dealership (Sochi)

SkyVault series is selected individually according to the project. Despite the dimensions of the structure, ISs simple to install and don't require subsequent servicing. In Table 1, the structural variations of *Solatube® M74* model*,* and in Table 2, some characteristics of *Solatube® Daylighting Systems* IS are provided.

The illuminated area of a room using different *Solatube®* models (approximately) for the standard daylight factor and for a typical room (aver-

Fig. 10. Illumination of the sports hall of the Peking University using Solatube® systems.
The hall with a capacity of more than 8000 spectators (about 2400 m²) was illuminated with 148 models of Solatube® 750 DS (530 mm, of *Solatube® SolaMaster®* series) with *OptiView®* diffuser for open ceiling and with *Daylight Dimmer ᵀᴹ* control device

age HTLG length is 1.82 m, ceiling height is 2.4 m) is as follows: *160 DS* (250 mm) − up to 14 m²; *290 DS* (350 mm) − up to 23 m²; *21-O/21-C* (530 mm) − up to 37 m²; *M74* (740 mm) − up to 100 m² (for installation height of 6 m).

When comparing optical and heat-insulating characteristics of the *Solatube®* ISs with traditional windows, there is no conflict between luminous transmission and heat conduction.

Solatube® (Table 3) provides effective light transmission with a minimum inflow of solar heat creating a comfortable medium in a room.

Operational and investment characteristics

Solatube® ISs are tight. All units (dome, flashing, light guide system, scattering diffuser) have seals which prevent insects and dust getting inside. Unlike zenith lanterns, the *Solatube®* does not require regular servicing. The *Solatube®* payback period is from three to five years, the service life is 30 years, and the warranty period is 10 years. .

Solatube® − **fields of application**

Solatube® ISs fall into the green (ecologically clean) category. Buildings equipped with them, meet the requirements of СП 52.13330.2011, of the Sanitary regulations and standards law 2.2.1/2.1.1.1278−03, of 261-ФЗ (Section 3, Art.11) and come under the energy efficient and ecologically safe category. This energy saving and ecologically clean technology of transmitting natural light by means of the *Solatube®* provides an aesthetic,

Table 1. Complete sets versions of the *Solatube® M74* model

Basic model	With an amplifier of luminous flux	With a collector	With a collector and amplifier
Classical version: • vault, border flashing, HTLG, prismatic diffuser; • diameter of the light guide is 740 mm; • recommended height of the light diffuser installation is (5–8) m; • average luminous flux is 18500 lm.	• increases luminous flux by 15–16%; • promotes formation of an optimum light intensity distribution curve LIDC of the diffuser and effective application at any installation height; • diffuser installation height is 8м; • amplifier height is 600 mm; • diameter of the light diffuser of the amplifier is 949 mm; • average luminous flux is 21500 lm.	• expands the area and raises efficiency of light collection three time over, including at low sun positions; • collector height is 1067 mm; • recommended height of the light diffuser installation is higher than 8 m; • average luminous flux is 35000 lm.	an integrated structure uniting the advantages of all three previous models

functional and environmentally friendly illumination of rooms.

The application of *Solatube®* IS in offices, buildings of industrial purposes and warehouses, along with the significant reduction in illumination costs, adds an important social impact by forming a healthy and environmentally safe light medium. The production of such a light medium helps ensure the economic prosperity of a business [10], they promote capitalisation of investments into modernisation of ISs with HTLGs, and the investments are paid off within four to five years. At present, design enterprises have started an active development of architectural-and-planning solutions using *Solatube®* ISs, which allows full meeting requirements of the sanitary regulations and standards for natural illumination.

An important application field for *Solatube®* is public service buildings; schools and kindergartens, hospitals, etc., where the human benefits are fully realised, creating complete light comfort and safety (Fig. 7). Continuing global urbanisation presses for radical measures to improve the city medium. One of the ways to tackle the creeping environmental crisis is the development of an underground infrastructure.

Fig. 11. Distributor network of *Solatube®* Daylighting Systems technology in Russia

Table 2. Comparative indicators of the *Solatube*® system and artificial light sources (a criterion is luminous flux)

System model *Solatube*®	Luminous flux *, lm	Comparison artificial light source**
SolaMaster® series (530 mm)	from 13500 (average) up to 20500 (max)	Analogues: • a luminaire with MHLs, 150–250 W; • three two-lamp luminaires with *T 8*, 36 W lamps; • four four-lamp luminaires of the Armstrong type with *T 5*, 14 W lamps.
290 DS (350 mm) of *Brighten Up*® series	from 6000 (average) up to 9100 (max)	Analogue: two four-lamp luminaires of the Armstrong type with *T 5*, 14 W lamps.
160 DS (250 mm) of *Brighten Up*® series	from 3000 (average) up to 4600 (max)	• four-lamp luminaire of Armstrong type with T 5, 14W lamps • a luminaire with four CFL, 18W.
M74 of *Skycalotte* series	from 18000 (average) up to 35000 (max)	Analogue: a luminaire with MHLs 250–400W;
Power and luminous flux values of discharge lamps		

MHLs:
 150 W 11250 lm
 250 W 20000 lm
 400 W 35000 lm
		Fluorescent lamps:
		 T-5: 14 W 1200 lm
		      28 W 2600 lm
		 T-8: 18 W 1350 lm
		     36 W 3350 lm
		 CFL: 18 W 1100–1200 lm

Notes:

* The data are given for a Solatube® system with HTLGs 1.82 m in length. Limit and average values of the luminous flux are obtained during the diurnal peak light periods.

** Light efficiency of the luminaire is accepted to be equal to 0.75.

Without drastically increasing energy consumption, such spaces must be lit by ISs with HTLGs (Fig. 8 and 9). *Solatube*® products are also attractive for sports buildings [3]. An impressive example of this is the wide use of such ISs in the sports hall of the Peking Scientific and Technical University, where judo and taekwondo competitions took during the 2008 Olympics (Fig. 10). As traditional zenith lanterns did not meet the illumination quality requirements, the sports hall was illuminated with the *Solatube*® ISs, which completely resolved the illumination problems in the context of a complex steel roof structure, and transmitting natural light over a distance more than 8 m.

During the last ten years, Solar Open Company as a representative of the *Solatube*® Daylighting Systems technology, installed many *Solatube*® ISs on buildings of different purposes: from private apartment houses to large-scale industrial and public buildings over a huge territory: from St. – Petersburg to Vladivostok and from Moscow to Alma-Ata. This became possible thanks to an active participation of the interested professionals in different places of the post-Soviet territory. At present, *Solatube*® Daylighting Systems technology is presented in this huge territory by the largest distribution network in the world (Fig. 11). Such a managing structure allows the clients to obtain effective information and maintenance services at any place within this region.

The record optical and heat-insulating characteristics of the *Solatube*® ISs with HTLGs offer prospects for their wide use for natural illumination. Undoubtedly, the application of such ISs hails progress in indoor illumination and a development their aesthetic concepts. It is evident that *Solatube*® products will play a notable role in the future of such indoor illumination.

REFERENCES

1. *Aizenberg Yu.B.* Hollow light guides, or light through tubes // Illuminator. 2003, № 4(6)–5(7), pp. 134–141.

Table 3. Comparative optical and heat-insulating characteristics of light-transmitting systems

Structure of light-transmitting system	Luminous transmission coefficient (LTC)	Heat input coefficient (HIC)	LTC/KT ratio
Triple glazed window with a specular film	0.22	0.16	1.38
Triple glazed window, specular coating with a low heat conduction	0.63	0.36	1.75
Double glazed window, glass with a low heat-reflecting ability	0.71	0.49	1.45
Solatube® of *SolaMaster®* series (530 mm)	0.60	0.20	3.0

2. *Kinny L., Mak-Kluny P, Stiles M.* Solar illumination is a new industry //Svetotekhnika. 1999, № 3, pp. 4–9.

3. *Selyanin Yu. N., Remizov A. N., Dobrovolsky A. N.* Solatube® systems of solar illumination. Daylighting Systems in architecture of sports constructions of the third millenium // Construction technologies. 2012, № 3, pp. 80–86.

4. *Bracale J.* Natural illumination of rooms by means of new passive light guide system "Solarspot" // Svetotekhnika. 2005, № 5, pp. 34–42.

5. *Solovyov A. K.* Tubular light guides: their application for natural building illumination and for energy saving // Svetotekhnika. 2011, № 5, pp. 41–47.

6. *Kuznetsov A. L., Oseledets E. Yu., Solovyov A. K., Stolyarov M. B.* Experience of application of hollow tubular light guides for natural illumination in Russia // Svetotekhnika. 2011, № 6, pp. 4–11.

7. URL: http://lightway.iricond.ru (Addressing date: 05.09.2015).

8. *Jenkins D., Munir T.* Characteristics of light guides and of light openings used in the systems of natural illumination // Svetotekhnika. 2003, № 6, pp. 34–38.

9. *Aizenberg J. B.* Hollow Light Guides. Moscow: Znack Publishing House, 2009, 208 p.

10. *Kinny L., Mak-Kluny P, Stiles M.* Solar illumination is a new industry //Svetotekhnika. 1999, № 3, pp. 4–9.

11. Answers to article notes // Svetotekhnika.1999, № 4, pp. 28–29.

Alexander T. Ovcharov,
Doctor of Engineering, Professor, graduated from the Tomsk Institute of Radio Electronics and Electronic Facilities in 1966. At present, he is Professor of the Chair "Architectural designing" of the Tomsk's State Architectural-Building University, the Director of Light systems Open Company, full member of the MANEB, associate editor of the Light and Engineering (Svetotekhnika) journal

Jury N. Selyanin,
an engineer, graduated from the Taganrog's Radio Engineering Institute in 1973, the Military academy of F.E. Dzerzhinsky in 1981 and its graduate military course in 1992. At present, he is the General Director of Solar Open Company, the official distributor of the Solatube® Daylighting Systems technology in the territory of the Russian Federation, Belarus and Kazakhstan

STUDIES AND EXPERIMENTS FOR DETERMINATION OF DEGRADATION OF PAINTINGS IN MUSEUM ART GALLERIES CAUSED BY ARTIFICIAL LIGHT SOURCES

Rajesh Sarkar and Saswati Mazumdar

School of Illumination Science, Engineering and Design, Jadavpur University, Kolkata, India
E-mail: saswati.mazumdar@gmail.com

ABSTRACT

Light displays a vital role in the exhibition environment especially in Art gallery. The exhibits' colour details cannot be realized without light. Both natural light and artificial light affect the exhibits, it reduces the strength of the paint and material, causes the fading of paper and paint colour, this damage cannot be recovered. So, the relationship between the exhibits protection and the art visual became one of the core issues of Art gallery design research. Museums and art galleries collect, preserve, and display historical /cultural artefacts and various achievements of historical days. Effective exhibit lighting must balance with exhibition and observation and museums visual lighting effects. This should be done by providing lighting levels as per standard as well as keeping the IR (infrared) and UV (ultraviolet) components of light sources minimum. There are different types of light sources (i.e. fluorescent, halogen and incandescent lamps) with IR and / or UV components, and those sources are being used for many years. Now in present days, there is tremendous development in lighting industries (i.e. lighting sources, lighting design etc.). Recently, solid state light sources (i.e. LEDs and OLEDs) are being developed and they have less power consumption and contains no IR range and minimum UV interval of radiation. So in modern art galleries, low wattage highly efficient LEDs are being used to minimize the fading effect on painting. It should be remembered that till now the inefficient halogen sources have best colour rendering property. The experimental work described in this paper reveals that colour rendering of a painting is different under different light sources, it is true but the colour fading of the painting fades very much slow when LEDs are being used.

Keywords: artificial light sources, degradation of museum paintings, infrared radiation −IR, ultraviolet radiation − UV, LEDs, photochemical and heat degradation

1. STUDIES

Museum is a non-profit making, permanent institution in the service of society and of its development, and open to the public, which acquires, conserves, researches, communicates and exhibits for purposes of study, education and enjoyment, material evidence of people and their environment. A museum is an institution that cares for (conserves) a collection of artefacts and other objects of scientific, artistic, cultural, or historical importance and makes them available for public viewing through exhibits that may be permanent or temporary. Different categories of museum are found i.e. fine arts, crafts, archaeology, anthropology, biography, history, science & technology etc. Lighting design should be based on the type of museum. A crucial restriction on illuminance levels for painting is more important because the materials are easily degraded by UV and IR exposure. It is necessary to use illumination with minimal or no UV at levels beneath a visible light threshold

considered safe for the media on display. Insufficient and unfocused lighting can make a museum un-presentable to its visitors. Many museums have been visited by the researcher in the State of West Bengal (e.g. Indian Museum, Gandhi Museum, Birla Museum, Bengal State Museum, Asutosh Museum of Indian Art) of India. In all those museums, Fluorescent Tube lamps (FTL, CFL etc.) and Halogen lamps (PAR, MR16 etc.) are being used mostly for Art galleries. Those museums are well maintained. But in-spite of that, the paintings have been faded. So, this study was made to analyse the degradation of the paintings by effect of different light sources [12, 13, 17].

The typical damage consists of:

1) Fading (Photochemical Degradation of the surface).

2) Degradation and cracking of paint and bindings (Heat damage caused by continuous heating)

The typical damage depends on:
- **Irradiation time**
- **Temperature**
- **Ultra-Violet Radiation**

Irradiation time: It is the length of time an object is exposed to irradiation. Irradiation is the product of irradiance and the length of exposure to it. The higher the irradiance and longer the exposure, the greater the potential risk [7, 10].

Temperature:

Paintings are essentially layered objects, built up from canvas, ground layer, paint layers and varnish layers. The layers contain materials that have differing physical characteristics including the rate, at which they expand and contract at varying temperatures, and the rate, at which they take up moisture from the surrounding air. A constant climate is, therefore, the ideal situation for keeping works of art stable. Changes of temperature will change the molecular damage of painting [3, 7, 10].

Ultra-Violet Radiation:

Ultraviolet radiation components (UVA, UVB & UVC) are very much damaging and must be eliminated by using UV absorbent filter. Daylight, fluorescent lamps, and halogen lamps emit high level of UV. UV level of efficiency over 70µW/lm are considered excessive for light sensitive objects. UV filtered screen are used in the following ways:

Table1. Different light sources used for experiment

Types of light sources	Wattage, W	Maker's name
CFL	15	Photonix
HALOGEN MIRCHI	60	Photonix
HALOGEN MR16	60	Photonix
UV LED with Phosphor	5	Photonix
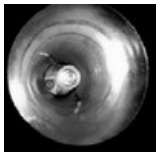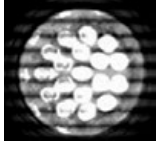
1. Laminated glass UV filter;
2. Acrylic/polycarbonate sheet;
3. UV absorbent varnish used in windows or display glass;
4. Polyester film used in windows or display glass.

The damaging effect of UV radiation on the museum can be eliminated using modern technology [9, 10, 12, 19].

2. EXPERIMENT

To analyse the damaging effect on art painting, different types of artificial light sources have been used for case study. Sources available in Kolkata Market such as CFL 15W, HALOGEN MIRCHI 60W and HALOGEN MR16 60W, Ultraviolet LED5W, coated with Phosphor, were taken. All the lamps were warm white in colour. At the time of experiment, no other types of LEDs were available in the Indian market. Different types of light sources used for experiment are shown in Ta-
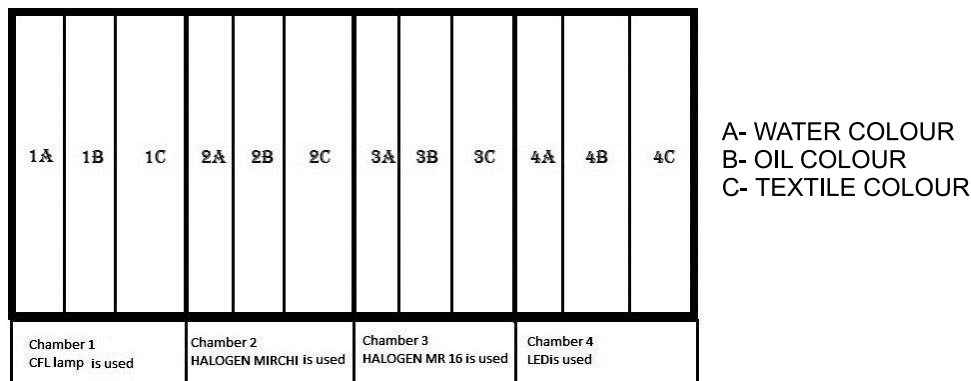
Fig. 1. Schematic diagram for experimental chamber

ble 1. Each lamp type has its own average intensity distribution property, i.e. CFL or HALOGEN MIRCHI, or HALOGEN MR16, or UV LED throws light in different beam angles.

2.1. Set-up Description

In Illumination Engineering laboratory of Electrical Engineering Department of Jadavpur University, four isolated chambers (not air-tight) had been made as models of museum showcases. In each chamber, there are provisions of three painting to be displayed and illuminated by a single artificial light source. Three types of paintings were exactly same coloured oil, textile and water colour paintings fixed in the wall of each isolated chamber. Distance between the painting and test lamp was made 0.7m. Each of the four chambers consisted from one type of lamps separately. Two track fitting small light sources have been installed in each chamber in the painting gallery model. The small zone of each painting was selected where the light beam was focused and the sensors were placed at that particular zone each time for checking the colour fading.

The schematic diagram is shown in Fig. 1, Chamber-1 stands for CFL light source, Chamber-2 stands for HALOGEN MIRCHI, Chamber-3 stands for HALOGEN MR16 and Chamber-4 stands for phosphor coated UV LED light source.

2.2. Procedure

Each lamp source was connected to specific control gear arrangement to control the light intensity as and when required. The aim was to illuminate all the paintings with fixed lighting level in each chamber. To analyse the effect of a particular light source on a particular painting, other two paintings were covered with white paper and the 100 lx level was fixed at a particular value at a time. This light source had been made ON for 6 hours per day, 5 days in a week (3000lx • h in a week) as per IESNA Hand Book 1987 standard. Then the light source position was changed to illuminate another painting, again other paintings being covered by white paper. This experiment was repeated in all chambers. The chambers were isolated from outside environment.

The illuminated coloured paintings were assumed as diffused coloured sources and its chromaticity co-ordinates and colour temperatures were measured at specific intervals for a long time to watch the change in its colour for its exposure under the specific light source. At starting, Spectral Power Distribution (SPD) of the reflected light from the paintings had been taken by the spectroradiometer, JETI-SPECBOS1200 type. According to the CIE1931 *xyz* colour space, the *x, y* and *u, v* colour coordinates of the painting have also been calculated from SPD measurements by this spectroradiometer.

According to the IESNA, for very sensitive exhibits, yearly 150000lx • h exposure is the limit for museum painting considering 50–75 lx over a day, 8 h per day, 6 days in a week, 300 days in a year being opened. So, per day average light exposure is 500lx • h, it is 3000lx • h per week and 150000 lx • h per year being the limit [1, 5, 13, 18].

For experimental purpose, the focus of the light was made at a fixed zone of each painting and light level was adjusted at 100 lx. The exposure time was being recorded regularly and the limited period of 30000 lx • h cycle (ten weeks exposure time) was chosen for each painting. Throughout the whole

period, all experimental values were analysed and the chamber temperature as well as outside ambient temperatures was recorded by non-contact laser thermometer ZMLT-550 type.

For the four chambers, lighting exposures on the painting, say "1A", was taken initially (keeping other paintings covered) by spectroradiometer instrument. After completion of every 3000lx • h, measurements were taken by spectroradiometer in each chamber until 30000lx • h was completed. A measurement data log was made for calculation purpose. The aging of lamps did not exceed 70% of rated burning hours otherwise lamp properties will be changed. The same procedure was repeated for painting "1B" and "1C". These were repeated for all other paintings in other chambers, e.g., 2A, 2B, 2C, 3A, 3B, 3C, 4A, 4B and 4C respectively.

Everyday temperature was measured in every chamber with respect to the ambient temperature. At the time of starting, the first readings were recorded. The sensor of the instrument was kept in the chamber when light was ON and measurement was taken after each 1 hour interval. Readings of temperature (°C) were noted at different places of the chamber and finally the average temperature was taken for that day.

2.3. Data Log On-Off Table Contents of the On-Off Log Table:

1. Date and time of the exposure of the four test lamps on each painting mentioned separately.

2. Total effective operating time (burning hours of test lamps) precisely maintained and mentioned in every day.

3. Total burning hours for each of the lamp in every day and throughout the entire time span (April, 2013 – January, 2014).

4. All the data have been noted after completion of every 3000lx • h exposure.

5. After completion of the 30, 000lx • h exposure on the water colour painting are changes from initial condition were observed.

2.4. Experimental Result

As per IESNA recommendation, total operating exposure will be 150000lx • h per year, but due to shortage of time span and other constraints, the experimental time of this project work reduced of April 2013 to January 2014. Only water colour

Table 2. Standard value temperature as per British Museum [3, 7, 10]

Type of Object	Degrees in Farenheit
Furniture	
Paintings and Paper	68 - 72°
Textiles	
Objects	

painting data exposed over one complete cycle (30000lx • h) in the span of April 2013 to January 2014 has been given here. To analyse the quality change all the measuring data reported here has been taken with respect to the water colour painting.

Following measuring data are given below:-
• Temperature of the chamber;
• Correlated Colour Temperature(CCT) of light reflected from painting;
• Chromaticity coordinates data (*x, y)/(u, v*) of the point where light was focused.

Temperature of the chamber:

It has already been discussed that painting is very much sensitive to temperature. In Table 2, it is shown that the accepted museum standard temperature is in the range of 20 °C ± 1 °C or 68 °F-72 °F for keeping the damage control of paintings. Changes of temperature will change the molecular damage of the painting. If the temperature is increased above the range then rate of change of damage of painting will also increase.

It is analysed by the experiment how the temperature of the chamber is responsible for damage of painting.

Sample data of temperature of the chamber taken during experiment is shown in a Table 3 from Nov. 2013 to Jan. 2014.

From Table 3 and Fig. 2, we found that chamber-4 with UV LED source ON had minimum temperature variation than the other light sources during the experiment. As per Table 2, temperature of the chamber with UV LED source is very nearer to the recommended value. All the sources radiate heat from front portion of the light sources but LEDs do not radiate heat. So, LEDs are preferred for painting lighting. Heat emits from back of the LED luminaires, but that does not affect the paintings too much.

Table 3. Temperature table

Temperature Measurement at Winter Session(Nov.-Feb)									
	AMBIENT ATMOSPHERE	CFL CHAMBER		HALOGEN MIRCHI		HALOGEN MR 16		LED	
DATE	TEMP °C	TEMP °C	Variation of chamber temp. and ambirnt temp.	TEMP °C	Variation of chamber temp. and ambient temp.	TEMP °C	Variation of chamber temp. and ambient temp.	TEMP °C	Variation of chamber temp. and ambient temp.
21-Nov	27.5	26.7	-0.8	28	0.5	27.7	0.2	26.4	-1.1
25-Nov	27.8	26.6	-1.2	28.5	0.7	28.1	0.3	26.3	-1.5
26-Nov	26.3	26.4	0.1	29.5	3.2	28.8	2.5	26.1	-0.2
27-Nov	26.7	27.4	0.7	30	3.3	29.7	3	26.3	-0.4
2-Dec	27.9	27.1	-0.8	29.4	1.5	28.2	1.3	26.8	-1.1
4-Dec	29.3	27.7	-1.6	28.8	-0.3	28.2	-0.9	26.9	-2.4
5-Dec	28.5	26.7	-1.8	29.8	1.3	29.5	1	26.1	-2.4
11-Dec	29	26.8	-2.2	29.4	0.4	29.3	0.3	26.4	-2.6
12-Dec	26.8	25.1	-1.7	28	1.2	27.8	1	24.8	-2
13-Dec	27.5	25.3	-2.2	27.5	0	27.3	0.2	25	-2.5
16-Dec	26.9	25.2	-1.7	27.4	0.5	27	0.1	24.8	-2.1
18-Dec	26.5	24.5	-2	26.5	0	26.9	0.4	24	-2.5
20-Dec	26.4	24.4	-2	28	1.6	27.9	1.5	23.9	-2.5
16-Jan	18.1	20.5	2.4	24	5.9	23.7	5.6	18.7	0.6
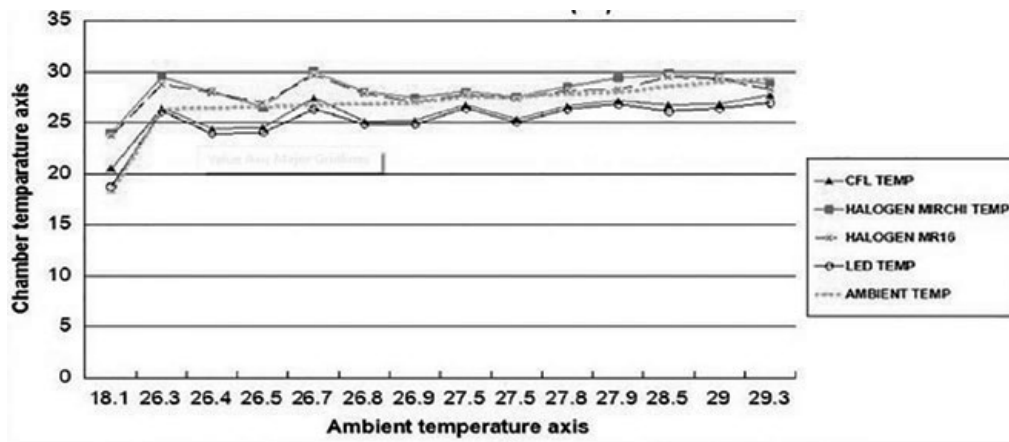
Fig.2. Temperature graph, [°C]

Effect of Ultraviolet Radiation:

Ultraviolet radiation is the most harmful on art or painting gallery, because depth of the penetration is very high by UV radiation. Ultraviolet (UV) light is Electromagnetic Radiation with a wavelength shorter than of visible light. It is in the range between 400nm and 100nm, corresponding to photon energies from 3eV to 12.4eV. Many polymers, textiles, papers, different types of paintings are degraded by UV light. The problem appears as discoloration or fading, cracking, and, sometimes disintegration. In addition, many pigments and dyes absorb UV and change colour, so paintings and textiles may need extra protection both from sunlight and artificial light sources, because they radiate UV. Old and antique paintings (such as water colour paintings) must be placed away from direct sunlight. Common window glass provides some protection by absorbing some of the harmful UV, but valuable artefacts need extra shielding. Many museums place black curtains over water colour paintings and ancient textiles. Since water colours can have very low pigment levels, they need extra protection from UV light. Tinted glasses, such as sunglasses also provide protection from UV rays.

There are different types of UV radiation (Table 4) depending upon their wavelength and energy levels [12].

From Table 4 it is seen that UVC is the most harmful than the other types i.e. UVA and UVB, because wavelength is very short as well as it has very high energy level. So, light sources containing UVC is more harmful and can damage many things.
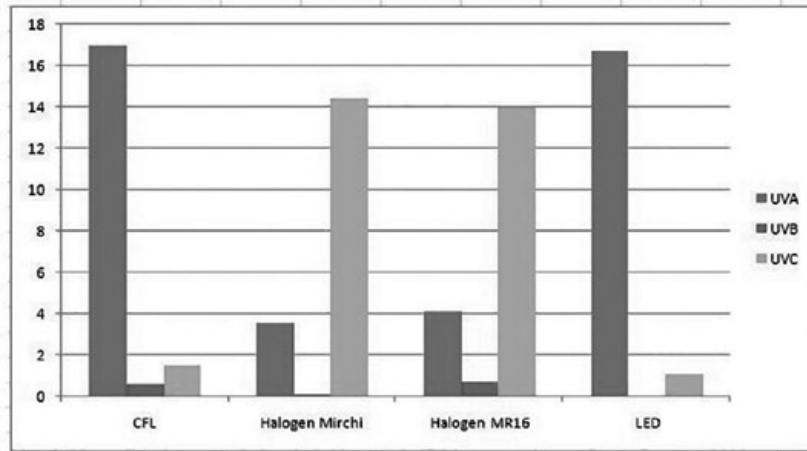
Fig. 3. UV component graphs of different light sources

UV component determination of the Test Light Sources:

There was an arrangement for varying the light output of the source. As our object painting was exposed to 100 lx from each of the source, UV meter sensor was placed to receive that 100 lx from each of the source. UV meter was placed at a distance of 0.7m from the source, this distance corresponds to that of the UV meter sensor was placed in experimental chamber. Data were taken by UV meter, Make- Konica Minolta, Model No. – UM-10 and shown in Table 5 in terms of $\mu W/cm^2$ of UV.

Table 5 depicts UV Components present in different light sources at a particular point of the painting (illumination level 100 lx) from 0.7m used in this experiment and Fig. 3 displays the bar graph representation of the UV components present in the lamp sources.

Our experimental results revealed that halogen and CFL had all the three components of UV. LED has no UVB component but other sources have it little. UVA component was higher in CFL and LED lights than halogen lights. UVC is minimised in LEDs, CFL has little more amount of it and halogen lamps have sufficient UVC component.

Table 4. Types of UV radiation

UV	wavelength	energy
UVA	400 – 315 nm	3.10 – 3.94 eV
UVB	315 – 280 nm	3.94 – 4.43 eV
UVC	280 – 100 nm	4.43 – 12.4 eV

SPD curves of these artificial light sources used in the experiment were taken by the JETI-SPEC-BOS1200 type spectroradiometer (curves not shown here). This instrument cannot show the exact values of UV and IR, but the nature of the curve confirmed the result, which were received by Konica Minolta UM-10 UV meter.

IR component determination of the Test Light Sources:

From the SPD curves, it was found that both of the halogen lamps had maximum IR component, CFL had very little amount of IR and LED lamp had no IR.

Table 5. UV components in different light sources rated at 230V and giving illumination level at 100lx at a particular point of the paintings being measured from 0.7m, [$\mu W/cm^2$]

UV-A,UV-B,UV-C Components in different light sources				
COMPONENTS	CFL	Halogen Mirchi	Halogen MR 16	LED
UV-A(400)	17	3.6	4.1	16.7
UV-B(360)	0.6	0.1	0.7	0
UV-C(250)	1.4	14.4	14	1.1

Table 6. Data of CCT value of reflected light from painting in period of 30000lx • h cycle

DATE	SL. NO.	CFL	HALOGEN MIRCHI	HALOGEN MR16	LED
			CCT VALUES after completion 30,000lx·h		
21-Nov	1	1634	1634	1634	1436
25-Nov	2	1294	1544	1435	1435
26-Nov	3	1419	2300	2300	1445
27-Nov	4	1668	2300	2300	1485
12-Dec	5	1684	2300	2300	1476
13-Dec	6	1688	2300	2300	1475
16-Dec	7	1483	2300	2300	1545
18-Dec	8	1491	2300	2300	1518
20-Dec	9	1545	2331	2336	1576
16-Jan	10	1477	2346	2359	1499

Table7. Chromaticity values of reflected light sources for 30, 000lx • h

DATE	CFL		HALOGEN MIRCHI		HALOGEN MR16		LED	
	X	Y	X	Y	X	Y	X	Y
21-Nov	0.5791	0.3333	0.6529	0.3325	0.652	0.3659	0.5487	0.3419
25-Nov	0.5708	0.3353	0.6504	0.3332	0.64	0.3533	0.5478	0.3408
26-Nov	0.5443	0.3347	0.6505	0.3329	0.6407	0.352	0.5474	0.3422
27-Nov	0.5053	0.3342	0.655	0.3369	0.6405	0.3447	0.5349	0.3371
12-Dec	0.5009	0.3314	0.6495	0.3331	0.6406	0.3422	0.5357	0.3362
13-Dec	0.5039	0.3355	0.6574	0.3294	0.6368	0.3463	0.5411	0.3415
16-Dec	0.5366	0.3382	0.6535	0.3315	0.625	0.3501	0.5277	0.3396
18-Dec	0.5368	0.3398	0.6526	0.3313	0.6203	0.3574	0.5318	0.3364
20-Dec	0.5274	0.3392	0.6486	0.3337	0.6339	0.3477	0.5205	0.3369
16-Jan	0.5404	0.341	0.6348	0.3403	0.621	0.3483	0.5367	0.3412

Correlated Colour Temperature (CCT) of light reflected by painting:

CCT of the reflected light from painting under different light sources was measured. If the CCT of the reflected from painting light is increased, it is understood that the colour of the painting is becoming whiter and fading of the painting has been occurred. By the experimental results, how the light sources changed the colour of the painting that was being observed.

The sample data of CCT values of reflected light from water colour painting illuminated by different light source are shown in Table 6.
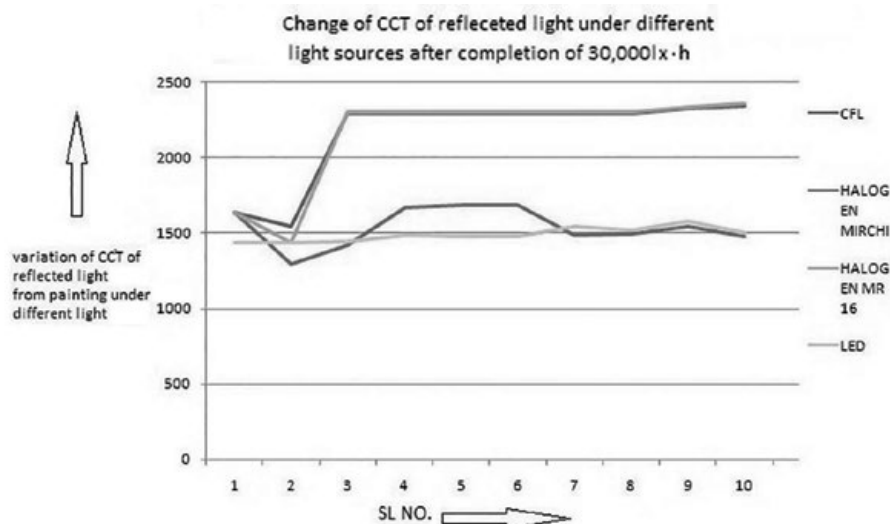
Fig.4. Graph of CCT value up to 30, 000lx•h of reflected light from water colour painting

Table 8. Change of Chromaticity Coordinate of painting under different light sources

Painting under different light sources	Initial Value of Chromaticity Coordinate (x, y)	Final Value of Chromaticity Coordinate (x, y)	Change of Initial to final value of Chromaticity Coordinate (x, y)	Remarks
CFL	x = 0.5791 y = 0.3333	x = 0.5404 y = 0.341	dx = 0.0387 dy = 0.0077	Change of Chromaticity Coordinate (x, y) from initial value to final value is very minimum of painting under UVLED with Phosphor coated light source. So the change of colour of painting under LED source also minimum.
Halogen Mirchi	x = 0.6529 y = 0.3325	x = 0.6348 y = 0.3403	dx = 0.0181 dy = 0.0078	
Halogen MR16	x = 0.652 y = 0.3659	x = 0.621 y = 0.3483	dx = 0.031 dy = 0.0176	
UVLED with Phosphor coated	x = 0.5487 y = 0.3419	x = 0.5367 y = 0.3412	***dx = 0.012*** ***dy = 0.0007***	

Change in Chromaticity of reflected light from painting under CFL Light Source

Chromaticity Graph using CFL Source after completion 30,000 lx · h
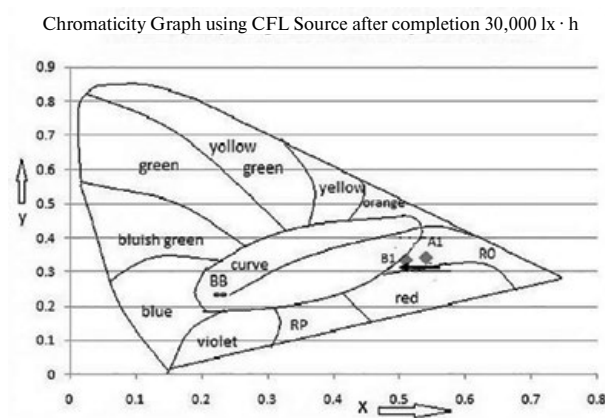
Fig. 5. Change of colour of painting by using CFL light source

Change in Chromaticity of reflected light from painting under HALOGEN MIRCHI Light Source

Chromaticity Graph using Halogen Mirchi after completion 30,000 lx · h
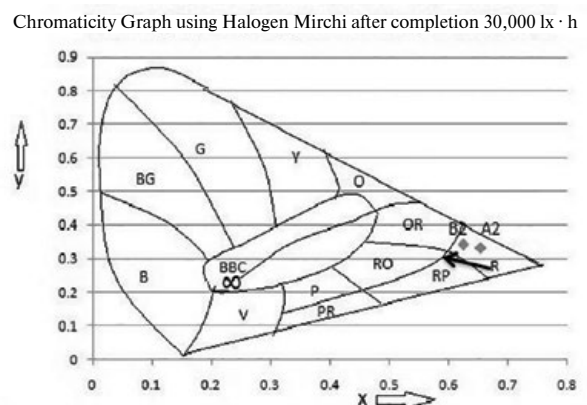
Fig. 6. Change of colour of painting by using Halogen Mirchi light source

Fig.4 shows the initial CCT values of the particular painting illuminated by different lamps and its change after 30 000lx • h. It is clear from Fig. 4 that the CCT effect remains nearly constant when the LED is used, but the initial CCT value is different from other sources; i.e. colour rendering is poorest for this source. For CFL, CCT value oscillated first and finally it was almost same as was found for LED lights. For HALOGEN MIRCHI and HALOGEN MR-16, there was steep rise in the CCT value of reflected light which means considerable change in colour of the painting occurred during this 30000lx • h cycle. So, these two sources should not be recommended for water colour painting lighting. The reflected light from paintings show higher CCT, i.e. the colour becomes whiter which proves more fading of the paintings when Halogen sources are used.

Chromaticity:

The experimental values of chromaticity co-ordinates on the water colour paintings, which were taken in different time span is given in Table 7. Chromaticity diagrams in Figs. .5–8 show the initial and final colour coordinates of the reflected light from the specific zone of the paintings, where the light beam was focused in experiment. Chromaticity *(x, y)* values of the light reflected by the painting have been taken for 30, 000lx • h. So, it determines the colour changes of the painting from initial exposure to final exposure (i.e. 30000lx • h) for each light source. For the same colour, the first reading under different sources show different co-ordinates for the same coloured painting. So, it is clear that colour rendering is different for exposure under different sources.

Change in Chromaticity of reflected light from painting under HALOGEN MR16 Light Source

Chromaticity Graph using Halogen MR16 after completion 30,000 lx · h
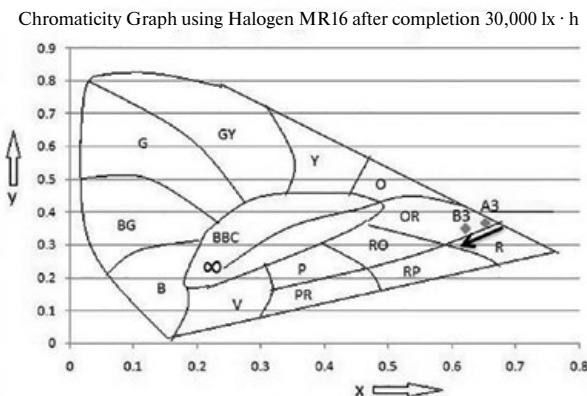
Fig. 7. Change of colour of painting by using Halogen MR16 light sources

Change in Chromaticity of reflected light from painting under LED Light Source

Chromaticity Graph using LED source after completion 30,000 lx · h
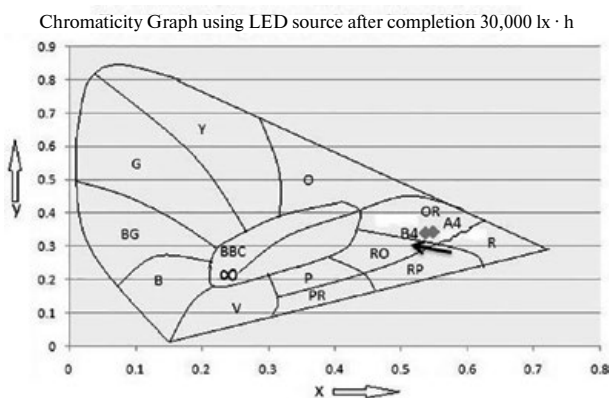
Fig. 8. Change of colour of painting by using phosphor coated UV LED light source
G-green, Y-yellow, B-blue, R-red, PR-pinkish red, RP- reddish pink, BG-bluish green, YO-yellowish orange, OR- orange-red, BBC-black-body curve, ∞-infinite

In CFL chamber, red water colour painting was exposed with 30, 000lx • h. Initially, chromaticity of the reflected light was found at position A1 on the red region, which is shown in the chromaticity graph of Fig. 5. Increasing the exposure limit up to 30, 000lx • h, the colour was found shifted from red to nearer to pink colour at position B1.

In Halogen (i.e. MIRCHI & MR16 both) chambers, red water colour painting was exposed for the same time. Initially chromaticity of the reflected light from the focused zone of the painting was found at position A2 and A3 on the red region which is shown in the chromaticity graph of Fig. 6 and Fig. 7. With increasing the exposure limit up to 30, 000lx • h, the colour was shifted more from

UV Components of Phosphor Based Blue LED
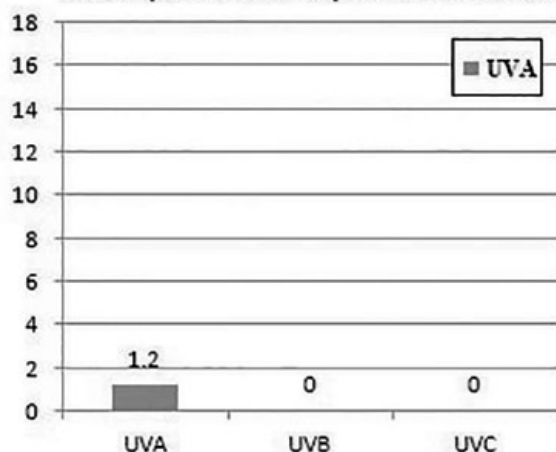
Fig-9 UV components of new phosphor based LED

red to nearer to bright pink colour at B2 and B3 respectively as shown in Fig. 6 (MIRCHI chromaticity graph) and Fig. 7 (MR16 chromaticity graph); so it is observed that the painting has been faded sufficiently.

In Phosphor coated UV LED light chamber, red water colour painting was again exposed with 30, 000lx • h,. Again, initially chromaticity of the reflected light was found at A4 on red region, which is shown in the chromaticity graph of Fig. 8. Increasing the exposure limit up to 30, 000lx • h, it was observed that the point shifted to B4. The change of chromaticity (at B4) was minimal for UV LED chamber in comparison with other light sources as found in Fig. 8. So, colour shifting of painting or fading occurs at very slow rate when LED sources are used.

From Table 8, it is understood that when LED light source is used, less colour fading occurs than with other light sources.

3. CONCLUSION

To obtain 100 lx at a particular point of the paintings, the power characteristics for all four types of lamps are measured. It was found that CFL consumed 15W, HALOGEN MIRCHI consumed 60W, HALOGEN MR16 consumed 60W and the phosphor coated UV LED consumed 5W. So, from energy efficiency point of view also LED was found best.

From the experimental data of various parameters already discussed e.g. Temperature, UV radiation, Correlated Colour Temperature (CCT), Chromaticity Coordinates data etc., the damaging

Table 9. UV components of new phosphor based LED, [µW/cm²]

UV-A(400nm)	UV-B(360nm)	UV–C(250nm)
1.2	0	0

of paintings have been explained, and it has been understood that different artificial light sources play a great role in the damage.

From the above discussion by thorough analysis of experimental data, it is found that the LED light sources are most efficient and minimum harmful than any other light sources for museum lighting design particularly for painting/textile galleries.

When the experiment was running, only ordinary UVLED (Phosphor Coated) was available in India. At that time, it was observed from previous data that used LED source had sufficient UVA component. Nova days Phosphor coated Blue LED is available in Indian market. Those types of LEDs have been purchased recently and it is tested by the same UV meter. The experimental value of UV components of new phosphor based Blue LED are given in Table 9.

Now it is found that there is very little component of UVA presented in it but there was no trace of UVB and UVC as shown in Table 9 and Fig. 9. It is also concluded that the same experiment should be repeated with this type of LEDs (Phosphor based Blue LED**).** If this new LEDs with better colour qualities, i.e. better SPD curves, better colour rendering properties, minimum UV and IR components are used for all types of paintings in museums, well protection of the paintings will be ensured in future .

REFERENCES

1. ANSI/ASHRAE/IESNA Standard 90.1.2007.

2. CIE52−1982: Calculations for Interior Lighting-Applied Method.

3. Design Guidelines, The British Museum, May 2012.

4. Energy Conservation Building Code-2011.

5. *Frost, M.* "Preserving Collections in Exhibitions." In *The Manual of Museum Exhibitions*, edited by B. Lord & G.D. Lord. Walnut Creek, CA: AltaMira Press, 2002.

6. Indian Standard: IS3646(Part I): 1992.

7. Timothy Ambrose, Crispin Paine. Museum Basic.

8. *Kevan Shaw and Malcolm Innes* "Museum and Gallery Lighting", October 27, 1993, revised June 1995.

9. NPS, Museum Handbook, Part I, 1999.

10. *Mary Claire Frazier* "Optimizing of Museum Lighting", Published in LD+A Magazine, September 2008.

11. Philips Lighting Handbook.

12. The Degradation of Coating by Ultraviolet Radiation, Clive H. Hare, Editor, Materials Technology Section, Journal of Protective Coating and Paint.

13. *Gary Thompson* "The Museum Environment", London, 1978.

14. http://apps1.eere.energy.gov/buildings/publications/pdfs/ssl/colour_rendering_index.pdf.

15. http://apps1.eere.energy.gov/buildings/publications/pdfs/ssl/arik_luminaire_raleigh2010.pdf.

16. http://apps1.eere.energy.gov/buildings/publications/pdfs/ssl/ns/rosenfeld_art_sandiego2011.pdf.

17. http://www.getty.edu/conservation/publications_resources/newsletters/19_1/news_in_cons1.html.

18. http://www.nouvir.com/pdfs/MuseumLighting.pdf.

19. http://www.philamuseum.org/conservation/10.html?page=3.

Rajesh Sarkar, Post Graduated (M. Tech.) in Illumination Engineering & Technology from Jadavpur University in 2014. He has more than 1 year experience in Teaching as an Assistant Professor in Electrical Engineering Department of Abacus Institute of Engineering & Management

Saswati Mazumdar, M.E., Ph.D., Professor of Electrical Engineering, and Director of School of Illumination Science, Engineering & Design in Jadavpur University, Kolkata, India. She has 26 years of experience in Lighting Research and Teaching and developed a modernized Illumination Engineering laboratory in Electrical Engineering Department of Jadavpur University. She has founded a Masters' Course on Illumination Engineering in J.U., executed a large no. of R&D and Consultancy Projects on Illumination and allied fields

RESEARCH INTO THE INFLUENCE OF LIGHT-MUSIC PERFORMANCES ON PSYCHOPHYSIOLOGICAL STATES

Nikolai V. Matveev[1], Victor T. Prokopenko[1], Natalia P. Sapunova[1*], and Daniil A. Fridman[2]

[1]The St.-Petersburg ITMO UNIVERSITY
[2] Lux Aeterna Theatre, St.-Petersburg
E-mail: modernns@yandex.ru

ABSTRACT

Each person in the modern world deals with a multitude of stimuli and stressors: the rhythms of urban life, stressful situations at work, difficulties in home life, domestic issues and many other things. The practice of targeted exposure of the audiovisual system to sensations can provide a possibility of using optoelectronic facilities for drug-free therapy, which improves psychological and emotional states, qualitatively raising living standards.

Keywords: colouristic, psychophysiology of spectator perception, sound design, colour design, light therapy, sound therapy

The research carried out in the period 2009–2012 within the «*IOSHA*» (*Improving Occupational Safety and Health Awareness of Employers and Employees in CEE*) project, showed that workplace illness accounts for 167,000 deaths annually in Europe. The primary factor (35.4%) is stress (23 million EU citizens annually need urgent treatment for workplace stress related issues); economic losses amount to 4% of Gross Domestic Product, or more than €500 billion. However, only 9.3% employers actively address rehabilitation, and 20.3% intend to introduce new initiatives [1]. An ideal method of relaxation is natural audiovisual stimulation. It has been shown that the spectral compositions of natural sounds (noise of waterfalls, birdsong, fire crackling, etc.) are similar to brain rhythms in a normal state. However, it is often difficult to obtain such stimulation in a big city environment. As a result, variuos methods and facilities of audiovisual stimulation are actively being developed, which can be applied both independently, and as part of the healthcare system.

Ideas around colour-music – the interaction of light, sound and music, were first developed by A.N. Skryabin in the 19th century. However, since then ideas about the synaptic connection between sound and colour have not been comprehensively explored, in a way which would imply potential abilities of joining art and modern facilities [2].

Colours and sounds create changes in the work of the brain, stimulating its activity and influencing the main feeling systems through hearing and sight. This raises questions about the level if interconnectedness and interaction between the sense organs, or more widely concerning interactions of eisodic systems [3]. Colours and sounds can be a terrible force as well, which is capable of harm; they can be a powerful weapon against a human body. Simultaneous exposure to sound and light is desirable, because it would allow implementing abilities of the light psychophysiological resonance strengthening music effect (or on the contrary, light effect) [4]. This creates a surprising sensation experienced by participants of a Sound and Light performance [5]. Moreover, recent research has shown that light therapy effectively deals with certain frustrations of mood, circadian rhythms and of sleep. [6]

Using different exposure types and methods, a resonance can be caused with different systems

or parts of our body. It is possible to activate both physiological (system) and emotional responses directly connected with the exposed area.

This research investigated the influence of fragments of a light-music performance by *Lux Aeterna* Theatre on the psychophysiological state of a person. The research was carried out at the St.-Petersburg National Research University of Information Technology, Mechanics and Optics (ITMO University).

Light images of the *Lux Aeterna* performance are formed as laser radiation passes through phase-amplitude transparencies (or when it is reflecting from them). The transparencies can be plastic or glass surfaces, optical elements (including those with defects), films and liquids. Abstract images are mainly as a result of radiation diffraction on non-uniformities of a transparency and represent interference pictures. One can add dynamics to the images using different methods. As light sources in the experiments, two semiconductor lasers and one solid-state laser with diode pumping at wavelengths of 445, 650 and 532 nm respectively were used.

The experimental method consisted of a sequential presentation of a test task to the test subject and in the exposure on the test subject to two different types of sound-colour content. As a test task, the respondents were set the Ring of Landolt test, in which the persons under test were offered to find and specify in the test table, rings of a certain type. The type of the rings was set in a random way.

The test results were analysed by speed and accuracy, from which an *efficiency indicator* was deduced. After the test was completed, the participant underwent a session of colour-sound exposure.

The experimental installation was a prototype relaxation office, in which a hemisphere with base diameter of 3 m was used as a screen.

In Fig. 1, a participant is shown sitting in a comfortable armchair in a semi-reclined position during a session of the colour-sound exposure.

The participants were 32 adults, both women, and men, 21 to 34 aged.

The action sequence of the experiment was as follows:

1. Participants were tested four consecutive times (to exclude the proficiency effect).

2. A session of the colour-sound exposure of the first type took place.

Fig. 1. A session of colour-sound exposure

3. Participants were tested again four consecutive times.

4. A session of the colour-sound exposure of the second type took place.

5. Finally, the participants were tested four consecutive times again.

The content of the two types of colour-sound exposure were chosen for the participants. The contents differed both by visual, and by sound stimuli. The content of the first type comprised a visual-sound track combining interaction of a sound track with a pleasant quiet melody and of three colours: green, dark blue and red. The content of the second type comprised a combination of the sound track, which was distinct from the first but similar in the essence, however this content contained one colour only: dark blue.

It should be noted that the contents of the sound-colour exposure did not just have different colour-music characteristics but also different directions of exposure. In particular, the first type of content aimed to arouse the participants emotionally, to raise their psycho-emotional and physical tone, to inspire a state of vivacity and vitality, and to provide as a whole, an effect of a "resurgence", which should influence an increase in the working capacity level. The second type of content, on the contrary aimed to calm and relax the participants, to immerse them in a state of inner rest similar to meditation.

The group as a whole, as well as gender subgroups, showed a gain in the efficiency indicator for 75% of participants. This means that exposure to the first type of content accomplishes its target function: increased working capacity. A positive effect of directed exposure to the second type of colour-music was also observed. In this latter case,
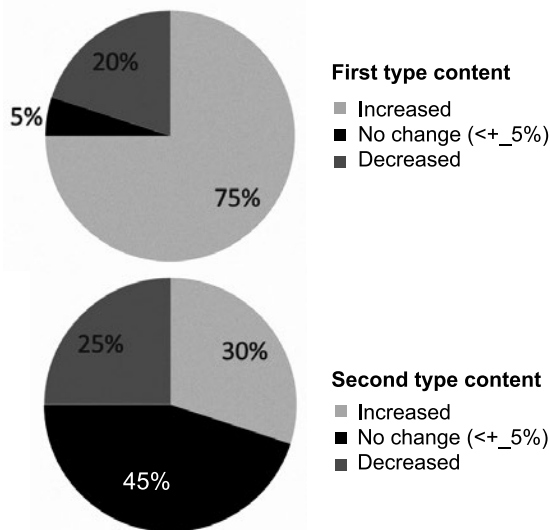
*Fig. 2. Change in the efficiency indicator after exposure
of the first type and of the second type contents*

the positive impact is confirmed by a decrease of the observed growth in the efficiency indicator of up to 30% and by an increase in the "efficiency decrease" indicator by no less than 25%. This is evidence of a decrease in the attention concentration level as a result of the relaxing effect of the second type content. General results of the change in the efficiency indicator are given in Fig. 2.

The performed research has provided evidence of a positive effect on the experiment participants, which also suggests the possibility of targeted application of this type of colour-music exposure as an effective instrument of influence on psycho-emotional, functional and other vital states.

Content developed in a specific way can both raise working capacity (content of the first type), and relax a person (content of the second type).

ACKNOWLEDGMENT

REFERENCES

1. IOSHA Survey Report. URL: http://www.iosha.eu/upload_files/IOSHA_survey_report_final.pdf (Addressing date: 15.06.2015).

2. *Sapunova N.P.* Music and light – back to the future // A collection of theses of reports of Scientific-and-practical conference "Light design – 2014". SPb, 2014, p. 44.

3. *Kravkov S.V.* Interaction of sense organs. Moscow – Leningrad.: Academy of Sciences of the USSR, 1948, 117 p.

4. *Yuryev F.I.* Light music. Kiev: Muzichna Ukraina, 1971, 98 p.

5. *Galeyev B.M.* Performances "Sound and Light" in the system of arts // Materials of the third conference on the Light and Music problem. Kazan: Prometei SDB, 1975, pp. 191–194.

6. *Breinard D.K., Khanifin D.P.* Use of light energy: from photons to human health // Svetotekhnika, 2014, № 4, pp. 18–22.

Nikolai V. Matveev,
Ph.D. Graduated from the St.-Petersburg National Research University of Information Technology, Mechanics and Optics with a degree in Technical Physics. A senior lecturer of the Chair "Light technologies and optoelectronics" of the ITMO University

Victor T. Prokopenko,
Doctor of Engineering, graduated from the St.-Petersburg State Electrotechnical University "LETI of V.I. Ulyanov (Lenin)" with a degree in "Dielectrics and semiconductors". At present, he is the Head of the Chair "Light Technologies and Optoelectronics" of the ITMO University, the Honoured Science Worker of the Russian Federation

Natalia P. Sapunova,
a musician and engineer, graduated from the department of arts of the St.-Petersburg University of Culture and Arts as well as from magistracy of the St.-Petersburg National Research University Information Technology, Mechanics and Optics with a degree in "Technical physics". At present, she is an engineer of the Chair "Light Technologies and Optoelectronics" of the ITMO University, the soloist of the State Academic Russian orchestra of V.V. Andreev

Daniil A. Fridman,
an historian and engineer, graduated from the Historical department (with a degree in "History of arts") and from the Polytechnic department (with a degree in "Electronic technology") of the Uzhgorod University. At present he is the artistic director and director of the Lux Aeterna theatre

HOW LED LIGHTING MAY AFFECT OFFICE ERGONOMICS: THE IMPACT OF PROVIDING ACCESS TO CONTINUOUS DIMMING CONTROLS ON TYPING AND COLOUR-MATCHING TASKS PERFORMANCE

Hongyi Cai and Linjie Li

Department of Civil, Environmental and Architectural Engineering, University of Kansas, USA.
E-mail: hycai@ku.edu

ABSTRACT

This study investigated the impact of providing young office workers individual access to continuous dimming controls of LED lighting on their performance of typing and colour-matching tasks and the subjective ratings of their task performance. A total of 30 young people participated. It was found that under the tested specific LED lighting providing access to continuous dimming controls didn't affect the participants' typing task performance and their subjective ratings of typing task difficulty, and satisfaction of their typing task performance. However, the participants' colour matching performance became worsen due to the perceived slight difference of CCT. Nonetheless, the perceived difficulty of the colour matching tasks and the subjective satisfaction of the colour matching task performance were not changed. The young participants' rating of the office lighting quality (e.g., brightness, uniformity, glare, CCT, CRI, flickering, noise) in the test room was also not affected.

Keywords: LED lighting, office ergonomics, lighting controls, typing task, colour matching

1. BACKGROUND

High quality lighting plays a critical role in office ergonomics. It is expected that LEDs will be predominant in future offices for illumination. Can LEDs increase the lighting quality in modern offices? Is there a perceived impact on colour perception, visual fatigue, glare, and office staff job satisfaction? Common office lighting, unless it was very good or very poor, had little influence on occupants' subjective feeling of the office environment [1]. Different lighting conditions had no effect on the sustained performance of cognitive tasks or on the mood and alertness of the participants [2–5]. However, these discoveries obtained under fluorescent lights may not continue to hold for LEDs. It is not yet proven that LED lighting can more easily improve the office lighting quality than fluorescent lighting. In fact, if misarranged, LED lights can cause problems as well since LEDs are tiny but very bright, like glare to office workers and extra high light levels on work surfaces. In the literature, several studies [6–10] did explore the effect of LED lighting on ergonomics, but not tested in office environments. It is still unclear about the ergonomic implications of LED lighting technologies in modern offices. The answers lie on a comprehensive investigation of all factors of lighting quality and their impact on office ergonomics, which is overwhelming. To narrow down the scope, this study focused on the role of access to continuous dimming controls of LED lighting in office ergonomics.

Providing office workers individual access to continuous dimming of LED lights will be common in future offices for the benefit of energy saving and individual needs [11]. In general, individual lighting control was highly desirable and

had significant effect on occupants' mood and job satisfaction [2, 4, 5, 12−16]. However, there was no proven effect of lighting control on office task performance, like typing and colour perception [13−16]. In fact, dimming light sources may change their colour rendering performance. That results in false colour perception. The saturation of colours gradually decreased as the adapting light intensity was lowered [17], while coloured objects' hues also shifted with changes in luminance under different light levels [18]. It was found that lower illuminance level and lower CCT (correlated colour temperature) could encourage participants' performance with higher self-set goals [19], while high CCT fluorescent lights could improve occupants' well-being and productivity in the corporate setting [20]. Unfortunately, most of those studies on individual lighting controls dealt with fluorescent lights, not LEDs. Continuous dimming over a wide range of light output, which is widely deployed in LED technologies, was seldom examined in previous studies.

What ergonomic benefits that office workers may gain when they are granted access to continuous dimming of LED lights have not been studied till Ono et al. [21]. However, Ono et al. did not study typical office tasks, like reading, typing, colour matching, etc. Thus, it is still not clear about the impact of granted access to continuous dimming of LED lighting on office workers' typing and colour-matching task performance, and their subjective rating of the lighting quality and task satisfaction. This study was aimed to address this topic.

2. EXPERIMENT

First, a survey of the luminous environments in 32 offices was conducted, including 21 offices at the University of Kansas and 11 offices disclosed in recent studies concerning lighting and office ergonomics [4, 5, 13, 14, 20, 22−24]. This survey was used to identify the typical lighting conditions and the layout of luminaires in those 32 offices, which were used to design the test conditions under which a null research hypothesis would be tested.

Null Hypothesis: Providing young office workers access to continuous diming of LED lighting in modern offices, including a general lighting system and a task lighting system with the same CRI but slightly different CCT, has no impact on their performance and subjective evaluations of typing and colour-matching tasks on prints and computer screens.

An experiment was then conducted in a windowless office to test the Null hypothesis using 30 young participants (19 female, 11 male) with age of 21.6 ± 3.3 years, eyesight of 20/20 or 20/16, normal colour vision and normal audio acuity. They were recruited on campus of the University of Kansas. Fig. 1 (a) shows the windowless office (2.90 m wide, 3.66 m deep and 2.87 m high) with suspended ceiling. A desk and an adjustable office chair were put in the test office. On the desk there were a Dell 23" LCD display with LED backlight, a keyboard, a mouse, a pair of speakers, and a document holder. A custom-manufactured adjustable chinrest was mounted on the edge of the desk, in front of the chair. As shown in Fig. 1 (b), the chinrest was titled toward the participant at adjustable angle and height to fix the position of his/her head during the experiment. A desktop PC computer was placed under the desk to run office task programs. A camcorder was mounted behind the participants to record the process of the experiments for time logging. Eight points, whose locations are shown in Fig. 1 (c), were selected for photometric measurements (illuminance, CCT) of the luminous environment during the experiment. Points 1−3 were on the desk surface. Point 4 was on the centre of a document holder. Point 5 was on the computer screen. Points 6−8 were on the background walls, 1.22 m above the ground at the eye level of the seated office occupants.

Four ceiling recessed 2' x 2' Cree LED luminaire (model # CR22−20L, CCT = 3500 K, CRI = 90), as shown in Fig. 2 (a), were used for providing general lighting in the test room. The layout of the four fixtures is shown in Fig. 1 (a) (c). In addition, a portable Lite Source floor-standing task light with adjustable arm and shade, as shown in Fig. 2 (b), was selected to supplement the general lighting with an A-19 shaped Philips LED lamp (CCT = 2700 K, CRI = 90, initial light output 940 lm). The shade blocks direct lights from entering the participant's eyes to prevent direct glare. This task light was put on the left side of the desk without producing any veiling reflection on the viewing materials attached on the document holder. This study adopted 2700 K instead of 3500 K for the task light, which reflects the different CCTs used in the surveyed 32 offices, to enable participants to
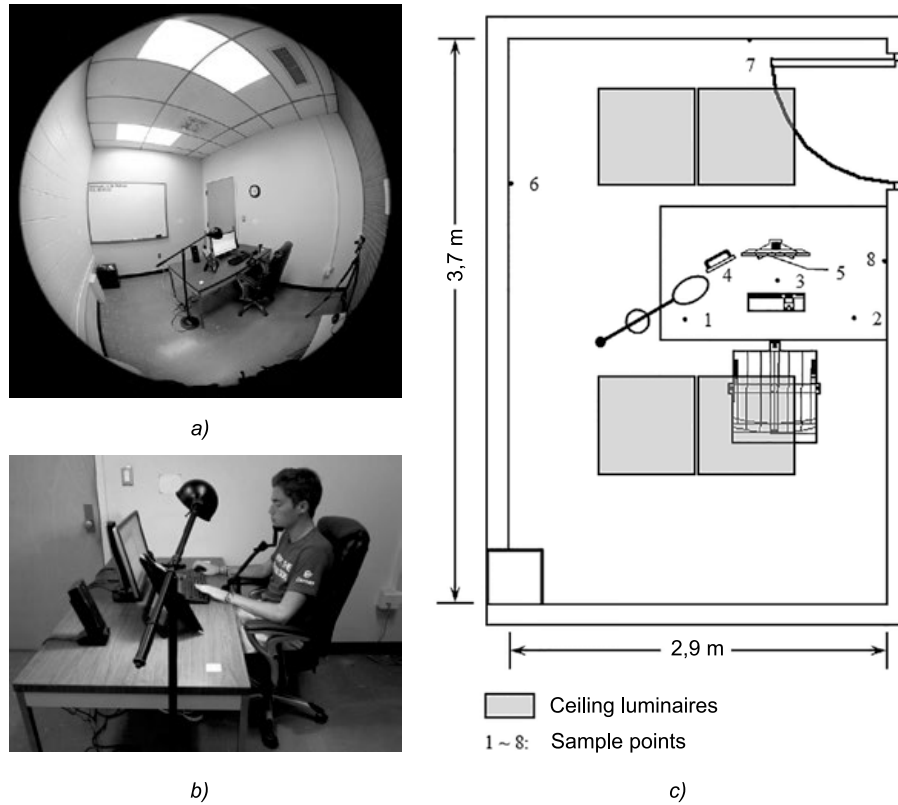
Fig. 1. Experiment setup in the windowless test room, (a) fisheye view of the test room, (b) a participant with his head on the adjustable chinrest, (c) plan view of the test room

adjust the CCT to personal preference via individual controls of both general and task lighting (the CRI of light sources could not be manipulated).

Continuous dimming of the LED lights was tested in this study. A Lutron DIVA wall dimmer (Fig. 2 (c)) was wired to the ceiling-recessed Cree CR22 LED luminaires to provide continuous dimming to 5%. The Lutron DIVA wall dimmer was mounted on the wall next to the desk, as shown in Fig. 1 (a) (b). A Lutron Credenza LED dimmer (Fig. 2 (d)) was also connected to the portable floor-standing task light to provide continuous dimming of the Philips LED lamp. The Lutron Credenza LED dimmer was put on the right side of the desk next to the mouse, where participants had easy access to it.

Throughout the entire experiment, the participants were not aware of the types and technical specifications of the lighting systems. They were also unknown of the real purposes of this study to prevent possible Hawthorne effect, if any, on the experiment results.

A typing task was designed in this study for covering simultaneous reading and typing performance on both paper and computer screen. Partic-
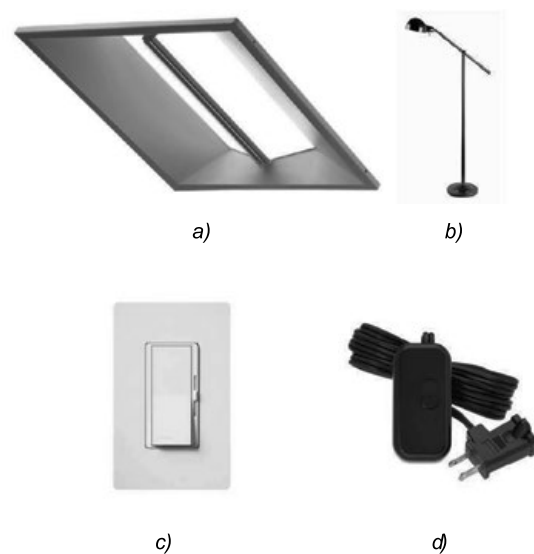
Fig. 2. Lighting fixtures and lighting control devices used in this study, (a) Cree CR22 LED luminaire (model # CR22–20L), (b) Lite Source floor-standing task light fitted with an A-19 shaped Philips LED lamp, (c) Lutron DIVA wall dimmer, (d) Lutron Credenza LED dimmer

ipants were asked to type printed text mounted on the document holder, as shown in Fig. 3 (a), with no time limit. All typing materials were printed black/white in high contrast on letter-sized sheets,

Fig. 3. Typing task, (a) text printed black/white on letter-sized sheets mounted on the document holder, (b) the interface of the NRC Typing Task software
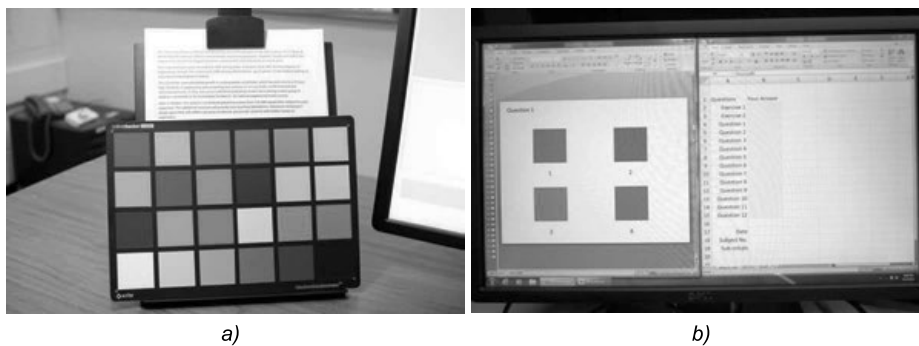
Fig. 4. Colour-matching task, (a) X-rite Classic Macbeth colour checker, (b) the interface of colour matching task showing the four candidate colours on the second PPT slide

with 12 point Calibri font, single spaced. The contents were daily news excerpted from the website of "The University Daily Kansan". To avoid getting practiced on typing the same text, two sets of text were used by each of the 30 participants under the two different test conditions (with/without lighting control). The order of the two sets of text was randomized for different participants. The selected text was very easy to read and understand, and was modified to unify the length to 1200 characters (including symbols and spaces), to avoid potential differences in typing difficulty that might result from differences in text. Additional materials (instructions to the experiment) were prepared for typing practice. The NRC Typing Task software [25] was used for evaluation of the typing performance. The interface of the software is shown in Fig. 3 (b). The NRC Typing Task software recorded the key stroke and time, and then calculated the typing speed (the number of net characters typed per second) using Equation (1) [25]. Such combined score was deemed better than two dependent measures, e.g., accuracy and speed, to simplify the quantification of the tying performance. Once completed, the accuracy of the typing task was 100%.

$$
\textit{Typing task score} =
$$
$$
= \frac{TOTAL - (CurKey + 2 \times BSKey)}{Time}, \qquad (1)
$$

where:

CurKey = the number of cursor keys pressed;

BSKey = the number of backspace keys pressed;

TOTAL = the total number of all keys pressed including cursor and backspace keys;

Time = the time spent in seconds.

In addition, a colour-matching task was used to evaluate the colour rendering performance of the tested office lighting with/without access to continuous dimming controls. An X-rite classic Macbeth colour checker was mounted on the document holder (Fig. 4 (a)). Without time limit, participants were asked to match a bench colour on the Macbeth colour checker with one of four option colours provided on the left side of the computer screen and then type the number of the identified colour in an answer sheet on the right side,

Table 1. The algorithm of generating candidate colours*

Colours	RGB values
Bench colour	R, G, B
Colour 1: more green	R-10, G+20, B-10
Colour 2: more yellow	R+10, G+10, B-20
Colour 3: more red	R+20, G-10, B-10
Colour 4: more purple	R+10, G-20, B+10
Colour 5: more blue	R-10, G-10, B+20
Colour 6: more cyan	R-20, G+10, B+10

*Any GRB value drops below 0 or exceeds 255 were discarded.

as shown in Fig. 5 (b). In case participants could not identify a match, they were asked to choose the closest one. The colour options were generated by slightly adjusting the RGB values of the bench colour on the Macbeth colour checker, using an algorithm (Table 1) developed by Colour Blender [26] for web design. Of the six new colours generated, only three were randomly selected, together with the bench colour, to form the four colour options shown on the screen. At the beginning, the experimenter showed an example to the participant using the dark skin colour on the Macbeth colour checker, followed with two practices using light skin and blue sky colours. The twelve colours in the second and third lines of the Macbeth colour checker were then used in the formal task consisted of 12 questions (Fig. 4 (b)). The sequence of the 12 questions was also randomized in different test trials. Both the number of correct answers and the time to complete the task were recorded. The score of the colour-matching task (the number of correct answers per minute) was calculated using Equation 2.

$$Color\ mathcing\ task\ score = $$
$$= \frac{No.\ of\ correct\ answers}{Time} \qquad (2)$$

Note that the RGB colour space is device-dependent. The same colour may look slightly different on the computer screen from that on the Macbeth colour checker, which commonly occurs in modern offices. Such colour discrepancy was examined under the LED lighting with or without continuous dimming controls, to test the impact on subjective evaluation of colour fidelity. To avoid colour shifts caused by changes of light levels and adaptation [17, 18], the task light was adjusted to remain the same illuminance levels on the Macbeth colour checker and the computer screen. The computer LCD display also fixed at the default factory settings without change throughout all lighting conditions.

A questionnaire was developed to survey participants' attitude toward lighting quality and task satisfaction right after they finished all office tasks. The questionnaire consists of 21 questions divided into two sections (Appendix A). The first section is a survey on office lighting quality, developed based on the work of Eklund and Boyce [27]. A total of 17 questions cover evaluation of lighting level, light distribution, glare, colour rendering, CCT, noise, flicker and overall impression. They are close-ended questions with only two options: agree or disagree, suitable for assessing participants' attitudes towards many clearly defined lighting quality issues in a short period of time [28]. The second section contains four questions covering subjective ratings on a 0–4 semantic scale (0 means the least difficult or satisfied, 4 means the most difficult or satisfied) of the difficulty of the two office tasks and performance satisfaction.

The two office tasks were conducted by each participant under the tested LED lighting conditions with or without access to the continuous dimming controls. The sequence of access to lighting controls was randomized for different participants so that 15 participants worked without lighting control first and then with lighting control, while the other 15 participants worked the other way, to exclude the confounding effect of control sequence. The experiment procedure was divid-

ed into a total of 14 steps. Below is the procedure first without lighting control and then with lighting control. For the reversed sequence, Steps 4, 5, 6 were swapped with Steps 9, 10, 11.

Step 1: The experimenter dimmed the general lighting to approximately 400 lx on the desktop, averaged on points 1–3 shown in Fig. 1 (c), when the task light was turned off. Then, the task light was turned on at maximum light level.

Step 2: Upon arrival, participants were screened by self-reporting their age and self-declaring if they have abnormal colour vision or abnormal audio acuity. Qualified participants were then asked to test their eyesight by reading two Snellen eye charts pasted on the back wall of the test room. The experimenter then explained the experiment to the participant, and asked he/she to sign the consent form.

Step 3: The participant adjusted the chair, the document holder, the display, the keyboard, and the chin rest till he/she felt completely comfortable. Once the adjustments were completed, their positions and/or title angles were fixed during the experiment and recorded for reconstruction later. The participant's chin sat on the chin rest throughout the experiment.

Step 4: The experimenter asked the participant to step out of the test room, then dimmed the task lighting until the illuminance values on the surface of the colour checker (on the document holder) and the screen were the same, about 350 lx. Then the participant came back in and sat down. The participant was given at least 2 minutes for eye adaptation.

Step 5: The participant conducted the typing task without individual lighting control. The participant practiced by typing the instructions to the experiment as long as he/she needed before he/she conducted the formal typing task. The participant was then given a short break.

Step 6: The participant conducted the colour matching tasks without lighting control. The participant also practiced twice before he/she started the formal colour-matching task.

Step 7: The participant completed the questionnaire. The 21 questions were presented on the computer screen. Participants were asked to click on the answers with the mouse.

Step 8: The participant stepped out of the test room for a 20-minute long break. The experimenter measured the illuminance and CCT at the eight

points using a Minolta Chroma Meter CL-200A. Then, the participant came back in for the second part of the experiment.

Step 9: The participant adjusted (either increasing or dimming) the general lighting and the task lighting to their preferred levels. Then, the participant was given a typing exercise to evaluate the lighting. Further adjustments were allowed without time limitation till the participant was completely satisfied with the adjusted lighting condition. Once the adjustment was finalized, the lighting condition was fixed throughout the rest of the experiment. Next, the participant was given at least 2 minutes for eye adaptation.

Step 10: The participant conducted the typing task again using different text. The participant practiced before he/she conducted the formal typing task. A short break was then given to the participant.

Sep 11: The participant conducted the colour-matching task again with different colour-matching questions. The participant practiced before he/she did the formal colour-matching task.

Step 12: The participant completed the questionnaire again.

Step 13: The experiment was completed. The participant left with pay.

Step 14: Photometric measurement again, including the illuminance and CCT at those eight reference points.

To complete the experiment, the 30 participants took 52–91 minutes, with an average 69.9 minutes and standard deviation (SD) of 9.0 minutes. It is worth to mention that the participants conducted each typing or colour-matching task only within several minutes, which may not reflect a whole-day-long office experience. Such short-time tasks were purposely designed to avoid fatigue of the participants over time, which was a distracting factor in this study.

3. RESULTS AND DISCUSSION

In this study, one independent variable (*IV*) was examined: (with or without) access to continuous dimming controls of the tested LED lighting. Four dependent variables (*DV*) were measured, including (a) net characters typed per second in the typing task, (b) number of correct responses per minute in the colour-matching task, (c) subjective rating of the lighting quality, and (d) subjective rating
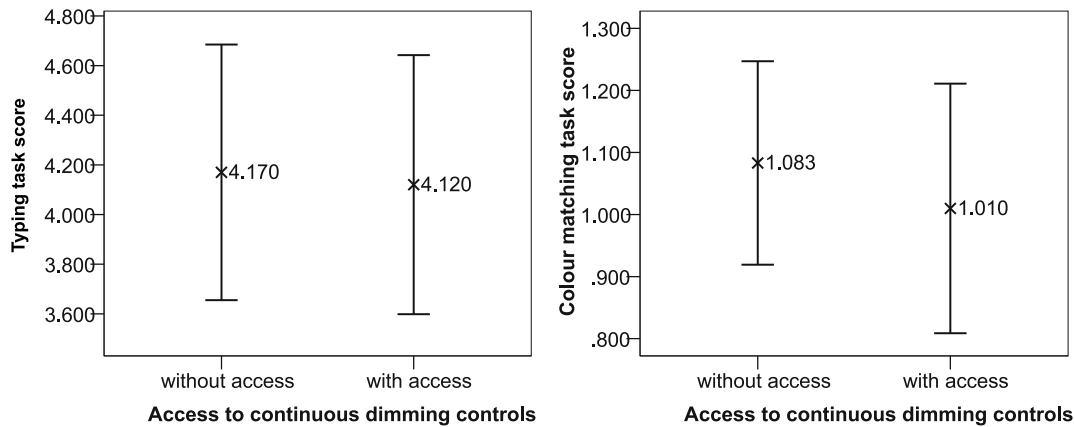
Fig. 5. Typing task scores (net characters typed per second) and colour-matching task scores
under each of the two test conditions

of the task satisfaction. All other variables not examined in this study were pre-set with fixed values to preclude their distracting effect.

The data collected in the experiment were used to calculate the four dependent variables (*DV*). The calculated *DVs* in each of the two test conditions (with/without lighting control) were compared to test the null hypothesis. Since the 30 participants went through the two test conditions in turn, two-way within-participants (repeated measure) ANOVA was calculated for testing the equality of means of the performance of the typing and colour matching tasks. A two-way repeated measure ANOVA was also conducted for analysis of the 30 participants' answers to the last four questions on task satisfaction in the questionnaire. Nonetheless, because answers to the first 17 questions on lighting quality in the questionnaire were discrete (agree or disagree), Chi-square test was used, which was capable of analysing discrete variables. All tests were analysed at a confidence level of 0.05 ($\alpha = 0.05$) with IBM SPSS.

The illuminance and CCT values were measured on the eight points in all tests conducted by the 30 participants under the two test conditions. As expected, the initial light levels measured at Points 1−3 on the desktop without controls were very close in the 30 tests (averagely (394.5 ± 58.7) lx on point 1, (595.9 ± 108.9) lx on point 2, and (320.9 ± 6.6) lx on point 3). However, the preferred light levels adjusted via individual controls were slightly lower and in a larger span of range ((367.5 ± 135.6) lx on point 1, (571.0 ± 230.0) lx on point 2, and (237.8 ± 107.5) lx on point 3). To avoid colour shift, the initial light levels on Point 4 (on the document holder) and Point 5 (the com-

puter screen) before the continuous dimming controls were introduced were almost the same (averagely (351.2 ± 20.3) lx on point 4, (336.2 ± 17.1) lx on point 5). Nonetheless, the access to individual lighting controls broke this balance and introduced a large variation ((467.5 ± 223.9) lx on point 4 vs. (318.9 ± 131.5) lx on point 5). Points 6−8 were on the background walls. The initial ambient light levels (averagely (217.2 ± 6.4) lux on point 6, (278.2 ± 6.2) lux on point 7, and (269.8 ± 7.6) lux on point 8) were much higher than the adjusted ambient light levels ((165.9 ± 68.5) lx on point 6, (204.0 ± 95.1) lx on point 7, and (198.4 ± 88.7) lx on point 8). The larger span of the initial light levels on the desktop before lighting controls was due to the different locations and tilt angles of the document holder and the display screen adjusted by different participants, which affected the initial adjustment of the task light by the experimenter to balance the light levels on points 4 and 5, thus, the initial light levels on the desktop. The average CCTs measured at the eight sample points under fixed LED lighting without lighting controls were 3125 K ± 92 K. After individual lighting controls were introduced, the measured CCTs changed to 3071 K ± 120 K. Note that a chromaticity difference in CCT of ± 60K is barely noticeable, while CCT of ± 100K is the recommended maximum colour difference that a lighting installation could tolerate [29].

The mean scores of net characters typed per second (with 100% accuracy) and the mean scores of the number of correct responses per minute under each test condition are shown in Fig. 5. Fig. 5 is the error bar plot. Based on the results of repeated measures ANOVA, the access to individual lighting controls did not make any statistically sig-

**Table 2. Descriptive statistics and Chi-square test results for subjective ratings
of the lighting quality under four different test conditions**

Question no.	Percentage of responses to positive lighting quality		Chi-square test p value
	without lighting control	with lighting control	
1	86.7%	93.3%	0.389
2	96.7%	93.3%	0.554
3	80.0%	86.7%	0.488
4	90.0%	93.3%	0.640
5	93.3%	90.0%	0.640
6	83.3%	86.7%	0.718
7	86.7%	96.7%	0.161
8	90.0%	93.3%	0.640
9	96.7%	86.7%	0.161
10	93.3%	93.3%	1.000
11	93.3%	100.0%	0.150
12	86.7%	93.3%	0.389
13	96.7%	100.0%	0.313
14	100.0%	93.3%	0.150
15	86.7%	93.3%	0.389
16	90.0%	86.7%	0.688
17	80.0%	76.7%	0.754

nificant difference ($p = 0.527$) on the typing task performance. However, the lighting control had a significant difference on colour matching performance ($p = 0.047$). The participants' average accuracy of colour matching per minute with lighting controls (1.010) was lower than those without lighting controls (1.083), indicating that providing participants access to the continuous dimming lighting control had interruption on their colour rendering performance of the LED lighting.

Moreover, based on the descriptive statistics of participants' responses to the positive lighting quality and p values of the Chi-square test shown in Table 2, it was found that subjective ratings of the lighting quality did not differ significantly under different test conditions. With access to individual lighting controls, no significant difference of lighting quality was perceivable by the participants.

The descriptive statistics of task satisfaction ratings are shown in Table 3. The result of the two-way repeated measures ANOVA is shown in Ta-

ble 4. No p value is less than 0.05, indicating that providing access to the continuous dimming controls of the tested LED lighting did not affect participants' ratings of typing task difficulty ($p = 0.752$) and satisfaction of their typing task performance ($p = 0.677$), perceived difficulty of the colour matching tasks ($p = 0.245$), and subjective satisfaction of the colour matching task performance ($p = 0.758$).

6. CONCLUSIONS AND DISCUSSION

Conclusively, the null hypothesis tested in this study was partially rejected. Under the specific LED lighting technologies examined in this study, providing access to continuous dimming controls did not affect the participants' typing task performance ($p = 0.527$), nor their subjective ratings of typing task difficulty ($p = 0.752$) and satisfaction of their typing task performance ($p = 0.677$). This indicates that the LED lights tested in this study provided initial high quality lighting that can satis-

Table 3. Descriptive statistics of task satisfaction ratings

Question No.	LED w/o lighting control		LED with lighting control	
	Mean	SD*	Mean	SD
18	0.9	0.8	0.8	0.8
19	2.8	1.1	2.9	0.7
20	2.3	0.9	2.1	1.0
21	2.7	0.9	2.6	0.8

*SD= standard deviation

Table 4. Tests of 2 × 2 repeated measures ANOVA for Questions 18−21

Source	Type III Sum of Squares	df	Mean Square	F	Sig.
Question 18: How do you rate the difficulty of the typing task you did?					
Lighting control	0.033	1	0.033	0.102	0.752
Error (Lighting control)	9.467	29	0.326		
Question 19: How do you rate your satisfaction with your typing task performance?					
Lighting control	0.133	1	0.133	0.177	0.677
Error (Lighting control)	21.867	29	0.754		
Question 20: How do you rate the difficulty of the colour-matching task you did?					
Lighting control	0.533	1	0.533	1.410	0.245
Error (Lighting control)	10.967	29	0.378		
Question 21: How do you rate your satisfaction with your colour-matching task performance?					
Lighting control	0.033	1	0.033	0.097	0.758
Error (Lighting control)	9.967	29	0.344		

fy the participants' needs for conducting the office typing tasks in the test room at photopic light level. Further adjustment of the lighting conditions via the continuous dimming controls tailored to meet each participant's individual needs did not increase the lighting quality to a significant level that may affect the participant's typing task performance and their subjective rating. Also, this phenomenon is consistent with previous findings [2] under fluorescent lights that participants' satisfactions were not associated with cognitive task performance in that perception and recognition of text is a portion of the typing task.

However, under the specific LED lighting conditions examined in this study, providing access to individual lighting adjustments worsened the participants' colour matching performance ($p = 0.047$) but no significant difference of lighting quality was perceivable by the participants. The variance of CCTs of the LED lighting with or without access to continuous dimming controls measured on the eight sample points was caused by a mixture of different light levels of the general lighting (3500 K) and the task lighting (2700 K) tailored to participants' individual needs. The individual lighting adjustments broke the balance of light levels on the Macbeth colour checker and the computer screen on which the option colours were presented, which introduced colour shift and variation of colour saturation [17, 18], leading to the slightly lowered colour matching performance. Yet the perceived difficulty of the colour matching tasks ($p = 0.245$) and the subjective satisfaction of the colour matching task performance

($p = 0.758$) were not changed. The CRI value (90) of the tested LED lights was very good for accurate colour perception in offices, which helped minimizing the adverse effect of the lowered colour-matching task performance under the slightly different lighting conditions (with or without lighting controls).

Moreover, in this study, providing access to continuous dimming controls of the LED lighting did not affect the young participants' rating of the office lighting quality (e.g., brightness, uniformity, glare, CCT, CRI, flickering, noise) in the test room, indicating that the variations of other factors (e.g., luminance distribution across the task and background surfaces, potential glare, flickering and noise of the LED lighting systems, etc.) introduced by the access to the continuous dimming controls were insignificant in this study.

Note that these conclusions were drawn based on the tested LED lighting technologies and the particular short-time tying and colour-matching tasks used in this study. Such test settings may not represent all other possible types of contemporary office lighting environments. The test settings explored in this study may not represent all complex test settings in modern offices. Fortunately, LED light sources to be used in modern offices will have even better colour rendering ability and consistent colour rendering performance throughout the process of dimming. Further investigations are needed to cover test conditions beyond the scope of this study, e.g., older office workers, different types of spectral data, whole-day-long working experience of office workers.

ACKNOWLEDGMENTS

REFERENCES

1. *Leaman A, Bordass B.* Assessing building performance in use 4: the Probe occupant surveys and their implications. Building Research & Information, 2001, 29(2), pp.129−143.

2. *Veitch JA, Gifford R.* "Choice, Perceived Control, and Performance Decrements in the Physical Environment" Journal of Environmental Psychology, 1996, 16, pp.269−276.

3. *Eklund NH, Boyce PR, Simpson SN.* "Lighting and sustained performance". Journal of the Illuminating Engineering Society, 2000, 29, #1, pp. 116−30.

4. *Boyce PR, Veitch JA, Newsham GR, Myer M, Hunter C.* 'Lighting Quality and Office Work: A Field Simulation Study". Pacific Northwest National Laboratory, 2003.

5. *Boyce PR, Veitch JA, Newsham GR, Jones CC, Heerwagen J, Myer M, Hunter CM.* "Lighting Quality and Office Work: Two Field Simulation Experiments" Lighting Research & Technology, 2006, 38, 3, pp.191−223.

6. *M. Thompson, U.M. O'Reilly.* "An Investigation into the Perception of Colour under LED White Composite Spectra with Modulated Colour Rendering" Proceedings for the 6th Light Research Office Symposium in Light and Colour, Lake Buena Vista, FL, February 2006.

7. *Hawes B.K, Brunyé T.T., Mahoney C.R., Sullivan J.M., Aall C.D.* "Effects of four workplace lighting technologies on perception, cognition and affective state". International Journal of Industrial Ergonomics, 2012, 42, pp.122−128.

8. *Bhardwaj S, Özçelebi T, Lukkien JJ.* "Smart lighting using LED luminaries" The 8th IEEE International Conference on Pervasive Computing and Communications, Workshops PERCOM Workshops 2010, Mannheim, Germany, March 29-April 2, 2010, pp. 654−659.

9. *Reijula J, Gro¨hn M, Mu¨ller K, Reijula K.* "Human well-being and flowing work in an intelligent work environment", Intelligent Buildings International, 2011#3, pp. 223−237.

10. *Wilkins AJ, Veitch JA, Lehman B.* "LED Lighting Flicker and Potential Health Concerns: IEEE Standard PAR1789 Update. Recommending practices for modulating current in High Brightness LEDs for mitigating health risks to viewers". Retrieved 15 July, 2013 from http://grouper.ieee.org/groups/1789/.

11. *Cai, H. & Chung T.M.* "Evaluating discomfort glare from non-uniform electric light sources" Lighting Research & Technology Journal, 2013, V. 45, #3, pp. 267−294.

12. *Veitch JA, Newsham GR, Boyce PR, Jones CC.* "Lighting Appraisal, Well-Being and Performance in Open-Plan Offices: a Linked Mechanisms Approach". Lighting Research & Technology, 2008, 40, pp. 133−151.

13. *Veitch JA, Newsham GR.* Exercised control, lighting choices, and energy use: an office simulation experiment. Journal of Environmental Psychology, 2000; 20 (3): 219−237.

14. *Veitch JA, Newsham GR.* "Preferred Luminous Conditions in Open-Plan Offices: Research and Practice Recommendations". Lighting Research & Technology, 2000, 32(4), pp. 199–212.

15. *Boyce PR, Eklund NH, Simpson SN.* "Individual Lighting Control: Task Performance, Mood, and Illuminance". Journal of the Illuminating Engineering Society, 2000, 29(1), pp. 131–142.

16. *Newsham G, Veitch J, Arsenault C, Duval C.* "Effect of Dimming Control on Office Worker Satisfaction and Performance". IESNA Annual Conference Proceedings, Tampa, Florida, July 25–28, 2004, pp. 19–41.

17. Hunt RWG. "Light and Dark Adaptation and The Perception of Colour". Journal of the Optical Society of America, 1952, 42 (3), pp.190–199.

18. *Davis W, Ohno Y.* Studies on the effect of illuminance on color rendering. Light and Lighting Conference with Special Emphasis on LEDs and Solid State Lighting, 27–29 May 2009, Budapest, Hungary, 2009.

19. *Baron RA, Rea MS, Daniels SG.* "Effects of indoor lighting (illuminance and spectral distribution) on the performance of cognitive tasks and interpersonal behaviors: the potential mediating role of positive affect". Motivation and Emotion, 1992, 16 (1), pp. 1–33.

20. *Mills PR, Tomkins SC, Schlangen LJ.* "The Effect of High Correlated Colour Temperature Office Lighting on Employee Wellbeing and Work Performance". Journal of Circadian Rhythms, 2007, 5(2), pp.1–9.

21. *Ono K, Miki M, Yoshimi M, Nishimoto T, Omi T, Adachi H, Akita M, Kasahara Y.* "Development of an Intelligent Lighting System Using LED Ceiling Lights into an Actual Office". Electronics and Communications in Japan 2012, 95(10). Translated from Denki Gakkai Ronbunshi 2011; 131-A(5), pp.321–327.

22. *Newsham GR, Veitch JA.* "Lighting Quality Recommendations for VDT Offices: A New Method Of Derivation". Lighting Research & Technology, 2001; 33(2), pp. 97–116.

23. *Veitch JA,* Newsham GR, Jones CC, Arsenault CD, Mancini S. "High-quality lighting: energy-efficiency that enhances employee well-being". CIE2010 Lighting Quality and Energy Efficiency, Vienna, Austria, March 14–17, 2010, pp. 197–204.

24. *Boyce PR, Veitch JA,* Newsham GR, Jones CC, Heerwagen J, Myer M, Hunter CM. "Occupant Use of Switching and Dimming Controls in Offices". Lighting Research & Technology, 2006, 38(4), pp.358–378.

25. National Research Council (NRC). Manual of typing task software. Retrieved 11 October, 2012, from http://archive.nrc-cnrc.gc.ca/eng/projects/irc/task-performance.html.

26. Color Blender. Retrieved 9 November, 2012, from http://www.colorblender.com.

27. *Eklund NH, Boyce PR.* "The development of a reliable, valid, and simple office lighting survey". Journal of the Illuminating Engineering Society, 1996, 25(2), pp. 25–40.

28. Instructional Assessment Resources (IAR). 2007. Survey question types. Instructional Assessment Resources, the University of Texas at Austin. Retrieved 12 January, 2012, from http://www.utexas.edu/academic/ctl/assessment/iar/teaching/plan/method/survey/survey_tables_questiontypes.pdf.

29. *Harbers G, McGroddy K, Petluri R, Tseng PK, Yriberri J.* "Visual colour matching of LED and tungsten halogen light sources". Proceedings of CIE2010 Lighting Quality and Energy Efficiency, 14–17 March 2010, Vienna, Austria, CIE, pp. 482–487.

APPENDIX A: A Complete List of Questions in the Questionnaire

Questions	Question type
Lighting quality survey: (Light level related)	
1. The lighting is uncomfortably bright for the tasks that I perform	agree/disagree
2. The lighting is uncomfortably dim for the tasks that I perform (light distribution related)	agree/disagree
3. The lighting is poorly distributed with unacceptable non-uniformity	agree/disagree
4. The lighting causes undesired deep shadows	agree/disagree
5. The contrast between the task and background is too strong and uncomfortable (glare related)	agree/disagree
6. Reflections from the light fixtures hinder my work	agree/disagree

Questions	Question type
7. The light fixtures are too bright. (CRI related)	agree/disagree
8. My skin is an unnatural tone under the lighting	agree/disagree
9. Coloured objects in the room look unreal or less legible (CCT related)	agree/disagree
10. The lighting is too warm for me or my work	agree/disagree
11. The lighting is too cold for me or my work	agree/disagree
12. The lighting color temperature is just fine for me or my work (other physical factors)	agree/disagree
13. The lights flicker throughout the test	agree/disagree
14. There is an unwanted humming noise of the lighting system (overall attitudes)	agree/disagree
15. Overall, the lighting is comfortable	agree/disagree
16. Overall, lighting in the office environment is acceptable	agree/disagree
17. Overall, I like to live and work in this office lighting environment	agree/disagree
Task satisfactions:	
18. How do you rate the difficulty of the typing task you did? (0 means easiest, 4 means hardest)	5-scale, $0 \sim 4$
19. How do you rate your satisfaction with your typing task performance? (0 means the least satisfied, 4 means the most satisfied)	5-scale, $0 \sim 4$
20. How do you rate the difficulty of the color matching task you did? (0 means easiest, 4 means hardest)	5-scale, $0 \sim 4$
21. How do you rate your satisfaction with your color matching task performance? (0 means the least satisfied, 4 means the most satisfied)	5-scale, $0 \sim 4$

Hongyi Cai, Dr.
He is an assistant professor in the Department of Civil, Environmental and Architectural Engineering at the University of Kansas in the U.S. He is the founder and principal investigator (PI) of the University of Kansas Lighting Research Laboratory. Dr. Cai is a member of IES and IALD in lighting profession

Linjie Li, LC.
He is a Test Engineer in Cree, Inc. He received his M.S. degree in Architectural Engineering with a concentration in lighting from the University of Kansas in 2013. During his stay in the University of Kansas, he worked as a Research Assistant in the Lighting Research Laboratory (KU-LRL) and conducted multiple lighting research projects under the supervision of Dr. Hongyi Cai. Working as a Test Engineer, he conducted research and measurement of photometric and spectroradiometric characteristics of lighting products, and provided extensive technical support to Illumination Engineering Society (IES) Test Committee. Mr. Li is a member of IES and received Lighting Certification (LC) from the National Council on Qualifications for the Lighting Professions (NCQLP) in 2015

RESEARCH INTO THE "COLOURING" EFFECT USING DIFFERENT SPECTRAL RADIATIONS

Svetlana M. Lebedkova and Yuliya A. Lusina

National Research University "MPEI", Moscow
E-mail: lebed1200@yandex.ru

ABSTRACT

Methods of evaluating qualitative and quantitative characteristics of colour sensation have been studied. An analysis of the proposed illumination methods of colour objects for the purpose of their "colouring" has been carried out. An experimental installation has been developed, and visual experiments were made to evaluate the colouring effect of colour samples. A calculation of saturation and luminosity of colour samples has been carried out with illuminating by different spectral radiations. Spectra of the radiations colouring (making more attractive) different groups of colour samples have been determined.

Keywords: light emitting diodes, colouring effect, colour samples

INTRODUCTION

One of the major characteristics of modern light sources (LS) is the quality of colour reproduction (colour rendition) of illuminated objects. Colour rendition characterises an influence of radiation spectral composition of a considered source on the colour rendering of objects in comparison with their colour when illuminated by a reference source. It is accepted practice to estimate this using general colour rendering index R_a, which is recommended by CIE. The practice of using fluorescent lamps (FL) when illuminating multi-colour interiors, has shown that white light FLs with the same correlated chromatic temperature T_{cc} and with close R_a values but with a different nature of the spectrum, can strengthen or weaken some colours. This is expressed in the increase or decrease of the colour luminosity or saturation. From the point of view of colour rendition, this is a negative effect, because colour is distorted in comparison with the standard. But strengthening colour saturation makes the object more attractive and it becomes pleasant to the observer. The property of colour improvement is critical to modern light emitting diodes (LED), as well as to FLs with three- and four-lined phosphors. As a rule, their R_a is not very high, and special indices of colour rendition are often low. There are plenty of examples of FL application where colours of illuminated object appear to be brighter, more beautiful, and juicier. In Germany, special FLs are manufactured for meat, fish, fruits and vegetable illumination, so that the customers perceive them to be more fresh and beautiful. However, these are protected technologies, and little is published about them.

The colour of an object is determined by the nature of its reflection spectrum. The brighter the colour is expressed, the narrower is this spectrum: tomatoes mainly reflect red rays, oranges — orange and yellow rays, and a white paper sheet reflects the entire spectrum of the incident white light. Thus, in order for coloured objects to appear more beautiful (to be more colourful), it is necessary that the maximum in the LS spectrum falls within the wave length interval corresponding to the maximun spectral reflection factor of these objects. And in doing so, LS radiation should remain white, so that it can be used for general illumina-

tion and to create comfortable conditions for long term occupants.

It is obvious that with the emergence of LEDs, finding such a radiation spectrum becomes easier.

The colouring effect can have different applications. In retail, for example, that is to attract the customer's attention to certain groups of goods or for window dressings with display goods of certain colours. It should be noted that it is not a question of colour illumination but of white light LS application, which makes objects brighter and more expressive.

It is recommended to illuminate confectionary and pastry with LSs of low T_{cc}. Frozen produce is better illuminated using FLs with T_{cc} of 4000–6500 K and $R_a \geqslant 85$. To illuminate meat products, lamps with a special spectrum accentuating natural red and pink colours are often used. Vegetable and fruit departments are traditionally illuminated with bell type luminaires or with searchlights of directional light with MHLs equipped with ceramic torches.

To strengthen the colour and to increase the attractiveness of different types of products, LED LSs could be applied with a corresponding radiation spectrum. To illuminate multi-colour objects, LSs with $R_a > 90$ are applied as a rule, so that colour rendition can be more precise, especially for products with different spectral reflection. *Martini Light HD RETINA LED* Company has proposed a new technology specifically intended for illumination of multi-coloured objects and for giving them a saturated bright shade.

A purpose of this paper is to determine the nature of LED radiation spectra to create a colouring effect for colour objects, under conditions of white colour perception stability.

DEVELOPMENT AND CREATION OF THE EXPERIMENTAL INSTALLATION

An aim of this study was to simulate an LED LS spectrum, under which colour objects perceived by experts would seem more beautiful and brighter in comparison with the same objects under standard illumination conditions. It was also necessary to estimate the degree of colouring comfort. Therefore an installation simulating different spectra of LED radiation and different conditions of colour object illumination was created. The model

Fig. 1. Structure of the experimental installation

proposed in work [1] was taken as a base. The experimental installation contained a light source, an illumination device, a control device (CD) and adaptometer.

The LS was simulated by a LED set, which allowed creating spectra of white radiation corresponding in particular to different T_c and R_a. Colour LEDs of *XP-E* series of *CREE – Royal Blue* Company (3 pieces), *Green* (8 pieces), *Amber* (29 pieces) and *Red* (8 pieces) were used.

The illuminator looked like a metal rectangular parallelepiped with dimensions of 350×350×150 mm^3. It was covered inside with sheets of white microporous polyethylene terephtalate (*MCPET*) with high reflecting properties, produced by *Furukawa* Company. The cover, to which LEDs were attached, was made of aluminium alloy, 3mm in thickness, which provided an effective heat removal. For the diffuser material, a matted perspex was selected.

For operation of the illuminator, CD of *Rainbow Electronics* Company (driver) was used. For LED radiation flux control, *P-CPU-AT-RS485-P130x46-RT007* board was applied. It transformed digital eight-bit signals from a monochromatic screen, into PWM signals supplied to each CD.

A piece of plywood 12 mm in thickness was used as the material for the adjustable chamber. The size of the structure was 760×500×500 mm^3. To provide non selective reflection conditions and uniformity of illuminating colour samples placed into the adaptometer, its inner surface was painted with white matte paint. In Fig. 1, the adaptable chamber with illuminator is presented.

The experimental installation allows changing radiation spectral composition by means of dimming the luminous flux of colour LED chains. In that case, light remains white with a small shade. This makes it possible to illuminate colour

Table 1. Dimming levels of four signals of a light-emitting diode light source when simulating an incandescent lamp with $T_c = 2800\ K$

Dimming levels of LED LS components	LED LS components			
	B	*G*	*A*	*R*
IL with $T_c = 2800\ K$	60	115	100	65

objects placed in the adaptometer using radiation, which creates a colour strengthening effect.

Saturated colour samples of the Moscow Power Institute (18 pieces) were selected as observation objects. They were placed on a grey background with a reflection factor of 0.5 (in order to avoid a big contrast with the surface of the adaptometer, which had reflection factor of 0.7).

The luminous flux of the light emitting diodes was dimmed using *Python*: setting signals of correspondent components *R*, *G*, *B* and *A* (from 0 to 255) and obtaining different versions of the spectrum.

The vertical plane surface, where observation objects were placed, had an illuminance of 500 lx, which remained constant with each spectrum versions.

Strengthening object colours of different chromaticity was achieved by increasing the radiation portion in the reference LS spectrum within wavelength intervals correspondent to this chromaticity. An LS model of type A with T_{cc} of 2800 *K* comprising four LEDs as specified above was used as the reference LS, with which the investigated LS could be directly compared. Control signals set with *Python* for the reference LS are given in Table 1.

LED spectra in red, yellow, dark blue and green areas, which caused inadmissible colour strength-

ening, were experimentally derived. The interval from the reference LS spectrum to the spectrum, which caused inadmissible colour strengthening, was divided into five sites. As a result, we obtained six points that is by six LED LS radiations for each group of colour samples (red, yellow, dark blue and green samples).

CONDUCTING THE EXPERIMENT

The experimental part of the work consisted of two stages. In the beginning, the degree of attractiveness for red-yellow and then blue-green samples of the MEI was estimated using a five-point scale, going from illumination by an incandescent lamp to illumination by the simulated LED LS with T_{cc} of 2800 *K*. Experiments with observation of red-yellow and then of blue-green samples were made separately. Accordingly, histograms were plotted to estimate red-yellow (Fig. 2) and blue-green (Fig. 3) colour samples of the MEI. The x axis shows a categorical evaluation of the samples, and the y axis — the number of observers who reported in each category. According to the obtained results, luminous flux of the simulated LED LS is enough in the dark blue, green and yellow spectrum parts. In the red part, the luminous flux is not enough, causing the claret-coloured and
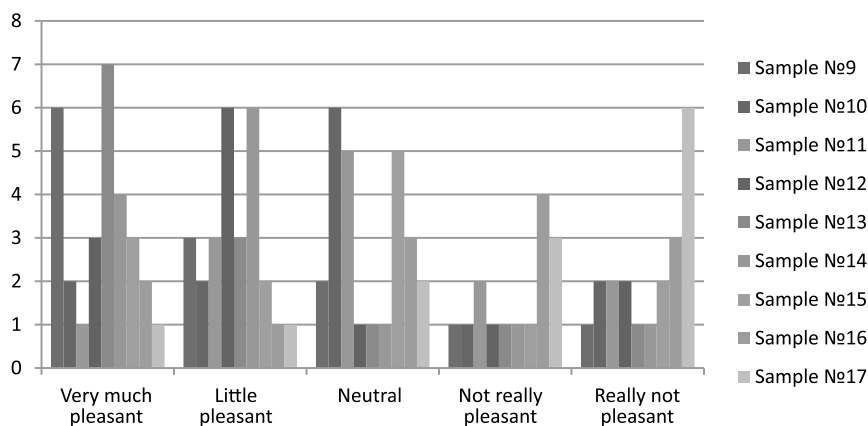
Fig. 2. A comparison histogram of subjective evaluation of colours of red-yellow samples with illumination using an incandescent lamp and the light-emitting diode reference source
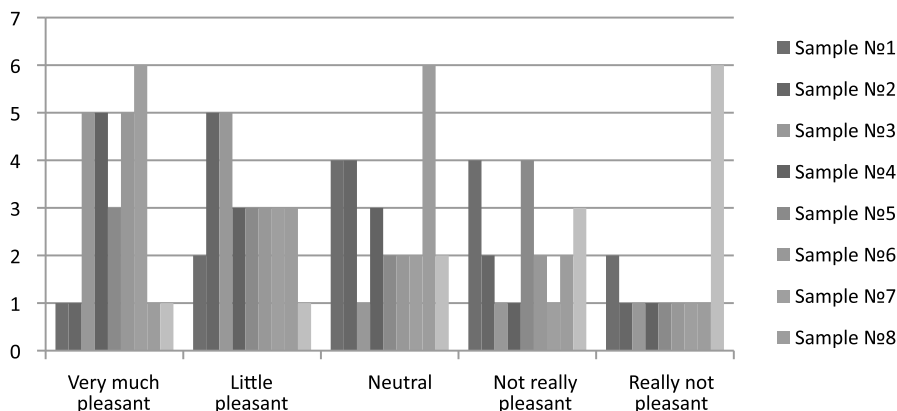
Fig. 3. A comparison histogram of subjective values of colours of blue-green samples with illumi-nation using an incandescent lamp and the light-emitting diode reference source

purple samples to darken and disappear. Spectrum of the reference LED LS is given in Fig. 4 (black dotted line).

The aim of the second part of the experiment was to find LED LS radiations, which would "embellish" some colour objects. Therefore, observations were carried out separately with red, yellow, dark blue and green samples of the MEI (since it was required to make recommendations concerning illumination of objects of specific shades). The colouring degree was evaluated using a binary system stimulus evaluation: "plus" and "minus", which was implemented by the presentation method.

The observers awarded a "plus" to radiation with which colour samples would become brighter, more saturated, "purer", more "flaring" and different by a comparison with the simulated reference radiation. In doing so, the white background of the adaptometer was perceived as white, and the skin of a person slightly changed its colour. Observance of this condition allows later on recommending the spectra obtained in the experiments both for accent illumination of specific objects, and for general illumination.

A "minus" evaluation was given to such a radiation, with which colour samples had a "dirty" shade, did not differ from others and were not very saturated. Or, on the contrary, it was given to radiation, with which samples were so bright and saturated that they caused discomfort, and skin colour became unrecognisable. According to work [2], in this case one could approximate distribution of the answers using a Gaussian distribution, processing the experiment results by statistical methods.

As noted above, six radiation spectra for each group of the MPEI samples were obtained, and they were shown to the observers by five times in an arbitrary order, which would exclude any guesswork. The observer was asked to say whether the simulated radiation strengthened the sample colour in comparison with the reference LS. The reference illumination version was shown to the observers in equal proportion with the other radiations. The responses were recorded into a visual evaluation report. The numbers of samples, which were most pleasant to the observers when illuminated with the best radiation, were also recorded.

Statistical processing of the observer answers in the second part of the experiment was performed by the probit method [3] based on the data of the reported visual evaluations. According to this method, values of the stimulus correspondent to the 50% probability of detection of the colouring effect and of the mean square deviation of this value were obtained. According to these data, weighed average values of the stimulus and of the dispersion were calculated. Thus to create the colouring effect when illuminating red samples, one should select red "radiation #3", when illuminating yellow samples, it should be yellow "radiation #2", when illuminating dark blue samples: dark blue "radiation #3" and green samples: green "radiation #3.

CALCULATION OF CHROMATIC CHARACTERISTICS OF RADIATIONS AND OF ILLUMINATED OBJECTS

Measuring spectra of the "embellishing" radiations was made using МДР-206 monochromator

Table 2. Saturation (*H*) and luminosity (*B*) values for red and yellow samples

Sample#	H_{graph_ref}	H_{graph_ls}	H_{CIELAB_ref}	H_{CIELAB_ls}	$H_{v_r v_g v_b\_ref}$	$H_{v_r v_g v_b\_ls}$	B_{ref}	B_{ls}
R radiation								
13	86	82	93	106	191	158	318	342
14	**95**	**94**	**76**	**91**	**368**	**313**	**228**	**256**
15	**93**	**99**	**63**	**80**	**528**	**456**	**171**	**197**
16	**83**	**90**	**52**	**67**	**656**	**586**	**139**	**158**
17	68	80	37	52	939	856	96	98
A radiation								
9	**30**	**28**	**70**	**75**	**39**	**41**	**434**	**437**
10	32	28	66	71	21	21	416	419
11	**45**	**40**	**84**	**88**	**40**	**35**	**399**	**404**
12	**59**	**52**	**89**	**93**	**85**	**75**	**375**	**382**

with grating groove of 1200 at 1 mm (the obtained spectra are given in Fig. 4).

Radiation colour and chromaticity coordinates were computed, and then plotted on the *XYZ* chromatic diagram together with the allowances for white radiation as ellipses. The chromaticity of the investigated radiations was outside of the FL allowances for white radiation. Nevertheless, during the experiments, the observers did not perceive a strong distortion of the white background and of hand skin colour.

According to the obtained results, chromatic characteristics of colour samples were computed when illuminating with reference and "embellishing" radiations. They showed that when illuminating colour samples with "embellishing" radiation, the integral reflection factor increases. Because of this, the samples under investigated radiation conditions seem more saturated, colourful and bright.

Then, by means of a uniform-chromaticity-scale diagram of the $v_r v_g v_b$ system corresponding to the luminance relation of the object and background $L_o/L_b = 2$, saturations of all the samples were determined when illuminated with the reference LED LS and with investigated radiation for each group accordingly. It was also found that the colour chromaticity of red samples moves to a redder spectrum area, of yellow samples — to
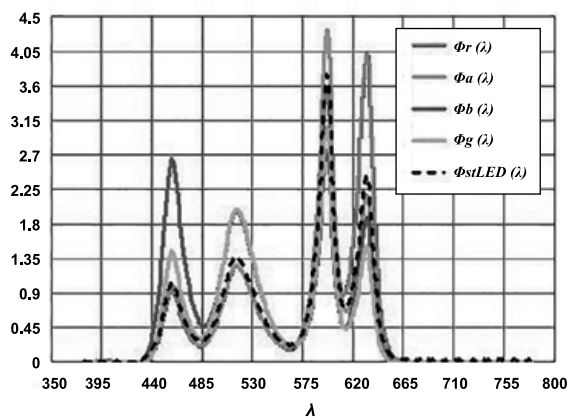
Fig. 4. Spectra of colouring red, yellow, dark blue, green and of the reference light-emitting diode radiations

Fig. 5. Illumination of a multi-colour composition using the reference radiation (at the left) and R radiation (on the right)
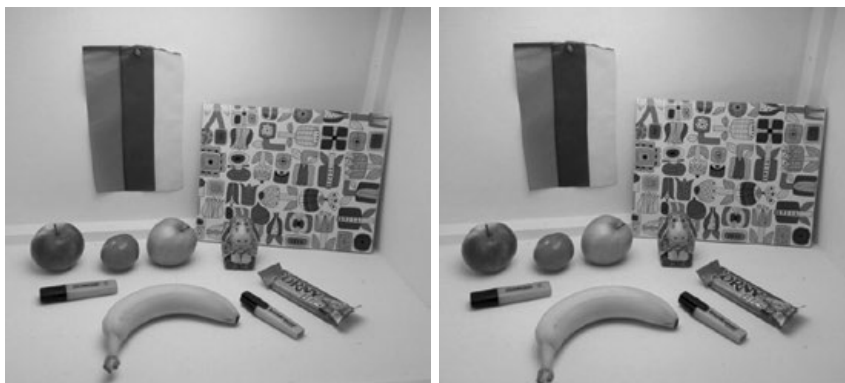
Fig. 6. Illumination of a multi-colour composition using the reference radiation (at the left) and A radiation (on the right)

Fig. 7. Illumination of a multi-colour composition using the reference radiation (at the left) and B radiation (on the right)

Fig. 8. Illumination of a multi-colour composition using the reference radiation (at the left) and G radiation (on the right)

Table 3. Saturation (H) and luminosity (B) values for dark blue and green samples

Sample#	H_{grapf_ref}	H_{graph_ls}	H_{CIELAB_ref}	H_{CIELAB_ls}	$H_{v_r v_g v_b\_ref}$	$H_{v_r v_g v_b\_ls}$	B_{ref}	B_{ls}
B radiation								
1	41	48	33	90	957	732	111	221
2	58	71	51	95	720	610	151	167
3	60	74	51	93	746	627	147	163
4	68	75	52	90	630	508	166	184
18	13	14	16	90	911	730	108	220
G radiation								
5	54	48	42	68	510	441	186	202
6	52	53	43	69	634	559	149	161
7	56	53	45	70	645	595	137	149
8	36	39	40	68	448	405	200	208

the yellow-orange area, dark blue samples moves to the blue-violet area, and that of green samples moves to the green area. These results correspond with the subjective estimations, when the observers perceived an increase of luminance and saturation of sample colours.

Calculations colour sample saturation in two uniform-chromaticity-scale systems: *CIELAB* and $v_r v_g v_b$ were performed. The results are given in Tables 2 and 3 for red and yellow, dark blue and green samples respectively.

An analysis of the calculation results shows that saturation in the *CIELAB* system for red samples increased from the reference radiation to the investigated. This is contrary to the calculation in the $v_r v_g v_b$ system. Luminosity in the $v_r v_g v_b$ system increases. In this case, it was minimal only for sample 17, and it was at maximum for sample 13, which is very different upon observation. Such a dispersion of the results can be explained by the fact that in the graphic method, an isoluminance plane was used with $L_o / L_b = 2$ ratio, and in our case, this relation is changed. Also, the *CIELAB* system does not account for the inductive influence of environmental fields [4] and does not de-

scribe the unequivocal connection of colour object luminosity with the luminance for any chromaticity, which in its turn excludes a possibility to descript colour "flaring" effect (Helmholtz-Kohlrausch phenomenon). Thus, due to the luminosity increase, red samples become more attractive to a greater extent.

To show the colouring effect of colour objects more obviously, a multi-colour composition was created, which was illuminated with the reference radiation and with the obtained investigated radiations (Figs. 5–8, see p. 63).

When analysing the results, it can be seen that going from the reference radiation to the investigated, saturation (according to the $v_r v_g v_b$ system) decreases, and luminosity increases. Thus with the colour "flaring" effect, our visual apparatus reacts precisely to the change in luminosity, rather than to saturation change. In this case, both samples with too high luminosity levels, and those where levels were too low, appear uncomfortable to the observer. In Table 4, intervals of saturation and luminosity values needed to create the colouring effect of colour objects of different chromaticity are given.

Table 4. Ranges of values of saturation (H) and lightness (B) for "embellishment" of colour objects

Colour of objects	H, thresholds	B, thresholds
Red	300–600	150–260
Yellow	35–75	380–440
Blue	500–630	160–190
Green	440–600	145–205

CONCLUSION

The experimental research results confirm that colour is strengthened under different-spectral radiations. The luminosity, saturation and colour chromaticity of objects changes. And the spectra of investigated radiations differ from the reference radiation spectrum and are characterised by lower R_a values. When evaluate the colouring effect of a colour, it turned out to be impossible to use the *CIELAB* system due to absence of an unequivocal connection of luminosity and luminance of colour objects. When using an "embellishing" radiation, the attractiveness of colour samples increased mainly because of an increase in their luminosity. The results of the work show that when illuminating colour objects, one should not use LSs with the R_a close to 100 in all cases. This invites a possibility to develop LEDs specifically for creating colouring effects in case of illumination of different destination objects with inner and external architectural illumination.

REFERENCES

1. *Lebedev I.S., Lebedkova S.M.* An installation to research object colouring with light-emitting diode illumination / the XXth International scientific and technical conference of students and post-graduate students "Radio engineering, electronics and power engineering", 27−28.02.2014, MEI National Research University: Theses of a report. V. 1. Moscow: Publishing house of the MEI, 2014, 168 p.

2. *Zhuravlyov G.E., Zabrodin J.M., Krylov V.Ju.* Psychology and mathematics. Moscow: Nauka, 1976, 296 p.

3. *Van der Varden B.L.* Mathematical statistics. Moscow: Publishing house of the foreign literature, 1960, 434 p.

4. *Mesckov V.V., Matveev A.B.* Foundations of light engineering: A teaching guide for high schools: In two parts. Part 2. Physiological optics and colorimetry. The second revised edition. Moscow: Energoatomizdat: 1989, 432 p.

Svetlana M. Lebedkova,
Ph.D, Professor. Graduated from the Light Engineering Chair of the MPEI in 1971. The Head of the Illumination installation department of the Svetotekhnika Chair of the National Research University "MPEI"

Yuliya A. Luzina,
Master of Engineering, graduated from the Svetotekhnika Chair of the National Research University "MPEI" in 2015

SIMULATION-BASED RETROFITTING OF AN EDUCATIONAL BUILDING IN TERMS OF OPTIMUM SHADING DEVICE AND ENERGY EFFICIENT ARTIFICIAL LIGHTING CRITERIA

Göze BAYRAM and Tuğçe KAZANASMAZ

Izmir Institute of Technology
Emails: tugcekazanasmaz@iyte.edu.tr; gozebayram@gmail.com

ABSTRACT

The high level of daylight performance is crucial to increase academic and work performance of students and staff in educational buildings which are mostly used during the daytime. New design solutions have potential to reach optimum lighting conditions and minimum energy consumption. So, the purpose of this study is to evaluate and propose an energy efficient lighting design for an educational building. The aim is to find the optimum type of shading device with appropriate slat angles, transmittance of glazing, and the luminaire type/layout as well. Utilizing DIALux simulations, scenarios for combinations of these inputs are tested for classrooms, offices and a laboratory, which are non-identical due to their orientation, size, window characterization and facade organization. The procedure covers all significant days (winter/summer solstice and equinoxes) during one year. Such an integrated approach would be proposed for lighting design and retrofit applications.

Keywords: retrofitting, shading device, energy, daylighting, artificial lighting, simulation

1. INTRODUCTION

The physical environment has significant impacts on academic performance and alertness of students in educational buildings which are occupied mostly during daytime [1, 2]. The utmost concern is to benefit from daylight efficiently, to avoid visually uncomfortable conditions (i.e. glare occurred by excessive illuminance) and to apply energy efficient lighting strategies simultaneously. A special attention is necessary in their design and in retrofitting process afterwards.

Though energy efficient artificial lighting fixtures and light sources are selected and located in their right positions and layout, improperly designed educational buildings, which do not meet the necessary illuminance and uniformity requirements, allow the use of artificial lighting unreasonably. To illustrate proper requirements, work plane horizontal illuminance range from 300 to 500 lx in classrooms and offices. Higher illuminance varying from 500 to 750 lx is necessary in laboratories [3]. Uniformity is recommended to be above 0.67 according to DIN5034 [4]. To exemplify such an improper design, uncontrolled direct sunlight passing through the glazing in a facade without any sun protection components can only be avoided using curtains, which also block daylight completely inside the room. On the contrary, excessive amount of daylight in the interior and unbalanced distribution lead to glare problems. In those cases, shading devices provide sun control to balance the illuminance levels.

Several studies figured out impacts of building orientation, shading devices on the daylight performance and energy efficiency [5, 6]. One study analysed users' responses to the visual comfort survey, percentage of facade glazing and the recommended daylight autonomy to reduce electrical lighting energy consumption in an office building

Table 1. Geometrical properties of selected rooms

DESCRIPTION		Room A	Room B	Room C	Room D	Room E	Room F
ORIENTATION		Southeast	Southwest	Northwest	Northeast	Southwest	Southeast
	Type	Class	Class	Office	Lab	Office	Lecture Hall
	Lighting Row No. & Total Lighting No.	3 & 9	3 & 9	6 & 18	3&30 - 3&24	3 & 3	4 & 24
	Width, m	6.40	6.40	6.50	22.90	3.10	13.00
	Depth, m	9.80	9.80	12.40	12.10	6.60	9.85
	Height, m	3.60	3.60	3.30	3.30	2.60	3.40
	Floor Area (m^2)	61.13	62.83	80.36	268.82	19.70	128.19
WINDOW	Width, m	2.90	2.90	2.90	2.90	0.95	0.95 & 1.40
	Height, m	2.55	2.55	1.80	1.80	2.50	2.35
	Height from Floor, m	1.05	1.05	1.05	1.05	0.10	1.05
	Total Glazed Area (m^2)	14.80	14.80	10.44	36.54	4.75	18.92
	Window-to-Wall Ratio (WWR %)	63	63	49	48	59	43

[7]. Another one focused on several lighting retrofit scenarios for a hall in the university campus. The study involved calculations of energy consumption relying on LEDs and different types of fluorescent lamps in each scenario [8]. One research proposed a simplified method to predict the energy savings of artificial lighting in relation to daylighting [9]; while others focused on the impact of external shading devices on daylight penetration and its performance [10].

The aim of this study is to retrofit an educational building in terms of lighting criteria by proposing the optimum slat angles and types of shading devices according to orientation. The other objective is to find the appropriate and energy efficient type and layout of luminaire to provide an adequate uniformity and support illuminance in deeper spaces and to attain minimum electricity consumption. So, both daylighting and artificial lighting are considered together as an integrated system. The values of parameters (slat angle and type of shading devices, transmittance of glazing,

and type of lamp and luminaire layout/type) are evaluated comparatively and determined correspondingly under different design scenarios for an educational building's lighting retrofit.

2. THE PROCEDURE

2.1. Description of the case rooms and measurements

The case building is an educational building in Izmir Institute of Technology (38°N latitude, 26°E longitude). A total of six rooms in this building were selected to conduct DIALux simulations [11]. Their physical and geometrical properties, the layout and technical properties of the artificial lighting system were obtained from architectural and electrical/lighting system drawings and field observation, Table 1, Fig. 1.

Measurements of horizontal work plane daylight illuminance were taken using a digital illumi-

Fig. 1. Interior and exterior views of windows in Room B
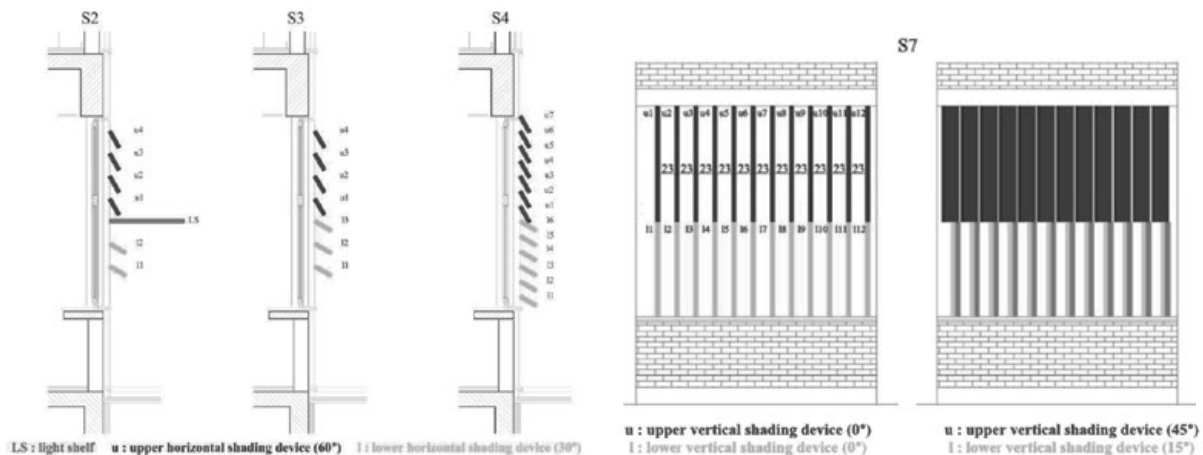
Fig. 2. Examples of options for shading devices

nance meter with an attached silicon photo diode receptor head, at 2.30 PM on December 4th, 2014. Its measuring range is 0.01−299, 900 lx. The sky condition was partly-cloudy. The optical properties of the glazing and surface materials were measured and calculated using both the illuminance and the luminance meter according to the method used in a previous study [12]. The reflectance of surface materials for walls, floor and ceiling were determined according to the Lambertian reflectance formulation. The reflectance of wall, floor and ceiling were 68%, 25% and 87% respectively. The transmittance of glazing was measured as 36% accordingly. Measured values were employed in DIALux model to correspond to the actual case before proposing retrofit scenarios.

2.2. Alternative retrofit scenarios using DIALux

DIALux performs daylight illuminance calculations, taking into consideration external obstructions, artificial lighting illuminance and its energy consumption as well [11]. The simulation-based models involved variants of shading devices, luminaires and glazings of sample rooms. Alternative retrofit solutions were proposed in terms of energy efficient lighting criteria. There are a total of nine alternative retrofit scenarios (S1-S9), which are derived from combinations of input values. These inputs are transmittance of glazing, type of shading devices, slat angles, type of luminaires and their layout. Three alternatives of transmittance of glazing (GT) were determined in retrofit simulations. GT1, GT2 and GT3 display the high (90%), medium (70%) and low (50%) transmittance, respectively.

A higher-reflected-wall surface (80%) rather than the actual one was attained as an input in retrofit proposals. The base case scenario (S0) was implemented using the actual measured values.

A shading device acts to balance the light distribution on the horizontal work plane, while prohibiting the excessive penetration of sunlight to prevents overheating. Three types of shading system, a light shelf, horizontal shading devices (HSD) and vertical shading devices (VSD) have been proposed for each window including variations of slat angles and slat distances (Fig. 2). Slats are movable from 0° to 90° with 15° intervals where 0° is accepted as open and 90° as closed. These slopes are valid for both HSD and VSD. The slat width is taken as 25 cm. Upper and lower slats move independently from each other. For example, scenario 3(S3) involves HSD with 30 cm distance between slats and all slopes (0°, 15°, 30°, 45°, 60°, 75°, 90°).

The actual luminaire used in this building is a recessed modular type holding 4 TL-D/18W fluorescent lamps. Its total power is 70W, total luminous flux is 3834 lm. The retrofit scenarios involved replacing existing type of luminaires with LEDs'. The total power of the new LED panel with a similar luminous flux (3400 lm) is 41W. As it is essential to minimize the lighting power density [13] for the energy efficiency, LED type of luminaire with a similar luminous flux was chosen in retrofit scenarios. Luminaire layout is defined according to the number of luminaire rows which are switched on. For example, one alternative of luminaire layout included one working row near to the rear wall and others were switched off, while another alternative represented two working rows.
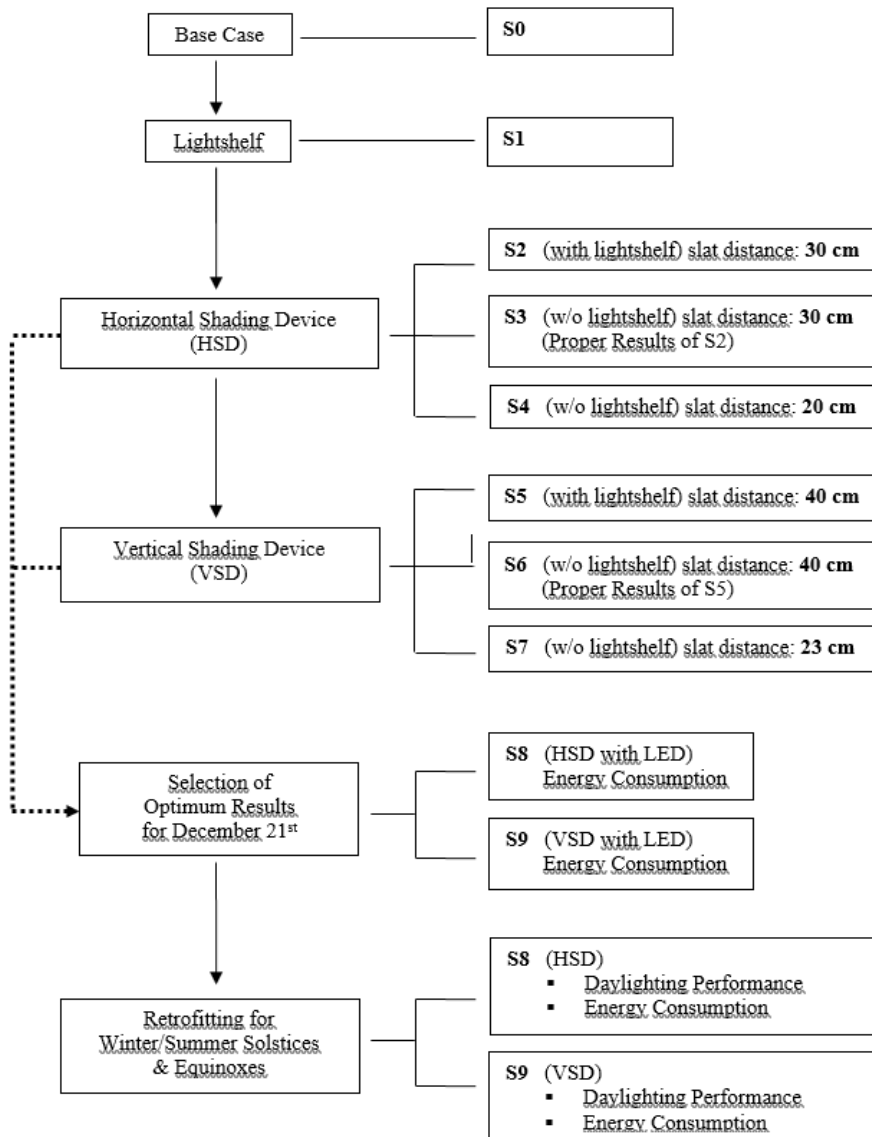
Fig. 3. Flowchart for scenario application steps (w/o: without).

The outputs are illuminance (lx), uniformity, LENI (Lighting Energy Numeric Indicator [kWh/yr.m^2] and the annual lighting electricity consumption [kWh/yr]. The European standard EN-15193 prescribes LENI values for educational buildings of (27−34.9) kWh/yr.m^2 with basic requirements [14].

As laboratories need higher illuminance (500−750) lx than classrooms and office rooms (300−500)lx [3], LENI are stated in a range of (41.8−51.9) kWh/yr.m^2 with comprehensive requirements [14]. Uniformity values should be above 0.67 according to DIN5034 [4]. In general, lighting consumes almost 10−50% of total electricity consumption in buildings; specifically 30−40% in office buildings. Recent studies search for new design/or technological strategies to reduce LENI below 10 kWh/yr.m^2 [13, 15]. To calculate lighting energy consumptions of buildings, Building Energy Performance Regulation (2008) and the Energy Calculation Method (BEP-TR) in Turkey have been adopted depending on the European Standard EN-15193[14], which defines the parameter of LENI. As it is known that LENI depends also on the daylight availability and is associated with the daylight climate; and climate in Izmir differs from the one in Europe, the recommended values may not fit the real situations in İzmir. Utilizing this kind of study, it is expected to provide useful information for developing such further standards and recommendations which are significant to our country's actual climatic conditions.

Comparison of Measured and Simulated Illuminance (EM and ES)
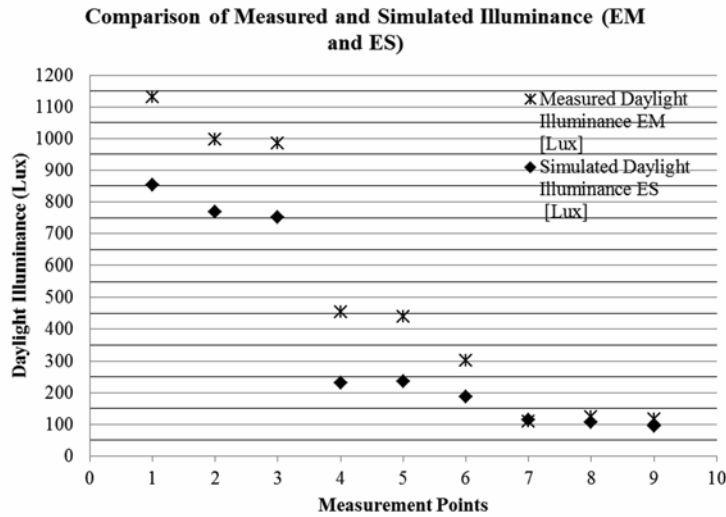
Fig. 4. Comparison of measured and simulated daylight illuminance for Room B

The electricity use was calculated for each single three-hour-periods (9:00 AM-12:00 PM; 12:00 PM-3:00 PM; 3:00 PM-6:00 PM) for winter/summer solstices and equinoxes. The whole year is subdivided into four periods due to seasons. The assumption here is that results for one significant day, i.e. winter solstice, are the same for other days in i.e. winter period. Each seasonal period identified by winter/summer solstices and equinoxes, covers 75 working days seperately. The annual electricity use corresponds to 300 days. Steps of scenario applications are given in Fig. 3.

In detail, retrofitting consists of a total of nine scenarios. First, DIALux performed the base case model for December 21st/June 21st and March 21st/September 21st. Second, simulations were run for a total of seven daylighting and energy efficiency improvement scenarios only for the day of December 21st. All simulations were produced under clear sky conditions. Third, one scenario including HSD, which resulted in the optimum illuminance and uniformity values; and another one including VSD were selected. Fourth, these two optimum scenarios were assigned as S8 and S9, respectively. They involved LED lighting fixtures, which replaced the existing fluorescent ones. So, it was possible to test their energy efficiency and to compare the results in terms of illuminance and uniformity. The calculation methodology for the annual lighting electricity consumption is simplified due to the standard EN15193. It takes into account the number of working luminaires and their working time i.e. for the winter solstice when S8 and S9 are the concern. For example, one row corresponds to three luminaires, which are switched on for only 3 hours, i.e. at noon.

$$\text{daily energy consumption} = \text{luminaire power} \\ \times \text{number of working luminaires} \times \text{working} \\ \text{time} \quad (1)$$

$$\text{seasonal energy consumption} = \text{Daily energy} \\ \text{consumption} \times 75 \text{ days} \quad (2)$$

$$\text{seasonal LENI} = \text{seasonal energy consumption} / \text{floor area} \quad (3)$$

Reduction and simplification of calculations, as above, make them flexible and available for short time stamp evaluations. The sum of seasonal electricity consumptions results in the annual one presently.

Fifth, the simulation generated outputs of the optimum case for HSD (S8) and the optimum case for VSD (S9) with fluorescent lighting fixtures for the equinoxes and the summer solstice over again. Sixth, models leading to unbalanced daylight distribution were retrofitted additionally by means of installing vertical and horizontal slats and of modifying the slat angles. Finally, the findings for the solstices and equinoxes showed us the improved scenarios containing the optimum shading device type, slat angle, lighting fixture layout and type. The calculations presented the electricity consumption of fluorescent and LED luminaires for all seasons. Seasonal LENI values (sLENI), which are identified here, are necessary to assess each scenario separately considering their response to seasonal conditions. According to this procedure
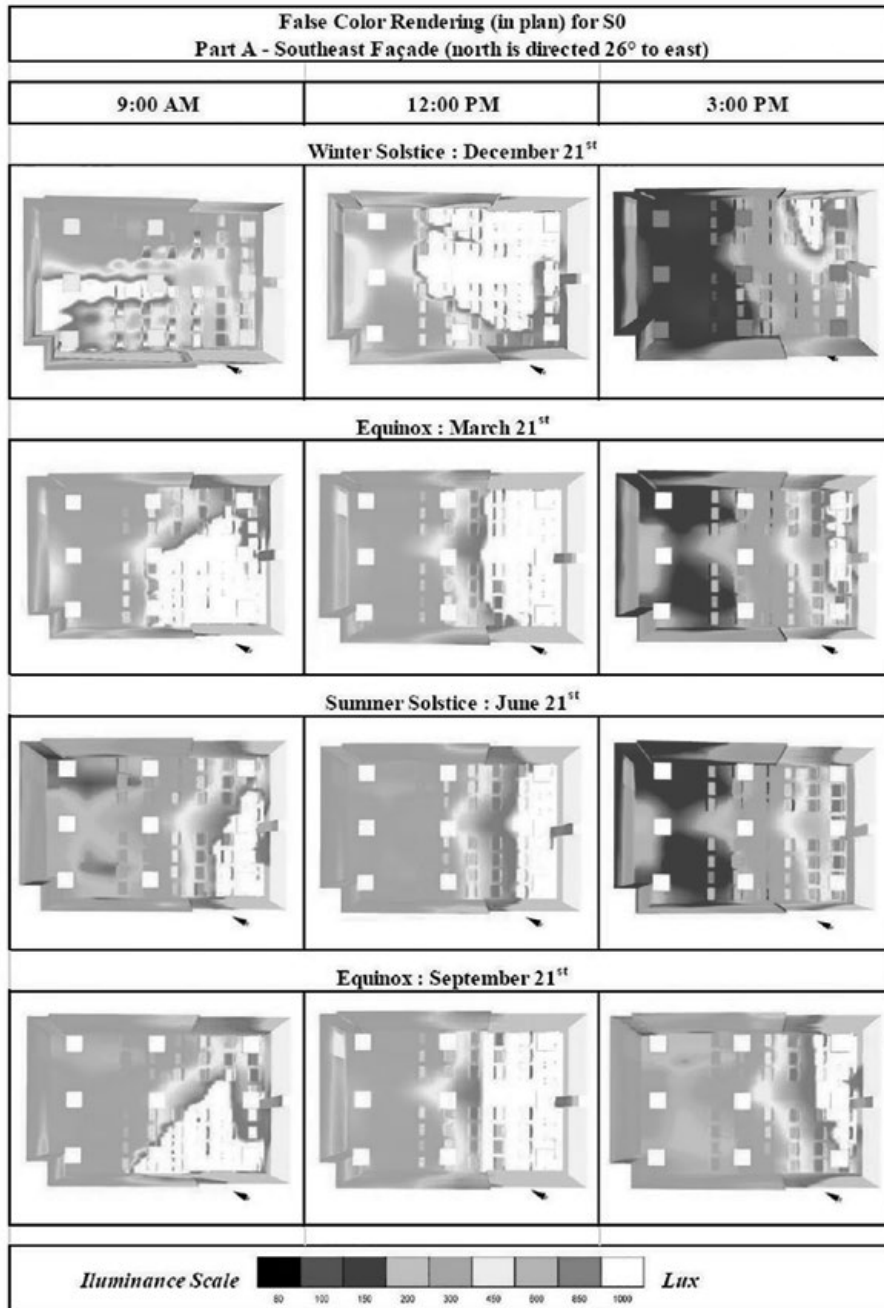
Fig. 5. Distribution of daylight illuminance for Room A in S0

the determination of the optimum HSD and VSD was based on the solstice and equinox conditions and LENI on the electricity consumption. The optimum application of HSD and/or VSD provides adequate conditions of daylight illuminance and uniformity while its role in the determination of the layout of working luminaires remains initially. The outcome designates the luminaires, which are counted in the energy consumption calculations and, by the way, in the LENI calculations. The subsequent step is to find out what would be

the least consumed energy if the fluorescent type of lamp replaced to be the LED.

3. RESEARCH FINDINGS

Field measurements aimed to determine the actual daylight performance and to validate the base case scenario by comparing illuminance and uniformity. The target daylight illuminance was set as 500 lx and the uniformity as 0.6 according to recommendations [12–14] in evaluation of sun

Table 2. Retrofitting the Results for the HSD for Room A facing with Southeast

SD: Shading Device (length=25cm);				Angle u: upper l: lower				
LL: Lighting Fixture Layout;				n: Number of Lighting Row (on)				
Panel length: 25 cm								
Vertical; height: window height				location: head of each side of window				

Hour	W/S Solstices & Equinoxes	SD Angle	LL n	ILLUMINANCE (lx)			UNIFORMITY	
				E_{avg}	E_{min}	E_{max}	U1 E_{min}/E_{avg}	U2 E_{min}/E_{max}
9 AM	December 21st	u=30° l=75°	2	487	396	591	0.81	0.67
	March 21st	u=60° l=75°	2	513	459	605	0.89	0.76
	June 21st	u=0° l=90°	1	478	300	589	0.63	0.51
	September 21st	u=45° l=75°	2	504	442	597	0.88	0.74
12 PM	December 21st	u=75° l=75°	2	487	394	598	0.81	0.66
	March 21st			446	326	577	0.73	0.57
	June 21st	u=75° l=45°		547	500	657	0.91	0.76
	September 21st	u=75° l=75°		450	338	579	0.75	0.58
3 PM	December 21st	u=15° l=60°	2	507	439	602	0.87	0.63
	March 21st			566	520	642	0.92	0.81
	June 21st			508	438	612	0.86	0.72
	September 21st	u=45° l=90°		488	387	593	0.79	0.65

shading systems. It was observed that there was an unbalanced daylight distribution in this classroom. Its uniformity (almost 0.1−0.2) was very low and the illuminance at approx. half of the measurement points was below the recommendations (500 lx). The area close to the windows was very bright when compared to the rear area, Fig. 4. Thus, it was necessary to propose a shading system to achieve a uniform daylight distribution.

A lineer regression diagram was used to validate the DIALux model. The coefficient of determination (R^2) and the lineer regression equation were calculated by using Excel. Value R^2 was equal to 97% and confirmed the high accuracy of the model. This is an indicator for approx. 97 % chance of prediction power of the measured values by using the simulated values. Consequently, the simulation outputs fit the field measurements very well.

Specifically, the measured illuminance was greater than the simulated ones (Fig. 4).

Retrofit simulations were conducted at 9:00 AM, 12:00 PM and 3:00 PM for winter/summer solstices and equinoxes under clear sky conditions. DIALux implemented every possible combination of slat angles, glazing and luminaire choices according to scenarios as mentioned in previous section. So, the analysis tool was run for almost 250 simulations for each case room. As this process was repeated for each six room, a total of 1500 simulation results were evaluated all together.

Regarding simulation results, which represent base case conditions for Room A, there was an unbalanced daylight distribution during the day due to the direct sunlight inside the room on December 21st. This day corresponds to the worst scenario; since, the sun elevation gets lowest inci-
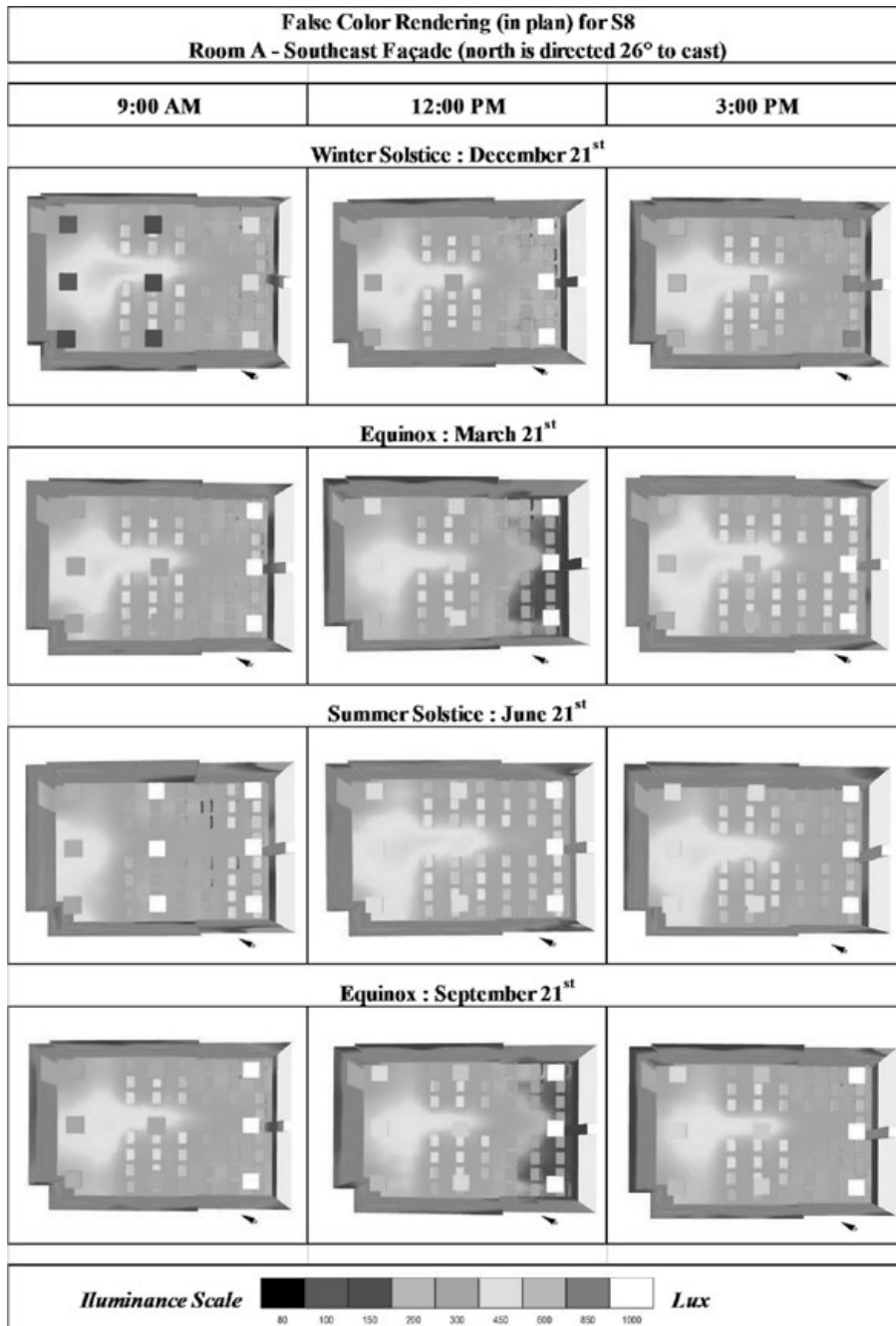
Fig. 6. Room A-False colour rendering (in plan) for retrofitted S8

dent values. The direct sunlight can reach at the rear wall during the morning hours; in the middle of the room at noon, Fig. 5. Daylight illuminance exceeds approximately 1000 lx mostly during the day. Even in summer period, disturbing bright area is almost one third of the whole floor area during the morning and at noon. The darkest region in this room received a very low level of daylight in the afternoon annually. Curtains are indispensable for such existing situations in the classroom to prevent direct sunlight. However,

they cause the use of artificial lighting system during the day.

To improve its uncomfortable lighting conditions, Scenario-S4 (Table 2) contained HSDs whose slat distances were 20 cm. They controlled the penetration of sunlight and daylight; thus, uniformity varied from 0.46 to 0.89. This led to a comfortable and stimulating visual environment. Using all glazing transmittance values (GT1, GT2 and GT3), daylight illuminance was within the range of recommended values (300–500) lx. S4-FT1 was
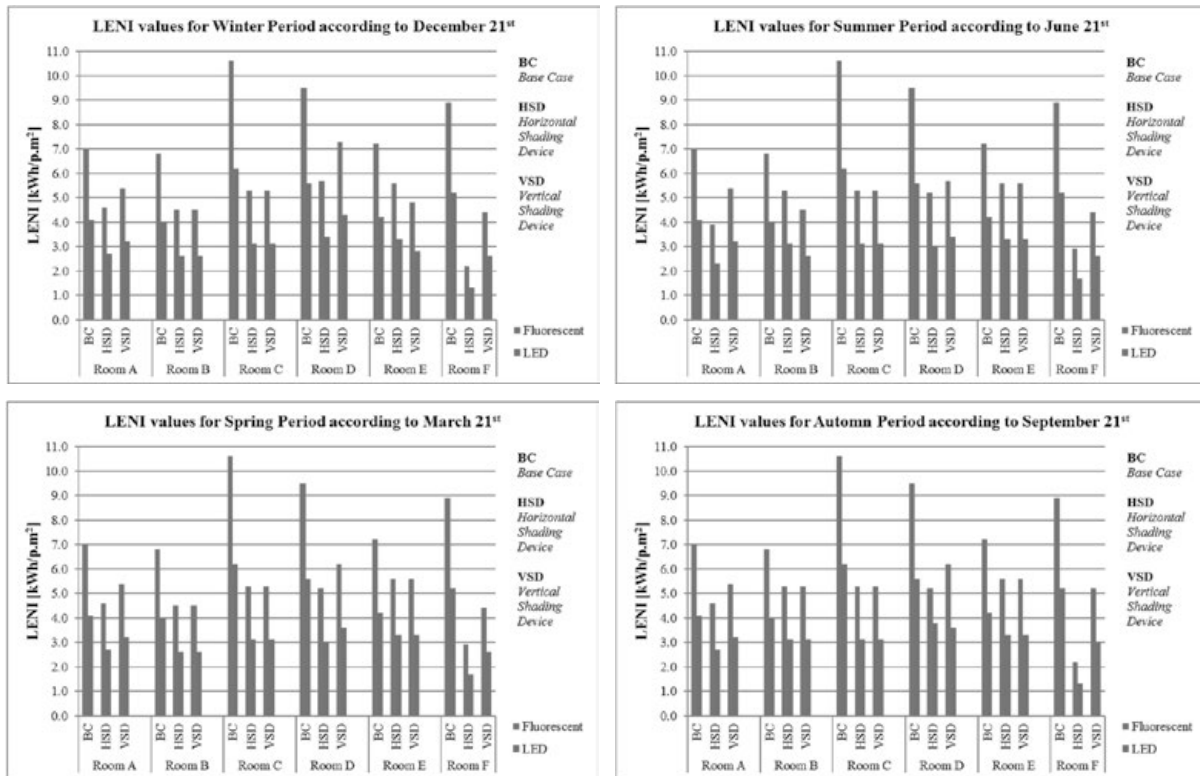
Fig. 7. sLENI values in winter/summer solstice and equinoxes for all case rooms.

found to be the most appropriate solution among the HSD scenarios in terms of uniformity. Upper and lower slat angles were 30° and 75° respectively in the morning, in this scenario. At noon, all the slat angles were 75° and two rows of luminaires are turned on. In the afternoon, upper and lower slat angles were 15° and 60° respectively and two rows of lighting fixtures are switched on.

S7-FT3 was proposed as the optimum one among the VSD scenarios. In S7-FT3, upper and lower slat angles were 45° and 30° respectively and two rows of lighting fixtures were in the working condition in the morning. At noon, upper and lower slat angles were 45° and 75° respectively. Only one row of luminaire was able to support the lighting level near the back wall. As all slat angles of the shading system were 75° in the afternoon, very low illuminance values were merely raised utilizing all artificial lighting system.

LED luminaires were integrated in S4-FT1 and S7-FT3 at this time. We named the former S8 and the latter S9. The photometric characterization of LED fixtures resulted in higher uniformity values. At noon, uniformity was increased from 0.79 (S4-FT1) to 0.92 (S8). It was rised up to 0.82 (S9) in the morning. Room A-False colour rendering (in plan) for retrofitted S8 is presented in Fig. 6.

Fig. 7 displays the sLENI values for all optimum HSD and VSD scenarios which initially fulfill the requirements of illuminance and uniformity. To discuss these scenarios furthermore due to desired energy consumptions, the proceeding step is to check which solution (HSD versus VSD) has the lower sLENI value; since both HSD-and VSD-retrofits are successful due to comfort levels. This process is accomplished for winter solstice; then, it covers the whole year to fig. out whether the optimum retrofit option for the worst time in a year would be additionally successful due to change in seasonal periods or not. Thus, the optimum solutions are obtained for HSD as S4-FT3 and for VSD as S7-FT3 on December 21st in Room B; for HSD as S4-FT1 and for VSD as S7-FT2 in Room C; for HSD as S4-FT1 and for VSD as S7-FT3 in Room D; for HSD as S4-FT3 and for VSD as S7-FT3 in Room E; for HSD as S4-FT2 and for VSD as S7-FT3 in Room F. A general conclusion depicts the dependency of sLENI on room orientation. Common retrofits are, conversely, valid in the whole year for each room. Specifically, HSD scenarios are found to be energy efficient solutions for Southeast and Southwest façade in relation to the geometric attributes (depth, width) of the room in this study.

4. DISCUSSIONS AND CONCLUSION

Reasons, which cause deficiencies in lighting conditions are stated as below:

• Facade configurations are independent of orientation and size in actual case. While there are large overhangs on North facade, preventing the penetration of diffuse daylight; there is no shading device on South facade resulting in the penetration of excessive direct sunlight.

• Despite the window-to-wall ratio is enough due to standards, room depth is higher than the required value. This caused insufficient amount of daylight in large rooms.

• The coated glazing, which is against high solar gain (the transmittance of glazing was almost 36%) minimizes the passage of daylight through the glass as well.

To improve above conditions, this study revealed scenarios bouncing design variants of shading devices and energy efficient lighting system relying on solstices and equinoxes.

Findings of illuminance derived from optimum solutions (S4-FT1 and S7-FT3) ranged from 480 to 532 lx on December 21th; similarly, that illuminance interval was kept similar in the whole year including a few exceptions observed at noon. Lower illuminance values were read at noon. The reason behind these exceptions may be the high protection of sun shading due to the higher slat angles. The uniformity varied between 0.46 and 0.89 during the year. Replacement of LEDs caused higher values of uniformity (0.63–0.92), but not significant change in illuminance.

The evaluation of the electricity use for periods was based on sLENI. Although Room E and Room B were two rooms facing Southwest (i.e. the same orientation), the installation of VSD in Room E was more energy efficient (4.8 kWh/p.m^2) than the use of HSD (5.5 kWh/p.m^2) in the same room on Dec 21st. Either the use of VSD or HDS did not make any difference in sLENI (5.5 kWh/p.m^2/flourescent) in the summer solstice and equinoxes. This condition was just the opposite when Room B was the concern. The application of VSD in Room B was more efficient (4.5 kWh/p.m^2/flourescent) than the use of HSD (5.2 kWh/p.m^2/flourescent) in the same room on June 21st. Their use did not influence sLENI either in winter solstice (4.5 kWh/p.m^2/flourescent) or equinoxes (4.5 kWh/p.m^2; 5.2 kWh/p.m^2/flourescent).

The reason behind this situation is related to the sun elevation and the depth of the room. In winter, when sun elevations are low, the use of VSD in the least depth rooms becomes the energy efficient solution. In summer, its installation in the rooms with the highest depth results in the lowest energy consumption. Consequently, findings are in accordance to literature. The HSDs remained as optimum solutions for Room A, D and F facing Southeast and Northeast.

The best options for Room B and Room E facing Southwest were the VSDs. Room C facing Northwest may involve either HSDs or VSDs and neither of them affect the energy consumption among solstices and equinoxes. The electricity consumption became constant throughout the year.

The sum of sLENI values using fluorecent lighting for each room were within the limiting benchmark values (27–34.9 kWh/yr.m^2) of energy efficient lighting design criteria defined in EN-15193–1. Input parameters concerned in this study do not match all strategies to reduce the electrical energy consumption in retrofitting [15], but there are many others related to electric lighting installation and daylight harvesting. Still the reduction in electricity use was almost in the range 56–83% with the contribution of LED luminaire, layout, transmittance of glazing and shading devices. There would be more reduction when sensors/dimming control systems are installed and the design criteria maintain room depth, ceiling height and window area satisfactorily.

Optimum scenarios lead to a high level of visual comfort conditions and a low level of energy consumption by positioning the slats with high angles (60° or 75°). That blocks the view mostly. It is obviously crucial to achieve visual comfort conditions and less energy consumption without ignoring the outdoor visual contact. The depth of slats may be decreased and their geometry may be re-shaped in this context.

It is best to set the slat angles by the control of an automation system containing intelligent sensors, which makes adjustments according to the daylight illuminance. The application steps for retrofitting scenarios would be an infrastructure for further researches. Yet, this study implied feedback information about deficiencies in the actual case and optimum solutions to satisfy energy efficient lighting criteria. Such a preceding study was con-

sidered and its methodology was built to provide foreknowledge for such a system design.

REFERENCES

1. Theodosiou, T. G., Ordoumpozanis, K.T. Energy, comfort and indoor in air quality in nursery and elemantary school buildings in the cold climatic zone of Greece. Energy & Buildings, 2008. V40, pp. 2207–2214.

2. Bellia, L., Pedace, A., Barbato, G. Lighting in educational environments: an example of complete analysis of the effects of daylight and electric light on occupants. Building & Environment, 2013. V68, pp. 50–65.

3. Chartered Institution of Building Services Engineers CIBSE. Code for lighting. London: CIBSE; 2002.

4. Licht UB. Lighting design, detail practice. Munich: Birkhauser, 2006.

5. Krüger, E. L., Dorigo, A.L. Daylighting analysis in a public school in Curitiba, Brazil. Renewable Energy, 2008. V33, pp. 1695–1702.

6. Li, D. H., Tsang, E.K. An analysis of daylighting performance for office buildings in Hong Kong. Building & Environment, 2008. V43, pp. 1446–1458.

7. Konis, K. Evaluating daylight effectiveness and occupant visual comfort in side-lit open plan office buildings in San Francisco, California. Building & Environment, 2013. V59, pp. 662–677.

8. Nayyar, R.A. Assessing the potential for energy and economic savings from lighting retrofits at Illick Hall. Master's Thesis, New York, State of University of New York College of Environmental Science and Forestry. 2010.

9. Krarti, M., Erickson, P. M., Hillman, T. C. A Simplified method to estimate energy Savings of artificial lighting use from daylighting. Building & Environment, 2005. V40, pp. 747–754.

10. Li, D.H., Cheung, K. L., Wong, S. L., Lam, T. L. An analysis of energy-efficient light fittings and lighting controls. Applied Energy, 2010. V87, pp. 558–567.

11. DIALux version 4.9. User manual. Software standard for calculating lighting layouts, Lüdenscheid; 2011.

12. Fontoynont, M. Daylight performance of buildings. New York, USA: Earthscan, 2013.

13. International Energy Agency (IEA). Guidebook on energy efficient electric lighting for buildings, (Annex45), Aalto University School of Science and Technology, 2010.

14. PrEN15193–1, Energy performance of buildings; Energy requirements for lighting, 2007.

15. Dubois M.C., Blomsterberg, A., Energy saving potential and strategies for electric lighting in future North European, low energy office buildings: A literature review, Energy & Buildings, 2011. V43, pp. 2572–2582.

Tuğçe Kazanasmaz,
Assoc. Prof., Dr. She held a Doctor of Philosophy in Building Science from Middle East Technical University (METU). She has 15 years academic experience in architectural lighting, building physics and energy efficient design. At present, she is an Associate Professor in the Department of Architecture in İzmir Institute of Technology, Turkey

Göze Bayram,
Ph.D. in field of Architecture from Izmir Institute of Technology, 2015. She holds double major undergraduate degrees obtained from Yeditepe University as BSc. (Eng) Electrical and Electronic Engineer in 2005 and B. Arch. from Eastern Mediterranean University in 2010. She got her Master's degree from Dokuz Eylul University Architectural Department/Restoration Program in 2012. Her research topics are energy efficiency in buildings, architectural lighting and computer based simulations. She has been working as Architectural Project Manager in TARKEM since 2013. TARKEM is a corporation working for social and economic revitalization of Izmir Kemeralti Historical City Center

EFFECT OF AMBIENT TEMPERATURE RISE ON THE LED LIFE TIME RESOURCE

Aniruddha Mukherjee[1] and Amit Soni[2]

[1]*Department of Electrical Engineering, Suresh Gyan Vihar University, Jaipur, India*
[2]*Department of Electrical and Electronics Engineering, Manipal University, Jaipur, India*
E-mail: mukherjeeanirudh73@gmail.com

ABSTRACT

The impact of ambient temperature rise and, therefore T-point temperature rise too, on the life time of LEDs is analysed in this paper. From the research conducted so far it is understood that life time resource of LEDs is mainly dependent on junction temperature. For most of the high power LEDs, which are enclosed inside a luminaire, dissipation of junction heat from the device is a major concern for most of the manufacturers. In this paper, an attempt has been made to investigate the underlying constraints of heat dissipation and subsequently using LEDs as a general light source.

The investigation is carried out in two steps. Firstly, the degradation in light output with corresponding increase in ambient temperature is explored. Secondly, the impact of increase in T-point temperature on the lifetime of the LEDs is observed. The experiment is conducted using high power LEDs and the same is subjected to external thermal stress. The temperature inside the environmental chamber represents the ambient temperature for the LED and thus by gradually increasing the ambient temperature the T-point temperature is also increased. The temperature of the chamber and the T-point are measured by using k-type thermocouple. The corresponding data hence obtained are tabulated and correlated with light output. The results are analysed using statistical tool to obtain the relation between the parameters.

Keywords: junction temperature, ambient temperature, T-point, lamp life time resource

1. INTRODUCTION

Narendran in 2001 concluded that LEDs are prone to short lifetime if issues of thermal management are not properly addressed. This particular aspect is the most dominating constraint for the LEDs as an alternative long term solution of the issues pertaining to energy management [1].

Bullough in 2003 investigated the photometric features of the LEDs as a replacement for less energy efficient light sources. Further to this, the composition and spectral distribution was also investigated. The importance of LED driver and the subsequent influence it has on the performance of the LEDs as a suitable light source was also explored. [2].

In 2004, Xi and Schubert suggested a theoretical expression of temperature coefficient for diode forward voltage. It was shown that the temperature coefficient is dependent on the following factors: (i) the intrinsic carrier concentration, (ii) the band gap energy, and (iii) the effective density of states. The results were verified with experimental observations for GaN UV LEDs [3].

Further to this in 2008, researchers discussed the effect of the rise in T-point temperature towards LED lifetime. The T-point temperature is a vital parameter as it gives sufficient information to the manufacturer on the issues of degradation of LED lifetime due to heat. With the aid of this piece of information a manufacturer can design accordingly the size of heat sink, the amount of drive current for the device [4]. The un-
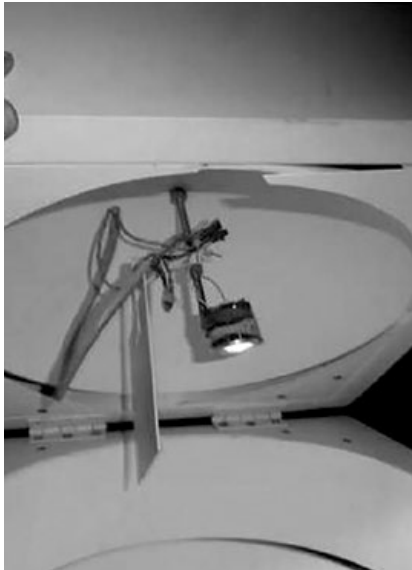
Fig.1. LED life test chamber

Fig. 2. LED life test rack

derstanding of T-point temperature is an important tool as it is related to the design of heat sinks and methods to vent out the heat from the device. A higher T-point temperature rating is an indication of a lower size of heat sink for the device.

The aspect of measurement of junction temperature has been widely investigated and innovative approach was derived from the research work of Jayawardena in 2012. The shift in wavelength is an effective method to determine the junction temperature in LEDs [5].

As observed, LED life predicted by manufacturers vary widely with actual lifespan as it involves the lifetime prediction of the LED device without considering the impact of an enclosed luminaire. Most of the lifetime prediction involves around the longevity of the LED without considering the impact of the enclosure it would have on the device.

The basic objective of this research is to determine the lifetime of enclosed LED luminaire considering the impact of rise in ambient and T-point temperature.

2. EXPERIMENTAL SET UP

The experiment is conducted using 3 mm high luminous flux LEDs from different manufacturers and having current rating of 100mA. The breakdown voltage is 3.8V and power consumed is 389mW for each LED at rated current. The basic reason to go for 3 mm LEDs is because most of the indoor retrofit LED luminaire used has 3 mm LEDs instead of the usual 5 mm. The en-

closed luminaire pose a major challenge to meet the thermal requirements for the device. However, similar experiments can also be conducted using 5 mm LEDs. The sample size selected for the experiment is fifteen and the material composition for the LEDs is GaAs. The LEDs are aged for 100 hours burning before the commencement of the test. The LEDs are labelled as LED1, LED2, LED3, LED4, LED5, LED6, LED7, LED8, LED9, LED10, LED11, LED12, LED13, LED14, LED15. The LEDs are placed inside the test chamber as shown in Fig. 1. The test chamber has two significant properties:

1. It maintains a constant ambient temperature inside the chamber;

2. It also serves as an intergrating sphere.

Each LED is mounted at the centre of the inside top surface of a life test chamber. A light meter is attached to measure the light output. A small white baffle is placed inside the chamber to shield the light meter from the direct light, allowing only the reflected light to reach the sensor. Two k-type thermocouples are placed on the top of the baffle, of which one thermocouple is used to measure the ambient temperature inside the chamber and the other one is used to measure the T-point temperature. The temperature inside the chamber is raised by a blowing hot air into the chamber manually through a temperature controller. Fig. 2 depicts the complete LED Life Test rack used for the experiment [6, 7, 8, 9].

The LED Life Test Rack is placed inside a room maintained at an ambient temperature of 25 °C (±1 °C). The driver is placed externally to supply the requisite current to the LEDs placed

Table 1. Variation of junction temperature with change in ambient temperature

$T_a(°C)$	T-point (°C)														
	LED1	LED2	LED3	LED4	LED5	LED6	LED7	LED8	LED9	LED10	LED11	LED12	LED13	LED14	LED15
27	37	40	38	37	38	40	41	36	40	42	37	37	40	38	41
30	42	43	40	40	41	45	43	41	42	45	40	39	45	40	46
35	45	45	43	42	43	47	45	46	44	47	43	44	47	43	49
40	49	49	46	44	46	50	47	49	47	50	45	50	50	46	53
45	53	52	52	53	52	54	50	52	50	53	51	56	52	51	57
50	60	56	59	60	58	57	57	55	58	56	53	60	55	53	61
55	63	63	61	64	62	61	61	59	62	59	58	64	60	57	65
60	67	71	69	72	71	68	65	67	70	68	65	70	68	69	68
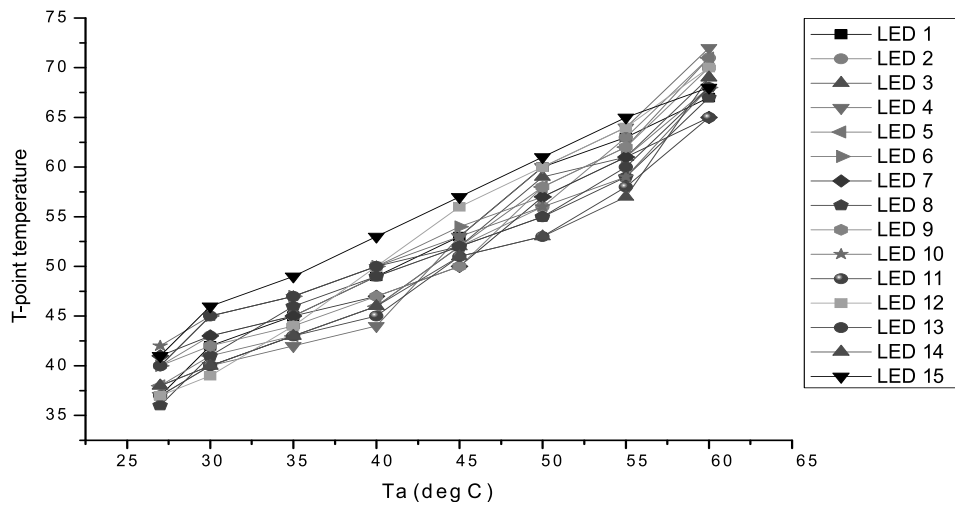
Fig. 3. T_a (°C) vs. T-point temperature for different LEDs.

inside. The experiment, as mentioned, is carried out in two steps.

2.1. Variation of junction temperature with change in ambient temperature

The first step includes the observation of junction temperature with respect to different ambient temperatures. The LEDs are subjected to different ambient temperatures and the corresponding changes in T-point temperature are observed. The results are tabulated (Table 1) and plotted as shown in Fig. 3. The ambient temperature is varied from 27 °C to 60 °C.

The data hence obtained are plotted using ORIGIN Pro 8 and as evident the T-point temperature increases exponentially with corresponding increase in ambient temperature. The equation fits the phenomenon with the value of R-square at 99.68%. The equation of the fit is analysed using ORIGIN Pro 8 and evaluated as hereunder:

$$y = A_1 e^{(-\frac{x}{t_1})} + y_0, \quad (1)$$

where 'y' and 'x' represents T-point temperature and ambient temperature (T_a) in degree Celsius respectively. The terms 'A_1', 't_1' and 'y_0' are constants having values as 1.5532, 19.23 and 35.75 respectively.

2.2. Variation in light output with change in T-point temperature

In the next step the variation in light output for corresponding changes in T-point temperature
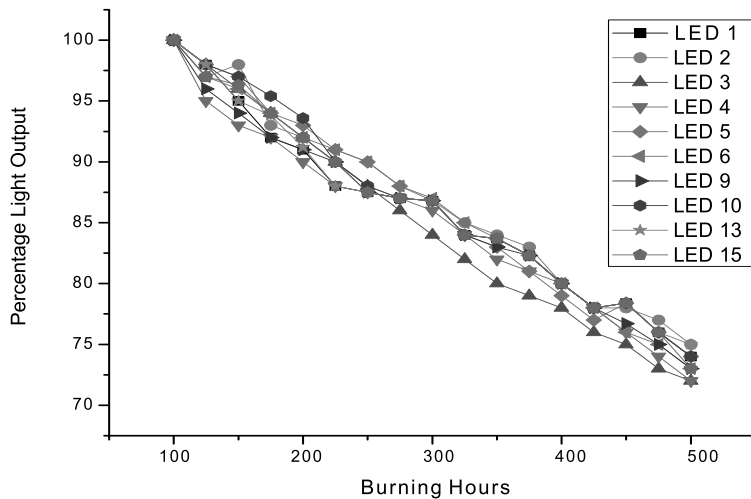
Fig.4. Percentage light output vs. burning hours under stressed condition

is observed. The LEDs are subjected to an ambient temperature of 50 °C and the percentage light output are measured for 500 burning hours. The ambient temperature corresponds to the operating temperature for the LEDs under test [10, 11]. This temperature creates sufficient stress for the LEDs [12, 13]. The interval between two successive measurements is 25 burning hours. The interval is to allow the junction heat to rise sufficiently before the next reading takes place. The results obtained are plotted as in Fig. 4. The set of regression fit hence obtained depicts the underlying aspect of LED light output with respect to stressed condition. The decrease in light output is extrapolated. It is understood that T-point temperature increases with increase in the burning hours and subsequently reduces the light output. The data are obtained for all the samples on test. The LEDs earmarked for these test are LED1, LED2, LED3, LED4, LED5, LED6, LED9, LED10, LED13 and LED15. The rest of the LEDs are unable to bear the stress and reached their end of life before the completion of the test. The cause of failure was yet to be investigated.

From Fig. 4 the decay in light output is observed to follow an exponential curve. The equation for the fit is as hereunder with an R-square of 99.05%:

$$y = A_2 e^{R_0 x} + y_0, \qquad (2)$$

where 'y' corresponds to percentage light output and 'x' relates to the burning hours for the LEDs under test. The constants 'A_2', 'R_0' and 'y_0' cor-

responds to the values of 48.61, 59.15 and −0.00159 respectively.

3. INFERENCE

The conducted test is mainly aimed at addressing the issues pertaining to ambient temperature and the corresponding effect it has on the performance of high flux LEDs. As observed with the rise in ambient temperature, the T-point temperature also increases. The information of T-point temperature is an important tool considering the fact that how easily the luminaire will dissipate heat. A low T-point temperature rating with a high ambient temperature will pose difficulties in heat dissipation with a passive heat sink. Thus, luminaires with a low T-point rating will require a fan or an active heat sink thus increasing the cost of the luminaire. On the contrary a higher T-point rating will allow passive heat sink to dissipate heat from the luminaire easily.

Again, from the second experiment the rise in operating temperature also decays the light output substantially. For LED1, LED5 and LED10 the percentage light output is decreased from 100% to 74%. In the case of LED2 and LED13 it reduces to 75%. The reduction in percentage light output for LED3 and LED4 is 72%. It degrades to 73% for LED6, LED9 and LED15. It is hence observed that the increase in operating temperature will affect the light output.

The mathematical relation also illustrates the inherent relation between ambient temperature and T-point temperature in the first case. In the second relation the relationship between light output and burning hours are observed.

These tests and similar tests offer the underlying aspect of LEDs sensitivity towards temperature. The ambient temperature plays a vital role as most of the LED luminaires are enclosed and the heat trapped inside the luminaires is very significant in reference to the light output of LEDs.

REFERENCES

1. J. Bullough, "Light Emitting Diode Lighting Systems, Lighting Answers," vol.7 no.3, National Lighting

Product Information Program, Lighting Research Centre, 2003, Troy, NY.

2. The Alliance for Solid State Illuminations and Technologies, ASSIST, Osram Opto Semiconductors, "LED Basics", 1st September 2010, pp. 1−26.

3. The Alliance for Solid State Illuminations and Technologies, ASSIST, PHILIPS LUMILEDS, "Technology White Paper, Understanding power LED lifetime analysis", 2008, pp. 1−11.

4. Y. Xi and E.F. Schubert, "Junction−Temperature Measurement in GaN Ultraviolet Light-Emitting Diodes Using Diode Forward Voltage Method," Applied Physics Letters, Sep. 2004, Vol. 85, # 12, p. 2163.

5. N. Narendran, J.D. Bullough, N. Maliyagoda and A. Bierman, "What is the Useful Life for White LEDs?" Journal Illuminating Engineering Society, January 2001, Vol. 30, issue 1, pp. 57−67.

6. A. Jayawardena, Yi-wei Liu, N. Narendran, "Methods for Estimating the Junction Temperature of AC LEDs", Council for Optical Radiation Measurements (CORM) 2012 Annual Technical Conference Ottawa, Ontario, 29 May − 1 June 2012.

7. IEC62612, "Self-Ballasted LED Lamps for General Lighting Services with Supply Voltages > 50 V − Performance Requirements", International Electrotechnical Commission, June 2013.

8. G. Meneghesso, S. Levada, R. Pierobon, F. Rampazzo, E. Zanoni, A. Cavallini, A. Castaldini, G. Scamarcio, S. Du, and I. Eliashevich, "Degradation Mechanisms of Gan-Based Leds after Accelerated DC Current Aging," in IEDM Tech. Dig., 2005, pp. 103−106.

9. L. Trevisanello, M. Meneghini, G. Mura, M. Vanzi, M. Pavesi, G. Meneghesso, and E. Zanoni, "Accelerated Life Test on High Brightness Light Emitting Diode", IEEE Transactions on Device and Materials Reliability, June 2008, Vol. 8, # 2, pp. 304−311.

10. E.Hong, N. Narendran, "A Method of Projecting Useful Life of LED Lighting Systems", Third International Conference on Solid State Lighting, Proceedings of Photo-Optical Instrumentation Engineers, 2004, SPIE: 5187, pp. 93−99.

11. N. Narendran and Y. Gu, "Life of LED based white light sources", IEEE / OSA,

Journal of Display Technology, 2005, Vol.1, #1, pp. 167−171.

12. C. H. Chen, W.L. Tsai, M.Y. Tsai, "Thermal Resistance and Reliability of Low Cost and High Power LED Packages under WHTOL Test", Electronics materials and packaging, EMAP2008, Taipei, Oct 2008, 22−24, pp. 271−276.

13. G. Farkas, Q. Van Voorst Vader, A. Poppe, and G. Bogná, "Thermal Investigation of High Power Optical Devices by Transient Testing", IEEE Transaction Components Packaging Technology, March 2005, Vol. 28, # 1, pp. 45−50.

Aniruddha Mukherjee
received his B.E. degree from NIT Silchar and his M.E. degree from Jadavpur University in Electrical Engineering. He has around eighteen years of experience including industry and teaching. He is currently associated with Suresh Gyan Vihar University Jaipur. His present field of research has been to explore the parameters involving the lifetime in CFLs, LEDs and HID lamps. He has also authored several papers in these areas of research

Amit Soni
received his M. Tech. and Ph.D. From MNIT Jaipur. His field of research has been on solar PV Materials & Its Applications, Renewable Energy, lighting applications. He has profound expertise in these areas and has good number of publications in reputed journals. He has more than fifteen years of experience in teaching and industry and is currently the Head of the department of Electrical and Electronics Engineering in Manipal University Jaipur

Solatube® Technology: Prospective Application in Architecture and Building in Russia

Fig. 4. *Solatube*® M74 collector of SkyVoult series (740 mm) on a roof of a building. A combination of the collector and Fresnel lenses on the dome (Raybender® technology) provides constancy of luminous flux within all light day, including morning and evening periods due to catching light rays at low angles of the sun above the horizon
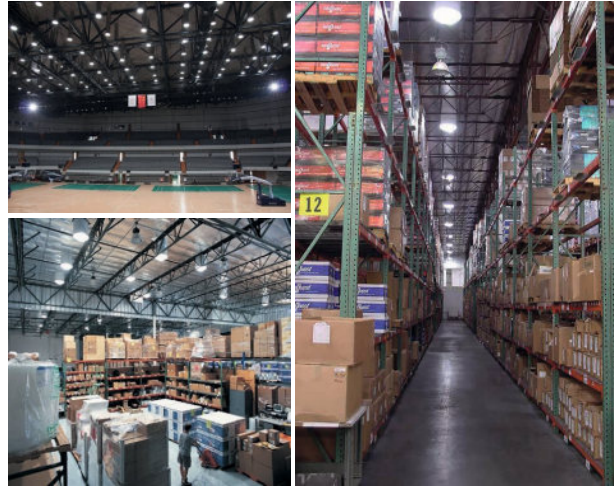
Fig. 6. *Solatube*® M74 model illuminating rooms with high ceilings

Fig. 7. *Solatube*® system illuminating a kindergarten (Krasnodar)

Fig. 9. *Solatube*® 330DS model illuminating underground car service centre of the KIA car dealership (Sochi)

Fig. 8. *Solatube*® 290DS model illuminating underground rooms of the Legal Academy (Nizhny Novgorod)

61

Fig. 2. A comparison histogram of subjective evaluation of colours of red-yellow samples with illumination using an incandescent lamp and the light-emitting diode reference source

Fig. 3. A comparison histogram of subjective values of colours of blue-green samples with illumi-nation using an incandescent lamp and the light-emitting diode reference source

Fig. 4. Spectra of colouring red, yellow, dark blue, green and of the reference light-emitting diode radiations

Fig. 5. Illumination of a multi-colour composition using the reference radiation (at the left) and R radiation (on the right)

Fig. 6. Illumination of a multi-colour composition using the reference radiation (at the left) and A radiation (on the right)

Fig. 7. Illumination of a multi-colour composition using the reference radiation (at the left) and B radiation (on the right)

Fig. 8. Illumination of a multi-colour composition using the reference radiation (at the left) and G radiation (on the right)

Hongyi Cai and Linjie Li

How LED Lighting May Affect Office Ergonomics: The Impact of Providing Access to Continuous Dimming Controls on Typing and Colour-Matching Tasks Performance

a)   b)

Fig. 1. Experiment setup in the windowless test room, (a) fisheye view of the test room, (b) a participant with his head on the adjustable chinrest, (c) plan view of the test room

a)   b)

Fig. 3. Typing task, (a) text printed black/white on letter-sized sheets mounted on the document holder, (b) the interface of the NRC Typing Task software
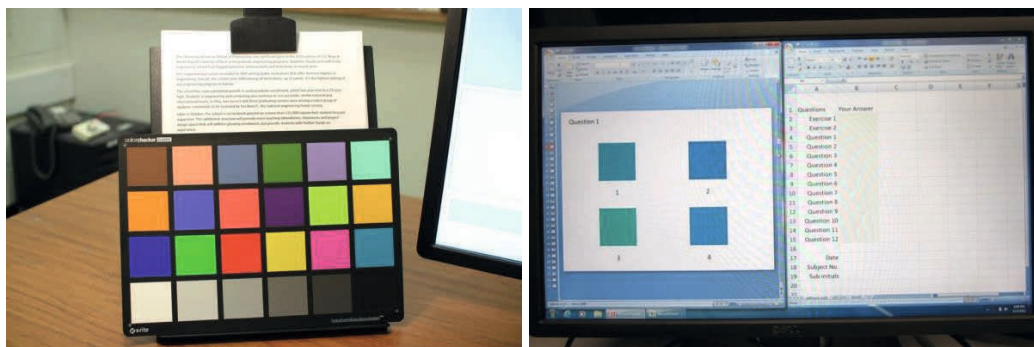
a)   b)

Fig. 4. Colour-matching task, (a) X-rite Classic Macbeth colour checker, (b) the interface of colour matching task showing the four candidate colours on the second PPT slide

DEVELOPMENT AND VALIDATION OF DYNAMIC CONDUCTANCE BASED WATTAGE INDEPENDENT MODEL FOR MAGNETIC BALLAST DRIVEN NON-RETROFIT CFLS

Biswadeep Gupta Bakshi[1], Aparajita Dutta[2], and Biswanath Roy[3]

[1]*Calcutta Institute of Engineering and Management, India*
[2]*AWA Lighting Designers, India*
[3]*Electrical Engineering Department, Jadavpur University, India*
E-mail: broy@ee.jdvu.ac.in

ABSTRACT

This paper presents a wattage independent mathematical model for non-retrofit Compact Fluorescent Lamps (CFLs) driven by magnetic ballast at nominal frequency (50 Hz), which is implemented using Matlab-Simulink. This developed model reproduces time-dependent electrical behavioural pattern of lamp system taking supply voltage as input and is modified form of existing dynamic conductance model, in which the rate of change of charge carriers inside the discharge tube is represented by physical phenomena, viz. ionization, recombination and wall diffusion. In the pre-existing model, four coefficients A, B, C and D are used to describe these physical phenomena for a particular wattage lamp and model implementation is done without considering electrical parameters of the ballast, however, it is replaced by a sinusoidal current source. Whereas, this modified wattage independent model includes magnetic ballast with its electrical parameters and applicable for a range of lamp wattage (7−18) W. The developed model is compared with a test lamp of 9 W throughout a wide range of supply voltage (200−260) V. Simulation results show close approximation of the actual lamp system and the developed model can be utilized for ballast design.

Keywords: wattage independent lamp model, magnetic ballast, Non-retrofit CFL, dynamic conductance

1. INTRODUCTION

Tubular and compact fluorescent lamps, which are basically low pressure mercury vapour lamp, are widely used light sources in indoor artificial lighting because of their good luminous efficacy and acceptable colour property. Even after the widespread availability of LEDs, fluorescent lamps are still most popularly used light sources in the developing countries, like India due to low initial cost, improved running performances and long burning hours [1]. Various complex physical processes are involved in light production from these discharge lamps. Mathematical modelling of such lamp system provides various benefits viz.: 1) Simulation of electrical behaviour; 2) Studies and analysis of complex V-I characteristics; 3) Design of ballasts; 4) Electrical power quality studies [2, 3].

One of the most commonly used modelling techniques is based on lamp heat balance equations [4−9]. In this approach, rate of change of arc temperature is described in terms of lamp power consumption, thermal radiation and conduction loss. Heat balance model is mostly implemented in PSpice and further incorporates cathode electrode voltage drop and starting warm-up phase [6, 7]. Recently, the same model is modified to produce a semi-theoretical model to include dimming process and tube temperature effects and it is validated using different tubular and compact fluorescent lamps [8, 9].

In comparison with the heat balance model, a simpler lamp model based on lamp dynamic conductance was first proposed by G. Zissis et al [10]. The authors introduced a model which was derived from Francis' energy balance equation [11] and theoretical basis of the model is the time-varying nature of arc column conductance within the discharge tube. More the charge carrier density inside the discharge tube more will be the conductance and less will be the arc resistance. The first dynamic conductance model is referred to as 'quadratic model' as the right hand side of the equation is actually a quadratic polynomial [12]. This quadratic model is modified by J.C. Anton et al to a polynomial model which gave better simulation results for high intensity discharge lamps [13]. In quadratic and polynomial model the recombination loss inside the discharge tube is modelled to be varying as the square of the conductance. Thereafter, J.C. Anton et al proposed that it would be a better approximation to express the recombination loss as an exponential function of conductance [14]. This exponential model is further validated for both low and high frequency operation [2].

Based on Francis energy balance equation, some researchers have also proposed physical discharge lamp model, which relates terminal electrical behaviours with lamp's geometric dimension, cold spot temperature, gas composition [15−17]. In this approach, thrust is given to micro-level discharge phenomena, viz. ion mobility, transportation rate, ambipolar diffusion coefficient, which make the model unsuitable to formulate through terminal electrical behaviour.
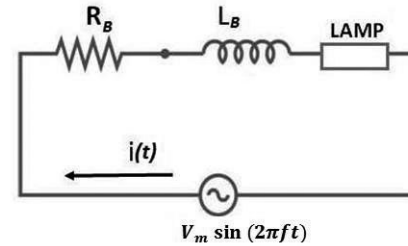
Fig. 1. Electrical circuit for lamp and magnetic ballast system

In the implementation of exponential dynamic conductance model [2], there are three main shortcomings, viz.:

1. In the pre-existing model, instead of physical parameters of the ballast itself, it is approximated to be a sinusoidal current source feeding the lamp (but in practice, due to highly non-linear nature of the lamp, the current distorted from a true sinusoid); 2. The lamp model input was sinusoidal rated current instead of voltage; 3. The existing conductance models are wattage-specific, i.e. the experimentally obtained model coefficients describe that particular lamp only and cannot be used for other lamps having different wattage.

In order to develop the proposed wattage independent model, a modified form of dynamic conductance model [2,10−14] is used. In this regard, other thermal and physical modelling techniques are not chosen due to their complexity and requirement of some data, which are quite difficult to find out experimentally, viz. arc temperature, electron temperature, gas pressure, electron mobility [4−9, 15−17]. As compared to these techniques, synthesis of dynamic conductance model requires
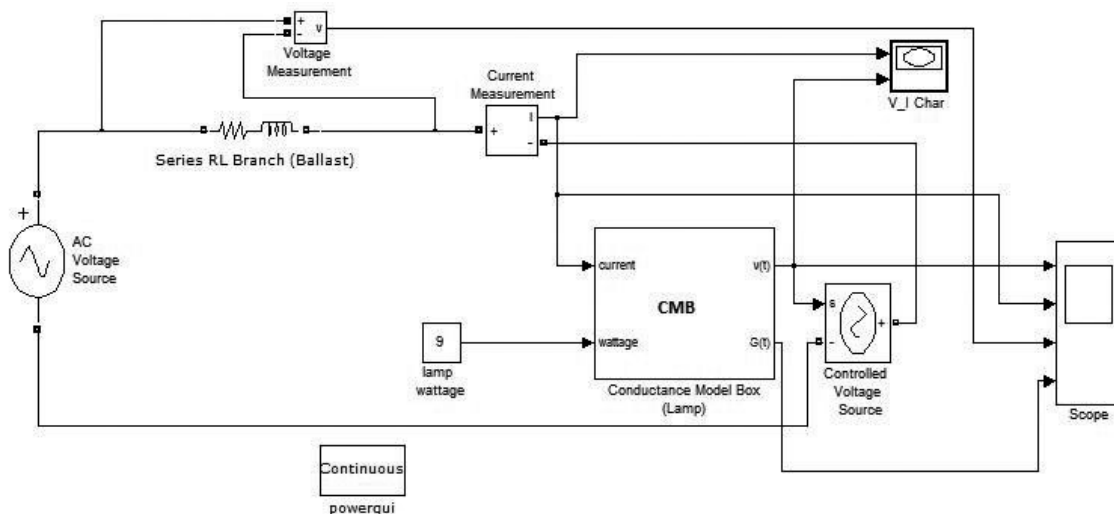
Fig. 2. Simulink Implementation of complete lamp-ballast system
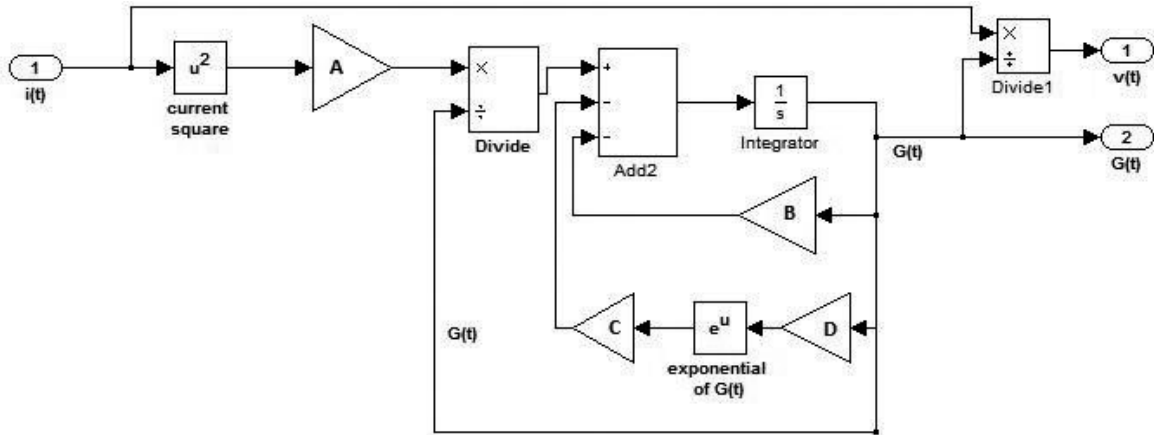
Fig. 3. Formulation of 'Conductance Model Box' subsystem based on lamp model eqn. (1)
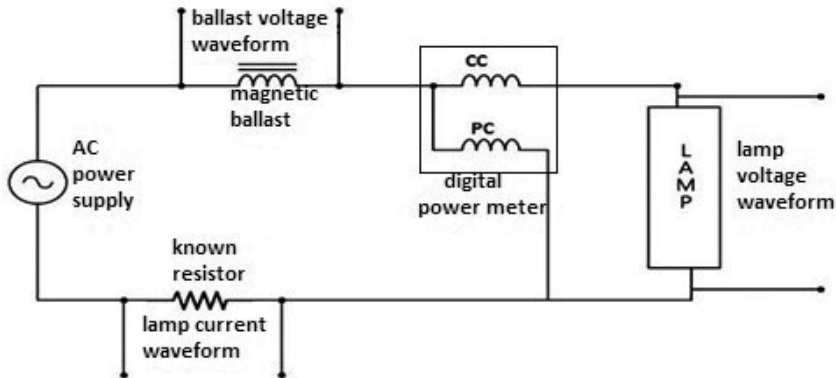
Fig. 4. Experimental circuit diagram used for coefficient synthesis and model validation

only the terminal electrical characteristics of the lamp [18]. The developed wattage independent model replaces the four wattage-specific model coefficients A, B, C, D with four user defined functions obtained from experimental measurements using a set of five lamps (7–18)W. After software implementation, the proposed model is validated using an Osram-made 9 W test lamp.

2. EXISTING DYNAMIC CONDUCTANCE MODEL OF LOW PRESSURE DISCHARGE LAMPS

The conductance (or resistance) inside the discharge tube of a lamp does not remain constant; it is directly proportional to the charge carrier (mainly electron) density inside the lamp [10]. Discharge tube contains gases (like argon, krypton etc.) and metal vapour under certain low pressure. When voltage is applied across the electrodes, electrons rush towards the anode from the cathode end and collide with neutral gas, metal atoms to make them ionized [19]. This ionization process is liable to increase the lamp conductance because more the number of charge carriers, more will be the conductance of the arc. On the other hand, some electrons recombine with the ions and reproduce neutral atoms. This recombination causes the reduction in lamp conductance [10, 13]. Apart from recombination, some electrons are diffused towards the lamp wall and do not participate in the discharge. As a whole, lamp conductance is a 'dynamic' quantity, which is dependent of three main factors: ionization, recombination and the tube wall loss [2].

Taking the three factors into consideration, the existing mathematical model based on dynamic conductance [2, 14] is expressed as:

$$\frac{dG(t)}{dt} = A*i(t)v(t) - B*G(t) - - C*\exp[D*G(t)], \tag{1}$$

where, $G(t)$ is lamp dynamic conductance, $i(t)$ is instantaneous lamp current, $v(t)$ is instanta-

Table 1. Computed lamp model coefficients (obtained at 240 V, 50 Hz)

Lamp Wattage W	Maker's Name & Model	Computed model coefficients			
		A	B	C	D
7	Osram Dulux S	0.9559	1574	1	1.671
10	Osram Dulux S	0.503	1497	0.5	2
11	Osram Dulux S	0.2514	1374	0.4	4.095
13	Osram Dulux S	0.1884	771.7	0.35	5.003
18	Osram Dulux D	0.06	494.2	0.1	9.99

neous lamp voltage, *A, B, C, D* is lamp model coefficients.

The first order differential equation (1) is the basic lamp model equation, which holds good for low pressure discharge lamps, i.e. fluorescent lamps and CFLs [2]. The implementation of eqn. (1) is referred to as 'conductance model box' (CMB) in the previous works [2, 14] where eqn. (1) is solved to get $G(t)$ taking current $i(t)$ as input. Then $i(t)$ itself is divided by $G(t)$ to produce lamp voltage $v(t)$. Electrical behaviour of a specific wattage lamp is entirely dependent on its A, B, C, D coefficients. The relationship of these coefficients with the physical discharge processes are discussed in the next section.

3. PHYSICAL BASIS OF MODEL COEFFICIENTS

The dynamic conductance model is developed in recent literatures on the basis of Francis' energy balance [11] equation:

$$\frac{d\eta_e}{dt} = P_e + L_e, \tag{2}$$

where η_e is average density of free electrons, P_e is production rate of electrons, L_e is rate of loss of electrons.

The production rate of electrons is directly proportional to the instantaneous input electrical power [2]:

$$P_e = k_1 i(t)v(t) \tag{3}$$

The loss rate of electrons can be divided as:

Table 2. Measured ballast parameters

Lamp Wattage, W	Ballast		Maker's Name
	Parameters		
	Resistance, R_B, Ω	Inductance, L_B, H	
7	139.15	3.88	ECB
10	195.36	4.48	Philips
11	138.82	4.84	ECB
13	195.25	4.03	Philips
18	104.39	3.51	Philips
9 (for model validation)	123.5	4.245	Philips

$$L_e = L_W + L_R, \tag{4}$$

where L_W is wall loss rate, L_R is recombination loss rate.

The above loss rates can be expressed in terms of average density of free electrons (η_e) as [2]:

$$L_W = -k_2\eta_e, \tag{5}$$

$$L_R = -k_3 \exp(k_4\eta_e). \tag{6}$$

In the right hand side of equation (5) and (6), negative sign indicates decrease in electron density. The dynamic conductance $G(t)$ can be expressed as:

$$G(t) = \frac{i(t)}{v(t)} = k_5\eta_e. \tag{7}$$

In eqns. (3–7) k_1, k_2, k_3, k_4, k_5 are proportionality constants [2]. Replacing the values of P_e and L_e, eqn. (2), it can be rewritten as:

Table 3. Result summary of the curve fitting process

Coefficient Function	Equation of the fitted curve	Type of fit	Value of the constants
A (W)	$A(W) = a*\exp(b*W) + c*\exp(d*W)$	exponential	$a = 18.95$, $b = -0.3703$ $c = -8.397 \times 10^{14}$, $d = -5.019$
B (W)	$B(W) = a_1 \exp[-\left(\dfrac{W - b_1}{c_1}\right)^2]$	Gaussian	$a_1 = 1460$, $b_1 = 7.55$, $c_1 = 9$
C (W)	$C(W) = a_2*\exp(b_2*W) + c_2*\exp(d_2*W)$	exponential	$a_2 = 4.7 \times 10^{12}$, $b_2 = -4.42$ $c_2 = -2.6$, $d_2 = -0.167$
D (W)	$D(W) = p_1 W^3 + p_2 W^2 + p_3 W + p_4$	Cubic polynomial	$p_1 = -0.0078$, $p_2 = 0.3273$ $p_3 = -3.536$, $p_4 = 13.01$
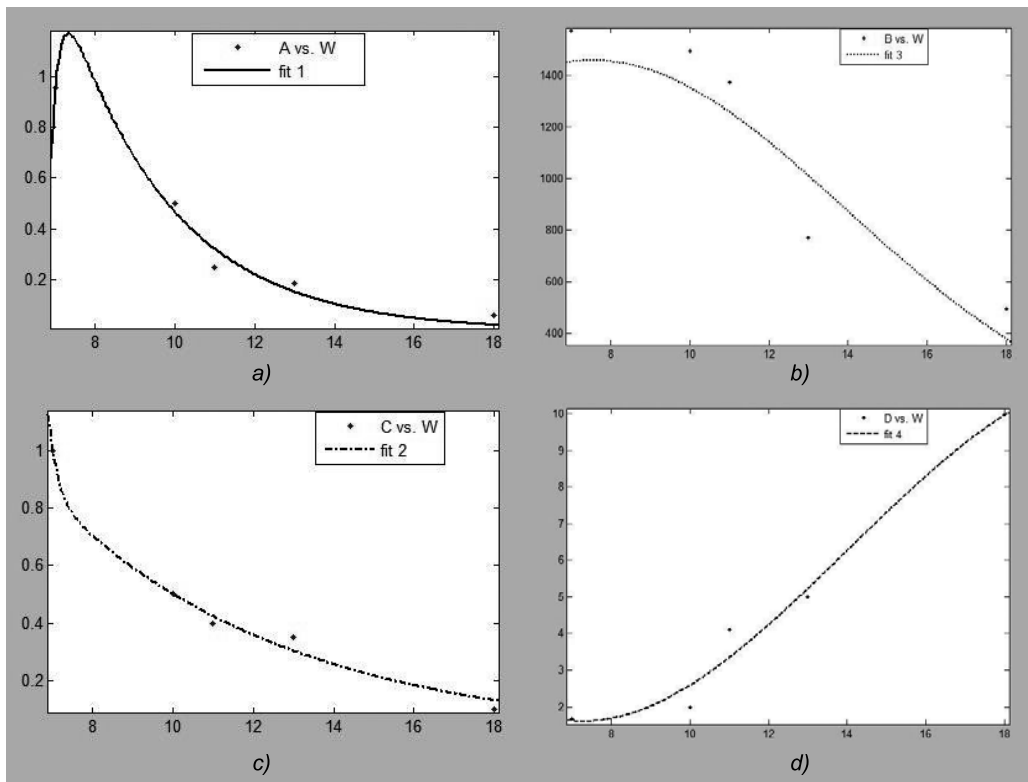
Fig. 5. Fitted curve with respect to lamp wattage for: (a) coefficient A, (b) coefficient B, (c) coefficient C and (d) coefficient D

$$\frac{d\eta_e}{dt} = k_1 i(t)v(t) - k_2\eta_e - k_3\exp(k_4\eta_e). \qquad (8)$$

Replacing η_e with $G(t)$ and multiplying both sides with k_5, eqn. (8) got its final form as:

$$\frac{dG(t)}{dt} = k_1 k_5 i(t)v(t) - $$
$$-k_2 G(t) - k_3 k_5 \exp[(k_4 / k_5)G(t)]. \qquad (9)$$

By comparing eqns. (1) and (9) we get:

Table 4. Lamp system quantities (measured and simulated)

Quantity	Supply Voltage					
	200 V		240 V (rated)		260 V	
Lamp Voltage (V-RMS)	Measured	55.1	Measured	51.2	Measured	49.4
	Simulated	52.67	Simulated	51.01	Simulated	50.4
Lamp Current (A-RMS)	Measured	0.1243	Measured	0.172	Measured	0.206
	Simulated	0.133	Simulated	0.165	Simulated	0.186
Ballast Voltage (V-RMS)	Measured	182	Measured	227	Measured	248
	Simulated	179.3	Simulated	221.42	Simulated	242.1
System Power (W)	Measured	9.7	Measured	12.7	Measured	15.75
	Simulated	9.41	Simulated	12.44	Simulated	14.25
Lamp conductance (mS)	Measured	2.26	Measured	3.36	Measured	4.18
	Simulated	2.53	Simulated	3.23	Simulated	3.76

$$A = k_1 k_5$$
$$B = k_2$$
$$C = k_3 k_5$$
$$D = k_4 / k_5$$

So it can be concluded that A, B, C, D coefficients are determining the discharge phenomena. The production rate of electrons and loss rate of electrons due to wall diffusion are related to coefficient A and B respectively, whereas the rate of recombination is related to coefficients C and D.

4. PROPOSED MODEL OF CFL-MAGNETIC BALLAST SYSTEM

For developing the complete lamp system model, following considerations are taken: 1. Lamp's behaviour is governed by exponential dynamic conductance model given in eqn. (1); 2. The lamp is driven by magnetic ballast, which is represented by inductance L_B having internal resistance R_B; 3. The supply voltage is sinusoidal having the frequency 50 Hz.

The lamp system considered for modelling is shown in Fig. 1, which is basically an AC series circuit [20, 21].

Matlab-Simulink implementation of the lamp system is shown in Fig. 2, in which the ballast is represented by a series R-L branch. A current measurement block is sensing the system cur-

Fig. 6. Function parameter settings of A (W) during model validation

rent, which is fed to a subsystem named as conductance model box (CMB). The CMB is actually representing the lamp itself and its details are shown in Fig. 3. CMB is having four gain blocks corresponding to four model coefficients A, B, C, D. The output of CMB is the instantaneous lamp voltage $v(t)$. The simulated lamp voltage drop is added in series with the ac voltage source and the ballast through a 'controlled voltage source' block taken from 'SimPowerSystems' library. In order to carry out mathematical computation, this library calls for an additional solver block 'powergui' [22]. To obtain the waveforms, 'scope' block is used whereas the lamp $v(t)$-$i(t)$ characteristic is observed using '*x-y*' graph.

Fig. 7. Modified Conductance Model Box (Wattage Independent Lamp Model)

a)   b)
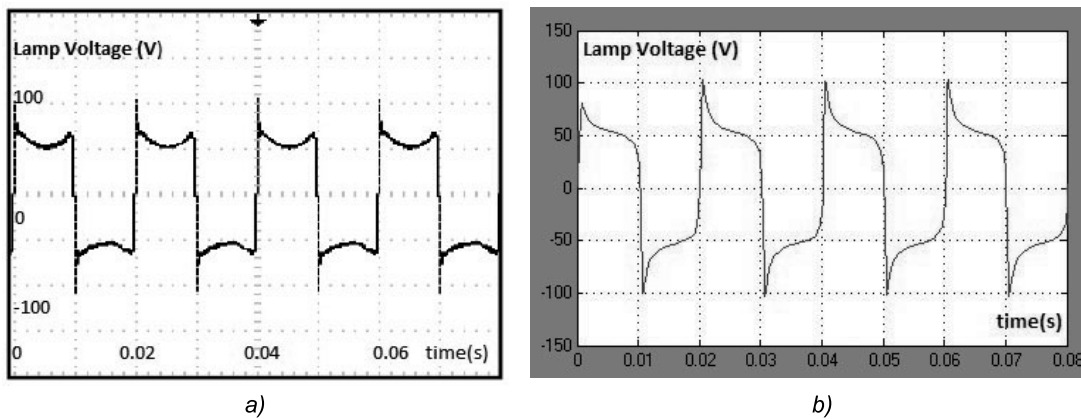
Fig. 8. Lamp Voltage waveform for 9 W CFL at 240 V, 50 Hz: (a) measured, (b) simulated

5. DEVELOPMENT AND IMPLEMENTATION OF WATTAGE INDEPENDENT LAMP SYSTEM MODEL

To develop the wattage independent lamp system model, firstly, the model coefficients A, B, C, D are computed for five different wattage non-retrofit CFLs (7–18) W using following steps:

1. First order differential eqn. (1) is converted into an algebraic difference equation (10) by Euler's method [2] as:

$$\frac{G(t_n)-G(t_{n-1})}{t_n-t_{n-1}} = Ai(t_n)v(t_n)- \\ -BG(t_n)-C\exp[DG(t_n)], \quad (10)$$

where t_n is time instant of taking lamp, *v(t)-i(t)* is data, $i(t_n)$ is current at n^{th} instant of time, $v(t_n)$ is lamp voltage at n^{th} instant of time, $G(t_n)=i(t_n)/v(t_n)$ is lamp conductance at t_n.

2. For curve fitting purpose, difference eqn. (10) is further expressed as:

$$y = AV^2x - Bx - C\exp(Dx), \quad (11)$$

where $x = G(t_n)$ is independent variable,

$y = \dfrac{G(t_n)-G(t_{n-1})}{t_n-t_{n-1}}$ is dependent variable, *V* is ave-

rage value of the lamp voltage $v(t_n)$, which is taken from the steady regions.

3. For a particular wattage lamp, x and y variables are obtained from experimentally measured lamp voltage and current data at rated supply voltage with respect to time and the corresponding circuit diagram is shown in Fig. 4. The voltage and current waveforms (in both, CSV and images formats) are measured using Tektronix 1012 B digital storage oscilloscope. A known low resistor of 0.66 Ω is used to obtain the current waveform indirectly in terms of equivalent voltage drop. Yokogawa WT

71
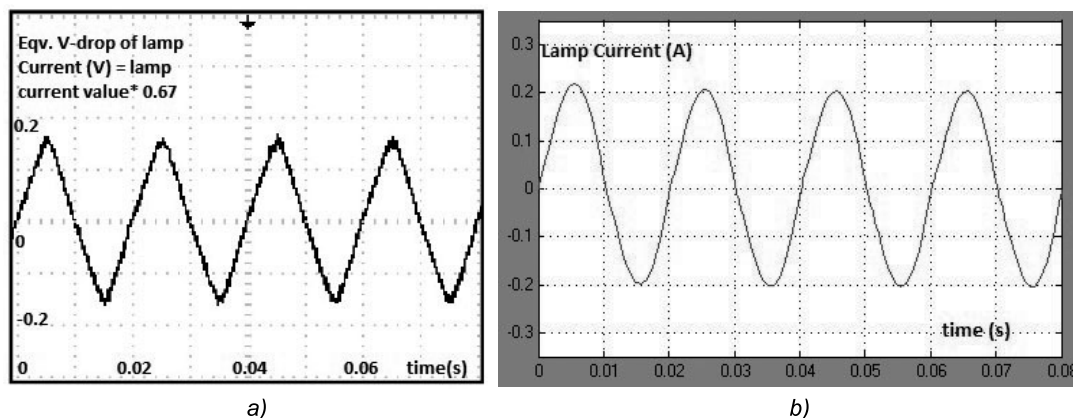
Fig. 9. Lamp Current waveform for 9 W CFL at 240 V, 50 Hz: (a) measured, (b) simulated

210 digital power meter is used to measure RMS values of lamp voltage, current, power consumption, power factor and ballast voltage.

4. Finally, Matlab curve fitting toolbox [23] is used to compute the numerical values of A, B, C, D coefficients for the specific lamp wattage. The data set is created as '*y vs x*' on the basis of experimental results and eqn. (11) is used as the custom equation. The best fitted curve is selected and the corresponding values of the model coefficients are shown in the Table 1. Along with the model coefficients, the measured ballast parameters are tabulated in Table 2.

The values of model coefficients A, B, C, D vary with lamp wattage as shown in Table 1 and it is expected since these coefficients determine the discharge process as discussed in section 3. Hence, the variation in model coefficient values ultimately causes change in the electrical and photometric properties of the lamp system, viz. current, voltage, ballast drop, light output. Considering this fact, the nature of coefficient variation is sought by curve fitting process, which is accomplished by Matlab curve fitting tool [23]. The fitted curves are shown in Figs. 5 a-5 d and corresponding results are summarized in Table 3.

Therefore, for any CFL (having wattage within the range considered) the model coefficients can be predicted from the four functions of lamp power. Hence Simulink implementation of the lamp model, i.e. CMB is modified: the four gain blocks are replaced by four user defined functions, viz., A (W), B (W), C (W) and D (W). For this purpose, four 'function blocks' are used, which take the lamp wattage as input and generates lamp model coefficients applicable for that particular lamp. For example, setting is shown for function A (W)

in Fig. 6. The outputs of the function blocks are multiplied with the required signals to accomplish the mathematical computation. The modified CMB for wattage independent model is shown in Fig. 7.

6. EXPERIMENTAL VALIDATION OF DEVELOPED WATTAGE INDEPENDENT MODEL

After Simulink implementation, the proposed wattage independent lamp model is validated through comparative analysis with experimental results obtained from an actual lamp. For validation purpose an Osram 9 W lamp is used, at the same time, in the simulation window, the lamp wattage is set to be 9 W. Firstly, the simulated waveforms are compared with the experimental waveforms obtained using Tektronix 1012 B DSO as given in Figs. 8–10. The simulated lamp voltage wave matches well with the experimental waveform, which can be characterized by an alternating square-shaped wave with pronounced restriking peaks at each zero crossings. The lamp current waveforms (both simulated and experimental) are slightly deviated from pure sinusoid, which proves the presence of non-linearity in the discharge lamp system. The ballast voltage waveform has been simulated and compared in this work, which is not reported in previous papers. It is seen that the alternating ballast voltage waveforms have two consecutive peaks: the first one has the higher altitude than the second one and the whole cycle repeats at supply frequency (50 Hz) at an interval of 20 ms. Moreover, as compared to the lamp voltage, the corresponding ballast voltage amplitude or the RMS values are nearly four times greater. Along
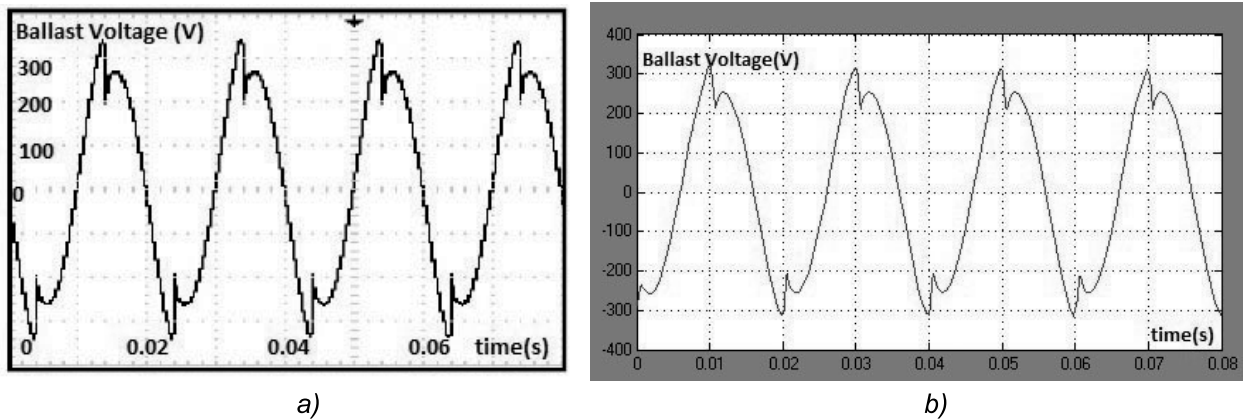
Fig. 10. Ballast Voltage waveform for 9 W CFL at 240 V, 50 Hz: (a) measured, (b) simulated
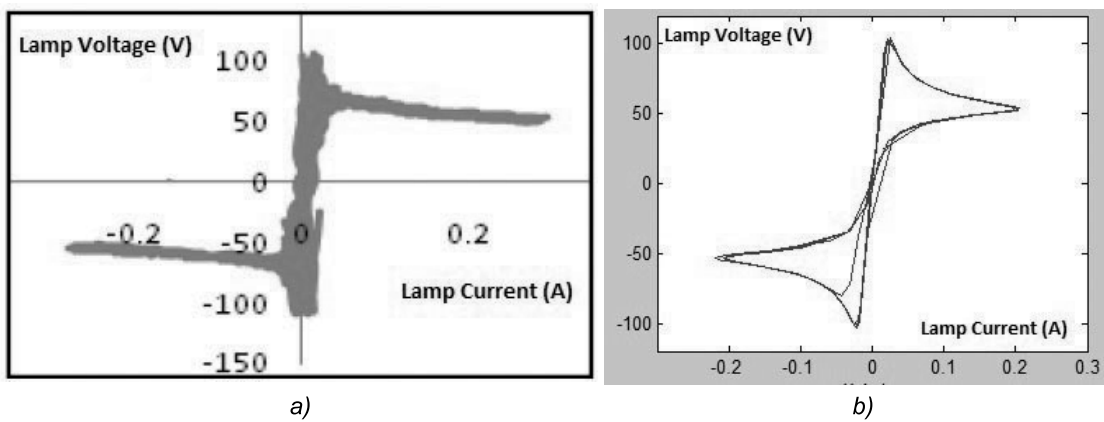
Fig. 11. Lamp V-I characteristics for 9 W CFL at 240 V, 50 Hz: (a) measured, (b) simulated
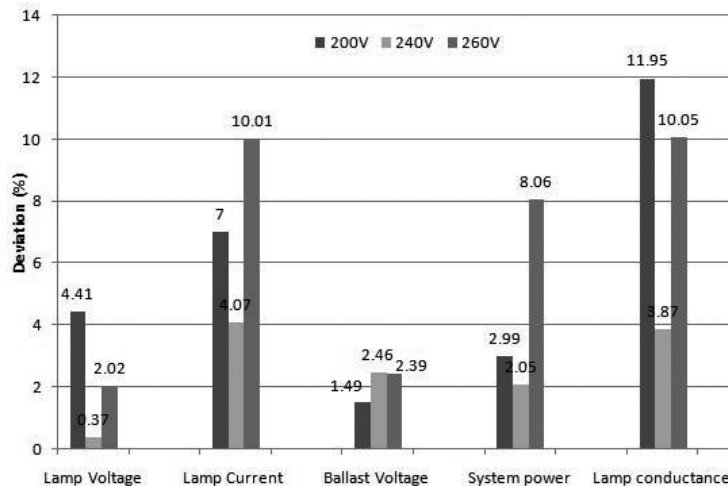
Fig. 12. Percentage deviation of the simulation results compared to the measured values (ref. Table 4)

with these waveforms, the complex lamp *v(t)-i(t)* characteristics (having 'loops' near positive and negative peak regions of the current wave) are depicted in Fig. 11.

In Figs. 8−10, the waveforms shown are the snapshots taken at rated supply voltage (240 V, 50 Hz). The nature of waveforms remains the same with the supply voltage variation, only their magnitudes differ provided the supply frequency remains constant. The measured and simulated lamp voltage, lamp current, power consumption, ballast voltage and lamp conductance are compared for minimum operating voltage (200 V), rated voltage (240 V) and maximum operating voltage (260
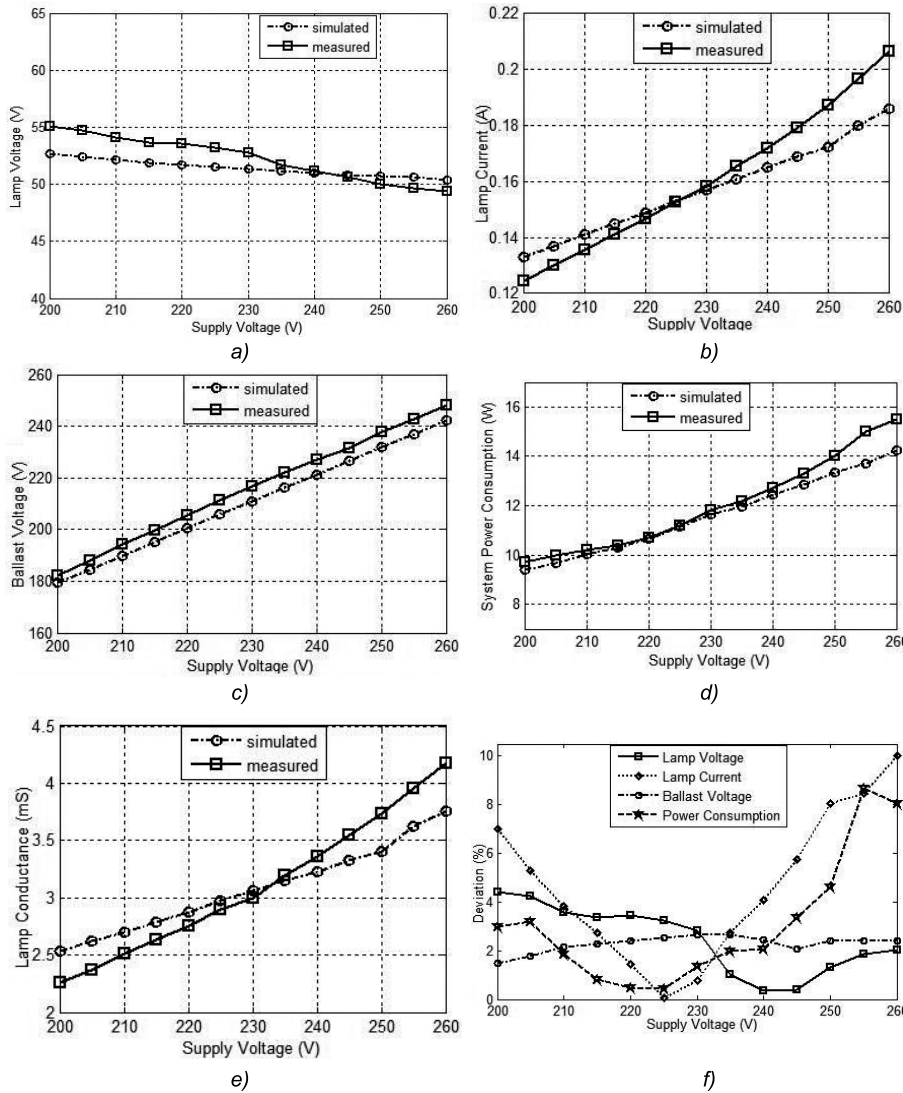
Fig. 13. Variation of electrical parameters with Supply Voltage for 9 W CFL: (a) Lamp Voltage (rms), (b) Lamp current (rms) (c) Ballast Voltage drop (rms), (d) Average power consumption by the lamp system, (e) Average Lamp conductance, and (e) Percentage deviation of simulated lamp system parameters plotted against Supply Voltage

V) at nominal frequency (50 Hz) as shown in Table 4. The percentage deviations are computed as:

$$deviation(\%) = \left| \frac{measured - simulated}{measured} \right| \times 100\% \quad \text{and}$$

represented using a bar chart given in Fig. 12.

Percentage deviations as shown in Fig. 12 reveal that minimum deviation occurs near the rated voltage (240 V), which is within 5% for all the electrical parameters. For the upper and lower supply voltages (200 V & 260 V respectively), deviations tend to increase. The maximum deviation observed to be 11.95% for lamp conductance at 200 V.

The final step of the model validation is to plot the magnitudes of various electrical quantities of the lamp system with respect to the supply volt-

age. For this purpose, the supply voltage is varied from 200 V to 260 V at 5 V interval keeping frequency fixed at 50 Hz and corresponding measured and simulated results are plotted in the same axes. The graphical variations as shown in Figs. 13 a-13 e reveal that lamp voltage decreases with the increment of supply voltage, whereas, lamp current and ballast voltage increase. The average power consumption by the lamp and the ballast also enhances with supply voltage due to increased Ohmic loss and core loss (for iron-core magnetic ballast) in the system. The simulated values lie close to that of the experimental values, especially near the usual operating range of the CFLs, i.e. 220–250 V. The percentage deviation of the simulation results with respect to the experimental results for lamp

voltage, current, ballast voltage and consumed average power plotted against the supply voltage is shown in Fig. 13 f for better representation of the model's accuracy.

7. CONCLUSION

In this paper, a wattage independent discharge lamp model applicable for low wattage non-integrated CFLs has been proposed, implemented and validated for low frequency (50 Hz) operation. Simulated waveforms and *v(t)-i(t)* characteristic gave the close resembles of the experimental data. Near the rated supply voltage (220−250) V model shows best performance to predict electrical parameters: the deviations are within 5% from the measured data.

The main advantages of the developed model are:

1. It is applicable for a wide range of lamp wattage (7−18) W, hence mitigates coefficient computational effort;

2. The model does not require any confidential data to be provided by lamp manufacturer;

3. The understanding and synthesis of the model is simple, as subatomic factors viz., ion mobility, electron energy distribution, are not taken into consideration. Such approximations, however, may have brought some inaccuracy in the model, especially near the upper 260 V and lower 200 V range of supply voltage.

The key application area of the developed model is to improve ballast design techniques. Although our proposed model is simulated under low frequency environment, the same can also be implemented for high frequency operation. Nowadays, power quality researchers need to study ballasted discharge lamp systems as they are considered to be a major cause of harmonics. For them, the proposed model can be useful. The wattage independent modelling approach presented here can also be applied for high intensity discharge (HID) lamps.

ACKNOWLEDGEMENT

REFERENCES

1. Griffiths, A.: '21 st Century Lighting Design', 1 st Edition, Bloomsbury Publication, UK, 2014, pp.160−200.

2. Blanco, C., Antón, J.C., Robles, A., et al. 'A discharge lamp model based on lamp dynamic conductance', IEEE Trans. Power Electron., 2007, Vol. 22, No.3, pp. 727−734.

3. Yan, W., Hui, S.Y.R., Chung, H., Cao, X.H. 'Genetic algorithm optimized high-intensity-discharge lamp model', IEE Electronic Letters, 2002, Vol.38, No.3, pp. 110−112.

4. Laskowski, E.L., Donoghue, J.F. 'A Model of Mercury Arc Lamp's Terminal V-I behavior', IEEE Trans. on Industry Applications, July/August 1981, Vol. IA-17, No. 4, pp. 419−426.

5. Yan, W., Hui, S.Y.R., 'A universal PSpice model for HID lamps', IEEE Trans. Ind. Appl., 2005, 41, pp. 1594−1602.

6. Yan, W., Hui, S.Y.R., Chung, H. 'Nonlinear high-intensity discharge lamp model including a dynamic electrode voltage drop', IEE Proc. Sci. Meas. Technol., 2003, 130, (4), pp. 161−167.

7. Lin, D., Yan, W., Hui, S.Y.R. 'Modelling the warm-up phase of the starting processes of high-intensity discharge lamps', IET Sci. Meas. Technol., 2011, Vol. 5, Iss. 6, pp. 199−205.

8. Lin, D., Yan, W., Hui, S.Y.R. 'Modeling of Dimmable Fluorescent Lamp Including the Tube Temperature Effects', IEEE Trans. on Ind. Electronics, Sept. 2011, Vol. 58, No. 9, pp. 4145−4152.

9. Yan, W., Tam, E., Hui, S.Y.R. 'A Semi-Theoretical Fluorescent Lamp Model for Time-Domain Transient and Steady-State Simulations', IEEE Trans. on Power Electronics, November 2007, Vol. 22, No. 6, pp. 2106−2115.

10. Zissis, G., Damelincourt, J.J., Bezanahary, T. 'Modelling discharge lamps for electronic circuit designers: A review of the existing methods', IEEE Proceedings of the Industrial Application Society, 2001, pp.1260−1262.

11. Francis, V.J., 'Fundamentals of Discharge Tube Circuits', Methuen and Co. LTD, London, 1948. pp. 39−48.

12. Koprnický, J.: 'Electric Conductivity Model Of Discharge Lamps −Self Report of PhD Thesis', Technical University of Liberec and Univer-

sity Paul Sabatier Toulouse, Laboratory of Plasma and Energy Conversion, 2007, pp 21–22.

13. Antón, J. C., Blanco, C., Ferrero, F., Roldán, P., Zissis, G. 'An equivalent conductance model for high intensity discharge lamps', Proc. IEEE IAS Conference, 2002, pp. 1494–1498.

14. Antón, J. C., Blanco, C., Ferrero, F., Roldán, P., Zissis, G. "Simulation of the dynamic behavior of HID lamps based on electrical conductance," in Proc. IEEE IECON, 2002, pp. 462–467.

15. Loo, K.H. et al 'A Dynamic Collisional-Radiative Model of A Low-Pressure Mercury–Argon Discharge Lamp: A Physical Approach to Modeling Fluorescent Lamps for Circuit Simulations', IEEE Trans. on Power Electronics, July 2004, Vol.19, No.4, pp.1117–1129.

16. Loo, K.H. et al 'A Dynamic Conductance Model of Fluorescent Lamp for Electronic Ballast Design Simulation', IEEE Trans. on Power Electronics, September 2005, Vol.20, No.5, pp.1178–1185.

17. Holloway, A.J. et al 'A Physically Based Fluorescent Lamp Model for a SPICE or a Simulink Environment', IEEE Trans. on Power Electronics, 2009, Vol.24, No.9, pp. 2101–2110.

18. Blanco, C., Antón, J.C., Robles, A., et al. 'Comparison between Different Discharge Lamp Models Based on Lamp Dynamic Conductance', IEEE Trans. Industry Applications, July/August 2011, Vol.47, No.4, pp.1983–1991.

19. Coaton, J.R., Marsden, A.M.: 'Lamps and Lighting', 3 rd Edition, Wiley Publication, 1996, pp.12, 57–69.

20. Spreadbury, F.G., 'Electric Discharge Lighting', Sir I. Pitman & Sons Ltd., 1946, pp.57–98.

21. Gupta Bakshi, B., Roy, B., 'Simulink simulation and experimental verification of magnetic ballast driven Compact Fluorescent Lamps', Proc. IEEE CALCON, 2014.

22. MATLAB SimPowerSystems, a toolbox product of Mathworks dedicated to electrical circuit and system simulation: *http://in.mathworks.com/products/simpower/,* last accessed on 31.10.2015.

23. MATLAB Curve Fitting Toolbox by Mathworks: *http://in.mathworks.com/help/curvefit/cftool.html*, last retrieved on 01.10.2015.

Biswadeep Gupta Bakshi is currently working as Assistant Professor of Electrical Engineering Department in Kolkata Institute of Engineering and Management. He did M.E. in Illumination Engineering from Electrical Engineering Department, Jadavpur University in 2013 after obtaining B.E. in Electrical Engineering from Bengal Engineering and Science University, Shibpur, India (currently IIEST, Shibpur) in 2011. His current research interest includes mathematical modelling of discharge lamp systems

Aparajita Dutta, did her M.E. in Illumination Engineering from Jadavpur University, Kolkata, India in 2014 after obtaining B.Tech. in Electrical Engineering from Meghnad Saha Institute of Technology (MSIT), India in 2012. Currently she is working as a Lighting Designer in AWA Lighting Designers, New Delhi, India – a New York based Architectural Lighting Design Company

Biswanath Roy is a Professor of Illumination Engineering at Electrical Engineering Department of Jadavpur University, India. He did Ph.D. (Engg.) on Daylighting in 1999 from Jadavpur University after having M.Sc. (Tech.) in Optics & Optoelectronics in 1993 and B.Sc. (Hons.) in Physics in 1989 from University of Kolkata. He is Life Fellow of Indian Society of Lighting Engineers (ISLE), Life Member of The Institution of Engineers (India) and Member of IESNA

ELECTRIC AND RADIATION CHARACTERISTICS OF A TRANSFORMER TYPE LAMP WITH A DISCHARGE TUBE OF 16.6 MM DIAMETER

Vladimir A. Levchenko[1], Oleg A. Popov[1], Sergei A. Svitnev[1], and Pavel V. Starshinov[*2]

[1]*National Research University "MPEI",Moscow*
[2]*LIT Open Company, Moscow*
E-mail: blitzzz-z@ya.ru

ABSTRACT

Experimental research of the electric and radiation characteristics of a transformer type lamp were performed in a closed discharge tube of 16.6 mm inner diameter, which operate in a mercury vapour (7 Torr) and inert gas (0.1−1.0 Torr) mixture at 265 kHz frequency with 180 W plasma discharge power. It is established that maximum values of energy efficiency in the mercury line of 254 nm and of HF electric field intensity in plasma, as well as minimum values of the lamp discharge current correspond to inert gas pressure of 0.3 Torr. Calculations of discharge current according to the induction discharge transformer model showed a good coincidence with the experimental results.

Keywords: induction discharge, LP mercury plasma, UV radiation, HF electric field intensity

1. INTRODUCTION

Induction mercury LP discharge lamps of the transformer type (TTL) are one of prospective sources of visible and UV radiation [1−3]. As they have no inner electrodes, TTLs can work in relatively low inert gas pressure of 0.05−0.5 Torr corresponding to as much as possible effective generation of mercury radiation in the 185 and 254 nm lines [4]. This opens up a possibility to develop effective sources of UV resonant radiation, of different power, to be used for water and air purification. Most research on TTL is concerned with the creation of durable (60−100) thousand hours and energy efficient ($\geqslant$ 100 lm/W) fluorescent TTLs with a low power load on the glass tube walls covered with a phosphor. This requires for the discharge tubes to be of relatively large diameters: about (50−70) mm [2, 4, 5]. This project is the first piece of research on TTLs with discharge tubes of a smaller diameter, equal to 15 − 25 mm, which are more effective for creating bactericidal lamps.

2. EXPERIMENTAL INSTALLATION AND MEASUREMENT METHODS

Induction discharge was fired at a frequency $f = 265$ kHz in a closed quartz tube with external and inner diameters of 19 and 16.6 mm respectively. The length of the lamp $L = 492$ mm and length of the plasma coil determined as length of the discharge tube axis, $\Lambda_{pl} = 815$ mm. The HF inductor consisted of two ring ferromagnetic cores (magnetic conductors) connected in parallel of 2 cm² section each, which were symmetrically placed on the closed discharge tube. Each of two inductance coils connected in parallel (16 turns each) enclosed its own core. Mercury vapour pressure in the discharge tube was maintained to be optimum (according to a maximum of energy efficiency of the lamp discharge part in the line of 254 nm $\eta_{e,\,254}$). 0.006−0.008 Torr by means of temperature of a mercury-indium amalgam placed on the tube wall. As buffer gases, krypton, argon and mixtures of argon with neon (30% *Ne* + 70% *Ar*) and Penning's mixture (60% *Ne* + 40% *Ar*) were used. The pressure of the buffer gas mixture ($p_{i.g.}$) was changed

from 0.1 to 1.0 Torr. The measurements were performed at a constant plasma power P_{pl} = 180 W.

The layout of the installation is presented in Fig. 1. Electric measurements were carried out using digital oscillograph *Tektronix TDS640A*. To measure specific radiation flux in the mercury line of 254 nm, *IL1700* radiometer of *International-LightTechnologies* Company with photometric head *SED240/W* with a cosine nozzle for angular characteristic correction was used. The lamp was placed in a black grounded metal box located on an immovable post with a black screen in the discharge tube plane. The box had a slit of 20 mm width for measurement of the above mentioned specific radiation flux of the lamp [3]. Distance from the radiation receiver (RR) to the slit was equal to 150 cm, and distance from the slit to the lamp was 10 cm. These sizes were selected on the assumption that irradiance sufficient for exact measurements should be provided on the RR surface, and that the lamp site accentuated by the slit can be considered as a point source.

The formula for calculation of a total radiation flux of the lamp in the 254 nm line $\Phi_{e,254}$ looks like [3]:

$$\Phi_{e,254} = \frac{\pi^2 \cdot h \cdot d \cdot i \cdot L}{\Delta \cdot S},$$

where L is length of the lamp; h is distance from the lamp to the detector; i is the RR photocurrent; S is integral sensitivity of the detector; d is distance from the slit to RR; Δ is width of the slit.

The measurements of the discharge current I_{pl} was carried out by means of a current transformer. To measure HF voltage U_{pl} of plasma coil, a wire turn placed along the external perimeter of the closed discharge tube was used.

3. RESULTS OF THE EXPERIMENT

3.1. Intensity of HF plasma electric field

In Fig. 2, HF electric field intensity in the plasma coil E dependence on argon pressure and on pressure of 30% *Ne*+70% *Ar* mixture are given. E was calculated according to the formula

$$E = U_{pl}/\Delta_{pl},$$
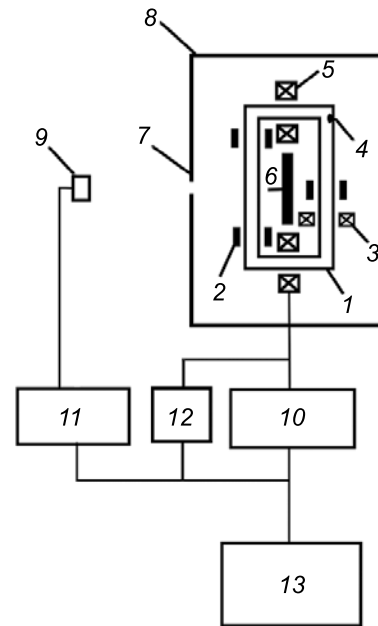
Fig. 1. Layout of the experimental installation:
1 – discharge tube, 2 – holder, 3 –current transformer, 4 – amalgam, 5 –inductor, 6 – screen, 7 – slit, 8 – box, 9 – radiation receiver, 10 – electron ballast, 11 – radiometer, 12 – digital oscillograph, 13 –personal computer

where $\Delta_{pl} = 81.5$ cm is the length of the plasma coil turn.

With an increase in $p_{i.g}$, E grows at first, and then decreases, with a maximum at $p_{i.g} = 0.2 - 0.3$ Torr. Such a dependence of E on $p_{i.g}$ is typical for low-temperature LP plasma in inert gases and in mercury vapour and corresponds to a known ratio connecting E with electron temperature T_e, working mixture pressure $p_{i.g}$ and the energy portion of energy lost by a normal electron between two impacts (elastic and not elastic) χ [6]:

$$E = 1{,}5 \cdot T_e \cdot \chi^{1/2} / \lambda_e,$$

where λ_e is an average length of electron path.

On the one hand, increase of p_{ig} reduces λ_e, which raises E, and on the other, growth of $p_{i.g}$ leads to decrease of T_e, and hence, to decrease of E. Complexities of χ dependence on $p_{i.g}$ is imposed on these relationships. As a result, the dependence of E on p_{ig} has a maximum value, the position of which moves towards a low $p_{i.g}$ with an increase in the atomic weight of an inert gas, and this increase reduces E (Fig. 2). So, in the TTL, which has a mercury vapour mixture with krypton at p_{ig} 1.0 and 0.5 Torr, E was equal to 0.48 and 0.55 V/cm accordingly.
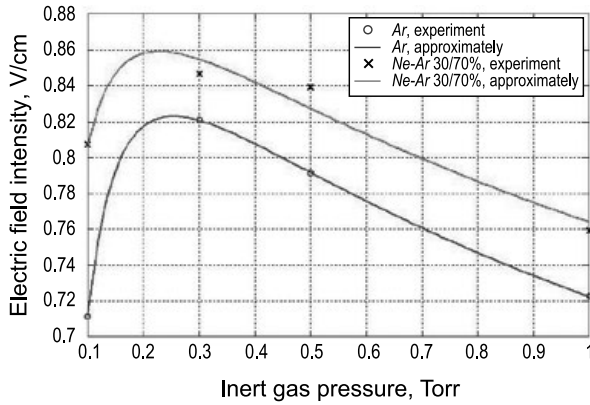
Fig. 2. Dependence of the plasma HF electric field intensity E on inert gas $p_{i.g}$ pressure at f = 265 kHz frequency of the discharge current and at power absorbed by plasma R_{pl} = 180 W

The obtained results are in keeping with the experimental data for tubular lamps with the same structure parameters but with inner electrodes operating at 50 Hz frequency [7].

3.2. Current of the plasma coil

The discharge current of the lamp (plasma coil current) I_{pl} was measured by means of a current transformer and calculated using the analytical ratios obtained within the induction discharge transformer model as [4, 5]:

$$I_{pl} = \frac{P_l - P_{ind}}{U_{pl} \cos\varphi},\qquad(1)$$

$$U_{pl} = nU_{ind}/N,\qquad(2)$$

where n is number of inductors connected in parallel, U_{ind} is HF volt age of the inductor, $N = 16$ is number of turns of the coil in the inductor, P_l is power consumed by the lamp, P_{ind} is power losses in the inductor measured during the work, φ is phase difference between U_{pl} and I_{pl}:

$$\cos\varphi = \frac{R_{pl}}{Z_{pl}},\qquad(3)$$

where R_{pl} and Z_{pl} are active and full resistances of plasma accordingly:

$$Z_{pl} = \sqrt{R_{pl}^2 + \left(\omega L_{pl}\right)^2}.\qquad(4)$$

where $\omega = 2\pi f$ is circular current frequency, L_{pl} is inductance of the plasma coil.

And one can find Z_{pl} using the measured U_{pl} and R_{pl}:

$$Z_{pl} = \frac{U_{pl}^2}{P_{pl}} = \frac{U_{pl}^2}{P_l - P_{ind}},\qquad(5)$$

L_{pl} can be found knowing mutual inductance M of the HF inductor and of the plasma coil:

$$M = k\sqrt{L_{ind}L_{pl}},\qquad(6)$$

where $k \approx 1$ is the connection coefficient of the inductor with the plasma coil, $L_{ind} = 500 \cdot 10^{-6}$ H is the inductance of the inductor, and M is determined using the formula [4]:

$$M = \frac{U_{pl}}{I_{ind}\omega},\qquad(7)$$

where I_{ind} is the current in the inductor.

It follows from (6) and (7):

$$L_{pl} = \frac{U_{pl}^2}{\left(I_{ind}\omega\right)^2 L_{ind}},\qquad(8)$$

and from (1−8) is following a calculation formula for I_{pl}, where all parameters of the lamp in the right part are determined experimentally:

$$I_{pl} = \frac{1}{\dfrac{nU_{ind}}{N}\sqrt{\left(\dfrac{1}{P_l - P_{ind}}\right)^2 + \left(\dfrac{1}{I_{ind}^2 \omega L_{ind}}\right)^2}}.\qquad(9)$$

In Fig. 3, the results of the measurements and calculations of I_{pl} dependences on p_{ig} pressure are given according to expression (9) carried out for two buffer gases: argon and 30% Ne + 70% Ar mixture. It can be seen from Fig. 2 and 3 that I_{pl} dependences on p_{ig} correlate with the correspondent E dependencies on p_{ig} and have minimum values at those p_{ig}, which E dependence on $p_{ig.}$ maximum accrues to. The I_{pl} dependencies on $p_{i.g}$ computed according to expression (9) correspond well
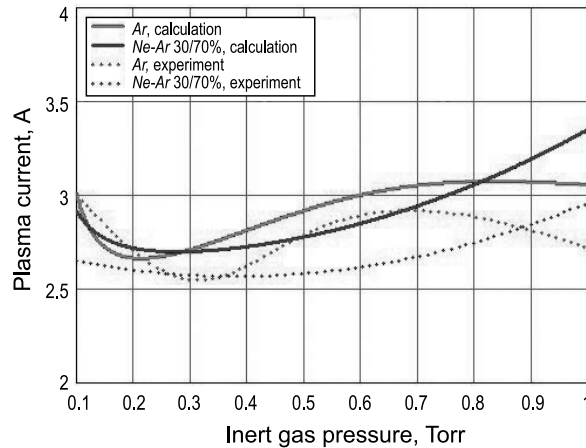
Fig. 3. Dependences of discharge current I_{pl} on inert gas pressure $p_{i.g}$. Lamp parameters are in accordance with Fig. 2
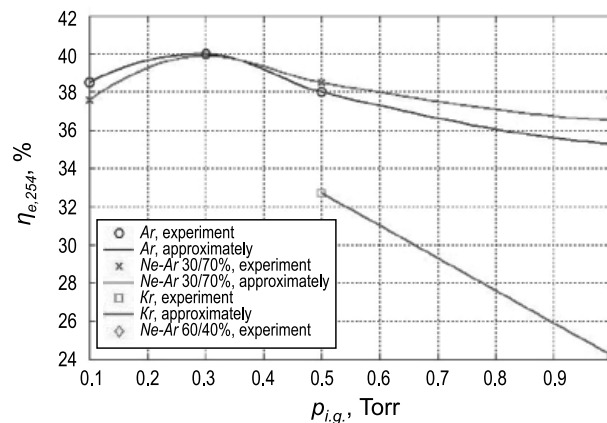
Fig. 4. Dependence of energy efficiency of the lamp in the 254 nm line $\eta_{e, 254}$ on of inert gas pressure $p_{i.g}$. Lamp parameters are in accordance with Fig. 2

to the experimental dependences obtained: the difference between I_{pl} measured and calculated values does not exceed 15%.

3.3. Energy efficiency of the lamp in the 254 nm line

In Fig. 4., experimental dependences of $\eta_{e, 254}$ ($= \Phi_{e,254}/P_{pl}$) on $p_{i.g}$ are presented for argon, krypton and for a mixture of argon with neon. It can be seen, that maximum $\eta_{e, 254}$ accrues to p_{ig} pressure 0.3 Torr, at which E has a maximum. One should not e that in a higher p_{ig} interval, $\eta_{e, 254}$ appears to be higher with an "easier" filling. However, at a lower p_{ig} pressure, $\eta_{e, 254}$ difference between pure argon and 30% Ne + 70% Ar mixture is practically not iceable. Unfortunately, radiation and electric characteristics of induction discharge with the easier filling of 60% Ne + 40% Ar were only obtained with p_{ig} of 1 Torr. With a lower $p_{i.g}$, induction discharge did not fire because to fire discharge in an "easy" gas with a high ionisation potential, an excessively high intensity of the electric field is required [6].

It follows from Fig. 4 that with a low p_{ig}, of 0.2–0.3 Torr, $\eta_{e, 254}$ at Δ_{pl} = 815 mm reaches 40%. As it was shown in [4], Δ_{pl} increase leads to $\eta_{e, 254}$ increase because of a decrease in plasma density and due to decreasing frequency of extinguishing impacts of resonantly-excited mercury atoms with plasma electrons.

CONCLUSIONS

• $\eta_{e,254}$ of mercury LP TTLs with an inert gas (or with a mixture of inert gases) with (0.1–0.5) Torr pressure and working current of (2.5–3.0) A reaches high values: to 40%.

• $\eta_{e,254}$ and E of these lamps non -monotonically depend on $p_{i.g}$ with a maximum at $p_{i.g.} \approx 0.3$ Torr.

• I_{pl} dependence on $p_{i.g.}$ computed according to the induction discharge transformer model is in keeping with the correspondent experimental dependence.

• The E calculations results are in keeping with the experimental values of this value obtained by other authors for a positive column of analogue lamps with inner electrodes but with the same other structure data and at the same discharge currents.

REFERENCES

1. Ultra-violet technology in the modern world: a cCollective monography / Under editorship of F.V.Karamzinov, S.V.Kostyuchenko, N.N.Kudryavtsev, S.V.Hramenkov. – Dolgoprudny: Publishing house "Intellekt", 2012. 391 p.

2. *Isupov M. V., Krotov S. V., Litvintsev A. Yu, Ulanov I. M.* Induction ultra-violet lamp // Svetotekhnika, 2007, № 5, pp. 37–40.

3. *Levchenko V.A., Popov O.A., Svitnev S.A., Starshinov P. V.* Experimental researches of electric and optical characteristics of an electrodeless UV lamp of the transformer type//Svetotekhnika. 2014, № 6, pp. 39–43.

4. *Popov O.A.* Research and development of induction fluorescent light sources at 100–15000 kHz frequencies / Synopsis of thesis of Dr. of engineering, Moscow: B. i., 2011. 41 p.

5. *Isupov M.V., Fedoseev A.V., Sukhinin G. I, Ulanov I. M.* Experimental and theoretical research of low-frequency induction discharge of the transformer type//Thermophysics and aeromechanics. 2014, V. 21, № 5, pp. 681–692.

6. *Rokhlin G. N.* Discharge light sources. – Moscow: Energoatomizdat. 1991. 720 p.

7. *Veselnitsky I. M.* Determination of optimum parametres and some questions of designing fluorescent lamps of a raised power / Synopsis of thesis of PhD. – Moscow: B.i., 1966. 20 p.

Vladimir A. Levchenko,
a physicist. Graduated from the MPhTI. A post-graduate student of the MPhTI SU

Sergei A. Svitnev,
Ph.D. Graduated from the "MPEI" in 2009. A leading engineer of LIT Joint-Stock Company

Oleg A. Popov,
Dr. of Technical Science. Graduated from the Moscow Power Institute in 1965. Professor of the Chair «Light and Engineering» of the "MPEI" National Research University

Pavel V. Starshinov,
master of engineering. Graduated from the Light and Engineering Chair of the National Research University "MPEI"in 2015

HYBRID LABORATORY LIGHT SOURCE FOR POLYGRAPHY SPECTRALLY CLOSE TO STANDARD *D* ILLUMINANT

Svetlana P. Arapova, Sergei Yu. Arapov, and Andrei G. Tyagunov

Ural Federal University of the first President of Russia B.N. Yeltsin, Ekaterinburg
E-mail: arapova66@el.ru

ABSTRACT

Based on a halogen incandescent lamp with an interference filter and light-emitting diode radiators, a laboratory light source (HLLS) was created, close in spectrum to standard CIE radiators of *D* series. Working values of correlated chromatic temperature of the HLLS can vary from 5000 to 6500 *K*. The HLLS characteristics obtained according to the *ISO 3664:2009* standard are provided. An algorithm for an automated luminous flux control system is described, and possible applications for the HLLS are considered.

Keywords: hybrid, laboratory, light source, standard CIE illuminant, light-emitting diode module, halogen lamp, interference filter, daylight source, visual control, chromaticity, luminous flux control

INTRODUCTION

The visual evaluation of colour of reflecting objects is a constantly arising problem in the lighting industry, which inevitably leads to questions surrounding the appropriate application of different artificial light sources. The evolution of standards for artificial illumination is well described process [1]. B and C standard radiators introduced by CIE in 1931 had a very specific structure, based on incandescent lamps with liquid filters; they were intended for the simulation of real natural light. An important disadvantage of these radiators is the fact that the violet part of their spectrum is underestimated in comparison with natural light. Later, as more and more fluorescent bleaches were used in paper, plastic and cloth production, B and C radiators became obsolete and were replaced in 1963 with the D radiator, which did not have this disadvantage. At the same time, no standard physical implementation was offered for the D radiator.

To date, D series radiators are successfully used for colorimetric calculations in different colour computer control systems, but the problem of creating correspondent conditions of artificial illumination for visual comparative evaluation of the results still stands. The quality of light sources applied in practice for this purpose, can be estimated using the techniques proposed in the CIE051.2−1999 publication and in the standard *ISO 3664:2009*. Best practice development of the D radiator simulator was later generalised in a CIE publication 192:2010, which to a large extent has something in common with paper [1], but the conclusion drawn suggested that the adoption of structures simulating a D radiator as standard would be inefficient.

In polygraphy, special fluorescent lamps are used with correlated chromatic temperature $T_{cc} = 5000−5500$ K and with a high colour rendition general index R_a of about 95−97. It has been noted repeatedly that at high R_a, the spectrum of fluorescent lamps is substantially different from natural daylight. Modern technology has made light sources specialised by spectrum based on other physical principles widely accessible. In the first place, these are modular light-emitting diode (LED) sources supplied with spectral component control systems [2, 3, 4−7]. Progress of nana-coating de-
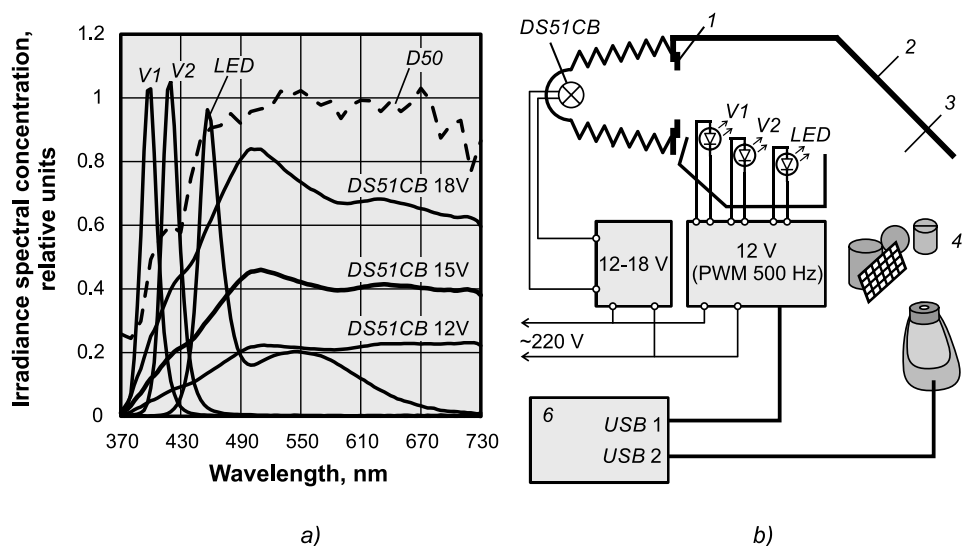
Fig. 1. A hybrid laboratory light source (HLLS):
a – spectra of radiators: V1 (400 nm) and V2 (420 nm) ultra-violet LEDs with $S_{V1}(\lambda)$ and $S_{V2}(\lambda)$ spectra, LED – cold-white LED with $S_{CW}(\lambda)$ spectrum, DS51CB – Decostar 51 Cool Blue HIL (with a dichroic filter) and its $S_{DS}(\lambda)$ spectra with different power supply voltages (12, 15 and 18 V). The dotted line is designation of one of the target spectra (D50);
b – HLLS structure: 1 – adjusted aperture diaphragm, 2 – diffuse reflector, 3 – radiating device alignment, 4 – operation area of the source with objects placed in it, 5 – i1Pro spectrophotometer, 6 – control computer

position technology allowed manufacturing halogen incandescent lamps (HIL), supplied with interference filters at quite reasonable prices. On the domestic market in Russia, *Decostar 51 Cool Blue* HILs (further – *DS51CB*) are well-known *Osram* products. These can also be used for laboratory research purposes [8]. HILs with interference filters can be considered modern versions of B and C illuminants, with their insufficiency in the violet part of the spectrum. At the same time, there exist many available LED light sources with a large portion of their short-wave radiation in the visible spectrum interval.

Therefore, creating an accessible light source, close in spectrum to the D radiator, using this element, enabling spectrum adjustments, is an interesting and topical task.

LIGHT SOURCE STRUCTURE

To obtain the desired spectral composition of a hybrid laboratory light source's (HLLS) radiation, light fluxes from various radiators need to be mixed. As a reference point, D radiator spectrum was selected with T_{cc} from 4500 to 6500 *K*, and as initial components, *DS51CB* HILs with interference filters were selected, as well as one white and two violet LED light sources.

Spectral composition of the component radiation (Fig. 1a) corresponded with the task parameters, and the difference in physical principles of light generation is reflected in the name "hybrid".

The structure of the HLLS is shown in Fig. 1b. The junction of the corrugated housing and aperture diaphragm *1* makes it possible to select HIL radiation with a sufficient spectrum and also to adjust the radiation flux to the reflector. Flux mixing is made using a diffuse reflector *2*. Power supply to the LED sources is from the *P16NF06* systems controlled by PWM outputs of an *Arduino Uno* (*ATmega328P*) controller. The frequency of PWM outputs of the *Arduino Uno* was about 500 Hz at eight-bit adjustment of on-off time ratio, which is acceptable for the task. The *Arduino Uno* was chosen also because of its *Arduino IO* open source package, which allows controlling it from the *Matlab* medium. In this case, a monitor program is loaded into the controller. This program transmits commands arriving via a *USB* interface from *Matlab* to the controller output. The HIL power supply was carried out by an independent pulse source with manual adjustment of output voltage from 12 to 18 V.

The spectra of the obtained radiation and of separate components were measured using *i1Pro*

widespread spectrophotometer from *X-Rite* along with the *Argyll CMS* open software.

The main purpose of the *i1Pro* is measuring the reflection spectra of printed impressions according to the requirements of standard *ISO 13655:2009*. This measurement is necessary when constructing *ICC* profiles in computer systems for colour adjustment. Addiitionally, the *i1Pro* has a mode for measuring spectral concentration of irradiance [mW/m²·nm], and a cosine-correcting attachment is included in the complete set. A mode for "the high permission" is also provided for, in which spectral data are generated at 3.33 nm step intervals (three readouts every 10 nm) for 109 spectral areas in the section interval from 370 to 730 nm.

On the official site of *X-Rite* Company, the list of *i1Pro* characteristics is quite limited. The *i1Pro* spectral analyser is constructed based on a diffraction lattice and on a 128-pixel photodiode ruler. The digitisation interval of the spectrum is 3.5 nm, the optical resolution is 10 nm. So, the broadband measuring path allows obtaining a high level of output signal and reaching a high speed of measurements, corresponding to *ISO 13655:2009* requirements (step of digitisation is 10 nm). When reading check prints, *i1Pro* makes 200 measurements per second. The radiation spectrum is calculated by an internal processor and transmitted to the control computer. Unfortunately, regular errors of *i1Pro* cannot be evaluated based on the presented information. These inevitably depend on the spectrum type. Random error in the experiments did not exceed 0.24 mW/m²·nm with $p = 0.95$.

It is clear that a 10 nm resolution is not suitable for exact colorimetry of radiators with narrow peaks in the spectrum. CIE127:2007 publication recommends performing exact measurements of LED spectra with a resolution of 5 nm and a digitization step of 2.5 nm. At the same time, the abilities of *i1Pro* in the high resolution mode are sufficient to evaluate the quality of the obtained radiation spectra according to *ISO 3664:2009* requirements.

CONTROL OF THE RADIATING COMPONENTS OF THE SOURCE

The radiation spectrum in the HLLS operation area is formed by a combination of spectra of its components:

$$s(\lambda) = a_1 \cdot s_{V1}(\lambda) + a_2 \cdot s_{V2}(\lambda) + \\ + a_3 \cdot s_{CW}(\lambda) + s_{DS}(\lambda), \quad (1)$$

where $s_i(\lambda)$ are spectra of the components (Fig. 1a) measured in the HLLS operation area with their continuous power supply, a_i are coefficients, which determine the contribution of i_{th} component in the HLLS total spectrum and are values of PWM on-off time ratios of LED power proportionally expressed. The HIL is not included in the automatic control, $s_{DS}(\lambda)$ spectrum is the «reference», and LEDs are used to complete the construction of HIL radiation in the shortwave part of the visible spectrum area to the desired result.

With due regard to discreteness of the obtained spectral data by wavelength (109 spectral areas), hereinafter it will be convenient to use vector-matrix configuration of the data presentation:

$$s = S_{LED}a + s_{DS}, \quad (2)$$

where S_{LED} is a matrix (109×3), where the columns are spectra of the light emitting diodes, $a = [a_1, a_2, a_3]^T$ is vector of on-off time ratios, s_{DS} is vector (109×1) of *DS51CB* HLN spectrum.

The target spectrum of the D radiator with set T_c can be computed according to CIE recommendations as

$$s_D = s_0 + M_1(T_c)s_1 + M_2(T_c)s_2, \quad (3)$$

where s_0, s_1, s_2 are vectors (109×1) of D radiator components; $M_1(T_c), M_2(T_c)$ are coefficients recommended by CIE. To evaluate coincidence of the spectra s and s_D configurations, the approximation quality coefficient *GFC* (*Goodness Fitting Coefficient*) is convenient [9], which should be minimised as follows:

$$GFC = 1 - \frac{(s_D, s)}{\|s_D\| \cdot \|s\|} = \\ = 1 - \frac{s_D^T s}{\sqrt{s_D^T s_D}\sqrt{s^T s}} \to \min, \quad (4)$$

where s_D is the target spectrum (3) of D radiator with set T_c, s is HLLS spectrum (2). Expres-
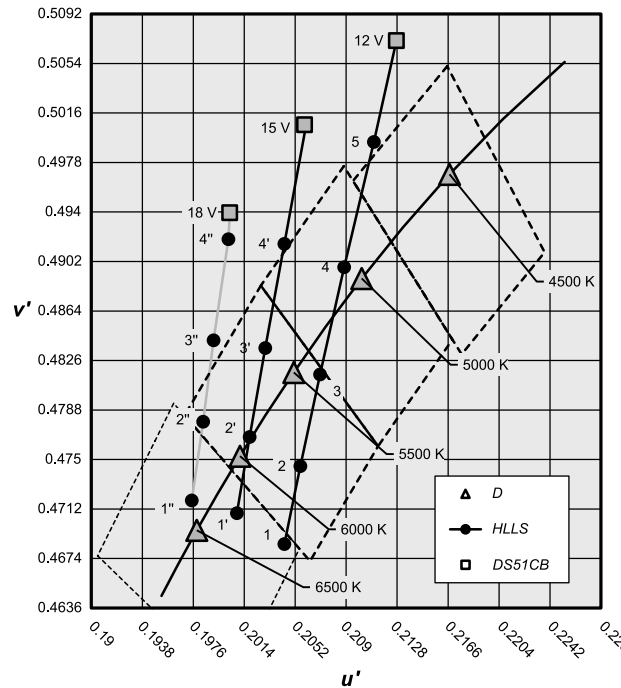
Fig. 2. HLLS chromaticity depending on T_c of D target radiator and DS51CB HIL power supply voltages. Points: 1, 1', 1'' – 6500 K; 2, 2', 2'' – 6000 K; 3, 3', 3'' – 5500 K; 4, 4', 4'' – 5000 K; 5 – 4500 K. Mesh step equal to 0.0038 corresponds to the threshold of perception of chromatic differences

sion (4) represents a difference from one of cosine of the angle between vectors s_D and s in 109-dimensional vector space of the spectra. Zero *GFC* means collinearity of the vectors, and hence a full coincidence of the spectra configurations (within the constant accuracy).

Thus the task of achieving the best HLLS spectrum with a set T_c (3) consists of obtaining $a = [a_1, a_2, a_3]^T$ in (2) providing a minimum *GFC* (4) under condition $0 ″ a_i ″ 1$ and a subsequent chromaticity control.

Let's consider a set of vectors $\{s^*\}$, which form a subspace L with basis s_{UV1}, s_{UV2}, s_{CW}, s_{DS}:

$$s^* = b_1^* s_{V1} + b_2^* s_{V2} + b_3^* s_{CW} + b_4^* s_{DS} = S b^*, \quad (5)$$

where S is a matrix with (109×4) columns $s_{V1}, s_{V2}, s_{CW}, s_{DS}$, and $b^* = \begin{bmatrix} b_1^* & b_2^* & b_3^* & b_4^* \end{bmatrix}^T$.

It is easy to show that the least angle with target vector s_D is formed by vectors from L lying on a straight line, which contains an orthogonal projection of s_D vector on subspace L. Coordinates b of such a projection in L can be easily found using standard least-square method:

$$b = \left(S^T S \right)^{-1} S^T s_D = S^+ s_D, \quad (6)$$

as one can see, with application of the Moore-Penrose pseudoinversion operation. The vectors, which minimise *GFC* (4), form a straight line:

$$s_{\min GFC} = k S b, \quad (7)$$

where k is an arbitrary constant.

Now we obtain a solution of the initial task (2) − (4). According to the condition, it should be an element of the linear variety (2) representing a hyperplane lying in L, as well as the straight line (7). In all practically interesting cases, the hyperplane (2) is not parallel to the straight line (7), and hence they have one general point. Thus, a singular solution of task (2) − (4) exists and can be obtained as

$$a_1 = b_1 / b_4, \quad a_2 = b_2 / b_4, \quad a_3 = b_3 / b_4. \quad (8)$$

It is also simple to show a stability of the proposed solution, however, this is beyond the scope of the present article.

The solution of the equation system (6) − (8) allows calculating an evaluation of HLLS characteristics by spectrum, chromaticity and il-
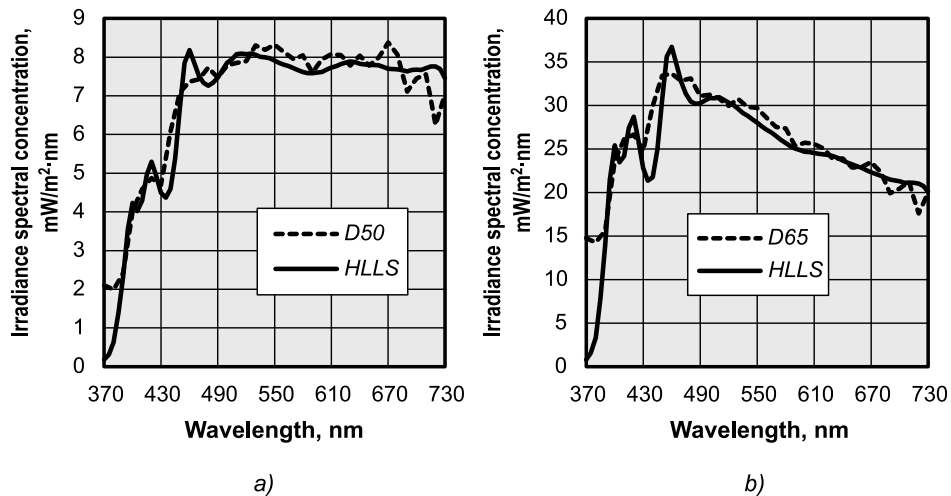
Fig. 3. HLLS Spectra:
a – D50 imitation (point 4 in Fig. 2). GFC = 0.0032, $\Delta E_{u'v'}$ = 0.0013, illuminance in the operation area is equal
to ≈ 570 lx; b – D65 imitation (point 1" in Fig. 2). GFC = 0.0078, $\Delta E_{u'v'}$ = 0.0022,
illuminance in the operation area is equal to ≈ 2000 lx

luminance in the operation area. In Fig. 2, the CIE1964 chromatic diagram with trajectories of chromaticity change is given at different HIL power supply voltages, corresponding to the best spectral approach of the target D radiator depending on T_c.

It is clear from Fig. 2 that the proposed procedure of searching for the best spectral approach together with a correct choice of the *DS51CB* HIL power supply voltage allows obtaining approached very close by chromaticity to D radiators with T_c from 5000 to 6500 *K*. *D65* and *D50* radiators can be found more often than others in colorimetric applications. The most successful version of *D50* imitation by means of HLLS is possible with *DS51CB* HIL at supplying voltage of 12 V (point *4* in Fig. 2), and with *D65* at 18 V (point *1* in Fig. 2). Design spectra of the HLLS for these cases are given in Fig. 3.

Thus, a successful selection of HLLS radiating components makes it possible to use elementary algorithms to control them.

EXPERIMENTALLY OBTAINED CHARACTERISTICS OF THE LIGHT SOURCE

Radiators in HLLS are essentially different by light distribution, and it is possible to estimate the efficiency of mixing radiations using a diffuse reflector (in terms of imitating *D50* radiator), as well as to estimate uniformity of illumination

in the HLLS operation area. In nine points of this area of about 18×18 cm size, measurements of irradiance spectral concentration were made. Illuminance deviation from its average value amounted to around 20%. Spectral irradiance distribution varied point-to-point but as a whole it corresponded well to a preliminary estimation (Fig. 3a). And in points of the operation area, the chromatic shift $\Delta E_{u'v'}$ (10 °CIE1964) being equal to ≤ 0.005, corresponds to *ISO* recommendation *3664:2009*.

Other indicators of *D50* imitation quality according to standard *ISO 3664:2009* also confirm that the result is acceptable. And R_a = 98.3 (according to the standard it is not less than 90), and as to special indices, R_1 = 98.9, R_2 = 98.7, R_3 = 99.2, R_4 = 96.9, R_5 = 98.0; R_6 = 98.9; R_7 = 97.5; R_8 = 98.0 (according to the standard, they are not less than 80). The metamerism index in the visible area M_{vis} = 0.14 (according to the standard, no more than 0.25), and in the violet area M_v = 0.09 (according to the standard, no more than 0.15).

The reached levels of the HLLS luminous flux allows using it in experimental colour control works in polygraph [10]. The *D50* radiator is basic for colorimetric calculations in colour adjustment computer systems based on the *International Colour Consortium* (*ICC*) methodology, and prints illuminated by means of HLLS were used for direct comparison with other experimental material. The developed HLLS was also successfully used for multispectral shooting of small objects [11].

CONCLUSION

An HLLS has been developed close by spectrum to standard radiators of D series. The control algorithm has been checked based on an analytical solution of the *GFC* minimisation task with a fixed reference spectrum of one of the HLLS components. A certain flexibility in T_{cc} choice is achieved but an essential dependence of illuminance level on T_{cc} in the HLLS operation area can be considered as a disadvantage.

When using HLLS, one should take into consideration that the LED component of the luminous flux adjustment was carried out by means of PWM (500 Hz). Besides, all of the obtained results are based on measurements by a spectrophotometer with a low spectral resolution (10 nm) intended for typical tasks connected with the chromatic perception by a person. When it comes to tasks beyond typical colorimetry, these characteristics may be insufficient.

For visual evaluation of prints in polygraphy, the obtained characteristics are even superfluous. Nevertheless, the spectral proximity to D radiators can be in demand in some specific applications. These include colorimetric researches, selection of paint mix formulas, evaluation of thermosublimation prints on textiles for outdoor advertising, and other tasks connected with the visual perception of products intended for viewing under natural illumination conditions.

Another interesting sphere of application for such hybrid sources, is in various biological research. In spite of the fact that the question of spectral efficiency of photosynthesis is studied sufficiently, and correspondent versions of optimising spectra of light-emitting diode sources [12] are proposed, it is reasonable to assume that in biological systems, other important photochemical processes specifically adapted for natural illumination also occur.

The energy efficiency of the developed HLLS was not analysed as part of this work, however, it is low.

Next steps in the perfection of the HLLS include an improvement of the radiation mixing system and an introduction of an additional element: a white LED with $T_{cc} = (500-3000)$K, which could lower HIL loading [8] and probably avoid overheat mode.

REFERENCES

1. *Hunt R.W.G.* Letter to the editor. Standard sources to represent daylight // Color Res. Appl. 1992, Vol. 17, № 4, pp. 293–294.

2. *Dowling K, Devis W, Zong U., Miller K.K., Ono Y.* Radiating installation of the National institute of standards and technologies (NIST) with adjusted spectrum for researches in the colour rendition field // Svetotekhnika. 2009, # 5, pp. 37–40.

3. *Sergeev Igor K.* Prospective Developments of UOMZ Production Association Open Society- in the Field of Lighting Devices with Light Emitting Diodes// Light & Engineering. 2011, V.19, # 4, pp. 59–66.

4. *Badgutdinov M. L, Galchina N.A., Kogan L.M., Rassokhin I.T., Soshchin N.P., Yunovich A.E.* Light-emitting diode module with adjustable correlated colour temperature // Light & Engineering, 2009, V.17, # 2, pp. 71–74.

5. *Galchina N.A., Guttsait E.M., Dvornikov E.A., Kogan L.M., Rassokhin I.T., Soshchin N.P., Turkin A.N., Yunovich A.E.* A light-emitting diode device with improved colour rendition // Light & Engineering, V.21, 2013, # 2, pp. 73–77.

6. *Aladov A.V., Zakgeim A.L., Mizerov M.N, Chernyakov A.E.* Polychrome spectrally changeable illumination devices with light emitting diodes: experience of development and application // Light & Engineering, 2014, V.22, #1, pp. 12–19.

7. *Guttsait E.M., Zakgeim A.L., Kogan L.M., Maslov V.E, Soshchin N.P.* Concerning simulation of standard light sources using light-emitting diode modules // Light & Engineering, V.21, 2013, № 4. pp. 75–80.

8. *Arapov S.Yu., Arapova S.P., Tarasov D.A.* Evaluation of applicability of the *Decostar 51 Cool Blue 50W 360 (Osram)* lamp as a specialised radiation source in polygraphy // Svetotekhnika. 2015, # 4, pp. 67–68.

9. *Imai F., Rosen M., Berns R.S.* Comparative Study of Metrics for Spectral Match Quality / The First European Conference on Colour Graphics Imaging and Vision., NY, USA, 2009, pp. 785–792.

10. *Arapova S.P., Arapov S.Yu., Solodova M.S.* A computer aided laboratory light source for colour rendition research when colorimetric illuminating / Materials of the International scientific-and-practical conference (Ekaterinburg, March,

19–20th, 2015)"Transmission, processing and perception of text and graphic information". – Ekaterinburg: Ural Federal University UrFU of the first President of Russia B.N.Yeltsin, 2015, pp. 34–46.

11. *Arapova S.P., Arapov S.Yu., Tyagunov A.G.* Experimental set of multispectral shooting based on a standard digital camera // Izvestiya vysshikh uchebnykx zavedeniy. Polygraphy and publishing problems, 2014, # 5, pp. 45–54.

12. *Valyaev D.B., Malyshev V.V.* Feasibility report on application of light-emitting diode luminaires in hothouses // Innovations in agriculture, 2013, #3 (1), pp. 55–57.

Svetlana P. Arapova,
physicist-engineer, graduated from physics-technics faculty of Ural Federal Polytechnic Institute in 1989, senior teacher of "Polygraphy and Web-design" chair of the Ural Federal University of the First President of Russia B.N.Yeltsin, the fields of scientific interests: prepress preparation, printing house, colorimetry, features of perception of colour in polygraphy, psychophysics

Sergei Yu. Arapov,
physicist-engineer, graduated from physics-technics faculty of Ural Federal Polytechnic Institute in 1988, senior teacher of "Polygraphy and Web-design" chair of the Ural Federal University of the First President of Russia B.N.Yeltsin, the fields of scientific interests: prepress preparation, colour management systems, colorimetry, multispectral photography

Andrei G. Tyagunov,
Ph.D., senior lecturer, graduated from the Metallurgical department of the UGTU-UPI in 1993. He is an organizer (2003) Federal University of the First President of Russia B.N.Yeltsin, a teacher of a number of the special subjects. Fields of scientific interests: printing processes and material technology

ENERGY-EFICIENT OPTICAL POWER CONTROL FOR DATA RATE AND ILLUMINANCE PROVISION IN VISIBLE LIGHT COMMUNICATION

Irfanud Din[1, 2] and Hoon Kim[2]

[1]*Department of Information and Communication Engineering, Inha University in Tashkent*
[2]*Department of Electronics Engineering,*
Incheon National University, South Korea
E-mails: hoon@incheon.ac.kr; irfan@inha.uzr

ABSTRACTS

The two main objectives of Visible Light Communication (VLC) systems are dimming support and communication. These objectives can be achieved simultaneously by reducing the total power consumption of VLC system. In this paper, we formulate the optimization problem that minimizes the total power consumption of Light Emitting Diode (LED) lamps in a VLC system, while satisfying the user's requirements of the illuminations as well as communication. Performance of proposed scheme is evaluated using computer simulation. Results show that the proposed scheme reduces the energy consumption of VLC system by 30% compared to existing schemes.

Keywords: optical power, energy efficiency, pulse width modulation, lighting control

I. INTRODUCTION

Visible light communication is a communication technology which utilize visible light source as a transmitter. Visible light refers to the visually-perceivable electromagnetic radiations i.e. radiations in visible spectrum. Visible spectrum covers the wavelengths from 380 nm to 780 nm, which correspond to a huge frequency band of approximately 400THz (from 384 THz to 789 THz) [1, 2]. In recent years, visible spectrum has received much attention to be used for high speed wireless communications in indoor environments.

Light Emitting Diode (LED) is considered to be very important source for lighting energy saving in indoor environments [3]. Taking advantages of fast switching characteristics of LED, it can be used as a communication source by modulating the LED light with data signal. Owing to the fact that VLC involves the combination of communication with lighting, VLC using LEDs has attracted considerable attention and has become a valuable mean for wireless communication.

Dimming is an essential functionality of modern lighting system, which is mostly achieved by Pulse Width Modulation (PWM) or changing the modulation depth of the input signal. Researchers have proposed different modulation schemes for dimming control and data transmission using LEDs [4–6]. A joint dimming and data transmission in VLC is proposed in [7], where the data is transmitted using Sub-Carrier Pulse Position Modulation (SC-PPM) and dimming is achieved using PWM or by changing the modulation depth. In our previous work [8], we had optimized the SC−LPPM parameters to minimize the power consumption of VLC system, while satisfying the user requirements of illumination as well as communication.

In this work, we use PWM for brightness control and communication. We are focusing on optimization of received optical power and illuminance to reduce the power consumption of VLC system with satisfaction of user's lighting and communication requirements. An optimization problem is for-
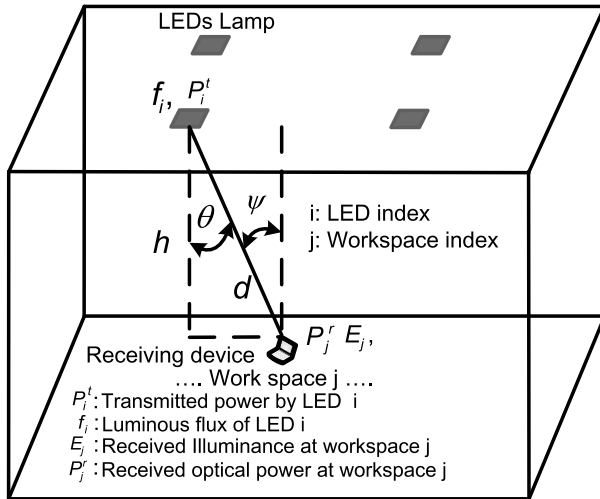
Fig. 1. System model for VLC indoor environment

mulated to find the optimal parameters i.e. widths of input waveform, PWM signals that satisfy both communication and illumination constraints.

The rest of the paper is organized as follows: paragraph 2 presents the system model used in this paper, data modulation scheme illumination and communication model for VLC system; the optimization problem is formulated in chapter 3, and performance evaluation of the proposed scheme is presented in paragraph 4.

2. SYSTEM MODEL

This work considers a VLC system in an indoor environment, as shown in Fig. 1. It is assumed that L identical LED lamps are equally spaced on the ceiling of a room, and that the floor is geographically divided into J identical square grids (or 'work places'). In the VLC system the LED lamps are considered to have capability of optical communication i.e., LED lamps works as VLC transmitters. The receiver devices at the users end are considered to have Photo Diodes (PDs) for optical communication. For simplicity we consider Line of sight channel only both for communication and illumination.

2.1. Modulation

We used On/Off keying (OOK) with PWM for data transmission and dimming control. OOK is the simplest modulation scheme, where the binary one and zero is represented by the presence and absence of carrier wave in a time slot, respec-

tively. Let A be the amplitude of the received optical power by a photo diode (PD), the received optical power is directly proportional to the amplitude A, which can be expressed as $P_r = A/2R$, where R represents the photo-detector responsivity and P is the average optical power. Let the transmission rate of an OOK transmitter be R_b, then it will transmit R_b rectangular pulses having duration $1/R_b$. For the binary 1 the pulse intensity will be $2P$, while for binary 0 the pulse intensity will be zero i.e. no pulse.

In order to evaluate the performance of a communication link, Bit Error Rate (BER) can be used as a key evaluation parameter used to. In general for an acceptable error probability the BER should be less than 10^{-6} [9]. BER for OOK can be compute as

$$BER_{ook} = Q\left(\sqrt{\frac{2R^2 P_r^2}{N_o R_b}}\right), \qquad (1)$$

where N_o is the Power Spectral Density (PSD) of Gaussian shot noise. Shot noise is the sum of noise due to artificial light and natural light, with PSD of N_i and PSD of N_s, respectively [10]. Mathematically N_o can be denoted as follow

$$N_o = N_i + N_s = q.(I_{bi} + I_{bs}), \qquad (2)$$

where q is the charge of one electron. Parameters I_{bi} and I_{bs} are the photocurrent due to artificial and natural light, respectively.

BER depend on the received power as all the other parameters in eq. 1 are constant. Therefore, the average optical power required to achieve a given BER, using OOK can be computed as

$$P_{req} = \frac{1}{R}\sqrt{\frac{N_0 R_b}{2}}Q^{-1}(BER) \qquad (3)$$

Fig. 2 illustrates the waveform of a PWM signal. The symbol period T_i^s is divided into two slots, T_i^{on} and T_i^{off}, where parameter i represents the index of signal waveform and corresponding LED. The slot T_i^{on} represents the signal interval. A data signal with amplitude k is transmitted during this slot. T_i^{off} has zero amplitude, i.e. no signal is transmitted during this slot. The width of slot T_i^{on} is directly proportional to the transmitted optical power and luminous intensity of LED. By changing the width

of slot T_i^{on}, signal with desired duty-cycle can be obtained as shown in Fig. 2.

2.2. Illumination

The amount of light emitted from an LED is represented by luminous flux, which is given as

$$f = K_m \int_{380}^{780} V(\lambda) f_e(\lambda) dx, \qquad (4)$$

where K_m is maximum visibility, $V(\lambda)$ is the standard luminosity curve and $f_e(\lambda)$ is the spectral flux [6]. Luminous intensity indicates the luminous flux per solid angle (Ω), which can be calculated as

$$I = \frac{df}{d\Omega}. \qquad (5)$$

The emitted luminous flux for a PWM signal waveform can be expressed as

$$f_i = N_i f_{max}, \qquad (6)$$

where N_i is the ratio of signal interval to symbol period, represented as $N_i = T_i^{on} / T_i^s$. f_i is luminous intensity of ith LED. The maximum transmitted luminous intensity is represented by f_{max}, which can be obtained with a PWM signal when $T_i^{on} = T_i^s$.

In design of lighting system the parameter of our interest is illuminance measured in lx and is given by luminous flux per unit area as [5]

$$e = \frac{d\Phi}{dA} = \frac{I(\theta)}{r^2}. \qquad (7)$$

Illuminance depends on source luminous intensity $I(\theta)$ in a θ angle direction, where r is the distance between source and point of interest. Considering Lambert radiation characteristic the horizontal illuminance at a point j located at r distance from light source can be calculated as

$$e_j = \frac{I_o cos^m(\theta) cos(\psi)}{r^2}, \qquad (8)$$

where I_o is the maximal luminous intensity, which is given by $I_o = I(0) = (m+1)f/(2\pi).\psi$ and θ represent angle of incidence and irradiance, respectively. In reference [11] m denotes the or-
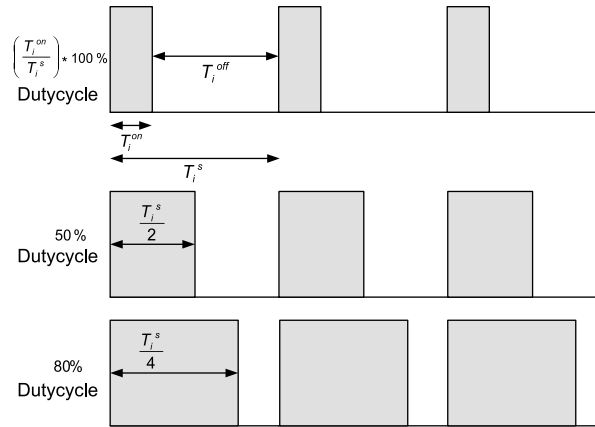
Fig. 2. Waveform of PWM signal with 100%, 50% and 80% duty cycle

der of Lambertian emission and is given by the semi-angle at half illuminance of an LED as

$$m = \frac{\ln 2}{\ln \cos(hpa)}, \qquad (9)$$

where hpa is the half power angle of LED. For example, $m=1$ at $hpa=60^o$. By replacing I_o in equation 7, the illuminance at a point j from i^{th} LED lamp can be expressed as

$$e_{ij} = \frac{f_i(m+1)cos^m(\theta)cos(\psi)}{2\pi r^2}. \qquad (10)$$

The total illuminance received at point j from L LED lamps can be computed as the summation of illumination from all LED lamps and can be represented as

$$E_j = \sum_{i=1}^{L} e_{ij}. \qquad (11)$$

2.3. Communication

Optical power transmitted by an LED is the integral of energy flux in all directions and given by

$$P_t = \int_{\lambda_{min}}^{\lambda_{max}} \int_0^{2\pi} f_e d\theta d\lambda \qquad (12)$$

where λ_{max} and λ_{min} are derived from the sensitivity curve of PD [5].

Optical power transmitted by an LED with an input PWM signal waveform can be computed as
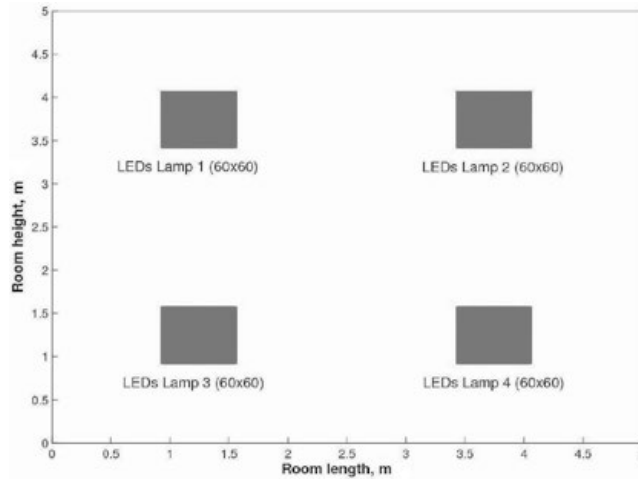
Fig. 3. LED Lamps placement scenario

$$P_i^t = N_i P_{max}^t, \qquad (13)$$

where P_i^t is the transmitted optical power by i^{th} LED lamp. The maximum transmitted optical power is given by P_{max}^t, which can be obtained with a PWM for which $T_i^{on} = T_i^s$.

Considering a receiver (PD) located at point j as shown in Fig. 1, the received optical power (LOS only) at PD from i^{th} LED with transmitted power P_i^t, is given by

$$P_{ij}^r = H(0) P_i^t, \qquad (14)$$

where H(0) is the channel DC gain, which is expressed as [12]

$$H(0) = \begin{cases} \dfrac{A(m+1)}{2\pi r^2} \cos^m(\theta)\cos(\psi)g(\psi)T_s(\psi), \\ \qquad 0 \le \psi \le \psi_c \\ \\ 0, \ \psi > \psi_c \end{cases} \qquad (15)$$

where A_r is the effective receiver area, $g(\psi)$ and $T_s(\psi)$ are the gain of optical concentrator and optical filter, respectively. $g(\psi)$ is given as

$$g(\psi) = \begin{cases} \dfrac{n^2}{\sin^2\psi_c}, 0 \le \psi \le \psi_c, \\ \\ 0, \ \psi > \psi_c \end{cases} \qquad (16)$$

where n is the reflective index. The received optical power at a point j from i^{th} LED can be expressed as
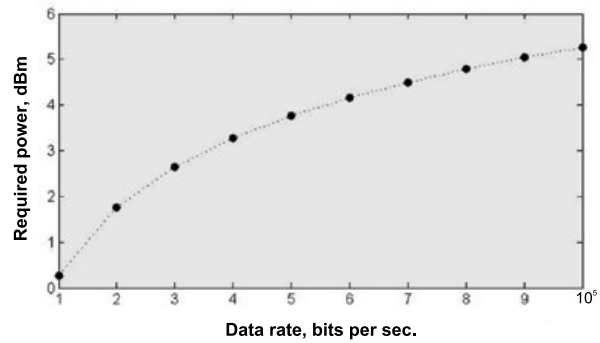
Fig. 4. Required power verses data rate plot for a target BER of 10⁻⁶

$$P_{ij}^r = P_i^t \frac{A_r(m+1)}{2\pi r^2} \times$$
$$\times \cos^m(\theta)\cos(\psi)g(\psi)T_s(\psi), \qquad (17)$$

where the total received optical power P_j^r at a point j from L LED lamps can be computed as the summation of optical power received from all LED lamps and can be expressed as

$$P_j^r = \sum_{i=1}^{L} P_{ij}^r. \qquad (18)$$

III. PROBLEM FORMULATION

The objective of the proposed scheme is to minimize the total power consumption under the constraints that the user's requirements of illuminations and communication must be satisfied. Assuming that the power consumption is propor-

tional to the signal interval of PWM signal waveform then the objective can be achieved by minimizing N_i i.e., minimizing the signals interval T_i^{on}. The goal is to find the optimal value of T_i^{on} that satisfies the requirements of illuminance and communication. The optimization problem can be stated as following:

$$\min_{N_i} \sum_{i}^{L} f_i. \tag{19}$$

$$Subject\ to \quad P_j^r \geq P_{req}, \quad for\ all\ j's \tag{20}$$

$$E_j \geq E_{req}, \quad for\ all\ j's \tag{21}$$

$$0 \leq T_i^{on} \leq T_i^s, \tag{22}$$

where P_{req} and E_{req} are the required received power and illuminance, respectively. The objective function is shown in Eq. (19), which aims to minimize the total luminous flux of LED lamps, hence minimizing the total power consumption of the system. The constraints are stated in Eq. (20) to (22). Eq. (20) and (21) are the constraints for required minimum levels of received optical power and illuminance, respectively. The constraint for the signal interval duration of PWM waveform is shown in (22), which can be varied from 0 to T_i^s, this constraint also sets the dimming capabilities and limits of transmitted optical power of LED.

IV. PERFORMANCE EVALUATION

Simulations were performed to evaluate the performance of the proposed scheme. An indoor

Table 1. System Parameters

Parameter	Value
Room size	5m*5m*3m
Number of LED Lamps	4
Height of desk surface	0.85m
Number of LEDs per Lamp	3600(60*60)
Space between LEDs	1cm
Single LED power	20.0 mW
Center luminous intensity	0.73 cd
Semi angle at half power	60 deg.
Photodiode responsivity	0.4
Detector physical area of PD	1 cm
FOV at the receiver	120 deg.
Reflective index of concentrator	1.5

room environment as shown in Fig. 1 is considered. Four LED lamps, capable of optical transmission installed at a height of 3m above the floor are considered. It is further assumed that each LED lamp consists of 60×60 LEDs with a separation distance of 1 cm. The centre luminous intensity of an LED is 0.73 cd, and semi-angle at half-power of LED is 60 deg. Fig. 3 shows the placement of the LED lamps at ceiling of the room, while Table 1 summarizes the typical system model parameter used in simulation.

Fig. 4 compares the required optical power for a PWM input waveform to achieve data rates of 1 Mbps to 10 Mbps with required BER of 10^{-6}.
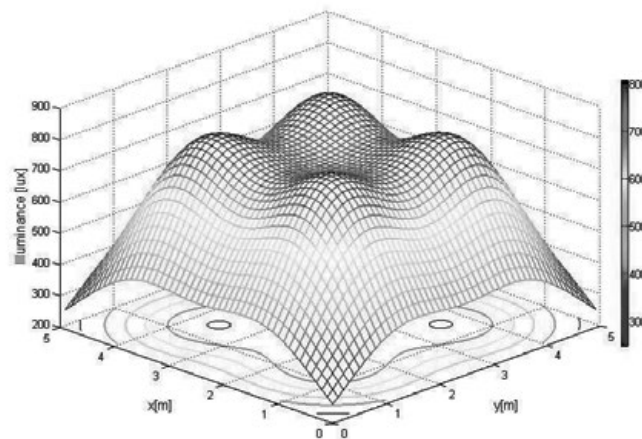
Fig 5. The distribution of illuminance
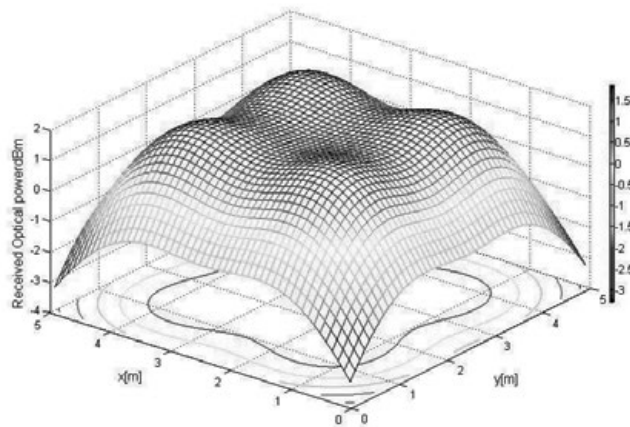
Fig. 6. The distribution of received optical power

It can be noticed that the required power increases with increasing data rate for a given BER.

Received optical power and illuminance at a desk surface of height 0.85m at the center of each workspace, are calculated by Eq. (17), (18) and (10) and (11), respectively. Fig. 5 show the illuminance distribution, computed on the desk surface. It can be noticed that illuminance level throughout the room is greater than the required illuminance level i.e. 400 lx, except at the corners, where the illuminance level is slightly below 400 lx. The corner area is very small and usually users are not located in these areas.

Fig. 6 shows the distribution of received optical power of direct light from LED lamps. The minimum received optical power at [13] is -2.8 dB, which is considered as minimum requirement for received optical power. This minimum optical power level is obtained at all places of the room.

Figs. 4 and 5 indicate that sufficient illuminance and optical power are obtained throughout the room, which therefore meet requirements for illumination and communication throughout the room. The power consumption of the proposed scheme is compared the conventional scheme, which used PWM signal waveform with fixed duty cycle of 50%. It is found that the proposed scheme reduce the energy consumption of VLC system by 32% compared with conventional scheme.

CONCLUSION

In this work, an optimization problem that minimizes the total power consumption of LED lamps in a VLC system, while satisfying the user's requirements of the illuminations as well as communication are formulated. Simulation results show that the proposed scheme reduces the energy consumption of VLC system by 30% compared to existing schemes.

REFERENCES:

1. Christian P. "Visible Light Communication", Seminar Kommunikations standards in der Medizintechnik [Online] http://www-old.itm. uni-luebeck.de/teaching/ss10/sem_kim/ausarbeitungen/2010−06−29%20Pohlmann.%20Visible%20Light%2°Communication.pdf?lang=en.
2. http://www.lificonsortium.org/.
3. Julia B. Babanova and Vadim A. Lunchev, "Energy Saving Capabilities when using Control Systems for Interior Illumination", Light & Engineering, 2012, Vol. 20, No. 1, pp. 58−65.
4. Z. Wu, J. Chau, T. Little, "Modeling and Designing of a New Indoor Free Space Visible Light Communication System", 16th European Conference on Networks and Optical Communications (NOC), IEEE, 2011, pp. 72−75.
5. H. J. Jang, J. H. Choi, Z. Ghassemlooy and C. G. Lee, "PWM-based PPM Format for Dimming control in visible light communication" 8th International Symposium on Communication Systems, Networks & Digital Signal Processing (CSNDSP), 2012, pp. 1−5.

6. K. Lee and H. Park, "Modulations for Visible light Communications with Dimming Control", IEEE Photonics Technology Letters, IEEE, 2011, Vol. 23, pp. 1136−1138.

7. H. Sugiyama, S. Haruyama, and M. Nakagawa, "Brightness Control Methods for Illumination and Visible-Light Communication Systems", Proc. Third International Conference on Wireless and Mobile Communications (ICWMC'07), 2007.

8. Irfanud Din and Hoon Kim, "Energy-Efficient Brightness Control and Data Transmission for Visible Light Communication", IEEE Photonics Technology Letters, 2014, Vol. 26, No. 8, April 15.

9. João Ascenso, e-Business and Telecommunication Networks, Springer, 2006.

10. Liu Yuan-jian, Shi Qin-jian, Ma Xue, and Zhang Ye-rong "Simulation and Analysis of Indoor Visible Light Propagation Characteristics Based on the Method of SBR/Image" International Journal of Antennas and Propagation, Vol. ID905916, 2014.

11. Grubor J., Jamett O.C. G., Walewski J.W., Randel S., Langer K.D., (2007), "High-Speed Wireless Indoor Communication via Visible Light", ITG Bachbericht.

12. J. M. Kahn, and J. R. Barry, "Wireless infrared communication" Proceedings of the IEEE, IEEE, Feb 1997, pp. 265−298.

13. T. Komine, and M. N.akagawa, "Fundamental Analysis for Visible-Light Communication System using LED Lights", IEEE Transactions on Consumer Electronics, IEEE, February 2004, pp. 100−107.

Irfanud Din
is working as Assistant Professor at Inha University at Tashkent. He has done his Ph.D. from Incheon National University South Korea. He received his M.S. in Mechanical Engineering with minor in Computer Engineering from Myongji University, South Korea. He did his B.S. in Computer Systems Engineering from University of Engineering and Technology Peshawar, Pakistan. His field of research focuses on Visible Light Communication, Radio Recourse Management and optimization, and next generation wireless communication systems

Hoon Kim
received his B.S., M.S., and Ph.D. degrees in Electrical Engineering from Korea Advanced Institute of Science and Technology (KAIST) in 1998, 1999, and 2004 respectively. He had been working with Samsung Advanced Institute of Technology (SAIT) during 2004 to 2005, while serving as a Senior Engineer in Communications and Networks Laboratory Division joining the project of design and performance analysis of radio transmission technology for beyond 3G and 4G mobile communication systems. He also had been working with Ministry of Information and Communications (MIC) from 2005 to 2007 as a deputy director in Broadband Communications Division in charge of promotion policies on broadband communications industry such as WiMAX. He joined Stanford University as a visiting scholar during 2007 to 2008 and worked on developing radio resource management algorithms and cross layer optimization schemes for 4G mobile communications systems. He is currently an Associate Professor of the Department of Electronics Engineering at Incheon National University where he has been working with the same department since 2008. His research interests include radio resource management, optimization techniques, 5G mobile communication systems, and internet of things. He is a Member of KICS, IEIE, IEEE, and IEICE

EXPERIMENTAL INDOOR VISIBLE-LIGHT COMMUNICATION SYSTEM USING SOLAR PANEL RECEIVER IN THE PRESENCE OF AMBIENT LIGHT NOISE

Kadirvel Sindhubala and Baba Vijayalakshmi

ECE Department B.S. Abdur Rahman University Chennai, India
E-mails: sindhumtech@yahoo.com; vijayalakshmibaba@gmail.com

ABSTRACT

Solar panels are traditionally used as one of the most promising eco-friendly, emission free energy sources. Instead of photodiode, solar panel can be replaced at the receiver side in the visible-light communication (VLC) system due to the additional advantage of easier targeting of light from white LED and having large collection area. In the proposed system, the transmitter uses white light emitting diode (LED) for providing illumination and communication, atmospheric channel and solar panel at the receiver. However, ambient light noise due to indirect sunlight and fluorescent light is a major concern that affects the performance of the communication system. Hence, adaptive minimum voltage detection (AMD) is used to track minimum voltage produced by the ambient light with the difference amplifier combined with Sallen-Key high pass filter to filter the ambient light noise. Using the proposed experimental system, data rate of 5.78 Kbps and a distance of 1.10 m is achieved between the transmitter and receiver for binary data transmission. The same receiver circuit with ambient noise reduction technique is tested for audio mp3 file and a distance of 0.40 m is achieved.

Keywords: ambient light noise, light emitting diode (LED), solar panel, visible-light communication (VLC)

1. INTRODUCTION

VLC technologies has been identified as an supplement technology for radio frequency(RF) based communication that can be utilized in critical environments such as hospitals, aircrafts, under water communications etc. [1—3]. Moreover, VLC offers advantages such as high security, hazardless to human, huge amount of unregulated bandwidth and licence-free [4]. Commercially available light emitting diode (LEDs) and solar panel are used for **data transmission and reception. The solar panel is** a passive device and it does not require
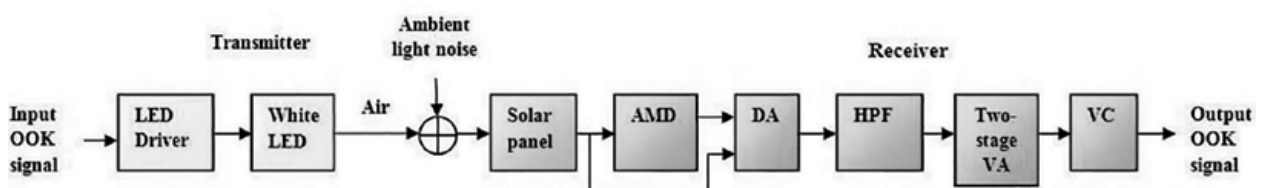
Fig. 1. Block diagram of our proposed of VLC system using solar panel receiver, where
AMD: adaptive minimum voltage detector, DA: difference amplifier, HPF: high pass filter, VA: voltage amplifier,
VC: voltage comparator
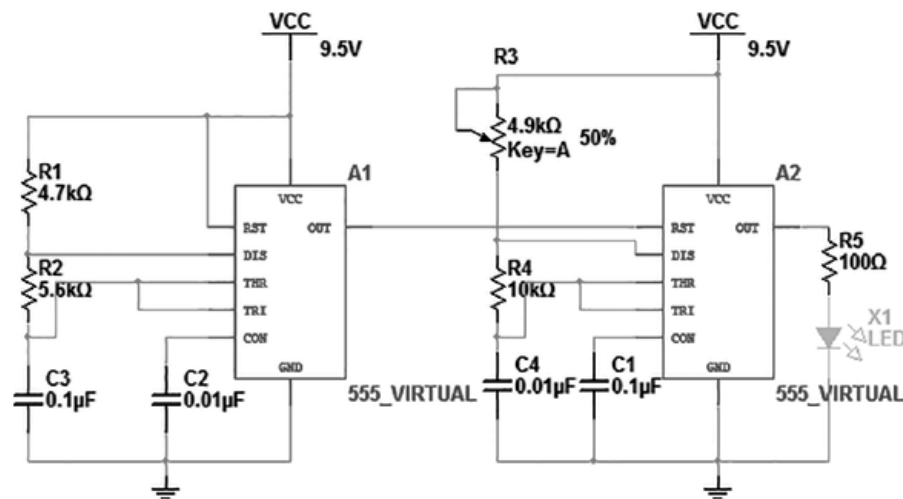
Fig. 2. Schematic design of proposed VLC transmitter
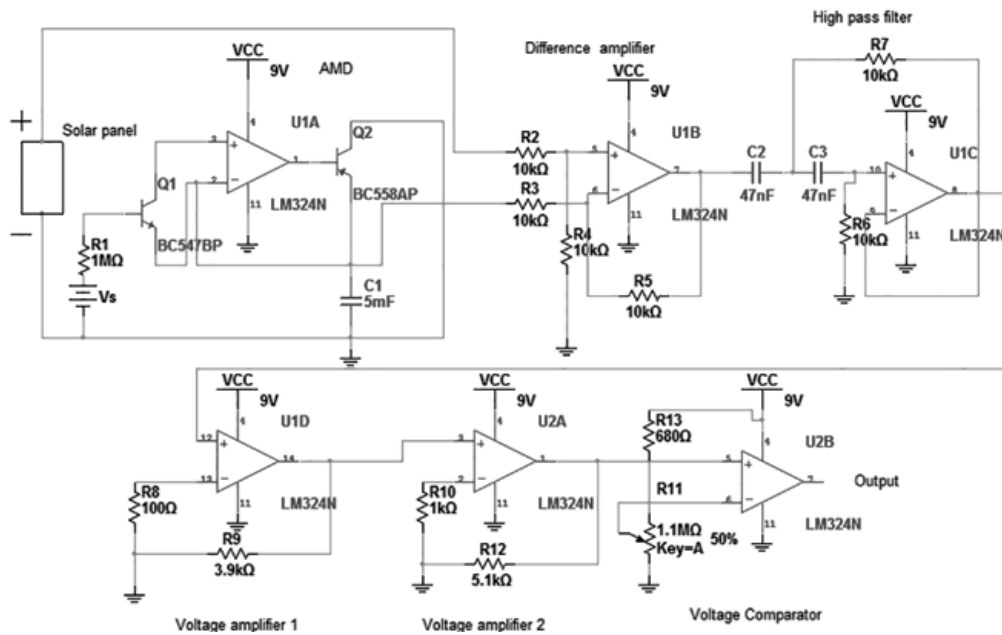
Fig. 3. Receiver circuit solar panel, adaptive minimum voltage detector (AMD), difference amplifier (DA), Sallen-Key high pass filter, voltage amplifiers and a voltage compactor are cascaded

an additional power supplies and has advantages of eco-friendly, large collection area, targeting of light easier. Natural and artificial ambient-light noise has average power larger than the desired input signal power. Therefore, the adverse effect from ambient-light noise for indoor VLC application needs to be addressed to achieve better signal retrieval [5–9].

In [10], a technique to receive optical energy and VLC signal using solar cell is implemented for the data rate of 3Kb/s and the distance achieved between the transmitter and receiver was

40 cm. The effect of sunlight interference was also investigated. However, the transmission distance of this system is only 40cm which is not suitable for practical application. This technique considers only ambient light noise produced by sunlight, fluorescent light noise is not considered.

In [11], experimental investigation of solar panel for communication and energy harvesting was done. Using on/off keying modulation, data rate of 1Mbps and transmission distance of 39 cm was achieved. Using the same transmission distance data rate of 7.01 Mbps was achieved for orthog-
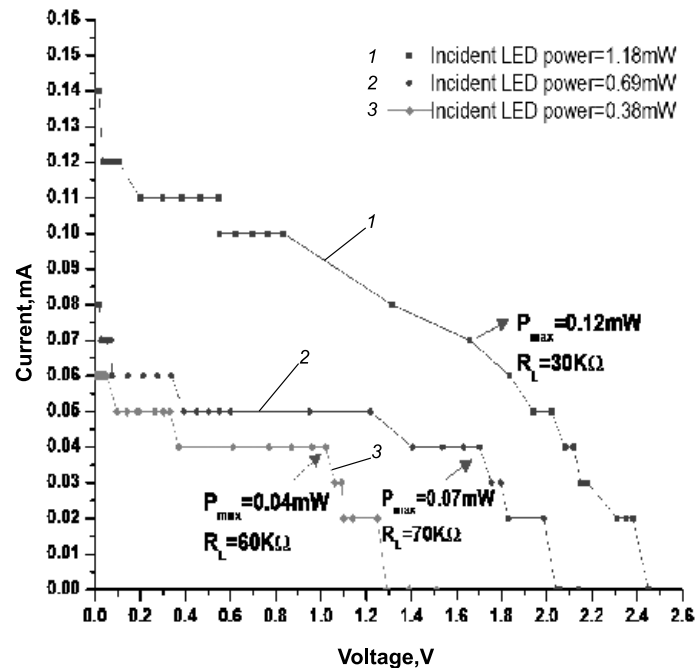
Fig. 4. I/V characteristics of solar panel for different optical power from white LED

onal frequency division multiplexing (OFDM). However, the transmission distance of this system is only 39 cm using on-off keying modulation, which is very minimum for practical applications and it employs capacitor to filter DC component and conventional low pass filter to filter the noise. Using low pass filter, ambient light noise cannot be eliminated completely.

In [12], audio signal transmission in VLC system using solar cell receiver was illustrated. The analytical and experimental studies showed the LED had small divergence beam and transmission distance of 35 cm was achieved. However, the distance achieved is very small.

In [13], design of VLC receiver to remove the noise from ambient lights using OOK modulation was done and tested. This VLC receiver uses photodiode at the receiver side and distance of 1m is achieved. However, photodiode can be replaced with the eco-friendly solar panel and the performance is tested using the same receiver circuit in the presence of ambient light noise.

In this paper, we present the inexpensive experimental design of VLC transmitter using on-off keying (OOK) modulation and receiver using solar panel for the data rate of 5.78 Kbps and distance of 1.10m. The ambient light noise from indirect sunlight and fluorescent light in indoor environment is also considered in the receiver design

to achieve better signal retrieval. The performance analysis is done for different distances with respect to output voltage at the solar panel, and optical power at the photodiode. The paper is organized as follows. Section 2 describes the indoor VLC system with solar panel receiver and provides the characteristics of solar panel, the results and discussion. Section 3, describes the audio transmission using solar panel receiver in VLC system with their testing and results. Finally, our conclusions are given in section 4.

2. SYSTEM DESCRIPTION OF PROPOSED INDOOR VLC SYSTEM USING SOLAR PANEL RECEIVER

VLC system mainly consists of two parts, one is the transmitter module and the other is the receiver module. Line of Sight (LOS) channel model is considered between the transmitter and receiver.

Fig. 1. shows the overall VLC system block diagram of the proposed VLC system using solar panel receiver employing ambient light noise reduction technique

2.1. Transmitter module

In the transmitter module, the commercial high power white LED is chosen to make sure that the
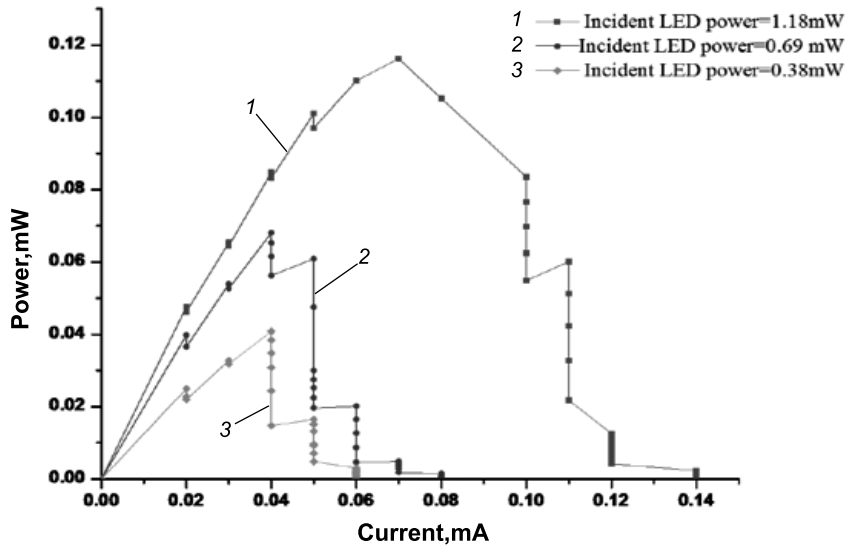
Fig. 5. P/I characteristics of solar panel for different optical power from white LED

colour temperature are both safe and comfortable for the human eyes. Luminous intensity in angle ϕ is given by

$$I(\varphi) = I(0)\cos^{m}(\varphi). \quad (1)$$

The order of Lambert emission m is related to the LED semiangle at half-power $\varphi_{1/2}$ by

$$m = \frac{-\ln 2}{\ln\left(\cos\phi_{1/2}\right)}, \quad (2)$$

where $\phi_{1/2}$ is the half-power semiangle of LED.

A horizontal illuminance E_{hor} at a point (x, y) is given by

$$E_{hor} = I(0)\cos^{m}(\varphi)d^{2}\cos(\psi), \quad (3)$$

where $I(0)$ is the centre luminous intensity of an LED, φ is the angle of irradiance, ψ is the angle of incidence, d is the distance between the transmitter and receiver.

Light emitting source of 1 Watt with the viewing angle as 90°, forward current of 0.35A/3.2W, power dissipation of 1.6 W and luminous intensity of 80 lm is used. OOK (on/off keying) is applied to modulate the LED. Reflector is used in the transmitter side to improve the communication range and results. The schematic circuit of proposed VLC transmitter is shown in Fig. 2

2. 2. Line of sight (LOS) channel

In the paper, atmospheric channel is considered between the transmitter and receiver. LOS Channel DC gain for the LED source is given by

$$H(0) =$$

$$= \begin{cases} \dfrac{A(m+1)}{2\pi d^{2}}\cos^{m}(\theta)\cos(\Psi), & 0 \leq \Psi \leq \Psi_{c} \\ 0 & \Psi > \Psi_{c} \end{cases}, \quad (4)$$

where d is the distance between the transmitter and receiver, ψ is the angle of incidence with respect to the receiver axis, Ψ_{c} is the FOV of the receiver.

The received power is given by $p_{r} = H(0) \cdot p_{t}$. (5)

$H(0)$ is the DC channel gain and p_{t} is the transmitted optical power of LED source.

2. 3. Receiver module

The receiver module mainly consists of solar panel and signal conditioning devices. Primarily, solar panel is used to accumulate optical energy from the sun. On the other hand, solar panel can also be used to collect the optical signal from LED. Thus, energy convergent VLC receiver is implemented without photodiode and other power supply systems. In this work, multi crystalline silicon photovoltaic solar panel of size (250×145×15) mm, module efficiency of 10 % is used as it is cost efficient and space requirements are lesser com-
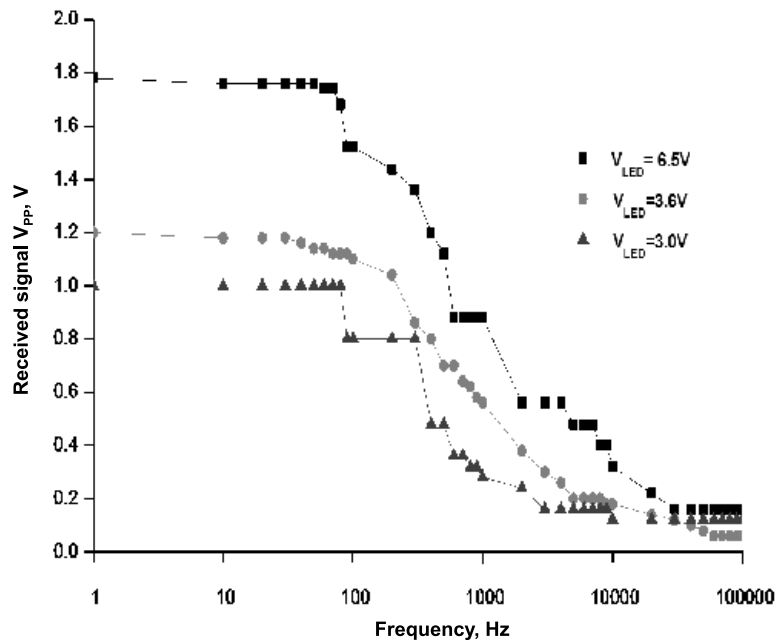
Fig. 6. Frequency response of solar panel for different voltage across white LED
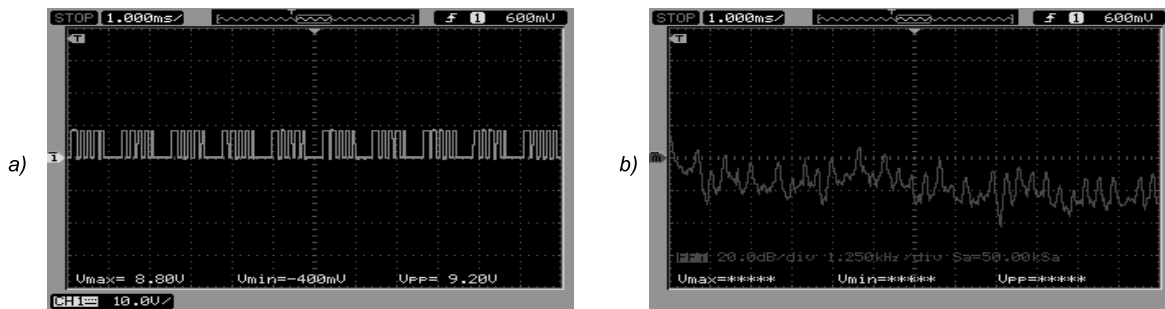
Fig.7. a) Output time-domain waveform of the transmitted input signal

b) Spectrum of the transmitted input signal
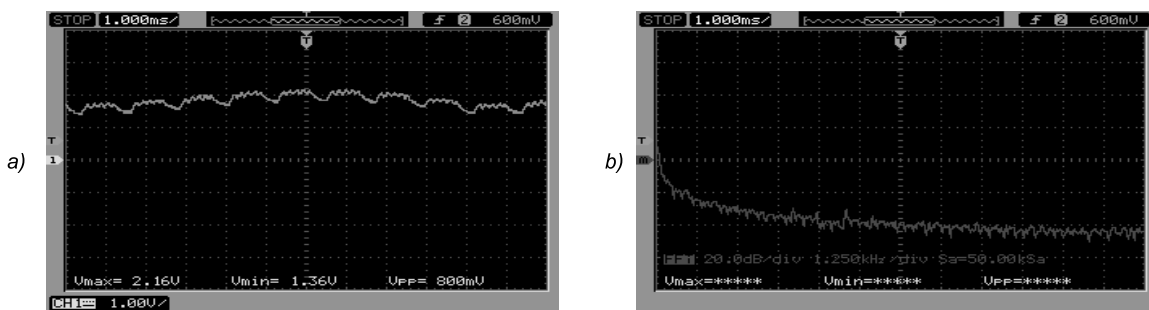
Fig.8. a) Output time-domain waveform of the solar panel output signal

b) Spectrum of the solar panel output signal

pared to monocrystalline PV module. The output signal from the solar panel is weak with lot of background ambient light noises and wireless communication distance also makes the situation worse. Therefore, the ambient noise reduction circuit becomes the critical part of our VLC system. Firstly, the solar panel is used in the receiver side to convert the optical signal into electrical signal. Adaptive minimum-voltage detector is used to track the minimum voltage produced from the ambient light. Difference amplifier (DA) is used for removing the minimum voltage. However, the ambient light noise is not completely removed using this stage. Hence, Sallen-Key high pass filter with a cut-off frequency of around 300 Hz is used to by-pass the ambient light noise. Two stage am-
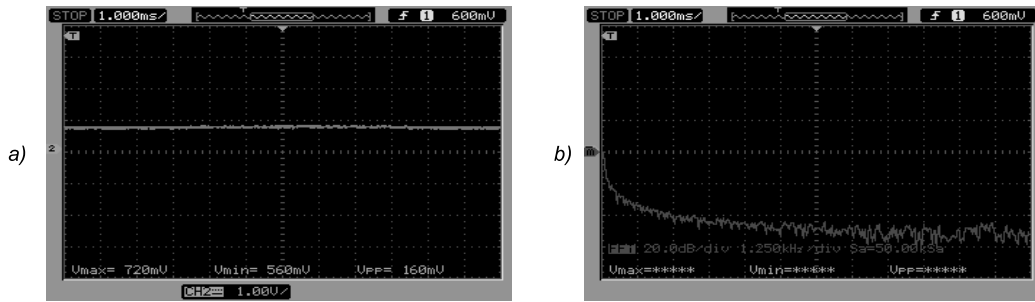
Fig.9. a) Output time-domain waveform of the sunlight signal

b) Spectrum of the sunlight signal
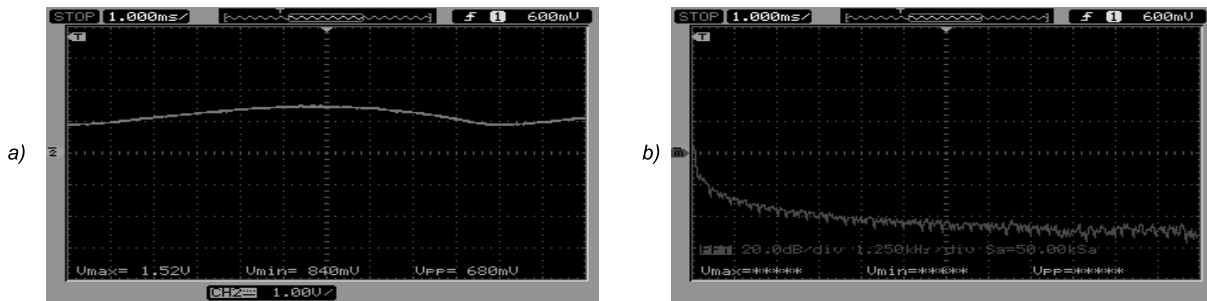
Fig.10. a) Output time-domain waveform of the sunlight and fluorescent light signal

b) Spectrum of the sunlight and fluorescent light signal
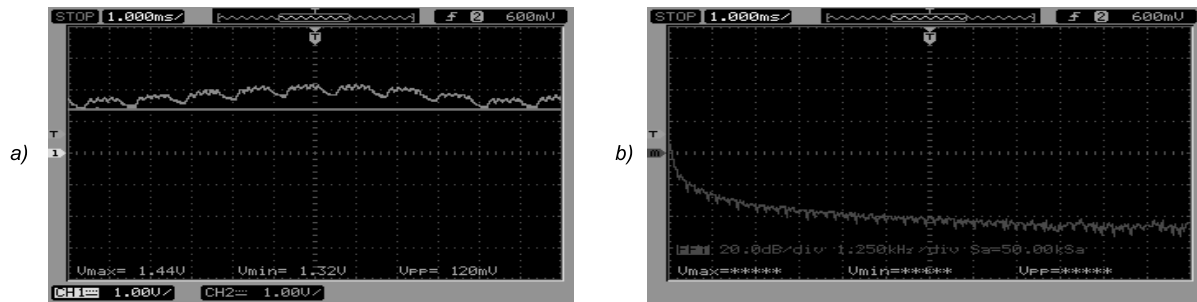
Fig.11. a) Time domain waveform of the adaptive minimum voltage detection (AMD) signal

b) Spectrum of the adaptive minimum voltage detection (AMD) signal
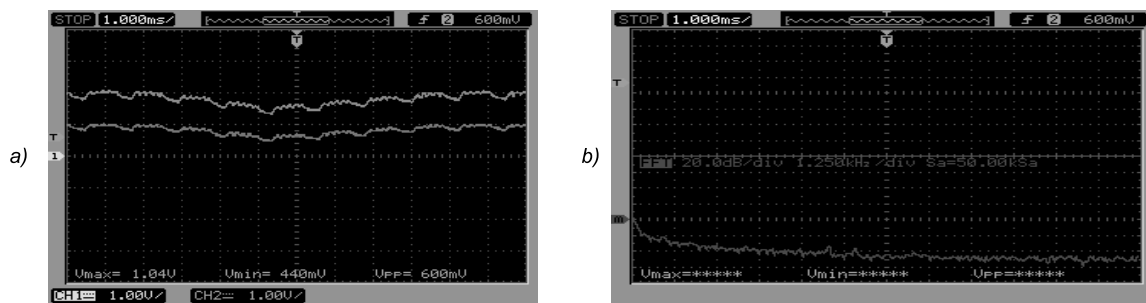
Fig.12. a) Time domain waveform of the difference amplifier (DA) signal

b) Spectrum of the difference amplifier (DA)signal

plifiers are used to amplify the weak signal to appropriate amplitude. Finally, the amplified signal is reshaped into the digital data signal using voltage comparator. Thus the transmitted signal is recovered back in the receiver side. Fig. 3 shows the VLC receiver circuit.

2.4. Solar panel characteristics

The solar panel used is multicrystalline silicon photovoltaic solar panel of size 250×145×15 mm, module efficiency of 10%. Fig. 4 shows the voltage vs. current graph of the solar panel for dif-
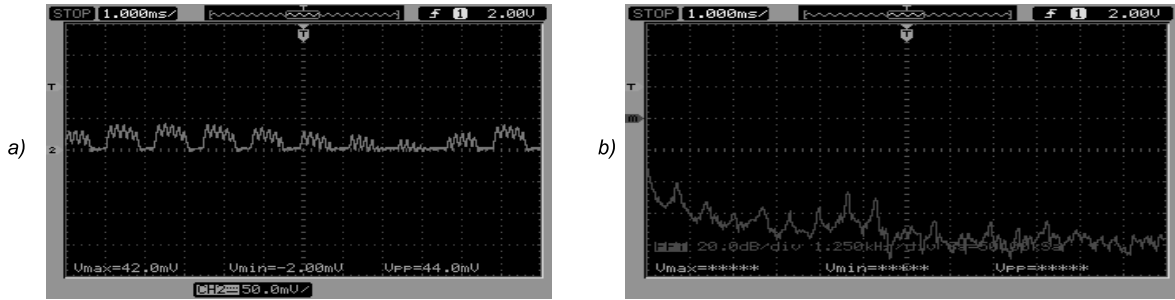
Fig.13. a)Time-domain waveform of the high pass filter signal

b) Spectrum of the high pass filter filter signal
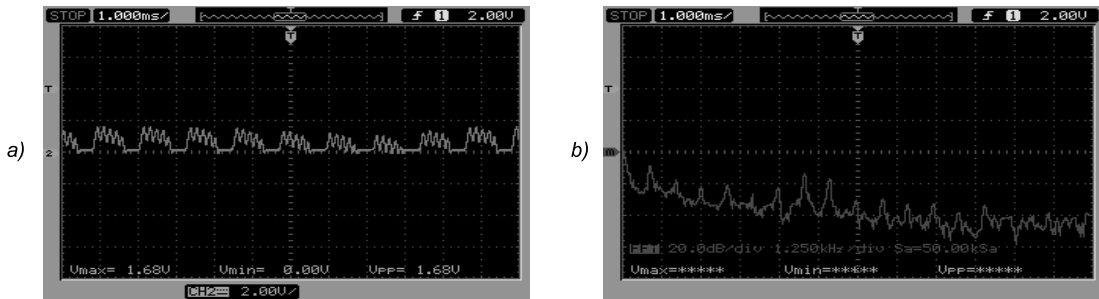
Fig.14. a)Time-domain waveform of the voltage amplifier stage1 signal

b) Spectrum of the voltage amplifier stage1 signal
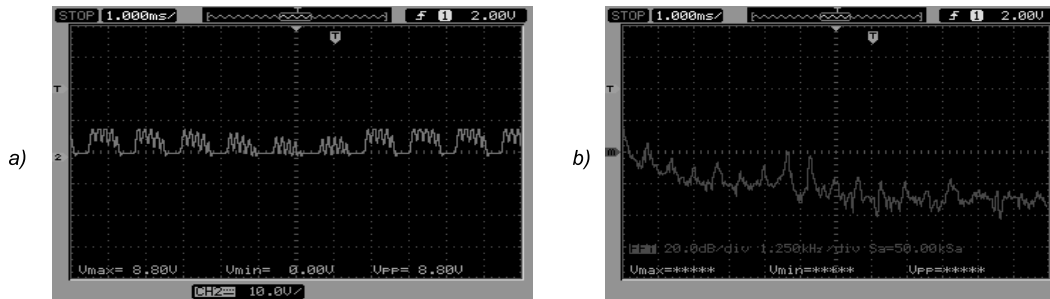
Fig.15. a)Time-domain waveform of the voltage amplifier stage2 signal

b) Spectrum of the voltage amplifier stage 2 signal
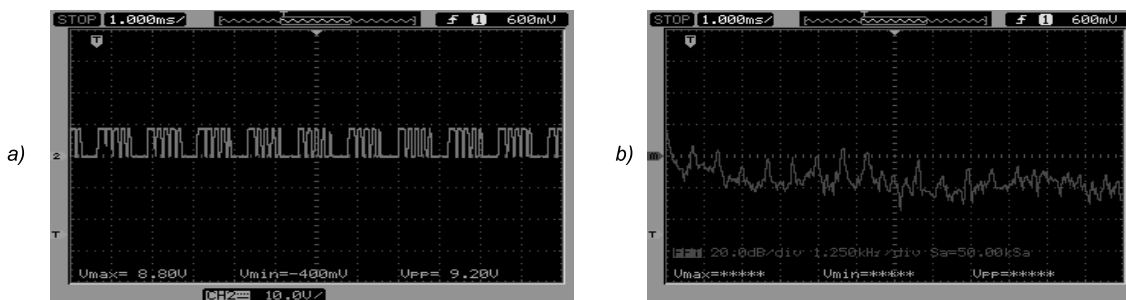
Fig.16. a) Time-domain waveform of the voltage comparator signal

b) Spectrum of the voltage comparator signal

ferent optical power from the white LED source. In Fig. 4 the electrical power from the solar panel is obtained by the multiplication of current and voltage. For the first case, the incident optical power is 0.38 mW. The maximum electrical power obtained from the solar panel is 0.04 mW at the load resistance of 60KΩ. Therefore, the optical to electrical conversion efficiency is 9.5%. For the second case, the incident optical power is varied to 0.69 mW.The maximum electrical power obtained from the solar panel is 0.07 mW at the load resistance of 70KΩ.Optical to electrical

conversion efficiency is 9.8%. For the third case, the incident optical power is varied to 1.22 mW. The maximum electrical power obtained from the solar panel is 0.12 mW at the load resistance of 30KΩ. Optical to electrical conversion efficiency is 9.83%.

Fig. 4 I/V characteristics of solar panel for different optical power from white LED is presenting and Fig. 5 shows the electrical power vs. current characteristics of solar panel for different optical power from white LED.

Fig. 6 shows the frequency response of solar panel for different voltage across the white LED. It is observed, the maximum achievable bandwidth of solar panel is 10 KHz, and the solar panel can receive even low frequency signals.

2.5. Experimentation and results

That proposed VLC system consists of transmitter, optical wireless channel and the receiver consisting of solar panel. Ambient light noise due to indirect sunlight and fluorescent light is a major concern that affects the performance of the communication system. Hence, ambient light noise reduction circuitry is introduced to reduce the noise. Thus the transmitted signal is recovered back at the receiver with the reduced ambient light noise. The experiment was performed inside the electronics laboratory of B.S Abdur Rahman University which is considered as an indoor VLC system. The experiments are carried out at the data rate of 5.78 Kbps, and the communication distance of 1.10m is considered between the transmitter and receiver. The analyses of observations are discussed in the succeeding section.
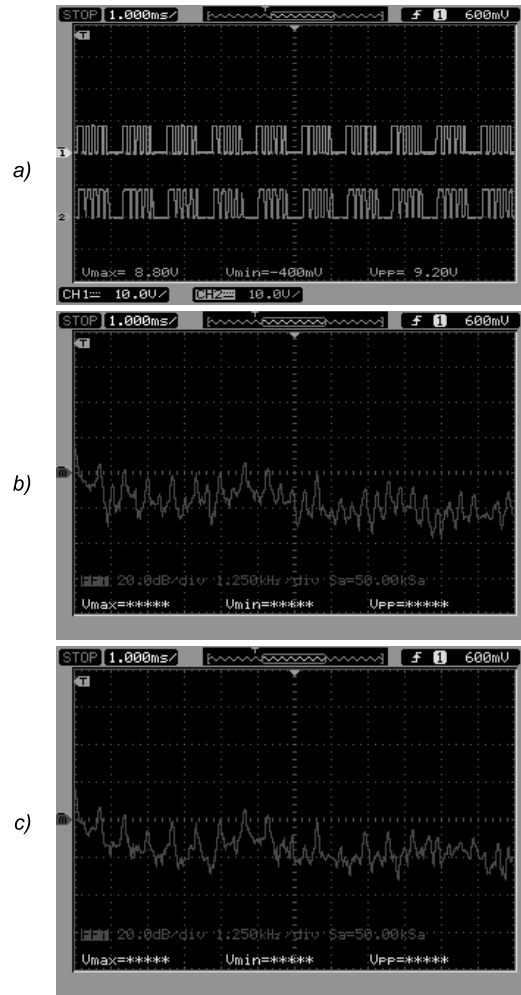
Fig.17. a)Time-domain waveform of the transmitted input and received output signal b) Spectrum of the transmitted input signal c) Spectrum of the received output signal

This proposed VLC system consists of transmitter where the OOK signal is transmitted via white LED and the electrical signal is converted
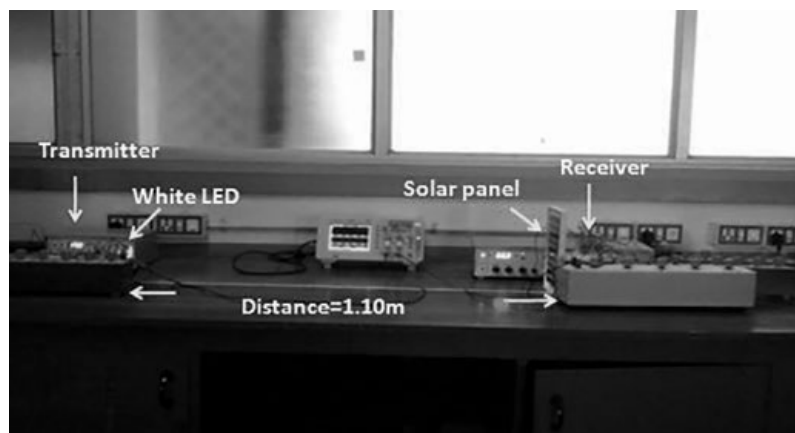
Fig. 18.Experimental test bench of the proposed VLC system using solar panel receiver
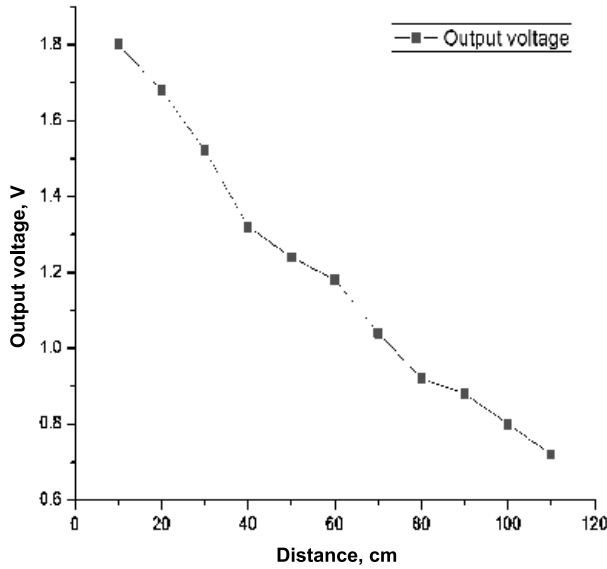
Fig. 19.The graph of the vertical distance between transmitter and receiver vs. output voltage produced at the solar panel
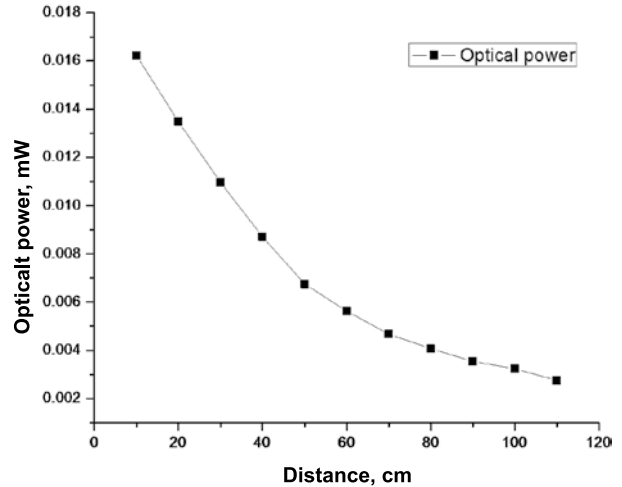
Fig. 20.The graph of the vertical distance between transmitter and receiver vs.optical power

as intensity modulated optical signal. Figs. 7a, b show the time-domain waveform and spectrum of the input electrical signal. The optical signal is transmitted via air as the free space medium and the optical signal is detected by the solar panel. Figs. 8a, b show the time-domain waveform and spectrum of the solar panel. The output signal retrieved from the solar panel suffers with the ambient light noise. The ambient sources of noise in the proposed VLC system include indirect sunlight and fluorescent light lamps operated by conventional ballast. The indirect sunlight induces strong direct current (DC) onto the solar panel. Figs. 9a, b show the time-domain waveform and spectrum of the indirect sunlight in the room, in which the experiment is carried out. The rectified sine wave form is emitted from the fluorescent light lamp operated by conventional ballast. Figs. 10a, b show time-domain waveform and spectrum of the indirect sunlight and fluorescent light. Adaptive minimum-voltage detector (AMD) is used to track the minimum voltage of the sig-

nal received from ambient light noise. Figs. 11a, b show the time domain waveform and spectrum of the adaptive minimum detection (AMD) signal. Difference amplifier (DA) is used for reducing the minimum voltage produced by the ambient light. Figs. 12a, b show the time domain waveform and spectrum of the difference amplifier (DA) signal. The ambient light noise is not completely reduced in DA stage; hence Sallen-Key high pass filter is used to reduce the ambient light noise. Figs. 13a, b show the time-domain waveform and spectrum of high pass filter signal. Two stage amplifiers are used to amplify the weak signal to the signal of appropriate amplitude to the input signal. Figs. 14a, b show the time-domain waveform and spectrum of voltage amplifier stage1 signal. Figs. 15a, b show the time-domain waveform and spectrum of voltage amplifier stage 2 signal. The amplified signal is converted to digital signal using voltage comparator. Figs. 16a, b show the time-domain waveform and spectrum of voltage comparator signal. Thus, the transmitted signal is recovered back in the receiver side. Figs. 17a, b, c show the time-domain waveform and spectrum of transmitted input signal, and the received output signal. The exper-
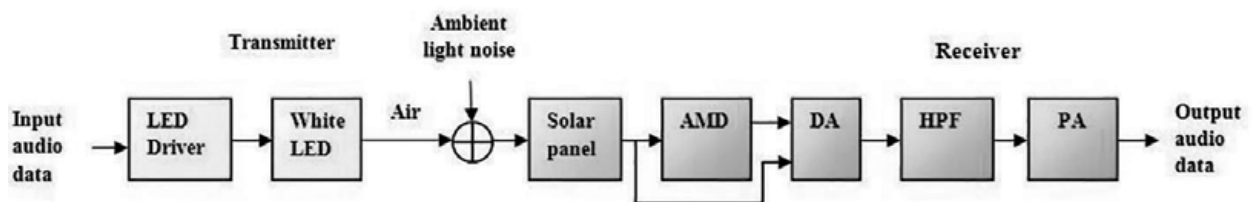
Fig. 21. Block diagram of proposed audio transmission in VLC system using solar panel receiver: AMD: adaptive minimum voltage detector, DA: difference amplifier, HPF: high pass filter, PA: power amplifier
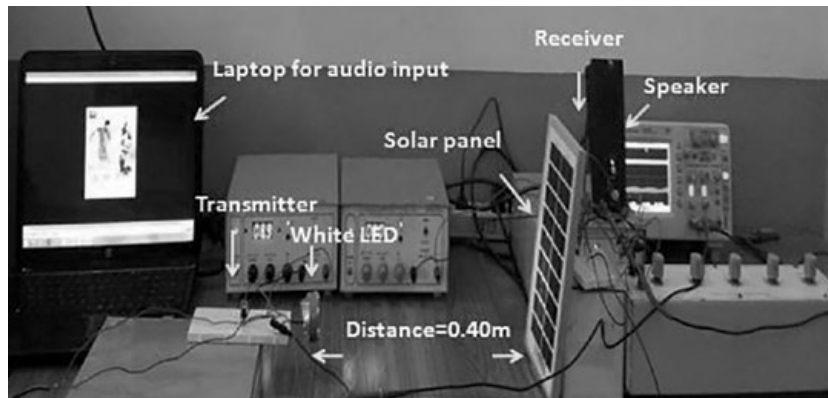
Fig. 22.Experimental test bench of the proposed audio transmission in VLC system

imental test bench of the proposed VLC system is shown in Fig. 18.

Fig. 19 shows the graph of the output voltage produced at the solar panel for the different vertical distance between the transmitter and receiver up to 1.10m.

It is observed from the Fig. 19, that the received output voltage decreases and is directly proportional to the increase in vertical distance between the transmitter and receiver. The maximum achievable distance of the proposed VLC system is 1.10m.

Fig. 20 shows the graph of the output optical power for the different vertical distance between the transmitter and receiver up to 1.10m.

It is observed from the Fig. 20, that the received optical power from LED decreases with the increase in vertical distance between the transmitter and receiver.

3. AUDIO SIGNAL TRANSMISSION IN VLC SYSTEM

The block diagram of our proposed audio transmission in VLC system using solar panel receiver is presented in Fig. 21.

3.1. Experimentation and results

The audio system in VLC system consists of the transmitter, atmospheric channel and the receiver. The transmitter consists of standard 3.5mm audio jack to supply the input of mp3 audio signal from laptop and TIP31 transistor is used for transmitting the audio via 1W white LED, which is driven by 9V DC power supply. Thus the electrical audio signals are converted into light pulses using white LED. The signal is transmitted via atmospheric channel
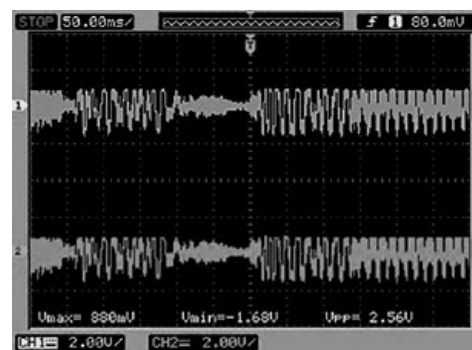
Fig. 23. Captured transmitted and received music waveforms

and received by the solar panel. The output signal received from the solar panel is very weak and the quality of the signal gets affected by the ambient light noise from indirect sunlight and fluorescent lamp driven by conventional ballast. Ambient light noise reduction circuit used for the above data transmission system is the same used for the proposed audio transmission in VLC system. Adaptive minimum-voltage detector is used to track the minimum voltage of the signal received from ambient light. Difference amplifier (DA) is used for removing the minimum voltage. However, the ambient light noise is not completely removed using this stage. Hence, Sallen-Key high pass filter with a cut-off frequency of around 300 Hz is used to bypass the ambient light noise. The ambient noise reduced signal is very weak. Hence, it is power amplified and the music signal is recovered back at the receiver. The distance achieved between the transmitter and receiver is 0.40m, Figs. 22, 23.

4. CONCLUSION

In this paper, an indoor VLC system using solar panel receiver with the ambient light noise re-

duction technique is implemented. The transmission rate of 5.78 Kbps and a distance of 1.10 m is achieved between the transmitter and receiver for the binary data transmission. After successful transmission and reception of data, we have considered the same ambient noise reduction circuit in the receiver side for audio data transmission and 0.40 m is achieved between the transmitter and receiver. Thus environmental friendly data transmission in VLC system is implemented using solar panel receiver.

REFERENCES

1. Shinichiro Haruyama, "Advances in Visible Light Communication Technologies" ECOC Technical Digest, 2012.

2. Y.Cheong, X.Weing, W.YounChung "Hazardless Biomedical Sensing Data Transmission Using VLC", IEEE sensors Journal, 2013, Vol. 13, pp. 3347–3348.

3. C Rust, H.H Asada," A dual-use visible light approach to integrated communication and localization of underwater robots with application to non-destructive nuclear reactor inspection", IEEE international conference on Robotics and Automation (ICRA), 14–18 May 2012, pp. 2445–2450.

4. J.Yoo, R. Lee, J. Oh, H. Seo, J. Kim, H. Kim and S.Yoon Jung, "Demonstration of Vehicular Visible Light Communication Based on LED Headlamp", International Conference on Ubiquitous and Future Networks (ICUFN), 2–5 July 2013, pp. 465–467.

5. C.W. Chow, C. H. Yeh, Y..F. Liu, P.Y. Huang, "Mitigation of Optical Background Noise in Light-Emitting Diode (LED) Optical Wireless Communication Systems", IEEE photonics Journal, Jan 2013, Vol. 5.

6. C.W Chow, C. H. Yeh, Y..F Liu, P.Y Huang, "Background Optical Noises Circumvention in LED Optical Wireless Systems Using OFDM", IEEE photonics Journal, Vol. 5, Apr 2013.

7. A. Nazmi Mohamed, M. Asmaa Aly, K. Ahmed, Aboul Seoud, H. Moustafa Aly, "Indoor wireless optical communication systems: effect of ambient noise", Optical Engineering, May 2014, Vol. 53.

8. A. Cailean, B. Cagneau, L. Chassagne, V. Popa, M. Dimian, "Evaluation of the noise effects on Visible Light Communications using Manchester and Miller coding" 12th International Conference on development and application systems, Romania, May 15–17, 2014.

9. C. Chang, Y. Su, U. Kurokawa, and B. Ichoi, "Interference Rejection Using Filter-Based Sensor Array in VLC Systems" IEEE Sensors Journal, May 2012, Vol. 12, pp. 1025–1032.

10. S. Kim, J. Won, S. Nahm, "Simultaneous reception of solar power and visible light communication using a solar cell", Optical Engineering, Apr.2014, Vol. 53.

11. Z. Wang, D. Tsonev, S. Videv, H. Haas, "On the Design of a Solar-panel Receiver for Optical Wireless Communications with Simultaneous Energy Harvesting" IEEE Journal on Selected Areas in Communications, 2015, Vol. 33, no. 8.

12. M. Syuhaimi Ab-Rahman, L. Al-Hakim Azizan, H. Ramza and Z. Musa, "The Comparison of Experimental and Analytical Study of the Gaussian Intensity Distribution for Light Emitting Diodes Beam", Journal of Computer Science, 2012, Vol. 8, #.6, pp. 913–919.

13. Y. Zhao and J. Vongkulbhisal, "Design of Visible Light Communication Receiver for On-Off Keying Modulation by Adaptive Minimum-Voltage Cancelation", Engineering Journal, Oct.2013, Vol. 17.

SURVEY ON NOISE SOURCES AND RESTRAIN TECHNIQUES IN VISIBLE-LIGHT COMMUNICATION

Kadirvel Sindhubala and Baba Vijayalakshmi

ECE Department B.S. Abdur Rahman University Chennai, India
E-mails: sindhumtech@yahoo.com; vijayalakshmibaba@gmail.com

ABSTRACT

Solid state lighting is revolutionizing in indoor illumination. Current incandescent and fluorescent lamps are replaced by light emitting diode (LED) at fast pace. LED offers low cost, power efficient, faster switching speed and it can be perceived by the human eye. Visible-light communication (VLC) is a wireless technology, which uses LED at the transmitter and suitable photodetector at the receiver.VLC overrides the drawbacks of radio frequency(RF) communication like restricted bandwidth, radiation hazards and environmental hazards. The main challenges in implementing the VLC systems are optimizing the optical background noise. It is produced by natural, artificial ambient light source and other kinds of noise at the receiver side, which limits the performance of the communication system. This survey provides the technology overview, review of different optical background noise sources, reduction techniques in VLC done by different researchers and a novel noise reduction technique at the receiver is proposed overcoming the drawbacks of the conventional methods.

Keywords: data communication, illumination, light emitting diode, radio frequency, visible-light communication, noise source

I. INTRODUCTION

Visible-light communication is an optical wireless communication technology, which uses spectrum of wavelength from 380 nm to 750 nm and is standardized by Institute of Electrical and Electronics Engineers (IEEE) [1]. VLC using LED is a promising technology to supplement existing RF communication. LED has properties such as energy efficient, low cost, high brightness and long life time. Hence, in VLC, the conventional lightings such as incandescent lamps and fluorescent lamps are replaced by the LEDs. Nowadays, in general, the LEDs are used in many places such as traffic lights, automobiles, indoor and outdoor lighting. Further, the on-off transient time of the LED is short, which offers high data rate transmission in VLC. VLC finds its application in many areas such as hospitals, underwater communications and road to vehicular communications as well as location based communications [2−7].

One of the main challenges, existing in VLC system are the optical background noises from natural and artificial ambient light and other noise sources contributed at the receiver side. To this, the indoor lighting sources such as incandescent lamps, fluorescent lamps driven by conventional and electronic ballast and outdoor lighting sources such as sunlight contributes the broad range of wavelength, which could overlap the transmission wavelength used in VLC [15−30, 32]. Hence, ambient noise reduction techniques are necessary to reduce the in band interferences occur from other lighting sources to improve the performance of the communication system.

In this paper, a survey of VLC system under the influence of noise sources is analyzed. The paper is organized in the following sections. In Section 2, the theory of VLC system is discussed. Section 3,
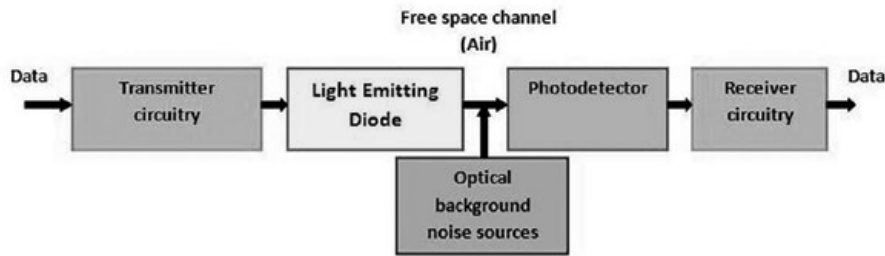
Fig. 1.Block diagram of VLC system

describes the noise at the receiver. Section 4, deals with the survey of existing methods applied for the noise reduction done by different researchers. Section 5, defines about the proposed method and the comparative study with the existing methods.

2. THEORY OF VLC SYSTEM

This section provides a brief overview of data transmission through VLC. It uses LED where the data is transmitted using intensity modulation (IM) technique. The detected intensity is converted as an equivalent electrical signal from the photodetector. This process is described as direct detection (DD). IM/DD methods are advantageous over the other methods, since they are simple and easy to implement. The basic blocks of VLC data transmission through IM/DD is represented in Fig. 1, followed by individual block function description.

2.1. VLC transmitter

The VLC transmitter uses visible white LEDs, which is different from the conventional lighting sources in the point of view that it must provide both illumination and data communication simultaneously. There are two different ways to generate white light using LEDs. Devices that use blue emitter in combination with a yellowish phosphor and trichromatic (RGB) LEDs are used to generate white light [8]. The comparison of RGB LEDS to phosphor based LEDS is described at the end of this paper as Table 1. Performances of two different types of white LEDs under various design challenges.

White LEDs are used as a modulation device on the optical carrier on visible light. The modulation bandwidth requirements of the LEDs are to be considered for data modulation. Visible white LEDs are usually high brightness LEDs and the manufacturers do not develop high brightness LEDs for communication purposes. But very high modulation band width is required for high data rate communication. Consequently, the research work is motivated to improve the modulation bandwidth of LED. Secondly, VLC transmitter must provide illumination as well at the time of data communication. For office work, general illumination of 300 to 1500 lx is required. The high brightness LEDs operate with the forward current > 100 mA, which is quite large with the communication devices. Hence, the VLC transmitter is complex than the conventional transmitter design as it needs to provide both illumination and data communication [12].

2.2. Channel modeling

The noise model should also be included with the channel model. Thus VLC channel is modeled as a linear optical additive white Gaussian noise (AWGN) channel and is described by the following equation (1)

$$I(t) = \eta\, p_i(t) \otimes h(t) + N(t), \qquad (1)$$

where I(t) is the photodetector current, η is the photosensitivity of the Photodetector, $p_i(t)$ is the instantaneous input power, $\otimes$ the symbol denotes the convolution (t) denotes the impulse response and N(t) denotes the AWGN noise. VLC can be applied in two different scenarios, which are Line Of Sight (LOS) and Non Line Of Sight (NLOS) [15, 31]. Line Of Sight (LOS) is the unobstructed path of communication between the transmitter and the receiver. The transmitter directs the light beam in the direction of the receiver. In the LOS case the received power is given by equation (2)

$$P_rLOS = H_LOS(0)P_t, \qquad (2)$$
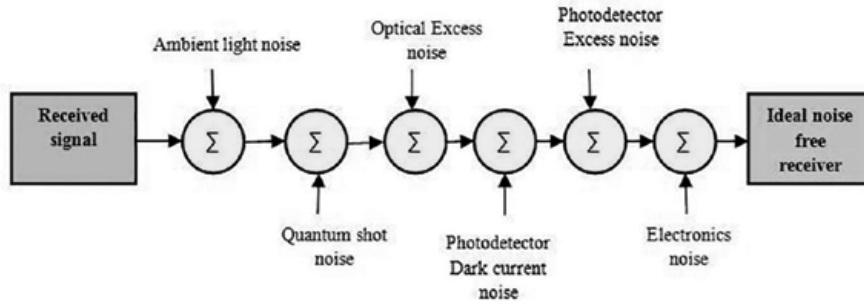
Fig. 2.Different sources of noise in optical wireless communication link

In the NLOS case, the light reflected by walls or by any other obstacles is taken under consideration. The received power is generally given by the channel DC gain on the LOS and reflected path $H_{ref}(0)$ is given by the equation (3)

$$P_r = H_{LOS}(0) + H_{NLOS}(0)P_t =$$
$$= H_{LOS}(0)P_t + \Sigma_{ref}H_{ref}(0)P_t. \qquad (3)$$

The non-directed LOS or diffused lighting achieves only limited data rate.

In the NLOS case, let us consider the effect of light reflected by walls or any other obstacles. The received power is generally given by the channel DC gain on LOS and reflected path $H_{ref}(0)$ is given by eq. (4)

$$P_r = H_{LOS}(0) + H_{NLOS}(0)P_t$$
$$= H_{LOS}(0)P_t + \Sigma_{ref}H_{ref}(0)P_t. \qquad (4)$$

The interference must be modelled along with the channel model. At the receiver side, the irradiance produced by the background light is given by eq. (5) [13]

$$H(t) = H_B + H_{interf}(t), \qquad (5)$$

where H_B is the average background irradiance and $H_{interf}(t)$ is the time varying component.

The optical power is converted into current in the receiver side by the photodiode. So the background irradiance produced by the light sources produces shot noise and there will be variations in the optical power due to the interference. The output current at the photodiode is given by eq. (6) [13]

$$i_d(t) = I_B + i_{interf}(t) + i_{noise}(t), \qquad (6)$$

where

$$I_B = A_r R_a H_B, \qquad (6a)$$

where

$$i_{interf}(t) = A_r R_i H_{interf}(t). \qquad (6b)$$

A_r is the photodetector active area and R_a and R_b are the responsivity of the photodetector for the average and interference irradiance.

2.3. VLC receiver

Two kinds of detectors such as PIN diodes and avalanche photodiodes (APDs) are used in the VLC. PIN photodiodes are mostly preferred, compared to APDs due to low cost, ability to withstand wide temperature fluctuations and it can be operated by an inexpensive low bias voltage power supply. The receiver sensitivity of PIN photodiode is 10 to 15 dB less compared to APDs. In order to compensate the reduced sensitivity of PIN receivers, the transmitter power is increased and larger diameter of lens is used. However, APDs can be operated with less transmitter power and has better internal gain. The signal to noise ratio (SNR) is increased, but APD receivers are costly and requires high operating voltages [8].

3. NOISE AT THE RECEIVER IN OPTICAL WIRELESS COMMUNICATION SYSTEM

There are different sources of noise, which degrades the performance of the optical wireless communication system [14]. Fig. 2 shows the different sources of noise in optical wireless communication link.

3.1. Optical excess noise

When laser is used in transmitter side, any noise that combines with the received signal other than the quantum shot noise is called optical excess noise.

3.2. Photodetector excess noise

Photodetector excess noise occurs due to gain multiplication process internal to the photodetector.This kind of noise is present only in photodetector with internal gain like avalanche photodiode or photomultiplier tube (PMT).

Both the above mentioned kinds of noise can be eliminated in VLC using LEDs and PIN photodiodes. The noise sources that are considered in the VLC system using white LEDs and the photodiode as receiver are ambient light noise, quantum shot noise, electronics noise and photodetector dark current noise.

3.3. Dark current noise

Dark current noise occurs in the photodetector due to random emission of electrons due to absorption of thermal energy at a fixed average rate when no field is being detected. It depends on the temperature and area of the photodetector. The dark current I_d is modeled as a DC current with noise PSD is given by eq. (7)

$$S_d(f) = I_d{}^2 \delta(f). \tag{7}$$

3.4. Ambient light noise

Different light sources such as natural and artificial background light contribute to the ambient light noise. Source of natural ambient light noise is sunlight. The artificial ambient light comes from many light sources such as incandescent lamps, and fluorescent lamps driven by conventional and electronic ballasts.

3.5. Quantum shot noise

The mean of photocurrent is taken from the sunlight, ambient light interference and dark current contains the desired signal of interest that varies with the received optical power, where the vari-

ance act as distortion to the desired signal received and it represents how much amount of noise power is present in the photodetector's output. Quantum shot noise exists due to quantum mechanical nature of light. The PSD of quantum shot noise due to unmodulated ambient and dark current is given by eq. (8)

$$
S_{ds}(f) = \\
= 2e[\frac{e}{hc} \int_{\lambda rL}^{\lambda rH} \eta(\lambda)\lambda S_b(\lambda) R_f(\lambda)\,\mathrm{d}\lambda + I_d], \tag{8}
$$

where $S_b(\lambda)$ represents the ambient light noise power spectral density.

3.6. Electronics noise

The electronics noise occurs at the pre-amplifier front end. Four kinds of front end amplifier designs such as resistor termination with a low-impedance voltage amplifier, high impedance amplifier, transimpedance amplifier, and noise matched or resonant amplifier are used in the optical receivers. Among all these four types of amplifiers, transimpedance amplifiers are widely used in VLC because of the capacity to achieve high bandwidth and low noise at the same time. It shows the transimpedance amplifier circuit with the feedback impedance *Zfb (ω)* and open loop gain *A_v (ω)*.

The equivalent input current noise PSD of Transimpedance amplifier is given by eq. (9)

$$
s_a(f) = i_n{}^2 + \frac{4kT}{R_{fb}} + \frac{v_n{}^2}{R_t{}^2}\left[1 + (2\pi R_{fb}c_t f)^2\right], \tag{9}
$$

where $R_t = Rf_b A_0 R_d / [(A_0 +1)R_d + Rf_b]$, $c_t = c_{fb} + c_d$, Rf_b is the feedback resistance, A_0 is the core amplifier DC gain $A_v(0)$, c_{fb} is the feedback capacitance, C_d, R_d are the resistive and capacitive parts of the combined impedance. The noise performance of the core amplifier is characterized by spectral densities $v_n{}^2$ and $i_n{}^2$ of the internal voltage and current random sources. The electronics noise can be treated as zero-mean additive Gaussian random process with variance as the noise power.

If the field effect transistor (FET) is used for the transimpedance amplifier, the equivalent noise power spectral density is given by eq. (10)

$$
s_{aFET}(f) =
$$

$$
= \begin{bmatrix} \dfrac{4kT}{R_{fb}} + 2e_{I_L} + \dfrac{4KT\Gamma}{g_m}\left(2\pi_{c_t}\right)^2 f_c f + \\[3mm] + \dfrac{4KT\Gamma}{g_m}\left(2\pi_{c_t}\right)^2 f^2 \end{bmatrix}, \qquad (10)
$$

where I_L is the leakage current, g_m is the FET transconductance, C_t the total input capacitance, f_c is the *1/f* noise corner frequency of the FET, Γ is the numerical constant (0.7 for Si JFETs, 1.03 for Si MOSFETs and GaAs MESFETs). In the above equation, first noise term and second is due to feedback resistance thermal noise and leakage current. The third and the fourth noise term corresponding to channel thermal and induced gate noise.

4. LITERATURE SURVEY ON EXSISTING METHODS

This section discusses about the survey of optical background noise sources exist in VLC system and the techniques to reduce the optical background noise, which has been implemented previously by different researchers are discussed in this section.

4.1. Optical filtering

Optical filters such as long pass filter and band pass filters are the two different kinds of optical filters which are used in most systems to reduce the ambient light. Optical band pass filters are mostly used to mitigate the noise in VLC communication system. The optical receiver consists of optical band pass filter, optical concentrator, optical lens, photodetector and preamplifier. The optical band pass filter is deposited on the outer surface of the hemispherical concentrator to reduce the ambient light noise. The optical lens of different refractive index for different colours is used on the inner surface of the hemispherical lens and a silicon photodiode is attached at the bottom of the optical lens. Transimpedance amplifier is used to convert the photocurrent produced into voltage. Then all the received signals of different wavelength is combined using the MRC circuit and thus the signal is demodulated to restore the original input signal [15].

The optical concentrator is used in front of the photodiode with the optical band pass filter, which has centre wavelength of 450nm and full width half maximum (FWHM) of 40nm [16].In the outdoor environment also ambient light noise from daylight causes severe degradation in the performance of the communication.The combining receiver structure using optical band pass filter is used to suppress the ambient light noise due to sunlight [17]. The optical filters, such as light control films that contain a special layer called micro louver can be used be placed on the top of the photodiode. That blocks the incident sunlight interference at an angle of 30° or higher. The micro louver film consists of transparent layer, absorption layer and blocking layer. The light incident from only specified angle is passed and the other light beyond that angle is blocked via absorption and blocking layers. Thus, optical filtering using micro louver is an efficient method to sunlight interference in outdoor environments. The distance achieved here is 1m, which can be increased by using high power driven LEDs [21].

4.2. Electrical filtering

High pass RC filters can be used to filter out the low frequency noise components due to ambient light [18]. A low pass filter is used to eliminate the high frequency noise components [19, 20]. The use of high pass filter or low pass filter is related to the high or low noise frequency component to the input signal.

4.3. Adaptive filtering

The received optical signal is divided into temporal signal frame of 20 milliseconds. Then characterize the channel, and decides for each temporal frames whether the channel model is noise free or polluted with fluorescent light using the classifier. The channel characterization is done using the high frequency obtained the wavelet of the temporal frames using a Daubechies window type I. The inverse filter of the channel is done to remove the effects of the ambient light noise produced by fluorescent light [22].

4.4. Wavelength filtering

When the adjacent cells transmit different signals and wavelength, interference occurs. Due

Table 1. The comparison of RGB LEDS and phosphor based LEDS

VLC Optical source (White LEDs)	Data rate	Uplink and down-link provision	Noise sources	Multipath dispersion
Phosphor based white LED	• The modulation bandwidth of LED is limited to about 2–3 MHz due to slow response of the phosphor • The limited bandwidth is overcome by using blue filter is used at the receiver front end to suppress the slow phosphorescence components. It increases the bandwidth up to 20 MHz. • The data rate can be increased by spectrally efficient complex modulation, equalization and filtering techniques • For example using phosphor based white LED and DMT modulation data rate of 1 Gb/s is achieved [10].	Phosphor based LEDs provide upstream up to 225Mb/s [9].	Sunlight, other artificial ambient light sources [8].	• Wide band of phosphor topped white LEDs results in multipath dispersion • Data rate is limited due to inter-symbol interference (ISI) caused by multipath dispersion.
RGB based white LED	• RGB LED consists of three different wavelength colours which are used to carry multiple data stream and it is multiplexed over wireless channel, hence high data rates are achieved. • For example using RGB LEDs and DMT modulation data rate of 3.43.4Gb/s is achieved [11].	RGB LEDs are used to provide downstream up to 575 Mb/s [9].	Sunlight, other artificial ambient light sources [8].	• Multipath dispersion occurs due to characteristic changes of RGB colour in RGB LED. The junctions that produce and green light are not as efficient as the junction that produces blue light. Efficiency of blue light is about 80% whereas it is only it is only about 60% and 30% for red and green light respectively[8].

to the interference, the Signal to Noise Ratio (SNR) also gets affected. To solve the above problem of ambient interference, hexagonal cell structure based on RGB LED and is used. Different wavelength must be used between adjacent cells. If the cells are far located, same wavelength is used. Optical filters are used to separate the modulated signals from adjacent cells. Hence, the SNR is improved by using RGB-LED hexagonal structure and optical filtering [23].

4.5. Filter-based sensor array

Currently, the optical receivers use photoelectric-diodes to convert optical signals to electrical signals. But it cannot distinguish an input of different wavelength. Because of these disadvantages spectrum sensor array is used to achieve interference rejection. A single chip sensor array from nano lambda made up of different spectral transmission characteristics has been developed. The received optical signal contains the inband interference from the ambient fluorescent light. Two signal fusion methods such as maximum SIR combination (MSC) and matched filter combination (MFC) are compared. It is noticed that MFC outperforms MSC under the influence of ambient light noise. There are drawbacks that still exists in this system are the noise amplification issues due to the equivalent transmission from a combination of sensors and the timing synchronization among the sensors. However, the proposed receiver is proved to be a promising solution to the in-band interference problems in VLC systems [24].

4.6. Adaptive minimum voltage cancellation method

In the indoor environment sunlight and fluorescent light interference affects the performance of the communication system. The received optical signal from the channel contains DC component from sunlight and a rectified sine wave from indoor fluorescent lights. The VLC receiver enabled with adaptive minimum voltage detection to track the minimum voltage and differential amplifier is used to cancel the noise from the received signal. Bit rate of 1.25 Mbps and 1m distance is achieved using this method [25]

4.7. Line coding techniques

The Manchester coding is a line code that is used to provide synchronization; it can also be used in the communications. The Manchester decoding performed is similar to the received signal corrupted with ambient light noise passing through the band pass filter. Thus, the optical noise from AC−LEDs and fluorescent light noise frequency was < 500 kHz, is filtered and the signal quality is improved. Manchester coding performs better than the conventional NRZ when the frequency is less than 500 kHz.

In addition to the Manchester coding, forward error correction (FEC) techniques can also be used to improve the transmission performance. Data rates of 1.25 Mb/s and 2.5 Mb/s are evaluated with the transmitter and receiver distance is 1.65 m [26]. Non-return-to-zero-inverted (NRZI) is also used to reduce the background optical interference in the low noise frequency band. The external interference signal used is another white LED driven by AWG. In general, NRZI decoding is done using XOR gate. The waveform processing in the NRZI decoding process is used instead of using XOR gate. The waveform processing consists of the received waveform delayed with the duration of one bit and the original received waveform delayed with the one bit duration.

Thus, NRZI decoding using waveform processing can be effectively used to reduce the optical interference in low-frequency band from DC to over 200 KHz. NRZI coding performs better than the conventional NRZ. The data rate achieved is 10 Mbps at the range of 1 m [27]. Miller coded signal is less affected by noise and other distortions.

So, that Miller code can be used in Multiple Input Multiple Output (MIMO) applications. The distance upto 50 m is achieved [33].

4.8. Orthogonal frequency division multiplexing (OFDM)

The optical wireless channel is affected by the optical background noises such as the AC-power LED operated at 60 Hz and the fluorescent lamp. In the OFDM receiver side, the received signal is down sampled, CP removed and FFT is performed. Equalization is performed in order to enhance the channel bandwidth of LED. Data rate of 5 Mb/s and 12 Mb/s, 32 and 64 OFDM subcarriers are used. AC-power LED has negligible effect if the OFDM is used. Fluorescent noise can be mitigated using different number of subcarriers [28].

4.9. Differential detector with two polarizers

Differential detectors (PD1 and PD2) and two linear polarizers (PL1 and PL2) are used to reduce the ambient light noise caused by the tungsten filament lamp effectively when compared to the Differential detectors (PD1 and PD2) and one linear polarizer. Using differential detectors with two linear polarizers (SNR) achieved is more[29].

4.10. Wavelet neural network VLC receiver

Fluorescent light interference degrades the performance of the communication system. Wavelet denoising outperforms high pass filter (HPF) in reducing the ambient light interference. In VLC receiver there exists another challenge added to the Fluorescent light interference (FLI) is the inter-symbol interference (ISI), which also needs to be simultaneously addressed. Artificial neural network (ANN) based equalizer is combined along with the wavelet denoising. Wavelet denoising isolates the spectral components of the FLI from the modulated signals using different levels of wavelet decomposition. The feed forward multilayer perceptron (MLP) ANN equalizer is used due to its greater performance when compared to other linear equalizers. Thus the data rate of up to 150 Mb/s is achieved with a BER of 10^{-6} by using wavelet and neural network based receiver [30].
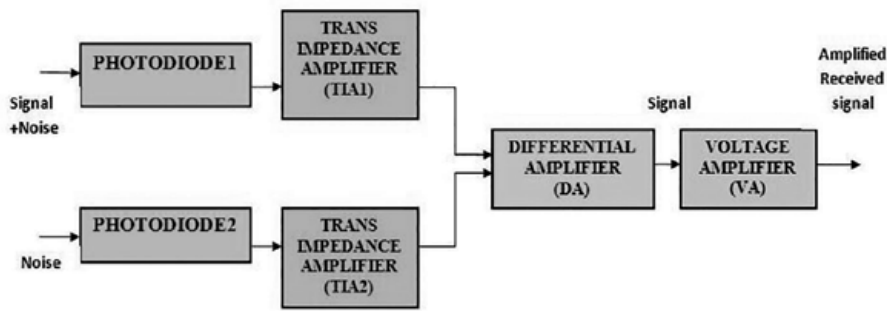
Fig. 3. Block diagram of proposed VLC receiver

4.11. Differential receiver using photocells

Traditional optical receivers use optical filters, colored, neural neutral density filters, low pass, band pass and high pass filters to reduce the ambient light interference. In a number of receivers they use computers to sift through all the signals to get the correct received data instead of filtering. All these methods reduce the signal from unwanted bandwidth while it passes the received signal. These methods only reduce the noise but do not cancel the noise caused due to interference. Hence, differential receiver using photocells is used to mitigate the ambient light interference [32].

4.12. Differential threshold with optical and color filters

In this method differential detection threshold (DDT) using optical filter and red color filter is employed in the receiver side to reduce the sunlight or artificial light in the outdoor environment. This method proves to be efficient like other methods such as spread spectrum techniques, combining techniques etc as it prevents the unwanted ambient light entering the photodiode [34].

5. PROPOSED METHOD

The optical wireless channel in the indoor environment is affected by the optical background noises such as indirect sunlight, fluorescent lamps generated by conventional ballasts operating at 50 Hz. The above conventional methods use optical filter, low pass filter, high pass filter etc. to reduce the optical background noises but it does not mitigate the noise completely and it still affects the performance of the communication system. Wavelet neural network, adaptive filtering, wavelength

filtering, OFDM also reduces the optical background noise but the receiver structure is complex. Miller code, filter based sensor array has also been used previously to reduce the noise but no practical experimentation is performed. Hence, the VLC receiver structure designed must be simple, it must improve the performance of the communication system and it must have the capability to reduce the optical background noise in the indoor environment.

The proposed receiver consists of two photodiode, transimpedance amplifier, differential amplifier and voltage amplifier. On the transmitter side on-off keying signals are used to drive the white LED, which is used for both illumination and communication purpose. We can able to achieve 500Kb/s and distance of 0.50m using the proposed receiver. Fig. 3 shows the block diagram of proposed VLC receiver.

The received optical signal from the optical wireless channel consisting of the optical background noise is collected at the photodiode1. The optical power is converted into current in the receiver side of the photodiode. So the background irradiance produced by the light sources produces shot noise and there will be variations in the optical power due to the interference.

The photocurrent produced at the photodiode1 is given by the eq. (11)

$$I_{P1} = I_{signal} + I_{interf}(t) + I_{noise}(t), \qquad (11)$$

$$I_{signal} = R \cdot P_{signal}, \qquad (12)$$

where R is the responsivity of the photodiode. P_{signal} is the input optical power of the LED.

$$I_{interf}(t) = R \cdot P_{interf}(t), \qquad (13)$$

114

where $P_{interf(t)}$ is the power of the ambient light interference signal.

$$< I^2_{noise}(t) >= 2q(I_{signal} + I_{interf}(t)). B, \qquad (14)$$

where q is the electronic charge and B is the receiver bandwidth.

The electrical current is converted into voltage using the transimpedance amplifier (TIA1). The output voltage at the TIA is given by eq. (15)

$$V_{out1} = R_f \cdot I_{P1}, \qquad (15)$$

where R_f is the feedback resistance and I_{P1} is the current produced at the photodiode #1.

The photocurrent produced at the photodiode #2 without the input signal is given by the eq. (16)

$$I_{P2} = I_{interf}(t) + I_{noise}(t), \qquad (16)$$

$$I_{interf}(t) = R \cdot P_{interf}(t), \qquad (17)$$

where $P_{interf(t)}$ is the power of the ambient light interference signal.

$$< I^2_{noise}(t) >= 2q(I_{signal} + I_{interf}(t)). B, \qquad (18)$$

where q is the electronic charge and B is the receiver bandwidth.

The electrical current is converted into voltage using the transimpedance amplifier (TIA2).

$$V_{out2} = R_f \cdot I_{P2}, \qquad (19)$$

where R_f is the feedback resistance and I_{P2} is the current produced by the photodiode #2.

The differential amplifier is used to mitigate the noise and helps to recover back the original received signal. The output voltage at the differential amplifier stage is given by eq. (20):

$$V_{DA} = A (V_{out1} - V_{out2}) \qquad (20)$$

$$= A (R_f \cdot I_{P1} - R_f \cdot I_{P1}) \qquad (21)$$

$$= A (R_f \cdot I_{signal} + I_{interf}(t) + I_{noise}(t) \\ -R_f + I_{interf}(t) + I_{noise}(t)), \qquad (22)$$

$$V_{DA} = A (I_{signal}), \qquad (23)$$

$$V_{DA} = A (R \cdot P_{signal}), \qquad (24)$$

where, A is the open loop gain.

The received signal will be a weak signal and voltage amplifier is used to amplify the received signal from the differential amplifier (DA). The output voltage at the voltage amplifier stage is given by eq. (25)

$$V_{VA} = A_V (V_{DA}), \qquad (25)$$

where A_V the voltage is gain and V_{DA} is the voltage at the differential stage.

Thus, the transmitted input signal is recovered back at the receiver side with the mitigation of optical background noise sources such as indirect sunlight and conventional fluorescent lamp operating at 50 Hz in indoor environment.

6. CONCLUSION

In this paper, we have analyzed the optical background noise sources and its reduction techniques in VLC system. Fluorescent light and sunlight are considered to be the important sources of ambient light noise among all the other ambient light noise sources. Based on the previous method analysis, the modified VLC receiver is proposed to reduce the optical background noises caused due to indirect sunlight and fluorescent lamps generated by conventional ballasts in the indoor environment. By overcoming the challenges of optical background noise, the error free transmission is achieved and SNR is improved. Thus highly efficient LED communication is established for many hazardless applications. It is most expected that VLC system will reach the market soon and benefit the users with data communication and illumination.

REFERENCES

1. IEEE Standards Association, IEEE Standard for Local and metropolitan area networks – Part 15.7: Short-Range Wireless Optical Communication Using Visible Light (IEEE Std 802.15.7), 2011.

2. A.K Das, A. Ghosh, A.M Vibin, S.Prince "Underwater communication system for deep sea divers using visible light", Photonics Global Conference (PGC), Dec 2012, pp. 1–3.

3. I.C Rust, H.H Asada," A dual-use visible light approach to integrated communication and localization of underwater robots with application to non-destructive nuclear reactor inspection", IEEE international conference on robotics and automation(ICRA). May 2012, pp. 2445–2450.

4. S.Iwasaki, C.Premachandra, T.Endo, T, Fujii, M.Tanimoto, Y.Kimura, "Visible light road to vehicle communication using high speed camera", IEEE Intelligent Vehicles Symposium, June 2008, pp. 13–18.

5. J.Yoo, R. Lee, J. Oh, H. Seo, J. Kim, H. Kim and S.Yoon Jung, "Demonstration of Vehicular Visible Light Communication Based on LED Headlamp", International Conference on Ubiquitous and Future Networks (ICUFN), July 2013, pp. 465–467.

6. Y.Cheong, X.Weing, W.YounCungCheong, X.Weing, W.YounChung"Hazardless Biomedical Sensing Data Transmission Using VLC", IEEE sensors journal, 2013, vol. 13, pp. 3347–3348.

7. R.Murai, T.Sakai, H.Kawano, Y.Matsukawa, Y.Kitano, Y.Honda, K.C Campbell "A novel visible light communication system for enhanced control of autonomous delivery robots in a hospital", IEEE/SICE International Symposium on System Integration (SII), Dec 2012, pp. 510–516.

8. Saadi, L. Wattisuttikulkij, Y. Zhao, P. Sangwongngam, "Visible Light Communication: Opportunities, Challenges and Channel Models", International Journal of Electronics and Informatics, 2012.

9. Y.Wang, Y.Wang, N.Chi, J.Yu, and H.Shang, "Demonstration of 575-Mb/s downlink and 225-Mb/s uplink bi-directional SCM-WDM visible light communication using RGB LED and phosphor-based LED", Optics Express, 2013, Vol. 21, pp. 1203–1208.

10. A. M. Khalid, G. Cossu, R. Corsini, P. Choudhury, E. Ciaramella,"1-Gb/s Transmission Over a Phosphorescent White LED by Using Rate-Adaptive Discrete Multitone Modulation", IEEE Photonics Journal, 2012, Vol. 4, pp. 1465–1473.

11. G.Cossu, A.M. Khalid, P. Choudhury, R., E. Ciaramella, "3.4 Gbit/s visible optical wireless transmission based on RGB LED", Optics Express, 2012, Vol. 20, pp. B501-B506.

12. http://cdn.intechweb.org/pdfs/14261.pdf.

13. H. Elgala, R. Mesleh, H. Haas and B.Pricope, "OFDM Visible Light Wireless Communication Based on White LEDs", Proc. of IEEE, 2007.

14. S.B. Alexander, "Optical Communication Receiver Design", SPIE Opt. Eng. Press/IEE, London UK, 1997.

15. M.Shahin Uddin, J.Cha, J. Kim and Y. Min Jang, "Mitigation Technique for Receiver Performance Variation of Multi-Color Channels in Visible Light Communication, IEEE Sensors Journal, 2011, Vol. 11, pp. 6131–6144.

16. K. Cui, G. Chen, Z. Xu, and R. D. Roberts, "Line-of-sight visible light communication system design and demonstration," Proc. of 7th IEEE, IET International Symposium on Communication Systems, Networks & Digital Signal Processing: 2nd Colloquium on Optical Wireless Communications, Newcastle, UK.,2010

17. I.E Lee, M.L Sim, F.W Kung "Performance Enhancement of Outdoor Visible-Light Communication System Using Selective Combining Receiver"IET Optoelectronics. 2009, Vol. 3, pp. 30–39.

18. K. Cui, G. Chen, Q. He and Z. Xu, "Indoor optical wireless communication by ultraviolet and visible light", Proc.of SPIE, Vol. 7464, 2009, pp. 74640D-1–74640D-9.

19. Y. Yong Tan, S. Jung, and W. Chung,"Real Time Biomedical Signal Transmission of Mixed ECG Signal and Patient Information using Visible Light Communication" 35th Annual International Conference of the IEEE EMBS, 3–7 July, 2013.

20. N.Kim, C.Jing, B. Zhou and Y. Kim "Smart Parking Information System Exploiting Visible Light Communication," International Journal of Smart Home, vol. 8, pp. 251–260, 2014.

21. Y.Chung, S.bin Oh, "Efficient Optical Filtering for Outdoor Visible Light Communications in the Presence of Sunlight or Artificial Light", ISPACS, 12–15 Nov.2013, pp. 749–752.

22. V. G. Ya´nez, J. R. Torres, J. B. Alonso, J. A. R. Borges, C. Q. Sa´nchez, C. T. Gonza´lez, R. P. Jime´nez, and F. D. Rajo, "Illumination interference reduction system for VLC Communications", Proc. WSEAS Int. Conf. Math. Methods, Comput. Tech. Intell. Syst, 2009, pp. 252–257.

23. S.H. Yang, H.S. Kim, Y.H. Son, and S.-K. Han, "Reduction of optical. Interference by wavelength filtering in RGB-LED based indoor VLC system", Proc. OECC2011, pp. 551–552.

24. C. Chang, Y. Su, U. Kurokawa, and B. Ichoi, "Interference Rejection Using Filter-Based Sensor Array in VLC Systems" IEEE Sensors Journal, 2012, vol. 12, pp. 1025–1032.

25. Y.Zhao and J.Vongkulbhisal, "Design of Visible Light Communication Receiver for On-Off Keying Modulation by Adaptive Minimum-Voltage Cancelation", Engineering Journal, 2013, vol. 17.

26. C.W.Chow, C.H.Yeh, Y.F.Liu, P.Y. Huang, "Mitigation of Optical Background Noise in Light-Emitting Diode (LED) Optical Wireless Communication Systems", IEEE photonics Journal, 2013, vol. 5.

27. Y. F. Liu, C. H. Yeh, Y. C. Wan, and C. W. Chow, "Employing NRZI Code for Reducing Background Noise in LED Visible Light Communication" in OptoElectronics and Communications Conference held jointly with International Conference on Photonics in Switching (OECC/PS), Jun 30-Jul 4, 2013, pp. 1–2.

28. C.W Chow, C.H Yeh, Y..F Liu, P.Y Huang "Background Optical Noises Circumvention in LED Optical Wireless Systems Using OFDM", IEEE photonics Journal, 2013, vol. 5.

29. A.Nazmi Mohamed, M.Asmaa Aly, K. Ahmed, AboulSeoud, H.Moustafa Aly, "Indoor wireless optical communication systems: effect of ambient noise", Optical Engineering, 2014, vol. 53.

30. S.Rajbhandari, P.Anthony Haigh, Z. Ghassemlooy and W.Popoola, "Wavelet-Neural Network VLC Receiver in the Presence of Artificial Light Interference", IEEE Photonics Letters, 2013vol. 25, no. 15, .

31. L.Grobe, A.Paraskevopoulos, J.Hilt, D.Schulz, F.Lassak, F.Hartlieb, C.Kottke, V. Jung nickel, and K.D Langer,"High-speed Visible Light Communication Systems", IEEE communications magazine, 2013, Vol. 51, pp. 60–66.

32. S.Faruque, S.Faruque, W.Semke,"Orthogonal on–off keying for free-space laser communications with ambient light cancellation", Optical Engineering, vol. 2, 2013.

33. A.Cailean, B.Cagneau, L.Chassagne, V. Popa, M. Dimian, "Evaluation of the noise effects on Visible Light Communications using Manchester and Miller coding"12th International Conference on development and application systems, May 2014.

34. Y.Kim, Y.Chung, "Experimental outdoor visible light data communication system using differential decision threshold with optical and color filters", Opt. Eng, 2015

Kadirvel Sindhubala
received her B.E. degree in Electronics and Communication Engineering from Anna University in 2009 and M.Tech in Communication Engineering from VIT University in 2011. From 2011 to 2013 she worked as software engineer. Currently, she is involved in her research on visible light communications at B.S. Abdur Rahman University, Chennai, India. She has published 5 papers in various international journals, national journals and in conferences

Baba Vijayalakshmi
received her AMIETE degree in Electronics and Telecommunication Engineering from IETE New Delhi in 2000 and M.E. in optical communication from Anna University, Chennai. She carried her research work in 3D scene generation using two 2D images through DRDO sponsored project. Since 2003, she has been a faculty in Electronics and Communication Engineering Department of different engineering colleges at Tamil nadu. Currently, she is serving as a professor in Electronics and Communication Engineering Department at B.S. Abdur Rahman University, Chennai. More than 24 papers are published in various International journals, National journals and in conferences. Her current research interests include image processing, visible light communication, optical communication, perceptual image analysis, 3D scene generation

MATLAB SIMULATION OF INDOOR GENERAL LIGHTING WITH LUMINAIRE IES FILE

Purnima Mandal and Biswanath Roy

Electrical Engineering Department, Jadavpur University, India.
E-mail: purnima.bhandari@gmail.com;
broy@ee.jdvu.ac.in

ABSTRACT

This paper deals with computation of lighting design parameters related with indoor general lighting scheme using MATLAB. Luminaire Intensity e-database, known as *.ies* file, is directly extracted by the developed MATLAB program and then utilized in subsequent lighting computation. Details of all computation steps and algorithms of developed MATLAB program are given in this paper. Simulated results are compared with DIALux lighting design software and percentage deviations are presented.

Keywords: lighting computation, MATLAB simulation, Indoor lighting

1. INTRODUCTION

The objective of this work is to simulate indoor general lighting in terms of numerical values of design parameters as well as graphical representation of computed results using MATLAB. Presently, four design parameters are considered in this developed programme without obstruction viz: a) Maintained Average Illuminance over horizontal working plane, b) Uniformity of Illuminance, c) Unified Glare Rating (UGR) and d) Lighting Power Density (LPD).

Flux transfer theory and other basic laws of illumination science are applied to compute direct and indirect illuminance separately on working plane to produce spatial distribution of light level. CIE guidelines are used to compute UGR at different observer's positions and for different line of observations.

Unique features of this presented work are:

1) Incorporation of luminaire photometric e-file (*.ies* file) in the developed MATLAB program and then extraction of relevant data for subsequent computation.

2) Computation of direct and indirect component of illuminance on working plane separately.

3) Modular form of computation of design parameters with algorithm and detailed theoretical background.

This approach of MATLAB simulation facilitaes the researchers to develop tailor-made program using existing MATLAB library functions, tools utilities for data analysis and optimization. This option is not available with the existing powerful lighting design software viz. DIALux, RELUX, AGi32.

2. INDOOR GENERAL LIGHTING SCHEME

The purpose of general lighting scheme is to achieve uniform illuminance all over the working plane. The luminaires are arranged in a matrix form and uniformity of Illuminance is measured. This type of lighting scheme is very useful in large office space where every workstation receives more or less same light from the lighting installation and hence ensures flexibility on the orientation of the workstations distributed within the floor space.

2.1 Design Parameters

The lighting ambience created with the general lighting scheme is characterized with following design parameters. The required value is recommended by National and International Lighting Standards to ensure visual performance related to intended visual task(s):

a) Maintained Average Illuminance over horizontal working plane ($\bar{E}$):

This parameter represents the quantity of light available throughout the working plane for entire space under the installation. For a new installation the initial average illuminance and maintained average illuminance are related by a factor known as Maintenance Factor (M.F) of the lighting systems, where

$$M.F. = \frac{Maintained\,average\,illuminance}{Initial\,average\,illuminance}.$$

b) Uniformity of Illuminance (U_1, U_2):

These parameters represent the uniformity of illuminance on the entire working plane and are assessed by the ratio of minimum to average illuminance and minimum to maximum illuminance. Usually minimum to average illuminance is considered to represent Overall Uniformity of illuminance.

c) Unified Glare Rating (UGR):

UGR is a quality criterion of indoor lighting installation. It indicates the visual discomfort experienced by the space users while engaged in visual tasks. The practical range of UGR lies within 10 to 30. The higher the value of UGR the more discomfort glare will be experienced by the user. UGR value less than 10 is assumed not to produce discomfort glare and hence globally it is represented as UGR<10.

d) Lighting Power Density (LPD):

This parameter indicates the installed electrical load of the lighting installation for a unit area of working plane and considered as an indicator to assess energy efficiency of the lighting installation. There are two ways to represent LPD as Installed electrical load (W) per unit area (m^2) of working plane and Installed electrical load (W) per unit area (m^2) of working plane per 100 lx. The second definition is more informative as it represents LPD value per 100 unit of average maintained illuminance level.

3. INTERFACING BETWEEN *IES* FILE AND MATLAB

IES file is Standard File Format for the Electronic Transfer of Photometric Data. It was first introduced in 1986 (IESNA LM-63−1986) and used by most of the luminaire manufacturers to create luminaire database. Moreover, wellknown lighting design softwares viz., DIALux, AGi32 are compatible with this *IES* file format of luminaire database. The *IES* file format, publish in IESNA LM-63−2002 [1] is used in this work. The manufacturer of luminaire supplies lumianire information as.*ies* file. A sample of *IES* file format specification is given in **Annexure-I**. MATLAB program is developed to interface between *IES* file and MATLAB to extract data from a given .*ies* file.

3.1. Algorithm: Luminaire data extraction from *IES* file

Algorithm start
Read IES file in ASCII mode from disk drive
Read each line in IES file
    If Line# is equal to 1
        Read IES file format version
    Else If Line starts with "["
        Extract Keyword name and value
    Else If Line contains "TILT" keyword
        Extract TILT information from file
    Else
Extract no of lamp, lumens per lamp, Candela Multiplier, number of vertical angles, number of horizontal angles, photometric type, unit's type, width of lumianire, length of luminaire and height of lumianire
    Go to next line in file
        Extract ballast factor, future use, and input watts
    Read remaining lines
        Extract intensity data
    End if
Algorithm end

4. COMPUTATIONAL METHODS

Theoretical details of computations are presented here.

4.1. Point-Specific Illuminance

In case of indoor lighting the total illuminance at a point comprises of two components:

1) Direct component − the contribution to illuminance directly from all light source(s) of the installation.

2) Indirect or inter-reflected component − the contribution to illuminance due to inter-reflection of light flux within the interior.

The entire working plane divided into a matrix of grid points, on which total illuminance are computed separately.

Direct Component: The computation of direct component of illuminance requires the following data: intensity distribution of luminaire, location of luminaire, position of grid points and dimension of luminaire light emitting surface.

The intensity distribution ($I_{c,\gamma}$) of luminaire is provided by luminaire manufacturer in *.ies* file, which contains I-values of luminaire corresponding to C-γ geometry.

The mathematical expression for point-specific horizontal illuminance (E_D^i) at i^{th} grid point is given by inverse square cosine law of illuminance [4, 5].

$$E_D^i = \frac{I_{c_i,\gamma_i} \cdot \left(\cos\gamma_i\right)^3}{h_m^2}, \qquad (1)$$

where, $I_{c,\gamma}$ is intensity along the direction pointing i^{th} grid point and the direction is specified by angles c_i and γ_i; h_m is mounting height of luminaire.

This law is applicable when the distance between the grid point and the source is at least five times of the largest dimension of the source. Under this condition, any finite area source is assumed as point-source. Above condition does not valid in most of the cases of Indoor General lighting. Under this situation, the light emitting surface of the luminaire is subdivided into a number of small area sources. The dimension of sub-sources is taken to meet the above requirement. The light distribution from each sub-source is calculated on the basis of principle of homogeneity of light distribution [4].

Let area of entire light emitting surface (A_s) be divided into m sub-sources of area (dA_s).

Then illuminance at i^{th} grid point due to j^{th} sub source is given by

$$dE_D^i = \frac{dI_{c_{ij},\gamma_{ij}} \cdot \left(\cos\gamma_{ij}\right)^3}{h_m^2},$$

where, $dI_{c,\gamma} \propto I_{c,\gamma}$.

According to principle of homogeneity of light distribution, $dI_{c,\gamma} = KI_{c,\gamma}$; K is proportionality constant, $K = \dfrac{dA_s}{A_s}$.

Thus total illuminance due to entire source will be

$$E_D^i = \sum_{j=1}^{m} dE_D^i. \qquad (2)$$

Equation (2) gives the direct illuminance value at i^{th} grid point due to a single finite area source. In presence of multiple sources, the contribution of individual source are to be calculated using equation (2) and then added to find out total contribution.

Indirect or Inter-reflected Component: This component depends on shape of the room, room surface reflectance factors, light distribution pattern of luminaire and position of grid point. The mathematical expression of point-specific indirect illuminance at i^{th} grid point is given by [2, 4]

$$E_R^i = \frac{\left(Total\,lamp\,lumens\,per\,luminaire\right) * RRC}{Working\,plane\,area\,per\,luminaire},$$

where, *RRC* is Reflected Radiation coefficient, $RRC = WEC + RPM\left(CCEC - WEC\right)$; *WEC* is Wall Exitance Coefficient; *CCEC* is Ceiling Cavity Exitance Coefficient; *RPM* is Room Position Multiplier.

Here, Total Lamp Lumen per luminaire is obtained by multiplying number of lamps (n) per luminaire with lumen per lamp (Φ_l) and these data are available in *.ies* file of luminaire.

The area per luminaire is obtained by dividing working plane area by number of luminaire (*N*). The value of '*N*' is usually estimated using Lumen Formula at the initial design stage.

Calculation of *RRC* requires the value of *WEC* and *CCEC* which are relatively complicated and it depends on [2, 4] 1) Direct Ratio (*DG*), 2) Downward Light Output Ratio (*DLOR*), 3) Upward Light Output Ratio (*ULOR*), 4) Room Cavity Ratio (G), 5) Room wall reflectance (ρ_1), 6) Ceiling and floor Cavity reflectances (ρ_2, ρ_3) and 7) Fraction of installed flux that reaches to wall, ceiling and floor (C_1, C_2, C_3).

The term *RPM* indicates the position of the grid point on working plane. The position is represent-

ed by an index comprising of two characters. This indexing is done by dividing the working plane into grid pattern where grid dimension is (10% of room length) X (10% of room width).

The value of *RPM* for a specific grid point is to be obtained from a chart [3] with the corresponding index and value of Room Cavity Ratio.

The total value of point-specific illuminance (E_T^i) at i^{th} grid point is equal to $E_T^i = E_D^i + E_R^i$

Computation of $\overline{E}$, U_1, U_2 and LPD: Initial average illuminance on working plane for *n* grid points is given by

$$\overline{E_{initial}} = \frac{1}{n}\sum_{i=1}^{n}E_T^i. \qquad (3)$$

Hence, maintained average illuminance is given by

$$\overline{E} = \overline{E_{initial}} * M.F., \qquad (4)$$

The uniformity of illuminance U_1 and U_2 are equal to

$$U_1 = E_{min}/\overline{E} \text{ and } U_2 = E_{min}/E_{max}, \qquad (5)$$

where E_{min} and E_{max} are maintained minimum and maximum values of the grid specific illuminance on working plane.

4.2. Lighting Power Density (LPD):

The parameter is calculated by

$$LPD = \frac{No.\ of\ luminaire*}{*Input\ wattage\ per\ luminaire}}{Area\ of\ the\ working\ plane}\left(\frac{W}{m^2}\right), \qquad (6)$$
OR
$$LPD = \frac{No.\ of\ luminaire*}{*Input\ wattage\ per\ luminaire}}{Area\ of\ the\ working\ plane*}\left(\frac{W}{m^2.100lx}\right)\cdot \\ *(\overline{E}/100) \qquad (7)$$

The value of input wattage per luminaire is to be taken from luminaire *.ies* file.

4.3 Unified Glare Rating (UGR):

The value of point-specific UGR is calculated based on position of observer's eye and line of sight of observer and depends on: 1) Background lumi-

nance (L_b, cd/m^2), 2)Luminance of luminous part of each luminaire in the direction of the observer's eye (L, cd/m^2), 3) Solid angle of the luminous part of each luminaire at the observer eye (ω, sr) and 4) Position of luminaire relative to line of sight and represented by Guth Position index for each luminaire(p).

The first two parameters are related to lighting and remaining two are the geometric parameters. The mathematical expression for UGR as given by CIE [3] is expressed as

$$UGR = 8*\log_{10}\left[\frac{0.25}{L_b}\sum_{k=1}^{N}\frac{L^2\omega}{p^2}\right]. \qquad (8)$$

The background luminance (L_b) is calculated with the assumption that room surfaces are diffuse surface and hence,

$$L_b = \frac{Average\,Wall\,Exitance}{\pi},$$

$$Average\,Wall\,Exitance = \\ = \frac{Total\,lamp\,lumen\,per\,luminaire*WRRC}{Working\,plane\,area\,per\,luminaire},$$

where WRRC is Wall Reflected Radiation Coefficient $= \frac{WEC}{\rho_w} - WDRC$; WDRC is Wall Direct Radiation Coefficient.

Now, the values of L, ω, p are to be calculated for each luminaire in the installation, which lie within the field of view of observer.

The luminance of source (L) is calculated by

$L = \frac{I_{c,\gamma}}{A_s\cos\gamma}$; A_s is Luminous area of the luminaire.; $I_{c,\gamma}$ is Intensity directed towards the eye of observer.

The solid angle 'ω' as subtended by the luminous part of the source at observer's eye is calculated by

$\omega = \frac{A_s\cos\gamma}{d^2}$; d is distance between source and observer eye.

The value of position index (p) is to be read/taken from Table of Position Indexed as given in CIE1l7 [3].

The value of *p* is given with respect to *H/R* ratio and *T/R* ratio where *H*, *R*, *T* are the distance parameters relating position of the source with respect to eye and corresponding coordinate system is shown in **Annexure-II**. To get exact value of '*p*' corresponding to different position of eye and sources interpolation is to be carried out.

5. ALGORITHM FOR LIGHTING SIMULATION

Algorithms of developed MATLAB simulations are presented here. Algorithms for computation of each lighting design parameter and also for graphical presentation of computed data are presented here.

5.1. Algorithm: Calculation of point-specific Direct Illuminance

Algorithm start
Capture room dimension as input
Capture number of luminaire to be used and their coordinates
Read Luminaire data from .ies file using **algorithm 3.1**
Prepare computation grid according to input
Devide light emitting surface to small area (virtual) source
Calculate distance (d) between grid point and virtual source
Calculate C angle and gamma angle
Interpolate through IES intensity data and determine I- values for C angle and gamma angle
Loop for all virtual area sources
Calculate direct illuminance (E) for the grid point
    $E_{Direct} = (I*((cosd(gama))\textasciicircum 3))/(mounting\ height\textasciicircum 2)$
Add up illuminance (E) to get grid specific total direct illuminance
Algorithm end

5.2. Algorithm: Calculation of point-specific reflected Illuminance

Algorithm start
Capture room dimension as input
Capture number of luminaire to be used and their coordinates
Read luminaire data from IES using **algorithm 3.1**

Calculate the average intensity value considering five plane photometry
    $I_{5-plane} = (I_0+2xI_{22.5}+2xI_{45}+2xI_{67.5}+I_{90})/8$
Prepare 18 conic solid angles (gamma) zones of 10-degree width
Loop through gamma value (i) 0° to 180° with an increment of 10°
    Calculate Zonal Costant = $= 2*pi*(cosd(i)-cosd(i+10))$
    Calculate mid-zone average intensity (I_{avg})
    Calculate Zonal Flux
      *Zonal Flux= I_{avg} * Zonal Costant*
    Sum up all Zonal Flux upto gamma$<=90^0$ to get total Downward Flux
    Sum up all Zonal Flux upto $90^0<=gamma<=180^0$ to get total Upward Flux
Calculate total installed lumens using.ies file
Calculate Fraction of Downward Flux (DLOR)
    DLOR=Total Downward Flux/ total installed lumens
Calculate Fraction of Upward Flux (ULOR)
    ULOR=Total Upward Flux/ total installed Lumens
Calculate Room Cavity Ratio (RCR)
Calculate Zonal Multiplier for zone 1 to 9
Sum up Direct Ratio for zone 1 to 9
    *DG= (1/((DLOR)*Total Installed Lumen)))*Zonal Multiplier * Zonal Flux;*
Calculate From Factor (f_{23})
    f_{23}=0.026+0.503e(−0.270RCR)+0.470e(−0.119RCR)
Calculate C_1, C_2, C_3 and C_0 where $C_0 = C_1+C_2+C_3$
Calculate Wall Exitance Co-efficent (WEC)
Calculate Ceiling Cavity Exitance Coefficent (CCEC)
Calculate Wall Direct Radiation Coefficent (WDRC)
Calculate Room Position Multiplier(RPM) for each Grid point
Calculate Reflected Radiation Coefficient (RRC)
    RRC=WEC+RPM (CCEC-WEC)
Calculate working plane area per luminaire
    Area per Luminaire=Working plane Area of the room/total no. of luminaries
Loop through grid points
Calculate Reflected illuminance at a point
    $E_{Reflected}$ =(installed lumens/luminaire)(R-RC)/Area per luminaire*
Algorithm end

5.3. Algorithm: Computation of $\bar{E}$, U_1, U_2

a) Maintained Average Illuminance ($\bar{E}$):
Algorithm start
*Calculate total initial illuminance at each grid point using **algorithm 5.1 and 5.2***
$E_{Total} = E_{Direct} + E_{Reflected}$
Sum up all illuminance vaules for all grid points to get the total initial illuminance values
Calculate total number of grid points
Calculate Initial Average Illuminance =(Total initial illuminance/Total number of grid points)
Calculate Maintained Average Illuminance
   $\bar{E}$ = *Initial Average Illuminance*M.F.*
Algorithm end

b) Uniformity of Illuminance (U_1, U_2):
Algorithm start
*Find out the minimum and maximum illuminance over working plane from the calculated total illuminance values of all grid points using **algorithm 5.3.a***
Calculate Maintained Minimum Illuminance = Minimum Illuminance* M.F.
Calculate Maintained Maximum Illuminance = Maximum Illuminance* M.F.
Calculate Uniformity of Illuminance
   U_1= *Maintained Minimum Illuminance / Maintained Average Illuminance*
   U_2= *Maintained Minimum Illuminance / Maintained Maximum Illuminance*
Algorithm end

5.4. Algorithm: Calculation of *LPD*

Algorithm start
Calculate the total lighting load of the Room
Total lighting load = Number of luminaire*Input Wattage to luminaire
Calculate area of the room
Calculate Lighting Power Density (W/m2)
   LPD = Total lighting load /Area of the room
   Calculate Lighting Power Density (W/m2 /100 lx)
   LPD per 100 lx = (Lighting Power Density / Maintained Average Illuminance)*100
Algorithm end

5.5. Algorithm: Calculation of *UGR*

Algorithm start
Read wall, ceiling and floor reflectances as input

*Read luminaire data from.ies file using **algorithm 3.1***
*Read the value WDRC from **algorithm 5.2***
*Read the value of WEC from **algorithm 5.2***
Calculate Wall Reflected Radiation Coefficient(WRRC)
   WRRC=(WEC/Reflectance of wall)-WDRC
Calculate indirect illuminance at Observer's Eye
   E_i=*Lumens per luminaire*WRRC/Working plane area per luminaire*
Calculate Background Luminance (L_b)
   L_b=E_v/(pi)
*Calculate area of light emitting surface of luminaire(A) using IES file data of **algorithm 3.1***
Calculate the height of the source above eye level (H)
   H=room height − user eye height
Calculate distance between eye to plane of source in the view direction(R)
Calculate distance between source and view direction (T)
Calculate distance between source and the observer in horizontal plane (Q)
   Q = square root of (T^2+R^2)
Calculate distance from the observer to the center of the luminous parts of the luminaire (D)
   D= square root of (Q^2+H^2)
Calculate gama angle
   gama=tan^{-1}(Q/H)
Calculate C angle
   C angle=atand(T/absolute value of R); where luminaire is mounted crosswise to the Line of Sight
   C angle=90-atand(T/ absolute value of R); where luminaire is mounted endwise to the Line of Sight
Interpolate through IES intensity data and determine Intensity (I) for C angle and gamma angle for each grid points
Calculate the projected area of the luminous part(A_p)
   A_p=*Area Of luminaire * cos (gama)*
Calculate luminance(L) of luminous parts of each luminaire in the direction of observer's eye
   L=I/A_p
Calculate solid angle(omega) of the luminous parts of each luminiare at the observer's eye
   omega=A_p/D^2
Interpolate the Guth Position Index (p) for corresponding forward ratio (H/R) and sideway Ratio = T/R
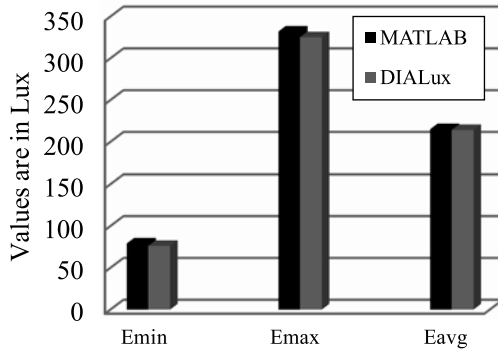
Fig. 1. Grid-specific Direct Illuminance for the model room
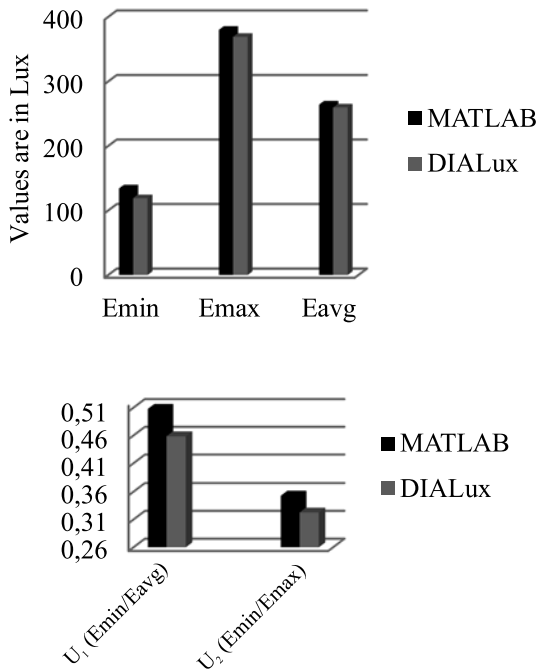
Fig. 2. Grid-specific Total Illuminance and Uniformity
for the model room

Loop through grid points
Calculate the UGR
   UGR = 8*log$_{10}$((0.25/L$_b$)*Sum of all the values of (L^2*omega/p^2) for all luminaires
Algorithm end

5.6. Algorithm: Isolux and Surface Plot

Algorithm start
Read the total illuminance value for all grid points
Plot Isolux diagram of illuminance distribution on working plane
Plot surface diagram of illuminance distribution on working plane
Algorithm end
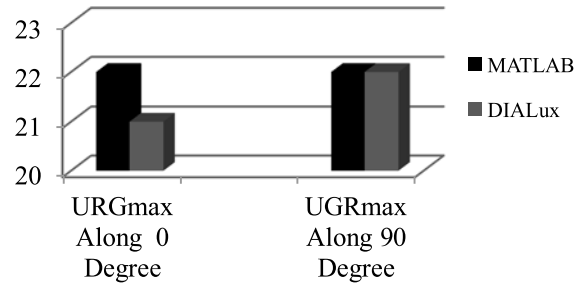
Fig. 3. Grid-specific Unified Glare Rating (*UGR*) for the
model room

6. SIMULATED RESULT AND COMPARISON

Developed MATLAB program is used for lighting simulation for an indoor enclosure with following room specifications:

a) Room dimensions: length 10m; width 10m; height 3.5m; b) room surface reflectances: ceiling − 80%; walls − 50%; floor − 20%; c) working plane: 0.76 m from floor; d) maintenance factor − 0.8; d) luminaire: mirroroptic, fluorescent lamp(TLD) 2×36W, H.F.

Graphical presentation of grid-specific total illuminance distribution i.e, isolux diagram is also obtained in MATLAB simulation and then compared with the same obtained from DIALux simulation. Results are presented in Figs. 1−5 and Table 1.

DIALux does not have any provision to calculate grid specific indirect illuminance.

Light Power Density (*LPD*): From MATLAB simulation, *LPD* is calculated as 6.66 W/m² and 2.50W/m²/100 lx (ground area: 100 m²) with ($\bar{E}$)-267 lx and from DIALux simulated *LPD* is found as 6.66 W/m² and 2.57 W/m²/100 lx (ground area: 100 m²) with ($\bar{E}$) − 260 lx.

The blue boxes shows only the schematic of the lumianires positions not the actual dimensions.

Develop MATLAB programme genates the surface plot of illuminance distribution over the working plane as shown in Fig. 6. Here illuminance values are plotted along Z-axis and grid coordinates are shown by X-axis and Y-axis. DIALux does not generate surface plot.

Simulated lighting design parameters are compared with DIALux simulation and deviations are computed with respect to DIALux simulated results as shown in Fig. 7.

Table 6.1. MATLAB simulated grid-specific indirect illuminance for the model room

9.545	56	55	54	54	53	53	53	54	54	55	56
8.636	55	54	53	52	52	51	52	52	53	54	55
7.727	54	53	51	51	50	49	50	51	51	53	54
6.818	54	52	51	50	49	49	49	50	51	52	54
5.909	53	52	50	49	49	48	49	49	50	52	53
5	53	51	49	49	48	48	48	49	49	51	53
4.091	53	52	50	49	49	48	49	49	50	52	53
3.182	54	52	51	50	49	49	49	50	51	52	54
2.273	54	53	51	51	50	49	50	51	51	53	54
1.364	55	54	53	52	52	51	52	52	53	54	55
0.455	56	55	54	54	53	53	53	54	54	55	56
m	0.455	1.364	2.273	3.182	4.091	5	5.909	6.818	7.727	8.636	9.545
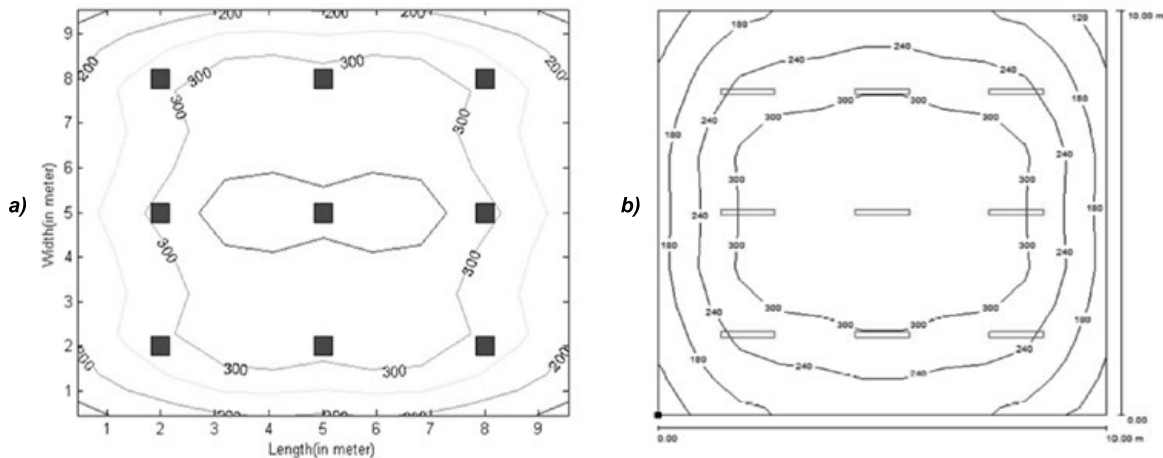
Fig. 4. Isolux diagram a) from MATLAB simulation b) from DIALux simulation

In case of direct illuminance computation, maximum deviation observed for minimum illuminance is 4%; whereas in case of total illuminance computation, maximum deviation observed again for minimum illuminance is 12%. This increase of deviation from 4% to 12% is due to the difference of results in indirect illuminance computation. It is not possible to compare MATLAB simulated indirect illuminance values as DIALux does not show indirect illuminance values. The error in uniformity computation (U_1 and U_2) is slightly higher (around 9%) due to deviation in minimum illuminance computation. Deviations of E_{avg}, E_{min}, LPD, UGR_{max} are less than 5%.
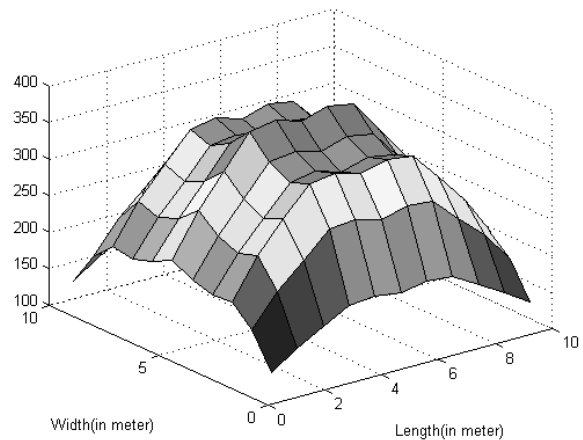
Fig. 5. Surface plot of total maintained illuminance
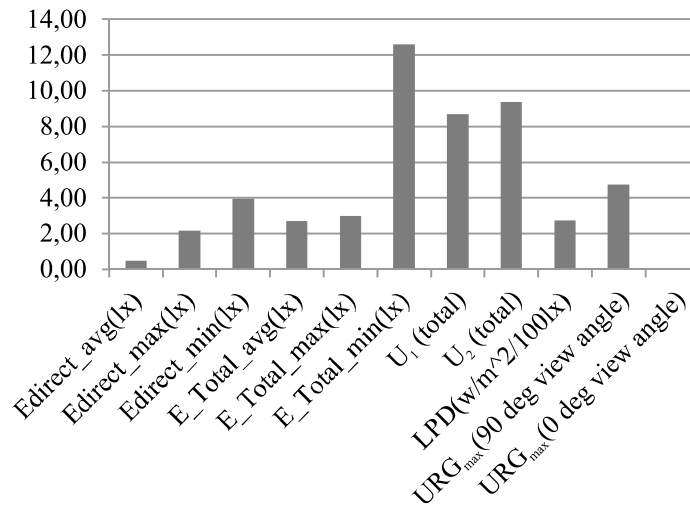
Fig. 6. Percentage deviation of design parameters
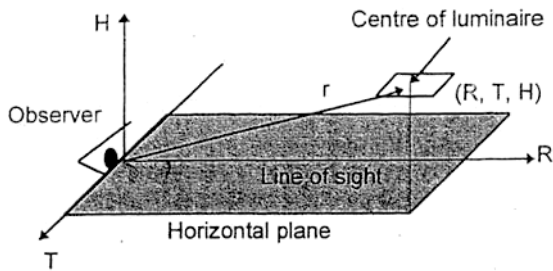
Fig. 7. The position index coordinate system [3]

7. CONCLUSION

It can be concluded that indoor lighting parameters viz., point-specific direct and indirect illuminance on working plane, source and background luminance as viewed by observer are computed using the developed MATLAB program using luminaire data from its *.ies* file as provided by manufacturer. Subsequently, indoor general lighting design parameters viz., maintained average illuminance, uniformity of illuminance and *UGR* are also found out with the above computed values. Results, obtained form the developed MATLAB program, are in good agreement with the DIALux simulation. This developed program can be utilized as MATLAB Tools for more complicated lighting computations and optimization.

ACKNOWLEDGMENT

REFERENCES

1. Standard File Format for the Electronic Transfer of Photometric Data, ANSI/IESNA LM-63–02, (2002)

2. Applied Illumination Engineering, Jack L. Lindsey, The Fairmont Press, Inc., 2nd Edition, p. 215−236, (1997).

3. Discomfort Glare in Interior Lighting, CIE117, p. 1−7, (1995).

4. IES Lighting Handbook, Reference Volume, p. 9−52−9−73, (1984).

5. Lamps and Lighting, Coaton J.R. and Marsden A.M., Arnold,4th Edition, p. 301−317, (1997).

6. Code of practice for Interior Illumination, IS-3646(Part1), (1992).

ANNEX-I

All ANSI/IESNA LM-63−2002 filenames shall end with the file extension *ies* or *IES* (the file extension is notcase-specific).The following file shows a sample of IES file format specification [1].

Sample .ies
· **IESNA: LM-63–2002**
· [Keyword 1] Keyword data
· [Keyword 2] Keyword data
· [Keyword 3] Keyword data
· :
· [Keyword n] Keyword data
· **TILT=<filename> or INCLUDE or NONE**
· <lamp to luminaire geometry>
· <number of tilt angles>
· <angles>

· <multiplying factors>
· <number of lamps> <lumens per lamp> <candela
   multiplier> <number of vertical angles> <number
   of horizontal angles> <photometric type> <units
   type> <width> <length> <height>
· <ballast factor> <future use> <input watts>
· <vertical angles>
· <horizontal angles>
· <candela values for all vertical angles at 1st horizontal angle>

· <candela values for all vertical angles as 2nd horizontal angle>
· :
· <candela values for all vertical angles at last horizontal angle>

ANNEX-II

The position index coordinate system(R, T, H) based on the observer. The ratios H/R and T/R are based on the centre of the luminaire Fig. 7 [3].

Purnima Mandal
is a research scholar at Electrical Engineering Department of Jadavpur University, India. She did M.E. in Illumination Engineering in 2007 after having B.E. in Electrical Engineering in 2005 both from Jadavpur University. She is now working on Daylight pipe integated lighting control system

Biswanath Roy
is Professor of Illumination Engineering at Electrical Engineering Department of Jadavpur University, India. He did Ph.D. (Engg.) on Daylighting in 1999 from Jadavpur University after having M.Sc. (Tech.) in Optics & Optoelectronics in 1993 and B.Sc. (Hons.) in Physics in 1989 both from University of Calcutta. He is Life Fellow of Indian Society of Lighting Engineers (ISLE), Life Member of The Institution of Engineers (India) and Member of IESNA

MODERN SYSTEMS OF OUTDOOR ILLUMINATION FOR COMPRESSOR STATIONS

Oleg V. Kryukov and Artyom V. Serebryakov

Giprogazcenter Joint-stock company, the Nizhegorodsky State Technical University (NSTU) of R.E.Alekseev, Nizhny Novgorod
E-mail: o.kryukov@ggc.nnov.ru

ABSTRACT

Principles of designing modern systems of outdoor illumination for compressor stations on principle gas transport lines are considered. Application of hardware based and circuit solutions for illumination of sites and buildings at compressor stations are presented.

Keywords: light sources (LS), light devices (LD), illumination control systems, energy saving LDs, compressor stations, design

Compressor stations (CSs) are one of the most significant electricity consumers of the gas pipeline grid [1, 2]. Most modern CSs are equipped with gas turbine pumps over units. Power consumed by a CS from the circuit using a gas turbine drive amounts to 2−4 MW, depending on the number of units. 10−20% of this is consumed for illumination, outdoor illumination (OI), of the CS and for illumination of production and auxiliary buildings [2, 3]. Therefore, the power consumption of all technological process of distant gas transport, and hence its cost to the consumer, depend to a large extent on the energy efficiency of the CS illumination installations [3−6].

Illumination installations of a CS should provide a level and quality of illumination at standard values; uninterrupted operation of illumination; convenience servicing and control.

Rationing of CS OI is carried out according to CП 52.13330.2011 "Artificial and natural illumination" and Gazprom Standard RD1.14−127−2005 "Standards of artificial illumination" [1 − 3].

Main light sources (LS) at CSs include (Fig. 1):
• For OI: high pressure gas-discharge sodium lamps (HPSL) (the power consumed by these is about 25% of the total power consumption of the CS illumination circuit);
• For the illumination of production rooms: FLs and arc discharge lamps of up to 150 W power, as well as light emitting diodes (LEDs). Nearly 35% of the total power consumption of the CS illumination network is spent for this purpose;
• For the illumination of office buildings, mainly FLs and CFLs are used; this uses nearly 50% of the total power consumption of the CS illumination network.

The electric power is supplied to the OI network by a third reliability degree electric power supply, using complete transformer substations suitable for power and repair units and gas cooling devices.

For the OI illumination installation's power supply, 220V or 380V of alternating current voltage is normally used. To improve the reliability of searchlight operation, mast mounted searchlights, with numerous lamps each (Fig. 2), are grouped in two's and three's, and connected to distributing switchboards. The switchboards are installed at the bottom of the mast, which allows switching on the required searchlights for undertaking repair and maintenance work on the mast at night without switching off all the searchlights. In the event of short circuit in one of the search-

lights or in the cable, only searchlights of a specific group are switched on.

For OI sites of CSs and of linear production base sites, searchlights with HPSLs of 1000 W power are installed on (20 − 30) m masts. The sufficient OI level is determined using standard documents.

This LD type has the following advantages: a long operational period; high luminous efficacy, up to 150 lm/W; long service life of about (20−30) thousand hours; broad power range, up to 1000 W; warm-up period after switching on of less than seven minutes; high stability of LS parameters during operation; operation in different temperature and weather conditions; reliability of LS ignition.

Currently, there is no conclusive evidence to suggest the superiority of lighting devices with LEDs instead of industrial purpose searchlights with high pressure mercury lamps (HPML) for this application.

Certainly, LDs with LEDs have a number of benefits [1−3]: a long service life; a wide LED temperature operation interval: (−50 − +60)°C; endurance for mechanical exposure; high luminous efficacy; wide radiation direction: the availability of a wide range of LEDs manufactured with radiation angles of (10 − 140)°, which means special reflectors or diffusers are not required; a zero lag and improved light and colour adjustment possibilities; better environmental and fire safety levels.

However, some technological factors limit the application of LDs with LEDs in CS OI, which is connected with features of the searchlight installation. As a rule, EI searchlight masts are spread wide apart, and searchlights are installed 20 to 30 metres up. This means that normalised illuminance cannot be achieved by replacing HPML searchlights with LED searchlights.

Powerful searchlights with LEDs sufficient to illuminate CS sites require special cooling due to the known features of LEDs. In this case, condensation forms over the entire LED board surface because of the temperature difference, leading to their failure. Therefore, the operation of LDs with LEDs is better in stable environmental conditions.

LEDs are susceptible to high steps in voltage. Lightning bolts can cause failures and parameter changes, worsening the operation of these LSs. Failures due to overloads and electric discharges is a very significant problem in LED application.
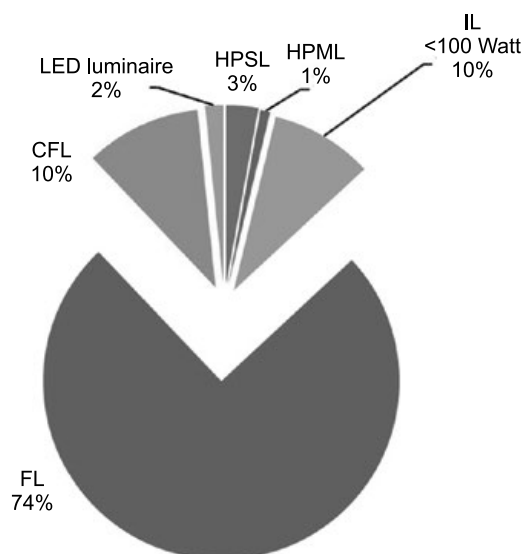
Fig. 1. Structure of light source application on CSs

Fig. 2. A mast with searchlights on a CS site

Besides, the luminous flux of LEDs decreases with time, and this decrease can reach (50 − 60)% of its initial value.

Contrary to the assumption that LDs with LEDs do not need servicing, they do require main-

tenance, sometimes more often than LDs with HPMLs, especially in low ambient temperatures and surface humidity. To address the problem of pollution, LDs with LEDs are used in projects with *IP55* protection degree and above.

LED disadvantages include a poor quality of colour rendition, relatively high price per lumen, relatively complex heat removal, etc.

LDs with LEDs can be applied, for example, for illuminating connection units, water-intake constructions, gas-distributing stations and points. These installations need smaller areas illuminated at a low LD height.

In accordance with СП 52.13330.2011 "Artificial and natural illumination, Actualised edition of Building regulations 23–05–95*, "Artificial and natural illumination" and Gazprom RD standards 1.14–127–2005, "Standards of artificial illumination" in the OI project, the following illuminance values should be provided:

— Cut-out and adjusting equipment: 10 lx;
— Sites and outflows from operation sites: 5 lx;
— Roads between tanks: 2 lx;
— Boards and control panels: 50 lx;
— Separate control devices: 50 lx.

DiaLux is normally used for illumination calculations.

According to the rules and standards, the control of the whole illumination CS OI network should be centralised: from one or minimum places number. In the OI control points, a signalling system concerning the OI state is provided for: "switched on/switched off". A centralized OI remote control is carried out from the attendant's room.

Depending on the number of searchlight LDs, and especially on their operating mode, their control version is selected. As a rule, control of all LDs is carried out simultaneously. Photo automatic control is widely applied, using magnetic starters in the illumination lines and program relays switching on LDs depending on the level of natural illumination or on the time of day or night. For this purpose, a EI control system based on control boxes ЯОУ-9600 is installed, which allows switching on/switching off from a photodetector signal when achieving a preset illuminance level; using buttons installed on the doors of the box, manually; by means of mechanics devices from control points.

However, the drive for energy efficiency dictates new design requirements for OI. At present, relay systems of OI remote centralised control are replaced with computer aided OI control systems (OI CACS).

The introduction of OI computer aided control systems allows for the following: centralised OI control (LD lighting mode operation, distant operation of timetabled site illumination with allowances for weather conditions); improved economic efficiency due to reduced power consumption and decreased servicing costs; operating objects in groups or individually; necessary levels of network safety; protocols of events and actions of the operators; to block switching on during periods of for assembly, starting-up and operation adjustment.

An increase in OI energy efficiency can be achieved due to the following reasons: rationalised selection, placing and optimisation of LD power using special software; replacement of outdated incandescent lamps and arc discharge lamps, with high pressure sodium lamps and with metal halogen lamps; use of computer aided remote control systems and of illumination installation work control; increase of stability of LS characteristics; improvement of LD operational properties; use of energy efficient ballasts (electron ballasts).

Further energy savings are reached by LIs with HPSL LDs and with electron ballast due to the stability of power consumption in a rated operating mode stabilised by voltage and in a LI power reduction mode, Power reduction systems gradually lower power and luminous efficacy in the set limits. As power reduction systems adjust illumination gradually, they are more acceptable for EI, although they are more expensive than simple systems of power switching.

As a whole, the experience of designing and operating, as well as the results of CS illumination research shows that:

• Most abnormal situations arising when illuminating are connected with inefficient choice and inefficient application of illumination equipment and LD control systems;

• Innovative illumination installations based on searchlights types ЖО-07 and ПСД 220/250 have confirmed their reliability and suitability for CS units. The declared time between failures of these searchlights reaches 50 thousand hours;

• One of main disadvantages of LED searchlights is their relatively high cost and insufficient luminous flux for CS. Nevertheless, the introduction of LDs with LEDs into CSs is a prospective approach due to the potential energy efficiency gains and the reliability of LDs main gas transport installations;

• Application of energy saving solutions in illumination control saves power and raises LS service life, LD reliability and comfort of the light medium.

REFERENCES

1. Energy saving and automation of electric equipment of compressor stations: a monography in three volumes. V. 2 / Under editorship of O.V.Kryukov. N.Novgorod: Vector TiS, 2011, 664 p.

2. Power installations and electric power supply of gas transport objects: Monography of series "Proceedings for the 45th anniversary of Giprogastcenter Open Society" V. 3 / Under editorship of O.V.Kryukov. Nizhny Novgorod: Istok, 2013, 300 p.

3. *Kalnynsh N.N., Kryukov O.V. Rubtsova I.E, Ryabkova E.Yu.* Innovative solutions in design of systems of compressor station illumination // Automation in the industry, 2011, # 9. pp. 19–21.

4. *Vasenin A.B., Kryukov O.V., Serebryakov A.V.* Electric power supply systems using SMART GRID principles for objects of main gas pipelines // Automation in the industry, 2012, # 4, pp. 36–38.

5. *Kryukov O.V., Titov V.V.* Development of CAC systems for autonomous wind-energy installations // Automation in the industry, 2009, # 4, pp. 35–37.

6. *Serebryakov A.V., Kryukov O.V.* About new abilities of SMART GRID technologies // Electric equipment: operation and repair, 2013, # 2, pp. 47–48.

Oleg V. Kryukov,
Doctor of Engineering, graduated from the Gorkovsky Polytechnical institute of A.A. Zhdanov in 1978 with a first class honours degree; the main specialist of Giprogascenter Joint-stock Company

Artyom V. Serebryakov,
Ph.D., graduated from the NGTU of R.E. Alekseev in 1978, a senior lecturer of the Chair "Electric equipment, electric drive and automatics"

CONTENTS

VOLUME 24   **NUMBER 3**   **2016**

LIGHT & ENGINEERING
(SVETOTEKHNIKA)

Vol. 24, No.3, 2016 is devoting to the selected high guality papers from the partnership of Light&Engineering Journal from CHINA, which are focused in the scope of the journal.

PARTNERS OF LIGHT & ENGINEERING JOURNAL

Editorial Board with big gratitude would like to inform international lighting community about the Journal Partners Institute establishment. The list with our partners and their Logo see below. The description of partner's collaboration you can found at journal site
www.sveto-tekhnika.ru

GENERAL PARTNER

 BL GROUP holding

 ITMO UNIVERSITY

PLATINUM PARTNERS

 VS LIGHTING SOLUTIONS

enercom СОЗДАЕМ ВОЗМОЖНОСТИ

 PHAROS-ALEF

ГЛОБАЛ ЛАЙТИНГ

GOLD PARTNERS

FAGERHULT

 ГСТЗ г. Гагарин

 ZUMTOBEL

SILVER PARTNERS	BRONZE PARTNERS

Светотехнический завод ВЛАДАСВЕТ

ВНИСИ · ВНИИОФИ ·

TENZOSENSOR

СВЕТОВЫЕ СИСТЕМЫ

НИИ

ИФ

СОЛАР МАГИЧЕСКИЙ СВЕТ